Developing fixed dose combinations for the geriatric population

University College London

UCL School of pharmacy Department of Pharmaceutics

Thesis submitted for the degree of Doctor of Philosophy by

Haitham Abdulrahim Bukhary

31 May 2019

UCL SCHOOL OF PHARMACY

29-39 Brunswick square

London, WC1N 1AX, UK

Declaration

This thesis describes research conducted in the UCL School of Pharmacy from June 2015 to May 2019 under the supervision of Dr Mine Orlu and Dr Gareth R. Williams.

I, Haitham Abdulrahim Bukhary confirm that the work presented in this thesis is my original work and I certify that I have written all the text herein. Where information has been derived from other sources, I confirm that this has been indicated in this thesis.

Signature: ---------- Date: ----------

Acknowledgments

I would like to express my gratitude to my supervisor's Dr Mine Orlu and Dr Gareth R. Williams for all their time, for giving me scientific guidance, for their valuable suggestions, and the constant encouragement throughout this PhD.

I would like to express my appreciation to all the staff at the UCL School of Pharmacy for the help and their administrative assistants.

I am also appreciative to all my colleagues at the UCL School of Pharmacy for providing an excellent environment of collaboration and for their friendship.

I want to give my deepest gratefulness to my home country, the Kingdom of Saudi Arabia, for giving me this outstanding opportunity of funding my scholarship sponsored by Umm Al Qura University.

Finally, I am truly indebted to all my family, specifically to my wife, my son, my parents, and my siblings, for their love, support, and encouragement throughout my life.

Abstract

Background: Successful therapeutic outcomes demand a patient's adherence to their dosage regimen, yet this is challenging to achieve among elderly people on multidrug therapies (polypharmacy). Therefore, it is the task of formulators to prepare medicines to minimise the burden on patients and maximise the likelihood of a dosage regimen being accurately followed. One route to improve adherence rates is to prepare fixed-dose-combinations (FDCs), in which multiple active ingredients are loaded into a single formulation. This thesis aims to develop different FDCs of multiple drug-polymer composite systems targeting specific conditions for the geriatric population utilising advanced pharmaceutical manufacturing techniques.

Methods: Different biocompatible polymers were selected for each formulation based on dissolution behaviour in aqueous media. The polymers were mixed with the selected combination of drugs and then formulated. Initially, fast-dissolving materials based on poly(vinylpyrrolidone) (PVP) were generated by either film casting (a conventional technique used to prepare orodispersible films), or single-needle electrospinning (to prepare FDCs in the form of nanoscale fibres). Further modification of the electrospinning setup was then undertaken to prepare oral FDCs containing ibuprofen, famotidine, and prednisone. Three polymers (PVP, Eudragit-L100, and Eudragit-RSPO) were used to generate fibres, and sequential and multi-jet electrospinning employed to fabricated FDCs. Finally, core/shell fibres made of Eudragit-RLPO/PVP, as a platform for levodopa and carbidopa both equally loaded in each layer of the core and shell, for biphasic release oral FDCs was performed using coaxial electrospinning.

Results: FDC in the form of PVP-based fast-dissolving oral films loaded with amlodipine besylate and valsartan were prepared by film casting between 5-30% w/w and electrospinning between 5-55% w/w. A comparison between the two types of formulations showed that 90% drug release could be achieved from the electrospun fibres within 2 minutes, while the cast film ODFs took 6 minutes. Next oral FDCs prepared from ibuprofen, famotidine, and prednisone proved the ability to generate different FDCs through modification of electrospinning setup by sequential and multi-jet electrospinning. Results from the in vitro drug release studies showed that the desired multi-phasic drug release could be obtained. This began with the immediate release of drug-loaded in the PVP layer instantly within ~1hr of sampling, followed by release from the Eudragit-L100 fibres triggered by the change of pH >6, and finally extended-release from the Eudragit-RSPO fibres to reach >80% after ~16 hours. Last FDC, the core/shell fibres gave similar release profiles for levodopa and carbidopa, with 50% immediate release from the PVP compartment, followed by 50% extended-release from Eudragit-RLPO. Overall the formulation provided the desired biphasic release profile.

Conclusions: The appropriate selection of polymer and manufacturing technique, can fabricate effective drug-polymer composite systems for multiple drug delivery via FDCs. Ultimately, it is believed these could be applied to enhance patient adherence.

Impact Statement

The majority of people age 65 years and older diagnosed with long term conditions require simultaneous treatment by multiple medicines, a situation termed polypharmacy. This raises many issues related to adverse effects, drug-drug interactions and medication errors. These issues often result in poor adherence to the prescribed drug regimen, which increases with long term management of multimorbidity. Designing appropriate and smart combined therapies will result in major benefits to multi-morbid patients, as well as their carers and health care providers.

The most common method of drug administration is through the oral route. Accordingly, it is the task of formulators to prepare oral patient-centric dosage forms specifically designed to minimise the burden on patients and optimise the adherence to the treatment regimen. A smart solution to overcome the administration challenge is delivering multiple drugs in a single dosage form, known as a fixed dose combination (FDC) drug product. Although this can be done with conventional formulation approaches, using novel techniques could allow the manufacturing of advanced formulations with improved specifications. In this work, solvent film casting and the electrospinning of nanofibres were explored as novel methods for FDC fabrication.

This research shows that FDCs in the form of drug/polymer composites were created with both techniques. A range of advanced formulations was prepared with electrospinning, and we were able to prepare systems giving varied release profiles of a number of drugs of relevance to the older population.

The results of this project show the feasibility of electrospinning as a promising low-cost smart manufacturing technique to create advanced drug delivery systems. The strategies employed here could be developed further for different applications in the pharmaceutical or food and nutrition industry. In the short term, the optimised platform can be used for preparing different FDCs that require multiple drug release profiles in an academic research setting. In the midterm, the scalability of electrospinning means it has the potential to provide an impact as a fabrication technology for the manufacturing of licensed FDCs. In the long term, implementation of these licensed

formulations into clinical practice will yield impact, particularly to meet the therapeutic needs of the ageing population.

Table of contents

List of Tables

List of Figures

List of Abbreviations

AADC l-amino acid decarboxylase

AB Amlodipine Besylate

APIs Active Pharmaceutical Ingredient

ASD Amorphous Solid Dispersion

BCS Biopharmaceutical Classification System

BP British Pharmacopeia

CD Carbidopa

DC Direct Current

DDS Drug Delivery System

DMAc N, N-dimethylacetamide

DSC Differential Scanning Calorimetry

EE Encapsulation Efficiency

EUDRAGIT® Poly(meth)acrylates

ER Extended-Release

E-L100 Eudragit-L100

E-RLPO Eudragit-RLPO

E-RSPO Eudragit-RSPO

FDC Fixed-Dose Combinations

FD-DDS Fast Dissolving Drug Delivery Systems

FDA Food and Drug Administration

FAM Famotidine

Glyc Glycerol

HIV Human Immunodeficiency Virus

IP Ibuprofen

IR Immediate Release

HCl Hydrochloric acid

HME Hot Melt Extrusion

HPLC High-performance liquid chromatography

LD Levodopa

MCAs Multi-Compartment Compliance Aids

MDS Monitored Dosage System

ML Mono-Layer nanofibre mats

ODFs Orodispersible films

OTC Over The Counter

PBS Phosphate Buffered Saline

PD Parkinson's disease

PCL Poly(ε-caprolactone)

PEG Poly(ethylene glycol)

PM Physical Mixtures

PRED Prednisone

PVP Polyvinylpyrrolidone

PVPVA Polyvinylpyrrolidone–Vinyl Acetate

RA Rheumatoid Arthritis

SEM Scanning Electron Microscopy

TEM Transmission Electron Microscopy

Tg Glass Transition Temperature

UN The United Nation

USP United States Pharmacopeia

VAL Valsartan

WHO World Health Organisation

XRD X-ray Diffraction

Research Publications from this thesis

Bukhary, H., Williams, G.R. and Orlu, M., 2018. Electrospun fixed dose formulations of amlodipine besylate and valsartan. International Journal of Pharmaceutics, **549** (1-2), pp.446-455.

Posters

Bukhary, H.; Williams, G.R.; Orlu, M, Utilisation of electrospinning to develop a fixed dose combination formulation. The International PharmTech Conference 2016. EPRSC EHDA Network at Devonshire Place, 78 London Road, Leicester, UK. November 2016.

Bukhary, H.; Williams, G.R.; Orlu, M, Fixed-dose combination of ibuprofen, famotidine, and prednisone prepared by multi-jet electrospinning. 3rd European Conference on Pharmaceutics. Bologna Congressi, Bologna, Italy, March 2019.

Chapter 1. General introduction

From the first decade of the twenty-first century, the growth of population over 65 years old was by 15.1% and with a faster increase of individuals aged over 85 years compared to any other age group (Yarbrough, 2016). The rapid growth of ageing population indicates a shift in life expectancy defined as the overall mortality level of a population (WHO, 2016). The United Nation (UN) estimates the change of human life expectancy from the current age of 71 years to 82 years by 2050 (Bongaarts, 2009). This increase in life expectancy brings the need for better medicines for geriatric patients (Orlu-Gul et al., 2014). In the UK, older people make 20% of the population and consume almost 50% of prescription drugs (Gorard, 2006).

The majority of people aged 65 and older are diagnosed with multiple diseases that require management with several active ingredients simultaneously, often to the extent of polypharmacy, which loosely defined in different literatures as the synchronous use of two medicines up to many different medicines together (Fulton and Riley Allen, 2005; Munger, 2010). Polypharmacy was recognised as a principal medication safety problem (Larsen and Martin, 1999), which raised the concerns due to many issues like the potential to cause adverse drug reactions or medication interactions (Payne and Avery, 2011). Furthermore, different medicines supply may lead to difficulties in self-administration such as mixing up similar looking medicines or wrong timing of medicine administration (Edirisinghe et al., 2015). Accumulation of these different issues might result in poor adherence to the prescribed drug regimen (Hughes, 2004).

At the WHO adherence meeting in 2001, the definition of adherence was concluded as the extent to which patient follows medical instructions given by the health care professionals including the plan of therapeutic regimen (Sabaté, 2003). The adherence of patients to their drug regimen is crucial for successful therapeutic outcomes (Jimmy and Jose, 2011). Patients adherence with their drug regimen affected by acceptability, which is the use a medicinal product as intended or authorised (Kozarewicz, 2014). It is generally assumed that the patients take the full course as prescribed medication. Unfortunately, for patients with long-term conditions there is a big chance for patients non-adherence with treatment plan (Haynes et al., 1996). The non-adherence can be intentional originating from the patient's opinions about the medicine (Lehane and McCarthy, 2007), or unintentional as passive process whereby patients fail to adhere to prescribing instructions as a result circumstances out of their control, e.g. forgotten (Gadkari and McHorney, 2012). For the geriatric population, the degree of functional disabilities, memory impairment, and other cognitive deficits might increase leading to increased outcome of unintentional non-adherence with treatment regimen (Hughes, 2004; Alldred et al., 2007). The problem may be more exacerbated since physiological functions might decrease, leading to altered pharmacokinetics and pharmacodynamics drug profile hence increased susceptibility for adverse drug events (Barber et al., 2009). At advanced age multiple drug therapy is more required (Hughes, 2004). The risk of non-adherence will be high when multiple morbidities last for a prolonged time. That necessitate public engagement to improve patient-centric products for the geriatric population which provide benefits for the patients, as well as family carers and health care providers (Orlu-Gul et al., 2014).

1.1 Strategies for managing polypharmacy

The aetiology of polypharmacy is multifactorial, yet different parts contribute to increase the incidence of multiple medicine use. Most of the drugs prescribed for the patients are through primary care providers, as reported that around 75% of all visits results in a written prescription (Larsen and Martin, 1999). Therefore, it is important for older patients to be able to reach a level of contact for their multiple prescriptions and hence receive advice on coordinating among medication regimens. The other important contributor to polypharmacy is the complementary and alternative therapies accessible over the counter medications (Prybys et al., 2002).

Different strategies to reduce polypharmacy was applied by some group like Pitkala et al. (2001) by simplifying drug regimen with tighter control conditions of day hospitals care in order to minimise the excessive prescribed medications. The final result was that day hospital care intervention did not significantly decrease the number of prescribed medicines for older patients, in facts there was a significant increase in the consumption of over the counter (OTC) drugs by the patients trying to self regulate their medications, and in the follow up after the experiment, the number of drugs returned to baseline level after 3 months only (Pitkala et al., 2001).

Electronic technologies have also been employed to enhance the lifestyle of polypharmacy patient and showed great potential to improve patient's medicine management by organising daily medication of an older person e.g. multi-compartment compliance aids (MCAs) and monitored dosage system (MDS), (Edirisinghe et al., 2015). These aids includes several sections that correspond to

single administration time, however as all medications removed from original containers and organised into each section of the MCA, this approach might invalidate the shelf life of the medicinal product (Edirisinghe et al., 2015).

Oral drug administration is highly effective and the most preferable method of drug administration to the majority of older (Liu et al., 2014). However, the complexity of many dosage regimens and impairments seen at older age such as dysphagia may affect medication adherence resulting in increased rates of morbidity and mortality (Carnaby-Mann and Crary, 2005). The proper pharmaceutical design is required to promote patient acceptability among the geriatric population (Liu et al., 2014).

Therefore, it is the task of formulators to prepare patient-centric dosage form specifically designed for these particular conditions to minimise the burden on patients and maximise the likelihood of a dosage regimen being accurately followed. Much work has been devoted to ensuring formulations exhibiting good patient acceptability (Liu et al., 2014), for instance, adding features into the oral medicinal product design to ensure ease of swallowingin order to prevent oesophageal retention and risk of aspiration (Liu et al., 2014). A smart solution to overcome the administration challenge is simplifying the treatment regimen for multiple drugs by combining them in a single dosage form.

1.2 Fixed dose combination

1.2.1 Definition of fixed dose combination

Fixed dose combination (FDC) drug products are defined as those which combine two or more active pharmaceutical ingredients (APIs) in a single dosage form at a fixed dose ratio (World Health Organization, 2005). According to the FDA (1975) “two or more drugs may be combined in a single dose when each component makes a contribution to the claimed effects, and the dosage of each component (i.e., amount, frequency, and duration) is such that the combination is safe and effective for a significant patient population requiring such concurrent therapy” (Hao et al., 2015).

FDC products are commonly used for the treatment of patients with chronic disease that require multidrug regimens, such as the population with human immunodeficiency virus (HIV) infection, hypertension, diabetes, and tuberculosis (Desai et al., 2012). The Food and Drug Administration (FDA) licensed a number of FDC products for targeting single disease condition or multiple disease condition (FDA, 2004). Between the years 1980 to 2000, the number of approved FDCs increased from 12 to 59 products (Hao et al., 2015). There is substantial evidence that increasing treatment regimen complexity (by multiple medications, multiple frequent dosing, and the need for specific time or diet) results in poorer adherence to treatments of hypertension, diabetes, and HIV infection (Ingersoll and Cohen, 2008). Examples of licensed products include the antiretroviral FDC products COMBIVIR® [zidovudine + lamivudine], and TRIZIVIR® [zidovudine + lamivudine + abacavir] (FDA, 2004) for treatment of HIV infection. EXFORGE® [amlodipine besylate + valsartan] is another

licenced FDC product which is indicated for the management of hypertension (Joint Formulary Committee, 2016). Other FDC products such as CADUET® (amlodipine besylate + atorvastatin calcium) are prescribed for multiple disease conditions (FDA, 2015).

1.2.2 Advantages and disadvantages of fixed dose combination formulations

FDC formulations created a number of advantages. First, it can facilitate simpler treatment plans for multiple drugs which have similarly timed regimens (Bangalore et al., 2007), and thereby reducing the burden on patient and improve patient compliance (European Medicines Agency, 2017), e,g TRIZIVIR® [zidovudine + lamivudine + abacavir] (FDA, 2004) an HIV treatment that gained patient's compliance with the reduced dosing burden of taking multi-dose formulation (Desai et al., 2012). FDC has also provided a therapeutic advantage in the antibacterial treatment with amoxicillin and potassium clavulanate by enhancing the effectiveness and broadening the antibacterial spectrum of amoxicillin (Desai et al., 2012). Moreover, FDC of anti-tuberculosis treatment minimised the drug resistance in the combination of rifampicin, isoniazid, pyrazinamide, and ethambutol (Wu et al., 2015).

Despite the previous advantages, FDC products include some limitations like the unclear cause of adverse drug reaction from multidrug combinations. (Desai et al., 2012). Also, the lack of flexible dosing that requires variant strength combinations to compensate for the standard doses making FDC tablets or capsules tends to be larger than the individual drug formulations, and thus if poorly designed FDCs could in fact

reduce patient compliance because of swallowing difficulties (European Medicines Agency, 2017).

1.3 The manufacturing techniques for the preparation of FDC

A number of conventional pharmaceutical technologies have been used for commercial FDC product manufacturing (Desai et al., 2012), such as the incorporation of multiple drugs in separate layers of multilayer tablets (Mitra and Wu, 2012). The most common process for making a chemically compatible FDC is through direct compression of tablets (Desai et al., 2012). The alternative method for chemically incompatible drugs is making a bi-layer or multi-layered tablet, or by adding partitioning buffer layer to provide better stability in the tablet (Desai et al., 2012).

Novel technologies have been employed for developing patient-centric dosage forms, able to enhance patient adherence in addition to improve bioavailability and absorption (Fina et al., 2018). Among those, 3D printing is an emerging technology that has been employed to produce an FDCs formulation containing five different APIs (Khaled et al., 2015). Hot melt extrusion (HME) is another example of a manufacturing technique used for the preparation of FDCs composed of multi-particulate pellets covered by multilayer film coating, to provide various release profiles for multiple drugs (Desai et al., 2012). An example of a marketed product made by HME includes contraceptive vaginal ring NUVARING®, and the contraceptive implants IMPLANON® (Dierickx et al., 2012).

FDCs could have several key strengths and limitations. As an advantage, FDCs could improve better patient adherence with the treatment regimen of multidrug formulation and complex drug formulation. It can have clinical benefits like synergistic therapeutic effects of two molecules, as in Aggrenox® 2 antiplatelet agents (dipyridamole and aspirin). And the reduction of the cost of manufacturing and distribution compared to the separate product. On the other hand, the limitations can be formed as a lack of flexible dosing, so a variety of strength combinations are required to compensate and cover the common doses. And finally, the challenge of specifying the cause of adverse drug reactions in the FDC.

Usually, the manufacturing of pharmaceutical products is performed in batches, which are transferred between processing steps, and off-line product quality testing and storage take place in between (Kelleher et al., 2018). While continuous manufacturing techniques such as hot melt extrusion enables a one-step continues feed input and product output if the required optimum parameters were maintained over the process (Gursch et al., 2015). The continuous manufacturing techniques characterised by the ability to increase product excellence, coordination, flexibility, and productivity (McKenzie et al., 2006), which makes it more promising for developing FDCs. Different alternative methods for manufacturing FDCs has to date not been widely explored. The approaches for utilising additional novel techniques can create additional chances of manufacturing advanced formulation with the intended specifications. In the next part, solvent film casting and electrospinning of nanofibres will be discussed as prospective methods for FDCs fabrication.

1.3.1 Solvent film casting

Solvent film casting is a commonly used conventional method for preparing orodispersible films (ODFs) (Buanz et al.,2015). ODF is a small size thin film usually made of a polymeric composite that fast dissolve once contacting with saliva (Scarpa et al., 2018).

1.3.1.1 Principle of solvent film casting

The principal of this method is to develop a drug-polymer composite from a film-forming polymer. The selected polymer dissolved in an organic solvent then mixed with an active pharmaceutical ingredient (APIs) readily dissolved in a suitable solvent (Hoffmann et al., 2011). Further excipient can be added such as glycerol as plasticisers if required (Dixit and Puthli, 2009). Next, the drug-polymer solution mixture poured into a casting container placed on a flat surface with application of temperature that allow solvent evaporation over time, which results in the molecular orientation of the polymer molecules resulting in a flexible film formation easy to handle and packaged (Deng et al., 2018).

1.3.1.2 Types of solvent film casting method

Solvent casting can be a non-continuous or continuous manufacturing process. In the non-continuous manufacturing process the collector plate covered with a fixed liner to produce a single batch collected once the ODF completely dry. In comparison continuous manufacturing done with bigger machines that depends on an intermediate

liner that continues rotate to collected film into big rolls, which then will be cut into smaller size for packaging (Hoffmann et al., 2011; Thabet and Breitkreutz, 2018). The non-continues production can be used at a small laboratory scale such as in a hospital-pharmacy (Visser et al., 2017), while continues batch production of ODFs applicable at the industrial level with larger equipment (Hoffmann et al., 2011).

1.3.1.3 Application of solvent film casting to formulate FDCs

Solvent film casting method has been employed to develop FDC loaded with a combination of low solubility drug: Posaconazole and Benznidazole to increase the apparent solubility and dissolution rate of both drug by developing amorphous solid dispersions (ASD) based on (vinylpyrrolidone–vinyl acetate copolymer; PVPVA 64), (Figueirêdo et al., 2018). The resulted ASD system based on PVPVA was an effective carrier for up to 50% (w/w) loaded FDC of both drugs, and proved an applicable technique to enhance the synergistic effect of both APIs as an ASD in PVPVA matrix with better dissolution that can potentially improve the bioavailability (Figueirêdo et al., 2018).

1.3.2 Electrospinning

Electrospinning is a simple technique in which electrical energy is applied to a polymer/drug solution to drive a liquid jet, usually resulting in amorphous solid dispersions (ASDs) in the form of nanoscale fibres (Khil et al, 2003). Since the 1980s, the attention on electrospinning has raised with the rising interest of nanotechnology, in which ultrafine fibres were made from different composites, semiconductors,

ceramics, and most commonly from polymers (Teo and Ramakrishna, 2006) into nano to micron size fibres (Huang et al, 2003). At these sizes, the formulations prepared from such fibres will gain many attractive features such as a large surface area to volume ratio, high porosity with tuneable pore size, the flexibility for efficient surface functionalization, and changeable surface morphology (Zamani et al, 2013). In recent years the number of publications on electrospinning noticed more increase (Tucker et al., 2012). Moreover, a variety of applications in the industrial fields and biomedical fields have made with electrospun fibres (Ramakrishna et al., 2005). For instance, a variety of natural and synthetic polymers was electrospun to fabricate a scaffold for tissue regeneration, wound dressing, and drug-delivery applications (Ma et al., 2011).

1.3.2.1 The general setup of electrospinning

The setup of electrospinning consists typically from four main parts: high voltage power supply, the syringe pump, the capillary needle (spinneret) usually metallic, and the grounded collector surface (Figure 1.1). Before electrospinning, the polymer solution loaded into the syringe then located in the syringe pump to run the solution at a constant flow rate through the needle. A high voltage power supply connect from direct current (DC) attached to the spinneret which is located at separating distance towards the surface of the grounded collector. (Sill and von Recum, 2008).

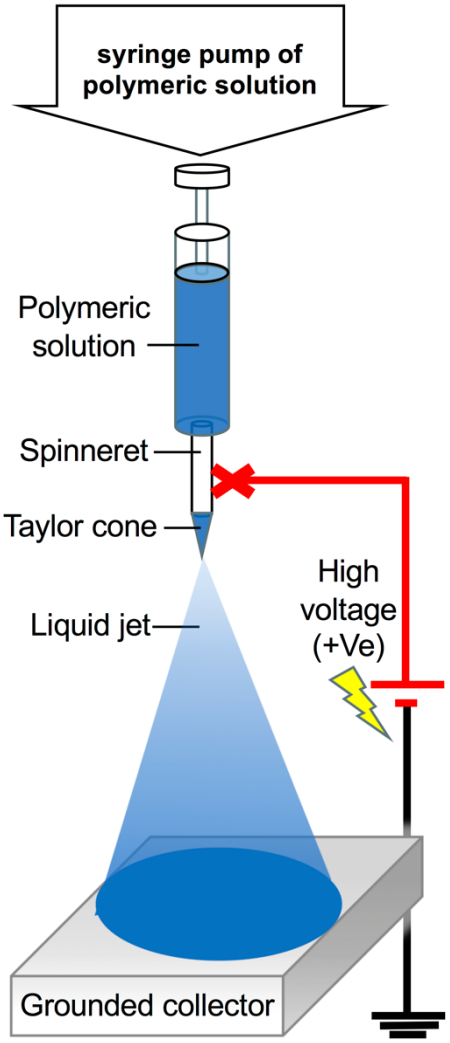

Figure 1.1. A schematic illustration of the setup of electrospinning technique. (Drawing made by PowerPoints software).

1.3.2.2 Principle of electrospinning

On the tip of the metallic needle (spinneret), the solution droplet makes a hemispherical shape by liquid surface tension (Deitzel et al., 2001). When high voltage power supply connected to the spinneret, polar charges (+ve or -ve) will charge the surface of polymeric solution depending on the level of applied voltages and the

solution probertites include conductivity, viscosity, and surface tension (Doshi and Reneker, 1995). By increasing the strength of applied voltage, similar charges will generate more electrostatic force Coulombic repulsions (Sill and von Recum, 2008; Zamani et al., 2013). The surface tension of the liquid is an opposing force to the force of electrostatic repulsion (Sill and von Recum, 2008). Therefore, with more power supply, the droplet shape will deform at the tip of spinneret from the hemispherical shape into a cone shape known as Taylor cone (Taylor, 1969). With continuous power supply on the charged solution, at critical voltage the force of electrostatic repulsion will overcome the surface tension and a liquid jet will be ejected from the tip of the cone to stretch by the potential difference between the charged polymeric solution and the collector ground connected (Renker and yarn, 2008; Zamani et al., 2013). During liquid jet stretching, it will reach to the point of whipping instability that will increase the flight time allowing to reduce diameter and solvent evaporation till discharge once collected as dry fibres (Li and Xia, 2004; Adomavičiūtė and Milašius, 2007).

1.3.2.3 Parameters affecting electrospinning

In order to achieve successful electrospinning of a selected polymeric solution, understanding the different parameter that controls the process is essential for formulation optimisation. The process of electrospinning to formulate fine fibres affected by a number of parameters (Huang et al, 2003). Explained by Doshi and Reneker (1995) into three categories; first is solution related parameters including the molecular weight, concentration, viscosity, solvent conductivity and surface tension of the electrospinning solution; second is processing parameters including the applied voltage, flow rate of polymeric solution, distance between spinneret and collector, and

type of collector; finally is ambient parameters including the surrounding temperature and humidity. (Doshi and Reneker, 1995). Next part will discuss the influence of each parameter on the process of electrospinning.

1.3.2.3.1 Solution parameters:

A- Concentration of the polymer solution: It has been confirmed that a minimum concentration of the polymer must be reached to the level of chain entanglement enabling continuous formation of fibres during polymer electrospinning (Shenoy et al., 2005). If the concentration is very low, this will produce beads as a process of electrospraying, as a result of low viscosity and high surface tension of the polymer solution (Deitzel et al., 2001). By increasing the concentration higher, beads mixed with the fibres will occur (Li and Wang, 2013). The optimum concentration for electrospinning is defined when uniform fibres with wide diameters formed (Deitzel et al., 2001).

B- Molecular weight: The overlapping molecular chains interlock physically by chain entanglement, that will finally result in building polymer chains (Shenoy et al., 2005). The increase of polymer molecular weight will increase the density of chain entanglements (Shenoy et al., 2005), which will lead into the continuous formation of fibres in electrospinning.

C- Viscosity: Both concentration and molecular weight of the polymer directly proportional to the density of polymer chain entanglements that will appear as the solution viscosity (Gupta et al., 2005). At very low viscosity, the liquid jet will break into

droplets due to high solution surface tension as a process of electrospraying (Deitzel et al., 2001). At high viscosity, more voltage is needed to overcome the solution surface tension, so at low surface tension will result in a continues fibres without beads formation (Demir et al., 2002). Solution viscosity influence the size of the fibres, as more solution viscosity associated with larger diameters, however, a very high viscosity will lead to solution drying at the tip of the spinneret (Doshi and Reneker, 1995).

D- Surface tension. The formation of fibres jet requires the electrostatic repulsion force between the charged polymer molecules to overcome the surface tension of a polymer solution at the spinneret tip (Hohman et al., 2001). This critical voltage is closely related to the surface tension of polymer solutions, therefore the higher surface tension value of the polymer solutions require higher applied voltage to initiate liquid jet formation (Lee et al., 2003). Surface tension drives the formation of beaded fibres during electrospinning by capillary breakup of the spinning jet to reduce the surface area from continuous fibres into spheres (Fong et al., 1999). The surface tension coefficient depends on the polymer and solvent, so decreasing the surface tension will support the formation of non-beaded fibres and favours the formation of fibres with large diameter (Fong et al., 1999).

E- Electrical conductivity: In the process of electrospinning, the net charge density carried by the liquid jet controlled more by the strength of applied voltage, then by solution conductivity (Fong et al., 1999). The higher conductivity of a solution the easier it can start electrospinning, while a solution with very low electrical conductivity, the applied voltage will be insufficient to create an elongation force of the liquid jet

(Bhardwaj and Kundu, 2010). High conductivity solution is the one has enough capacity for carrying density of charges on the surface (Sill and von Recum, 2008). The high electrical conductivity of a solution will increase the surface net charge density leading to the formation of electrospun nanofibers with smaller diameters size and less beaded (Fong et al., 1999). The conductivity of a solution affected by the type of polymer, solvent, and the presence of ionizable salts (Bhardwaj and Kundu, 2010). By adding ionic salt such as NaCl to the solution, the salt molecules separate to positive (+Ve) and negative (-Ve) ions, in which by free movement it will increase the electrical conductivity of the solution (Reneker and Yarin, 2008). Therefore, more uniform fibres with fewer beads can be obtained with the aid of ionic salt (Li and Wang, 2013).

1.3.2.3.2 Processing parameters:

A- Applied voltage: Only when the applied voltage reaches the threshold of initiation, it can overcome the surface tension of polymer droplet (Chakraborty et al., 2009). This will lead to change in the shape of polymer droplet to form Taylor cone at the surface of the pendant drop (Taylor, 1969; Deitzel et al., 2001). By increasing the voltage above the threshold of initiation, a liquid jet will elongate and eject from the capillary to start whipping instability (Sill and von Recum, 2008). It is required to control the strength of the electric field to allow slow travel speed across the distance to the collector, thereby enabling whipping instability and fibres elongation to increase diameter size (Kong and Ziegler, 2013). Further increase in the applied voltage will accelerate the fibres and reduce the flight time to a level that result of unsuccessful development of whipping instability (Sill and von Recum, 2008).

B- Flow rate. The flow rate of the polymer solution affects the shape of fibres. By increasing the flow rate, the pore size and fibres diameter will enlarge (Sill and von Recum, 2008). A high flow rate will also increase the amount of bead due to an inability of the fibres to completely dry from the solvent before reaching to the collector, accordingly flattened fibres might be produced (Sill and von Recum, 2008).

C- Distance from the spinneret to the collector: Increasing the distance between spinneret and collector (as shown in Fig. 1) will decrease fibres diameter size (Doshi and Reneker, 1995). Increasing the distance for more than 20 cm will make deposition of fibres jet on the ground surface significantly hard and result in fibres loss (Chakraborty et al., 2009). On the other hand very short electrospinning distance will not allow enough flight time or solvent evaporation, making the fibres susceptible to fusion due to the residual solution in the collected fibres (Megelski et al., 2002).

The type of a collector should be conductive like an aluminium plate and usually grounded so the charged polymer jet will accelerate toward it (Bhardwaj and Kundu, 2010). After whipping instability, the fibres jet deposited on the collector randomly (Renker et al., 2000), different types of the collector can be used where fibres uniformity is determined by the type of collector, and the speed of movement such as in the rotating collector (Kumbar et al, 2008).

1.3.2.3.3 Ambient parameters:

A- Temperature. At high temperature the molecular mobility will increase, that will increase the conductivity of the solution, and inversely decrease viscosity and surface tension (Chakraborty et al., 2009), this inverse relationship between temperature and viscosity result in a final outcome of decreasing the fibres diameter size (Mit-uppatham et al., 2004).

B- Humidity. Low humidity may lead to dry the solvent completely and cause fast solvent evaporation (Li and Wang, 2013). Wile high humidity will decrease evaporation of the solvent with the polymer, result in thick fibres diameter due to charges in fibres become neutralized so stretching force in the jet become small (Li and Wang, 2013). If humidity reaches 30%, pores formation on the electrospun fibres may appear, however, further increase in humidity will lead to pores coalescing (Kim et al, 2005; Pham at al., 2006).

1.3.2.4 Eelectrospinning applications in drug delivery

Electrospinning applications in drug delivery come from the ability to encapsulate multi-active pharmaceutical ingredients combined in the fibres (Wang et al., 2010), thus the technique was applied for designing FDCs products with different drug release profile. For instance, electrospinning has been explored as a method for fabricating fast dissolving thin films (Williams et al., 2012). The advantages of this fast-dissolving drug delivery system were to provide an immediate formulation disintegration and drug dissolving in the mouth to provide a rapid onset of action in a

few minutes (Seager, 1998). A study by Renner et al. (2007) showed that combination of paracetamol with caffeine have more significant analgesic effect than paracetamol alone in the management of pain related to cortical potentials during 3 hours' observation time. Illangakoon et al. (2014) performed a successful combination of paracetamol and caffeine in PVP electrospun nanofibers as an oral film for fast dissolving with simultaneous drug release.

Hence electrospinning is a promising smart fabrication method to design novel FDC formulations expected to contribute in enhancing the adherence of patients receiving multiple drug therapies, in particular for patients with chronic conditions, like hypertension, rheumatoid arthritis, and Parkinson's disease. Reduction of older patient non-adherence is expected to be 26% with the use of fixed-dose combination regimens. (Bangalore et al., 2007).

1.4 Oral drug delivery system

A drug delivery system defined as a device or formulation that safely facilitates the entrance of therapeutic materials into the body, and regulates the amount, timing, and site of drug release into the body for an effective outcome (Bruschi, 2015). The oral route is the most common and acceptable way for medication administration that improves patient compliance with the treatment regimen (Sugawara et al., 2005). Oral drug administration intended usually for the systemic therapeutic effects (Aulton, 2013). The most common oral dosage forms are solid and liquid dosage forms (Strickley et al., 2008). The liquid dosage forms could be easier to swallow for paediatric and geriatric patients; however, the problem of taste acceptability lead to

decreased patient compliance and non-adherence with the treatment (Jin et al., 2008). Compared to liquid dosage forms, the solid dosage form has some advantages including wider options for masking of the aversive taste of some APIs (Jin et al., 2008), and the predetermined dose ensuring dosing accuracy during administration (Marwaha et al., 2010). Solid dosage forms have a more attractive low cost of production for pharmaceutical industries and better stability with a long shelf life up to 5 years (Marwaha et al., 2010).

Despite the advantages of the solid dosage form, , it is essential to understand the physical and chemical properties of the APIs that will affect the successful design of a oral formulation with appropriate safety, efficacy and stability profile (Aulton, 2013).

1.4.1 Particle size and specific surface area

The reduction of drug molecule particle size will lead to a larger specific surface area per unit weight of drug powder (Aulton, 2013). The particle size and the range of particle size distribution influence performance of a pharmaceutical dosage form including dissolution rate, the content uniformity, and formulation stability (Merisko-Liversidge et al., 2003). A poor aqueous soluble drug exhibit a rate-limiting step dependent on the dissolution rate of the APIs from the dosage form, therefore increasing the specific surface area into fine particles at micro to nanometres will enhance the rate of dissolution and improve drug absorption (Aulton, 2013). Many of the new chemical entities show a remarkably poor aqueous solubility that requires enhancement of dissolution with different techniques such as complexation with hydrophilic polymers. However, particle size reduction might alter the crystalline

physical form of drug powder and change the particle surface energy that might reduce the chemical stability in a dosage form (Bhugra and Pikal, 2008).

1.4.2 Physical forms

The physical forms of APIs and pharmaceutical excipients affect on the performance of the final solid dosage form. Many of the APIs can exist in different physical forms, or could change physical form by temperature, humidity, or during processing of the formulation (Aulton, 2013). Also, it is known that only one form of the pure API is stable at the different level of temperature and humidity, and every other metastable form will convert to stable form in different rate (Zhang et al., 2004). Understanding the effect of physical form is important to choose the most stable form for the processing, and hence ensure the optimise the stability and therapeutic action of the API.

1.4.2.1 Crystal form

It is a condensation of the material molecules, that group together in a small structural arrangement to build the smallest block known as the unit cell, which will repeat in ordered three dimensional space to reflect the crystal lattice (Bravais lattice) that show the gross exterior of crystal habit (Gaisford and Saunders, 2012). In the crystalline material, the drug molecules are stuck together via non-covalent interactions of intermolecular forces such as van der Waals forces or hydrogen bonding to make the unit cell of the crystal lattice with energy and strength depending on the intermolecular forces (Florence and Attwood, 1988). A crystalline polymorph is an arrangement of similar drug molecules in different crystal packing or different conformations resulting

in the formation of different crystal structures with different lattice energy and consequently will significantly change the physical properties, such as density, hardness, melting point, enthalpy of fusion, solubility, and dissolution rate (Vippagunta et al., 2001). Pseudopolymorphs are a crystalline solid containing the API molecules with another secondary molecule within the unit cell in a stoichiometric amount of solvent molecules to make it a solvate or water molecules to make it a hydrate (Vippagunta et al., 2001).

1.4.2.2 Amorphous form

It is a high energy solid material which lacks the arrangement of repeating unit cell and loses the long-range structural order of the crystal (Gaisford and Saunders, 2012). The absence of intermolecular bonding will lead to a great excess enthalpy of the amorphous form over the stable crystalline form, and consequently higher energy to easily dissolve at a faster rate than a crystal form (Kaushal et al., 2004). The amorphous materials are thermodynamically unstable, in which the molecules in the amorphous matrix are susceptible to relax into the crystal structure arrangement with time due to the possible molecular movement in different modes as vibration, rotation, and translation (Gaisford and Saunders, 2012). This thermodynamic instability creates a problem of the amorphous material stability for a long time. Solid dispersion of pharmaceutical products implies one or many drug substances are homogeneously dispersed within a matrix of the carrier (Chiou, W.L. and Riegelman, S., 1971). Therefore, to keep the physical form stable for a long time, preparation methods can be used to blend the APIs with a polymer as amorphous solid dispersion (ASD), in

which the translational movement and orientation of the amorphous drug molecules are stabilised with the polymer through steric hindrance. (Williams et al., 2018).

1.4.3 Physical Stability

During the formation of amorphous material, a sufficiently fast cooling rate will be applied on the material at a molten state were molecules are freely moving towards an equilibrium state of supercooled liquid without structural alignment that gives it high volume and excess enthalpy. Therefore, as the temperature decrease, a molecular alignment will continue towards the perfect crystal until it reaches to glass transition (Tg) temperature. At which formation of glass occur preventing the volume and energy of supercooled liquid to go less than the formed perfect crystal. Below the Tg temperature, the rate of molecular mobility is reduced, and structural rearrangement will not respond to the change in temperature forming a glassy (or brittle) material (Hancock and Zografi, 1997).

The glassy material is a state of nonequilibrium and thermodynamic instability, that tend to change physical properties by partial or complete relaxation during storage (Santivarangkna et al., 2011). The approach of the material to change from glass state towards an equilibrium glassy state molecular mobility to align and loss it is excess enthalpy in the system represented as average relaxation time (Hancock et al., 1995). The rate of molecular alignment will increase with factors include increasing temperature and the addition of plasticisers (Levine and Slade, 1988). High relative humidity will increase the rate of water molecules penetration between the molecules matric of amorphous material, thus water act as plasticisers effect. Plasticisers are

small molecules that lower the Tg temperature of a material, so when the accumulating molecule of a plasticiser reach to the level sufficient to reduce the Tg temperature below the storage temperature, the amorphous material will easily recrystallise (Stajanca et al., 2016).

This changes in the formulation will lead to change of the physicochemical properties of the formulation and eventually change in its characters. From a pharmaceutical perspective, determining the formulation stability is critically important influencing the final drug product. Since relaxation affected by the molecular mobility, storage temperature, and the level of residual solvent in the system (Gaisford, 2009), slowing down relaxation is possible by limiting the effect of these factors such as the ensuring storage in the appropriate packaging or appropriate storage temperature.

1.5 Pharmaceutical polymers in drug delivery system (DDS)

Pharmaceutical materials have been conjugated to polymers as transporting carrier to modify or circulation half-life characteristics as well as to allow for passive and active targeting (Liechty et al., 2010). Polymers are large molecular weight materials that made up of repeating monomer units, that influence the polymer properties like chemical reactivity, size, shape, and asymmetry through their specific chemistry and arrangement (Florence and Attwood, 1988). Different shape of the polymer molecule can exist such as linear or branched or cross-linked among the separate polymers chain or branch. Cross-linking influence the formation of three-dimensional structured polymer; however excessive crosslinking usually will result in an insoluble polymer (Florence and Attwood, 1988).

Over 50 years, in the pharmaceutical industry, different pharmaceutical manufacturing techniques have been used to incorporate bioactive agents with polymers. e.g. compression, spray and dip coating, and encapsulation (Liechty et al., 2010). Polymers used for drug-delivery can be classified as water soluble and water insoluble polymers (Florence and Attwood, 1988). From the perspective of designing a DDS, the selection of polymer as a carrier can be categorized as: diffusion-controlled as a monolithic system, solvent activated by swelling or osmotically controlled, biodegradable chemically controlled polymer, and externally triggered systems by the change in the pH or temperature. (Langer and Peppas,1981; Verma et al., 2000; Liechty et al., 2010).

1.5.1 Polyvinylpyrrolidone (PVP)

Polyvinylpyrrolidone (PVP) is a linear homopolymer, consist of 1-vinyl-2-pyrrolidone monomers (Figure 1.2), (Florence and Attwood, 1988). For its low toxicity, biocompatibility, high water solubility PVP frequently used in pharmaceutical formulations as an excipient, binders, suspending or dispersing agent, emulsion stabilizer, and granulating agent (Nair, 1998; Osman et al., 2018). When PVP mixed with the APIs as a drug-polymer solid dispersion, PVP have shown to improves the bioavailability of APIs without affecting their thermal stability (Osman et al., 2018). Also, PVP as carriers inhibited the crystallization of the drug by increasing the Tg temperature for APIs as an ASD to be extensively higher by >50 °C above the storage temperature around 25 °C (Khougaz and Clas, 2000; Kaushal et al., 2004).

PVP

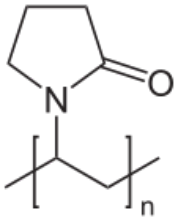

Figure 1.2. The chemical structure of PVP.

1.5.2 Poly(meth)acrylates (EUDRAGIT®)

The polymethacrylates based copolymers, principally marketed by (Evonik Industries, Germany) as the brand name Eudragit representing a group of copolymers. Eudragit obtained by polymerization of acrylic acid (prop-2-enoic acid; CH2=CHCOOH) and methacrylic acids or their esters like butyl ester or dimethylaminoethyl ester. It is a diverse range of anionic, cationic as well as neutral copolymers based on methacrylic acid and methacrylic or acrylic esters or their derivatives in varying proportions. Which gave it a varying degree of pH-dependent/independent solubility profiles. Eudragit polymers used as a functional excipient in various pharmaceutical dosage forms, e.g. coatings and matrix formers. The physical characterization of Eudragit grades copolymers demonstrates the amorphous nature of the polymers. Being a synthetic polymer, Eudragits display good reproducibility and other advantages associated with synthetic polymers as non-biodegradable, non-absorbable, and non- toxic functional excipients. (Thakral et al., 2013). The specific details and figures of each Eudragit polymer, are detailed specifically as used in each chapter.

1.6 Aims and objectives

The work described in this thesis aimed to develop FDCs targeting specific conditions for the geriatric population by utilising advanced pharmaceutical manufacturing techniques to prepare multiple drug-polymer composite systems. Specific objectives were as follows:

1- To investigate different pharmaceutical manufacturing techniques for the preparation of multiple drug-polymer composite systems.

2- To develop and fully characterise two types of FDC ODFs loaded with amlodipine besylate, valsartan, or both drugs, using the film casting approach or electrospinning.

3- To accelerate the release of amlodipine besylate and valsartan from these FDC formulations in conditions mimicking the oral cavity.

4- To create advanced pulsatile release FDCs from three different polymers and drugs, using two types of modified single-needle electrospinning process: sequential electrospinning to produce multilayer fibre mats, and multi-jet electrospinning to produce tangled fibres.

5- To assess the utility of this formulation as a platform for multiple phase release of three model drugs in separate doses (immediate, delayed, and finally extended-release).

6- To fabricate core/shell fibres as oral FDCs for biphasic drug release of multiple drugs to provide burst release followed by extended-release, targeting the treatment of Parkinson's Disease in the geriatric population.

1.7 References

Adomavičiūtė, E. and Milašius, R., 2007. The influence of applied voltage on poly (vinyl alcohol)(PVA) nanofibre diameter. Fibres & Textiles in Eastern Europe, 15(5-6), p.63.

Alldred, D.P., Zermansky, A.G., Petty, D.R., Raynor, D.K., Freemantle, N., Eastaugh, J. and Bowie, P., 2007. Clinical medication review by a pharmacist of elderly people living in care homes: pharmacist interventions. International Journal of Pharmacy Practice, 15(2), pp.93-99.

Aulton, M.E., 2013. Taylor K. Aulton's pharmaceutics: the design and manufacture of medicines. 4th ed. New York: Churchill Livingstone Elsevier.

Bhardwaj, N. and Kundu, S.C., 2010. Electrospinning: a fascinating fiber fabrication technique. Biotechnology Advances, 28(3), pp.325-347.

Bangalore, S., Kamalakkannan, G., Parkar, S. and Messerli, F.H., 2007. Fixed-dose combinations improve medication compliance: a meta-analysis. The American Journal of Medicine, 120(8), pp.713-719.

Barber, N.D., Alldred, D.P., Raynor, D.K., Dickinson, R., Garfield, S., Jesson, B., Lim, R., Savage, I., Standage, C., Buckle, P. and Carpenter, J., 2009. Care homes' use of medicines study: prevalence, causes and potential harm of medication errors in care homes for older people. BMJ Quality & Safety, 18(5), pp.341-346.

Bongaarts, J., 2009. Human population growth and the demographic transition. Philosophical Transactions of the Royal Society of London B: Biological Sciences, 364(1532), pp.2985-2990.

Bruschi, M.L., 2015. Strategies to modify the drug release from pharmaceutical systems. Woodhead Publishing.

Buanz, A.B., Belaunde, C.C., Soutari, N., Tuleu, C., Gul, M.O. and Gaisford, S., 2015. Ink-jet printing versus solvent casting to prepare oral films: effect on mechanical

properties and physical stability. International Journal of Pharmaceutics, 494(2), pp.611-618.

Bhugra, C. and Pikal, M.J., 2008. Role of thermodynamic, molecular, and kinetic factors in crystallization from the amorphous state. Journal of pharmaceutical sciences, 97(4), pp.1329-1349.

Carnaby-Mann, G. and Crary, M., 2005. Pill swallowing by adults with dysphagia. Archives of Otolaryngology–Head & Neck Surgery, 131(11), pp.970-975.

Chakraborty, S., Liao, I.C., Adler, A. and Leong, K.W., 2009. Electrohydrodynamics: a facile technique to fabricate drug delivery systems. Advanced Drug Delivery reviews, 61(12), pp.1043-1054.

Chiou, W.L. and Riegelman, S., 1971. Pharmaceutical applications of solid dispersion systems. Journal of pharmaceutical sciences, 60(9), pp.1281-1302.

Deng, L., Kang, X., Liu, Y., Feng, F. and Zhang, H., 2018. Characterization of gelatin/zein films fabricated by electrospinning vs solvent casting. Food Hydrocolloids, 74, pp.324-332.

Demir, M.M., Yilgor, I., Yilgor, E.E.A. and Erman, B., 2002. Electrospinning of polyurethane fibers. Polymer, 43(11), pp.3303-3309.

Deitzel, J.M., Kleinmeyer, J., Harris, D.E.A. and Tan, N.B., 2001. The effect of processing variables on the morphology of electrospun nanofibers and textiles. Polymer, 42(1), pp.261-272.

Desai, D., Wang, J., Wen, H., Li, X. and Timmins, P., 2012. Formulation design, challenges, and development considerations for fixed dose combination (FDC) of oral solid dosage forms. Pharmaceutical Development and Technology, 18(6), pp.1265-1276.

Dierickx, L., Saerens, L., Almeida, A., De Beer, T., Remon, J.P. and Vervaet, C., 2012. Co-extrusion as manufacturing technique for fixed-dose combination mini-matrices. European Journal of Pharmaceutics and Biopharmaceutics, 81(3), pp.683-689.

Dixit, R.P. and Puthli, S.P., 2009. Oral strip technology: overview and future potential. Journal of Controlled Release, 139(2), pp.94-107.

Doshi, J. and Reneker, D.H., 1995. Electrospinning process and applications of electrospun fibers. Journal of Electrostatics, 35(2-3), pp.151-160.

Edirisinghe, S., Raimi-Abraham, B.T., Gilmartin, J.M. and Orlu-Gul, M., 2015. Multi-compartment compliance aids (MCAs): application to the geriatric community. European Geriatric Medicine, 6(1), pp.65-68.

European Medicines Agency, 2017. Reflection paper on the pharmaceutical development of medicines for use in the older population.

Figueirêdo, C.B.M., Nadvorny, D., de Medeiros Vieira, A.C.Q., de Medeiros Schver, G.C.R., Sobrinho, J.L.S., Neto, P.J.R., Lee, P.I. and Soares, M.F.D.L.R., 2018. Enhanced delivery of fixed-dose combination of synergistic antichagasic agents posaconazole-benznidazole based on amorphous solid dispersions. European Journal of Pharmaceutical Sciences, 119, pp.208-218.

Fina, F., Goyanes, A., Madla, C.M., Awad, A., Trenfield, S.J., Kuek, J.M., Patel, P., Gaisford, S. and Basit, A.W., 2018. 3D printing of drug-loaded gyroid lattices using selective laser sintering. International Journal of Pharmaceutics, 547(1-2), pp.44-52.

Florence, A. T. & Attwood, D. 1988. Physicochemical principles of pharmacy, N ew Y ork , NY, Chapman and Hall.

Fong, H., Chun, I. and Reneker, D.H., 1999. Beaded nanofibers formed during electrospinning. Polymer, 40(16), pp.4585-4592.

Food and Drug Administration (FDA), 1975. 21-CFR-300.50: Fixed-combination prescription drugs for humans.

Food and Drug Administration, 2004, Fixed Dose Combination and Co-Packaged Drug Products for Treatment of HIV, Online available at:<http://www.fda.gov/RegulatoryInformation/Guidances/ucm125278.htm#30]]> [Accessed 29 May 2016].

Food and Drug Administration, 2015, Caduet (amlodipine besylate/ atorvastatin calcium) tablets. MD: U.S.

Fulton, M.M. and Riley Allen, E., 2005. Polypharmacy in the elderly: a literature review. Journal of the American Academy of Nurse Practitioners, 17(4), pp.123-132.

Gaisford, S. and Saunders, M., 2012. Essentials of pharmaceutical preformulation. John Wiley & Sons.

Gorard, D.A., 2006. Escalating polypharmacy. QJM, 99(11), pp.797-800.

Gupta, P., Elkins, C., Long, T.E. and Wilkes, G.L., 2005. Electrospinning of linear homopolymers of poly (methyl methacrylate): exploring relationships between fiber formation, viscosity, molecular weight and concentration in a good solvent. Polymer, 46(13), pp.4799-4810.

Gursch, J., Hohl, R., Armenante, M.E., Dujmovic, D., van der Wel, P., Brozio, J., Krumme, M., Rasenack, N. and Khinast, J., 2015. Continuous Drying of Small Particles for Pharmaceutical Applications, An Evaluation of Selected Lab-Scale Systems. Organic Process Research & Development, 19(12), pp.2055-2066.

Hancock, B.C., Shamblin, S.L. and Zografi, G., 1995. Molecular mobility of amorphous pharmaceutical solids below their glass transition temperatures. Pharmaceutical research, 12(6), pp.799-806.

Hancock, B.C. and Zografi, G., 1997. Characteristics and significance of the amorphous state in pharmaceutical systems. Journal of pharmaceutical sciences, 86(1), pp.1-12.

Hao, J., Rodriguez-Monguio, R. and Seoane-Vazquez, E., 2015. Fixed-dose combination drug approvals, patents and market exclusivities compared to single active ingredient pharmaceuticals. PloS One, 10(10), p.e0140708.

Haynes, R.B., McKibbon, K.A. and Kanani, R., 1996. Systematic review of randomised trials of interventions to assist patients to follow prescriptions for medications. The Lancet, 348(9024), pp.383-386.

Hoffmann, E.M., Breitenbach, A. and Breitkreutz, J., 2011. Advances in orodispersible films for drug delivery. Expert Opinion on Drug Delivery, 8(3), pp.299-316.

Hohman, M.M., Shin, M., Rutledge, G. and Brenner, M.P., 2001. Electrospinning and electrically forced jets. II. Applications. Physics of Fluids (1994-present), 13(8), pp.2221-2236.

Huang, Z.M., Zhang, Y.Z., Kotaki, M. and Ramakrishna, S., 2003. A review on polymer nanofibers by electrospinning and their applications in nanocomposites. Composites Science and Technology, 63(15), pp.2223-2253.

Hughes, C.M., 2004. Medication non-adherence in the elderly. Drugs & Aging, 21(12), pp.793-811.

Illangakoon, U.E., Gill, H., Shearman, G.C., Parhizkar, M., Mahalingam, S., Chatterton, N.P. and Williams, G.R., 2014. Fast dissolving paracetamol/caffeine nanofibers prepared by electrospinning. International Journal of Pharmaceutics, 477(1), pp.369-379.

Ingersoll, K.S. and Cohen, J., 2008. The impact of medication regimen factors on adherence to chronic treatment: a review of literature. Journal of Behavioral Medicine, 31(3), pp.213-224.

Jimmy, B. and Jose, J., 2011. Patient medication adherence: measures in daily practice. Oman Med J, 26(3), pp.155-159.

Jin, J., Sklar, G.E., Oh, V.M.S. and Li, S.C., 2008. Factors affecting therapeutic compliance: A review from the patient's perspective. Therapeutics and Clinical Risk Management, 4(1), p.269.

Joint Formulary Committee, 2016. British National Formulary. [online], London: BMJ Group and Pharmaceutical Press. Online available at: <http://dx.doi.org/10.18578/BNF.385405193> [Accessed on 28 May 2016].

Kaushal, A.M., Gupta, P. and Bansal, A.K., 2004. Amorphous drug delivery systems: molecular aspects, design, and performance. Critical Reviews™ in Therapeutic Drug Carrier Systems, 21(3).

Kelleher, J.F., Gilvary, G.C., Madi, A.M., Jones, D.S., Li, S., Tian, Y., Almajaan, A., Senta-Loys, Z., Andrews, G.P. and Healy, A.M., 2018. A comparative study between hot-melt extrusion and spray-drying for the manufacture of anti-hypertension compatible monolithic fixed-dose combination products. International Journal of Pharmaceutics, 545(1-2), pp.183-196.

Khaled, S.A., Burley, J.C., Alexander, M.R., Yang, J. and Roberts, C.J., 2015. 3D printing of five-in-one dose combination polypill with defined immediate and sustained release profiles. Journal of Controlled Release, 217, pp.308-314.

Kaushal, A.M., Gupta, P. and Bansal, A.K., 2004. Amorphous drug delivery systems: molecular aspects, design, and performance. CRITICAL REVIEWS IN THERAPEUTIC DRUG CARRIER SYSTEMS., 21, pp.133-194.

Khil, M.S., Cha, D.I., Kim, H.Y., Kim, I.S. and Bhattarai, N., 2003. Electrospun nanofibrous polyurethane membrane as wound dressing. Journal of Biomedical Materials Research Part B: Applied Biomaterials, 67(2), pp.675-679.

Khougaz, K. and Clas, S.D., 2000. Crystallization inhibition in solid dispersions of MK-0591 and poly (vinylpyrrolidone) polymers. Journal of Pharmaceutical Sciences, 89(10), pp.1325-1334.

Kim, G.T., Lee, J.S., Shin, J.H., Ahn, Y.C., Hwang, Y.J., Shin, H.S., Lee, J.K. and Sung, C.M., 2005. Investigation of pore formation for polystyrene electrospun fiber: effect of relative humidity. Korean Journal of Chemical Engineering, 22(5), pp.783-788.

Kong, L. and Ziegler, G.R., 2013. Quantitative relationship between electrospinning parameters and starch fiber diameter. Carbohydrate Polymers, 92(2), pp.1416-1422.

Kozarewicz, P., 2014. Regulatory perspectives on acceptability testing of dosage forms in children. International Journal of Pharmaceutics, 469(2), pp.245-248.

Kumbar, S.G., Nukavarapu, S.P., James, R., Nair, L.S. and Laurencin, C.T., 2008. Electrospun poly (lactic acid-co-glycolic acid) scaffolds for skin tissue engineering. Biomaterials, 29(30), pp.4100-4107.

Larsen, P.D. and Martin, J.L.H., 1999. Polypharmacy and elderly patients. AORN Journal, 69(3), pp.619-620.

Langer, R.S. and Peppas, N.A., 1981. Present and future applications of biomaterials in controlled drug delivery systems. Biomaterials, 2(4), pp.201-214.

Levine, H.A.R.R.Y. and Slade, L.O.U.I.S.E., 1988. Water as a plasticizer: physico-chemical aspects of low-moisture polymeric systems. Water science reviews, 3, pp.79-185.

Lee, K.H., Kim, H.Y., Bang, H.J., Jung, Y.H. and Lee, S.G., 2003. The change of bead morphology formed on electrospun polystyrene fibers. Polymer, 44(14), pp.4029-4034.

Lehane, E. and McCarthy, G., 2007. Intentional and unintentional medication non-adherence: a comprehensive framework for clinical research and practice? A discussion paper. International Journal of Nursing Studies, 44(8), pp.1468-1477.

Li, D. and Xia, Y., 2004. Electrospinning of nanofibers: reinventing the wheel?. Advanced Materials, 16(14), pp.1151-1170.

Li, Z. and Wang, C., 2013. Effects of working parameters on electrospinning. In One Dimensional Nanostructures (pp. 15-28). Springer Berlin Heidelberg.

Liechty, W.B., Kryscio, D.R., Slaughter, B.V. and Peppas, N.A., 2010. Polymers for drug delivery systems. Annual review of chemical and biomolecular engineering, 1, pp.149-173.

Liu, F., Ranmal, S., Batchelor, H.K., Orlu-Gul, M., Ernest, T.B., Thomas, I.W., Flanagan, T. and Tuleu, C., 2014. Patient-centered pharmaceutical design to improve acceptability of medicines: similarities and differences in paediatric and geriatric populations. Drugs, 74(16), pp.1871-1889.

Ma, G., Liu, Y., Peng, C., Fang, D., He, B. and Nie, J., 2011. Paclitaxel loaded electrospun porous nanofibers as mat potential application for chemotherapy against prostate cancer. Carbohydrate Polymers, 86(2), pp.505-512.

Marwaha, M., Sandhu, D. and Marwaha, R.K., 2010. Coprocessing of excipients: a review on excipient development for improved tabletting performance. International Journal of Applied Pharmaceutics, 2(3), pp.41-47.

McKenzie, P., Kiang, S., Tom, J., Rubin, A.E. and Futran, M., 2006. Can pharmaceutical process development become high tech?. AIChE Journal, 52(12), pp.3990-3994.

Megelski, S., Stephens, J.S., Chase, D.B. and Rabolt, J.F., 2002. Micro-and nanostructured surface morphology on electrospun polymer fibers. Macromolecules, 35(22), pp.8456-8466.

Merisko-Liversidge, E., Liversidge, G.G. and Cooper, E.R., 2003. Nanosizing: a formulation approach for poorly-water-soluble compounds. European journal of pharmaceutical sciences, 18(2), pp.113-120.

Mit-uppatham, C., Nithitanakul, M. and Supaphol, P., 2004. Ultrafine electrospun polyamide-6 fibers: effect of solution conditions on morphology and average fiber diameter. Macromolecular Chemistry and Physics, 205(17), pp.2327-2338.

Mitra, A. and Wu, Y., 2012. Challenges and opportunities in achieving bioequivalence for fixed-dose combination products. The AAPS journal, 14(3), pp.646-655.

Munger, M.A., 2010. Polypharmacy and combination therapy in the management of hypertension in elderly patients with co-morbid diabetes mellitus. Drugs & aging, 27(11), pp.871-883.

Nair, B., 1998. Final report on the safety assessment of polyvinylpyrrolidone (PVP). International Journal of Toxicology, 17(4_suppl), pp.95-130.

Orlu-Gul, M., Raimi-Abraham, B., Jamieson, E., Wei, L., Murray, M., Stawarz, K., Stegemann, S., Tuleu, C. and Smith, F.J., 2014. Public engagement workshop: how to improve medicines for older people?. International Journal of Pharmaceutics, 459(1-2), pp.65-69.

Osman, Y.B., Liavitskaya, T. and Vyazovkin, S., 2018. Polyvinylpyrrolidone affects thermal stability of drugs in solid dispersions. International Journal of Pharmaceutics, 551(1-2), pp.111-120.

Payne, R.A. and Avery, A.J., 2011. Polypharmacy: one of the greatest prescribing challenges in general practice. British Journal of General Practice, 2011: 83-84.

Pitkala, K.H., Strandberg, T.E. and Tilvis, R.S., 2001. Is it possible to reduce polypharmacy in the elderly?. Drugs & aging, 18(2), pp.143-149.

Prybys, K. and Gee, A., 2002. Polypharmacy in the elderly: clinical challenges in emergency practice. Part 1 Overview, Etiology, and Drug Interactions, Emergency Medicine Reports, 23(11), pp.145-151.

Ramakrishna S., Fujihara K., Teo W.E., Lim T.C., and Ma Z. 2005. An introduction to electrospinning and nanofibers, Singapore: World Scientific Pub Co Pte Ltd, pp. 155–191 [Chapter 4].

Renner, B., Clarke, G., Grattan, T., Beisel, A., Mueller, C., Werner, U., Kobal, G. and Brune, K., 2007. Caffeine accelerates absorption and enhances the analgesic effect of acetaminophen. The Journal of Clinical Pharmacology, 47(6), pp.715-726.

Reneker, D.H. and Yarin, A.L., 2008. Electrospinning jets and polymer nanofibers. Polymer, 49(10), pp.2387-2425.

Reneker, D.H., Yarin, A.L., Fong, H. and Koombhongse, S., 2000. Bending instability of electrically charged liquid jets of polymer solutions in electrospinning. Journal of Applied Physics, 87(9), pp.4531-4547.

Sabaté, E., 2003. Adherence to long-term therapies: evidence for action. World Health Organization. Geneva: WHO.

Santivarangkna, C., Aschenbrenner, M., Kulozik, U. and Foerst, P., 2011. Role of glassy state on stabilities of freeze-dried probiotics. Journal of food science, 76(8), pp.R152-R156.

Scarpa, M., Paudel, A., Kloprogge, F., Hsiao, W.K., Bresciani, M., Gaisford, S. and Orlu, M., 2018. Key acceptability attributes of orodispersible films. European Journal of Pharmaceutics and Biopharmaceutics, 125, pp.131-140.

Seager, H., 1998. Drug-delivery products and the Zydis fast-dissolving dosage form. Journal of Pharmacy and Pharmacology, 50(4), pp.375-382.

Shenoy, S.L., Bates, W.D., Frisch, H.L. and Wnek, G.E., 2005. Role of chain entanglements on fiber formation during electrospinning of polymer solutions: good solvent, non-specific polymer–polymer interaction limit. Polymer, 46(10), pp.3372-3384.

Sill, T.J. and von Recum, H.A., 2008. Electrospinning: applications in drug delivery and tissue engineering. Biomaterials, 29(13), pp.1989-2006.

Stajanca, P., Cetinkaya, O., Schukar, M., Mergo, P., Webb, D.J. and Krebber, K., 2016. Molecular alignment relaxation in polymer optical fibers for sensing applications. Optical Fiber Technology, 28, pp.11-17.

Strickley, R.G., Iwata, Q., Wu, S. and Dahl, T.C., 2008. Pediatric drugs—a review of commercially available oral formulations. Journal of Pharmaceutical Sciences, 97(5), pp.1731-1774.

Sugawara, M., Kadomura, S., He, X., Takekuma, Y., Kohri, N. and Miyazaki, K., 2005. The use of an in vitro dissolution and absorption system to evaluate oral absorption of two weak bases in pH-independent controlled-release formulations. European Journal of Pharmaceutical Sciences, 26(1), pp.1-8.

Taylor, G., 1969, December. Electrically driven jets. In Proceedings of the Royal Society of London A: Mathematical, Physical and Engineering Sciences (Vol. 313, No. 1515, pp. 453-475). The Royal Society.

Teo, W.E. and Ramakrishna, S., 2006. A review on electrospinning design and nanofibre assemblies. Nanotechnology, 17(14), p.R89.

Thabet, Y. and Breitkreutz, J., 2018. Orodispersible films: Product transfer from lab-scale to continuous manufacturing. International Journal of Pharmaceutics, 535(1-2), pp.285-292.

Thakral, S., Thakral, N.K. and Majumdar, D.K., 2013. Eudragit®: a technology evaluation. Expert opinion on drug delivery, 10(1), pp.131-149.

Tucker, N., Stanger, J.J., Staiger, M.P., Razzaq, H. and Hofman, K., 2012. The History of the Science and Technology of Electrospinning from 1600 to 1995. Journal of Engineered Fabrics & Fibers (JEFF), 7(3).

Verma, R.K., Mishra, B. and Garg, S., 2000. Osmotically controlled oral drug delivery. Drug development and industrial pharmacy, 26(7), pp.695-708.

Vippagunta, S.R., Brittain, H.G. and Grant, D.J., 2001. Crystalline solids. Advanced drug delivery reviews, 48(1), pp.3-26.

Visser, J.C., Woerdenbag, H.J., Hanff, L.M. and Frijlink, H.W., 2017. Personalized medicine in pediatrics: the clinical potential of orodispersible films. Aaps pharmscitech, 18(2), pp.267-272.

Wang, Y., Qiao, W. and Yin, T., 2010. A novel controlled release drug delivery system for multiple drugs based on electrospun nanofibers containing nanoparticles. Journal of Pharmaceutical Sciences, 99(12), pp.4805-4811.

Williams, G.R., Chatterton, N.P., Nazir, T., Yu, D.G., Zhu, L.M. and Branford-White, C.J., 2012. Electrospun nanofibers in drug delivery: recent developments and perspectives. Therapeutic Delivery, 3(4), pp.515-533.

Williams, G.R., Raimi-Abraham, B.T., and Luo, C.J., 2018. Nanofibres in drug delivery. UCL Press.

World Health Organization, 2005. Guidelines for registration of fixed-dose combination medicinal products. Annex 5 (No. 929). Technical Report Series.

Wu, J.T., Chiu, C.T., Wei, Y.F. and Lai, Y.F., 2015. Comparison of the safety and efficacy of a fixed-dose combination regimen and separate formulations for pulmonary tuberculosis treatment. Clinics, 70(6), pp.429-434.

Yarbrough, C. 2016. Formulating for patients. AAPS newsmagazine. [online]. Pp. 28-29.Availablefrom:http://www.aaps.org/AAPS_Newsmagazine/Science_and_Learning/eLearning/eLearning_May_16/> [Accessed 30 May 2016].

Zamani, M., Prabhakaran, M.P. and Ramakrishna, S., 2013. Advances in drug delivery via electrospun and electrosprayed nanomaterials. International journal of nanomedicine, 8, p.2997.

Zhang, G.G., Law, D., Schmitt, E.A. and Qiu, Y., 2004. Phase transformation considerations during process development and manufacture of solid oral dosage forms. Advanced drug delivery reviews, 56(3), pp.371-390.

Chapter 2. Materials and Methods

In this chapter, the general materials and methods used for this study, and instruments used for characterisation, are described. Precise details of sample preparation are given in subsequent chapters.

2.1 Materials

2.1.1 Materials used in Chapter 3 and Chapter 4

Polyvinylpyrrolidone (PVP; MW 360,000 Da), glycerol (80%W/V), and amlodipine besylate (AB) were purchased from Sigma-Aldrich, UK. Valsartan (VAL) was sourced from LKT Laboratories Inc., USA. Analytical grade ethanol, acetonitrile and methanol were procured from Sigma-Aldrich, UK. Deionised water was used for all studies requiring water, and all other chemicals used were of analytical grade.

2.1.2 Materials used in Chapter 5

Ibuprofen (IP) was purchased from Fagron, UK. Famotidine (FAM), prednisone (PRED), and Polyvinylpyrrolidone (PVP; MW 360,000 Da) were purchased from Sigma-Aldrich, UK. Eudragit® RSPO (E-RSPO; MW 15,000 Da), and Eudragit® L100 (E-L100; MW 135,000 Da) were a gift from Evonik, Germany. Analytical grade ethanol, acetonitrile, methanol, and N,N-dimethylacetamide (DMAc) were procured from Sigma-Aldrich, UK. Deionised water was used for all studies requiring water, and all other chemicals used were of analytical grade.

2.1.4 Materials used in Chapter 6

Levodopa (LD), carbidopa (CD), and PVP (MW 360,000 Da) were purchased from Sigma-Aldrich, UK. Eudragit® RLPO (E-RLPO; MW 150,000 Da) was a gift from Evonik Darmstadt, Germany. Analytical grade ethanol, acetonitrile, methanol, and N,N-dimethylacetamide (DMAc) were procured from Sigma-Aldrich, UK. Deionised water was used where needed, and all other chemicals used were of analytical grade.

2.2 Preparation of spinning solutions

The selected polymer was accurately weighed and dissolved in the selected solvent by mixed overnight with magnetic stirring to ensure complete dissolution was gained as a transparent clear solution. All the bottles were carefully taped and covered with parafilm to ensure no solvent evaporation. Information on the precise solution preparation will be detailed in the individual results chapters.

2.3 Electrospinning general details

For each electrospinning process, the polymer solutions were stirred overnight in the selected solvent to ensure complete drug dissolution. The polymer solutions were loaded into 5- or 10-mL plastic syringes (Terumo, MediSupplies, UK) with care taken to avoid any air bubbles. A stainless steel dispensing needles (20G, 0.61mm inner diameter, Nordson EFD, UK) were used as a spinneret for the single needle electrospinning process. Whereas concentric spinneret of stainless steel needles

(core: 18G, 0.83 mm inner diameter; shell: 13G, 1.83 mm inner diameter, Linari Engineering, Italy) was used as a spinneret for the coaxial needle electrospinning process. The feed rate of the solution was controlled with a syringe pump (KDS100, Cole Parmer, UK). A voltage was applied to the needle (spinneret) using a HCP 35-35000 power supply (FuG Elektronik GmbH, Germany). The fibres were collected on a grounded collector covered with aluminium foil and situated 12 cm from the spinneret tip. Electrospinning was carried out under ambient conditions (18–26 °C and relative humidity of 26–63%). After fabrication, the electrospun fibre mats were stored in a vacuum desiccator over silica gel beads to aid evaporation of the remaining organic solvents and moisture. Information on the precise samples prepared, flow rates, collector, and distance will be detailed in the individual results chapters.

2.4 Characterisation

2.4.1 Morphology

The surface morphology of all formulations was assessed by scanning electron microscopy. Imaging of the coaxial fibres internal structure was undertaken using transmission electron microscopy.

2.4.1.1 Scanning electron microscopy (SEM)

SEM images were obtained on a Quanta 200 FEG SEM, (FEI, USA). Prior to examination, samples were sputter-coated with gold under argon to make them electrically conductive. Images were taken at an excitation voltage of 5 kV. The

average diameter of the fibre formulations was determined from the SEM images by making manual measurements at 100 different points using the ImageJ software (National Institutes of Health, USA).

2.4.1.2 Transmission electron microscopy (TEM)

The samples of the electrospun fibres were collected on a lacy carbon coated copper grid (TAAB, UK). For each sample, the grid was held with a twicer and placed under the needle during electrospinning for only 5 seconds. The TEM images were taken on a Philips/FEI CM 120 Bio-Twin instrument (Netherlands).

2.4.1.3 Digital microscopy

The fibres from electrospinning process were collected onto on a glass slide for a few seconds and analysed using an inverted digital microscope (EVOS XL Cell Imaging System, Thermo Fisher Scientific, UK).

2.4.2 X-ray diffraction

X-ray diffraction (XRD) patterns were obtained on a MiniFlex 600 diffractometer (Rigaku, Japan) supplied with Cu Kα radiation (λ = 1.5418 Å) at a voltage of 40 kV and current of 15 mA. Samples were fixed on an aluminium holder and data recorded over the 2θ range between 3 to 43° at a scan speed of 5° min^{-1}.

2.4.3 Differential scanning calorimetry (DSC)

Differential scanning calorimetry (DSC) studies were conducted using a Q2000 calorimeter (TA Instruments, USA). Non-hermetically sealed samples in aluminium pans (Tzero premium pan/lid, TA instruments) were heated from 30 °C to an appropriate temperature (ideally above the melting point of the active ingredient of interest but below the degradation point of the polymer). Experiments were undertaken at a rate of 10 °C min^{-1} and under a nitrogen flow of 50 mL min^{-1}. Data were analysed using the TA instruments Universal Analysis software.

2.4.4 Fourier transform infrared spectroscopy (FTIR)

Samples from each formulation were cut small below 1 cm^2 and placed under the infrared source of the FTIR instrument. The analysis was carried out on attenuated total reflectance (ATR) FT-IR Spectrum 100 spectrometer (PerkinElmer, USA). Samples were studied over the range 4000 to 650 cm^{-1}, with the spectral resolution set at 1 cm^{-1}. Four scans per sample were recorded.

2.4.5 High performance liquid chromatography (HPLC)

Quantification of drug loading in each formulation was done by the following HPLC methods:

2.4.5.1 Amlodipine besylate and valsartan determination

An HPLC method was developed for simultaneous analysis of both AB and VAL simultaneously, based on that previously reported by Celebier et al. (2010). Samples (5 ± 0.5 mg of the electrospun fibres, or 50 ± 10 mg of the ODFs) were dissolved in 50 mL of methanol then diluted to a final volume of 100 mL with deionised water. The resultant solution was sonicated in a water bath for 30 min to ensure complete dissolution.

A calibration curve for AB and VAL was prepared from fresh solutions in the same solvent system on the day of the experiment. A quaternary HPLC pump (1200 Infinity Series, Agilent Technologies, USA) was used to mix the mobile phase, which comprised 30:35:35 v/v/v phosphate buffered saline (PBS; pH 3.6, 0.01 mol/L) : acetonitrile : methanol. Adjustment of the PBS pH was undertaken using orthophosphoric acid (85%, HPLC grade, Fisher Scientific, UK) and the solution filtered through a 0.45 μm membrane filters (Millex syringe filter, Merck Millipore, Germany) before use. The stationary phase used was a C18(2) column (00G-4252-E0, Phenomenex Luna, UK). The injection volume was 20 μL, the mobile phase flow rate 1 mL min^{-1}, and the column temperature 40 °C. A UV detector was used for quantification at 240 nm, where AB can be detected at t = 4.9 min and VAL at t = 7.2 min.

2.4.5.2 Ibuprofen, famotidine, and prednisone determination

An HPLC method for simultaneous analysis of the three APIs was developed on a 1200 Infinity Series instrument (Agilent Technologies, USA). The stationary phase used was a C18(2) column (00G-4252-E0, Phenomenex Luna, UK) held at 29 °C. The analysis was carried out at a flow rate of 0.6 mL/min, with an injection volume of 20 µL. A varied detection wavelength was used to detect FAM at 214 nm from 0 to 4.5 minutes, PRED at 243 nm from 4.5 to 6 minutes, and IP at 220 nm between 6 and 9 minutes. The mobile phase comprised 90:10 v/v methanol: phosphate buffered saline (PBS; pH 3.6, 0.01 mol/L). Adjustment of the PBS pH was undertaken using orthophosphoric acid (85%, HPLC grade, Fisher Scientific, UK). All mobile phase solutions were mixed and filtered through a 0.45 µm membrane filters (Millex syringe filter, Merck Millipore, Germany) before use. The retention times for FAM, PRED, and IP were 3.2, 5.5, and 7.2 min respectively.

The loading of each drug in the electrospun fibres was evaluated by taking100 ± 2 mg of the sample, dissolving this in 50 mL of methanol, and then diluting to a final volume of 100 mL with deionised water. The resultant solutions were mixed with a magnetic stirrer for 24 hours to ensure complete dissolution. A calibration curve for FAM, PRED, and IP was prepared from fresh stock solutions on the day of the experiment.

2.4.5.3 Levodopa and carbidopa determination

An HPLC assay for simultaneous analysis of both LD and CD was devised based on the method for Co-Careldopa detailed in the British Pharmacopeia (British

Pharmacopeia Commission, 2016). The analysis was performed on a 1200 Infinity Series instrument (Agilent Technologies, USA). The stationary phase was a C18(2) column (00G-4252-E0, Phenomenex Luna, UK) at temperature 25 °C. Analysis was carried out at a flow rate of 1.5 mL min^{-1}, and an injection volume of 20 µL used. Each assay ran for a total time of 6 min. A UV detector was used for quantification at 282 nm, where LD can be detected at t = 3.2 min and CD at t = 4.5 min. The mobile phase comprised 20:80 v/v methanol: phosphate buffered saline (PBS; pH 2.8, 0.01 mol/L). Adjustment of the PBS pH was undertaken using 1M orthophosphoric acid (85%, HPLC grade, Fisher Scientific, UK). The mobile phase solutions were mixed and filtered through a 0.22 µm membrane filters (Millex syringe filter, Merck Millipore, Germany) before use.

The loading of each drug in the electrospun fibres was evaluated by taking 20 ± 1 mg of each sample and dissolving this in 100 mL of 1M HCl under stirring. The vessels used all comprised darkened glass to protect the samples from light degradation. A calibration curve for LD and CD was prepared from stock solutions stored in the dark and freshly diluted on the day of the experiment.

2.5 Additional characterisation

2.5.1 Thickness of the formulations

10 mL of each orodispersible film casting solution was poured onto a glass plate, or. 5 mL of each electrospinning solution was spun onto aluminium foil. A 4 cm diameter circular section was cut from three different locations on each formulation with a biopsy

punch, and the thickness of each measured using electronic digital Vernier callipers. Data are presented as mean ± S.D. (n=3).

2.5.2 Folding endurance

The brittleness of the orodispersible films and the electrospun fibre mats was quantified in terms of the folding endurance, which is defined as the number of times the material can be folded at the same place without breaking or cracking (Mundargi et al., 2007). A circular section of 4 cm diameter cut with the biopsy punch was placed in a test apparatus built in-house (Figure 2.1). This is designed to sequentially fold the sample around the central diameter. Each fold rotates 180° around the central radius (+90° and -90°). The number of times the formulation could be folded before cracks appeared on the fold line was counted. Data from each sample are presented as mean ± S.D. (n=3).

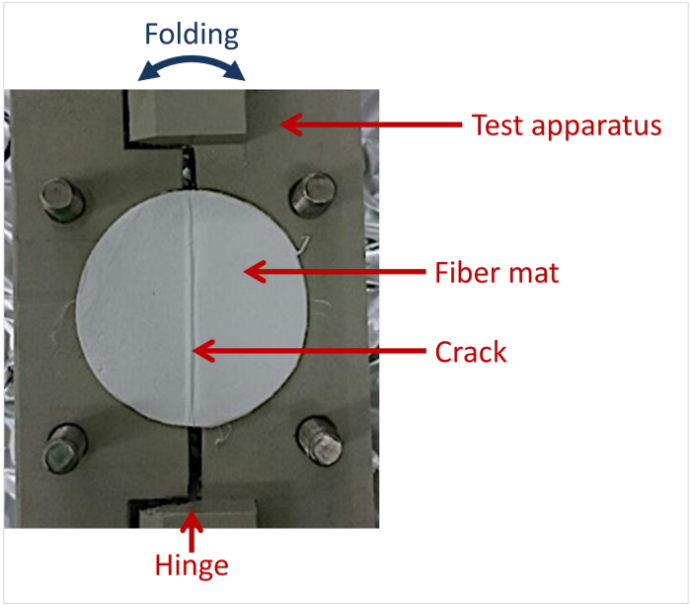

Figure 2.1. The folding endurance apparatus, showing the end point where the fibre formulation has cracked.

2.5.3 pH changes after formulation dissolution

4 ± 0.5 mg of each formulation was dissolved in 100 mL of deionised water. pH readings were obtained on a digital pH meter (HI 208, Hanna Instruments Ltd, UK) before and after dissolving the formulations. Results are reported as mean ± S.D. (n=3).

2.6 Functional performance

2.6.1 Wetting assays and disintegration time

This test was performed to evaluate the time taken for a fast dissolving film to fully disintegrate in simulated saliva (SS) solution. A 4 cm diameter circular section was dropped into an 8 cm Petri dish containing 15 mL of SS solution under stirring at 150 rpm. The latter was prepared by mixing 8 g NaCl, 0.19 g KH_2PO_4, and 2.38 g Na_2HPO_4 in 1 L of distilled water. Experiments were performed at room temperature. The wetting and disintegration of the formulations was recorded with a high-speed camera (HotShot 1280 CC, NAC Image Technology, Japan) at 500 frames per second.

2.6.2 Drug release dissolution studies

2.6.2.1 Fast dissolving formulations

The intended route of administration for fast dissolving fibres and the ODFs is as an oral film. Standard USP methods for dissolution testing do not accurately mimic this, and hence a more realistic in vitro release study was employed, similar that reported previously (Illangakoon et al., 2014). 15 mL SS was first pre-warmed to 37.5 ± 2 °C, and transferred into an 8 cm Petri dish held in an oil bath at 37 °C. A sample of the desired formulation (5 ± 0.5 mg) was dropped into the warm SS, and the mixture stirred with a 1 cm magnetic follower at 150 rpm. At predetermined time points, a 200 µL sample was taken from the Petri dish for HPLC analysis and replaced with an equal volume of fresh pre-warmed SS, to maintain a total volume of 15 mL. Three independent experiments were carried out and cumulative release percentages are reported as mean ± S.D.

2.6.2.2 Ibuprofen, famotidine, and prednisone loaded fibres

In vitro dissolution studies were carried out in two different media at pH 1.0 (0.1M HCL) and 6.8 (phosphate buffered saline; PBS). A sample of 100 mg was cut from each fibre mat and immersed in 200 mL of the desired release medium. The dissolution vessel was held at 37 °C and agitated at a speed of 100 rpm in a water bath incubator shaker (Metrex Water Bath Incubator Shaker, UK). At predetermined time points, 1 mL samples were withdrawn and replaced with an equal amount of fresh pre-headed medium to maintain a constant volume. The release of each API was quantified by

HPLC as detailed in Section (2.4.5.2). Three independent experiments were carried out, and cumulative release percentages are reported as mean ± S.D.

2.6.2.3 Levodopa and carbidopa formulations

Drug release experiments were carried out using USP apparatus type 1, with a rotating basket (Caleva ST7 dissolution tester, G.B. Caleva Ltd., Dorset, UK). Fibre samples of 30 ± 1 mg were loaded in hard gelatin capsules (size 0). Each capsule was placed in the rotating basket at 50 rpm, then immersed in a vessel containing 750 mL of 0.1M HCl, at a temperature of 37°. At predetermined time points, 1 mL samples were withdrawn and replaced with an equal amount of fresh pre-heated medium. The release of each API was quantified by HPLC as described in Section (2.4.5.3). Three independent experiments were carried out, and cumulative release percentages are reported as mean ± S.D.

2.7 Stability study

Initial stability studies were carried out the lead FDC formulations. The physical form of the components was assessed after storage for minimum of 4 months. Three different storage conditions were explored, as detailed in Table 2.1. Within each zone, the storage temperature and relative humidity (RH%) were recorded using a data logger (EL-USB-2-LCD, LASCAR, China). After the desired storage time, physical form characterisation for each formulation was undertaken using XRD and FTIR as detailed earlier.

Table 2.1. Details of the stability testing protocols

Zone	Container	Temperature (°C)	RH (%)
A	Fridge	6.5 – 7.6 °C	61 ± 6 %
B	Desiccator with silica gel in room temperature	16.5 – 27.5 °C	33.5 ± 1.6 %
C	Drying oven	30 - 40 °C	21.3 ± 4 %

2.8 References

Çelebier, M., Kaynak, M.S., Altınöz, S. and Sahin, S., 2010. HPLC method development for the simultaneous analysis of amlodipine and valsartan in combined dosage forms and in vitro dissolution studies. Brazilian Journal of Pharmaceutical Sciences, 46(4), pp.761-768.

British pharmacopeia commission, 2016, Appendix XII B. ANNEX: Recommendations on dissolution testing, British Pharmacopeia, London, England: stationary office.

Chapter 3. Amlodipine besylate and valsartan fixed-dose combinations prepared by film-casting

3.1 Introduction

The choice of an appropriate oral pharmaceutical dosage form is highly important, particularly for patient groups such as young children and the geriatric population. For instance, effective dosing using a formulation which required swallowing can be challenging for elderly patients who often suffer from dysphagia. Fast-dissolving oral drug delivery systems (FD-DDS) have the advantage of immediate disintegration and drug dissolution occurring in the mouth, providing rapid onset of action (Seager, 1998). Since the formulation does not need to be taken with water, FD-DDSs can be used for patients suffering from dysphagia and improve patient compliance. On such formulation type are the fast-dissolving orodispersible films (ODF) (Dixit and Puthli, 2009). ODFs could comprise a potential platform to create FDCs and enhance patient compliance.

ODF are thin films, usually made of a polymer composite, that readily dissolve in the oral cavity once in contact with an aqueous medium (saliva) (Hoffmann et al., 2011; Scarpa et al., 2018). They do not need to be swallowed, making them more convenient patients and improving adherence (Bala et al., 2013; Lai et al., 2018). ODFs do not necessarily need to be mucoadhesive, but often they do have mucoadhesive properties since most of the ODF are based on hydrophilic polymers (Borges et al., 2015a).

The flexibility of ODFs can give easier handling and better stability than other comparable formulations (e.g. orodispersible tablets, which might suffer from fragility and brittleness) (Borges et al., 2015a). However, there are some challenges in designing ODFs, the most significant of which is related to the physical instability of the loaded APIs, particularly in high relative humidity conditions (Borges et al., 2015a). Also, the drug-loaded capacity is often limited (Borges et al., 2015a), since the rapid dissolution obtained typically arises from the ODFs comprising amorphous solid dispersions. Increasing the drug content might result in crystallisation, and hence dissolution will slow (Abed et al., 2010; Ahmed and Aboul-Einien, 2007).

Here we aim to develop FDCs in the form of ODFs, using the film casting approach. The formulations will be made from a hydrophilic matrix (polyvinylpyrrolidone (PVP)) and loaded with amlodipine besylate (AB), valsartan (VAL), or both drugs combined (Figure 3.1). AB and VAL are frequently prescribed in combination as blood pressure lowering agents for the treatment of hypertension when monotherapy is not sufficient (Plosker and Robinson, 2008). An FDC (EXFORGE®) is available in the form of film-coated tablets containing AB and VAL in doses of 5/80 mg, 5/160 mg, and 10/160 mg. Therefore, these two drugs were selected as suitable candidates for FDC development.

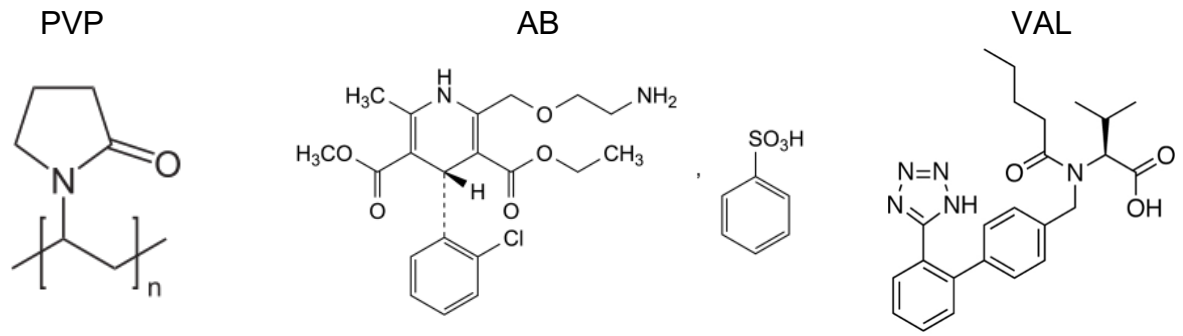

Figure 3.1. Chemical structures of polyvinylpyrrolidone (PVP), amlodipine besylate (AB), and valsartan (VAL).

The pharmaceutical characteristics of AB and VAL are listed in Table 3.1. The aqueous solubility of amlodipine besylate is 0.0753 mg/mL, and oral bioavailability reaches 64-80% from the licensed FDC formulation (Plosker and Robinson, 2008). VAL belongs to Biopharmaceutical Classification System (BCS) class II; it has very low solubility, and an absorption window limited to the upper gastrointestinal tract (Chella et al., 2015). These properties lead to variable absorption and low oral bioavailability of ~23% from the licensed FDC product (Plosker and Robinson, 2008), requiring the enhancement of aqueous solubility and dissolution rate to achieve higher oral bioavailability.

Table 3.1. The pharmaceutical characteristics for AB and VAL in their licensed product (EXFORGE®).

PK parameters	Amlodipine besylate (AB)	Valsartan (VAL)
pKa	8.6	4.7 and 3.9
Solubility	Soluble in acidic pH	Soluble in alkaline pH (>5)
Aqueous solubility	0.0753 mg/ml	0.0234 mg/mL
Bioavailability	64-80%	23%
Peak plasma concentration	6-8 h	2-4 h

3.2 Experimental

3.2.1 Solutions preparation

10% w/v (PVP; MW 360,000 Da; Sigma-Aldrich, UK) solutions were prepared in ethanol, with stirring overnight to ensure complete dissolution. Drug-loaded solutions were prepared as detailed in Table 3.2, by pre-dissolving the required amount of AB or/and VAL in 4 mL of ethanol, then combining this with 10 mL of the PVP solution plus 0.25 mL glycerol. Mechanical stirring was applied at room temperature for 20 min until homogeneous solutions were formed. Drug/polymer physical mixtures (PM) were prepared for control purposes.

Table 3.2. The composition of each formulation.

Formulation	Drug loading in the ODF %w/w	AB loading in the ODF mg	VAL loading in the ODF mg	Ethanol mL	PVP 10%w/v	Glycerol mL	Total volume (mL)
PVP	0	-	-	-	10	-	10
PVP+Glyc	0	-	-	-	10	0.25	10.25
FA1	5	69	-	4	10	0.25	14.25
FA2	15	231	-	4	10	0.25	14.25
FA3	30	563	-	4	10	0.25	14.25
FV1	5	-	69	4	10	0.25	14.25
FV2	15	-	232	4	10	0.25	14.25
FV3	30	-	563	4	10	0.25	14.25
FAV1	5 + 5	73.8	73.6	4	10	0.25	14.25
FAV2	15 + 15	282.3	282.7	4	10	0.25	14.25
FAV3	30 + 30	986	986	4	10	0.25	14.25

3.2.2 Solvent film casting

An initial blank orodispersible film (ODF) formulation was prepared by a film-casting a polymer solution mixed with glycerol (as detailed in Table 3.2). The polymer solution was prepared by dissolving PVP in ethanol (10 % w/v), and the resultant solution was blended with glycerol at ratios of 10:1 to 40:1 v/v, stirred until a fully homogeneous solution was obtained, and left to stand to remove any entrapped air bubbles. The optimal ratio was determined to be 40:1, which gave a fully dried ODF with acceptable flexibility.

Optimisation of the film-casting method was undertaken using a range of different collecting surfaces (stainless steel, plastic, and glass), and a range of temperatures up to 100 °C in attempts to obtain ODFs without bubbles present on their surface. Finally, after optimising the conditions, for each formulation the entire volume of the film casting solution mixture was poured into an 8 cm diameter film-casting mould on a glass plate, then placed into an oven at 50 °C for 24 hr to allow complete evaporation of the solvent (Figure 3.2). Drug-loaded ODFs were prepared similarly. The required mass of each APIs was dissolved in ethanol, then mixed with the PVP/glycerol mixture and cast as above.

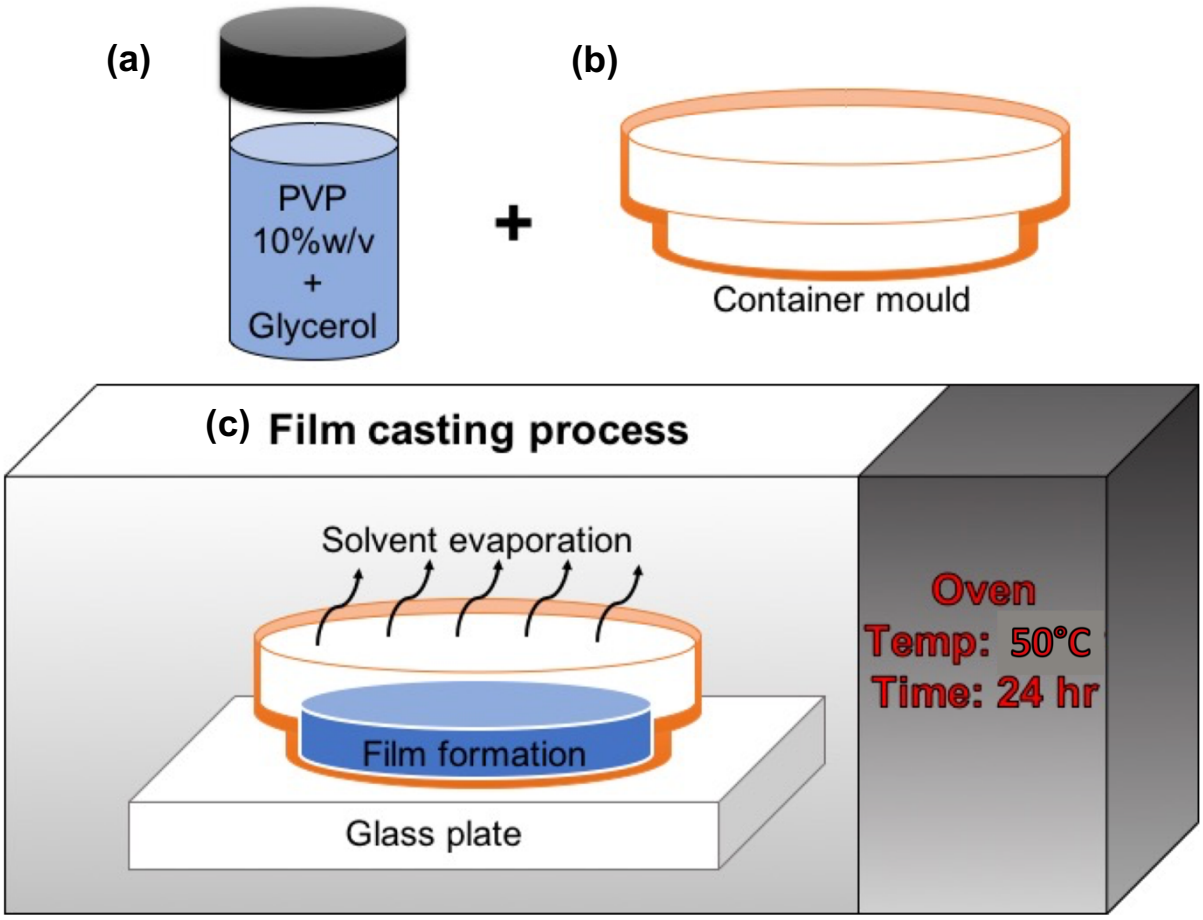

Figure 3.2. A schematic diagram of the orodispersible film preparation process. **(a)** A mixture of PVP solution with glycerol was made, and poured into **(b)** a container mould; **(c)** A film was then prepared through evaporation of the solvent.

3.3 Results and discussion

3.3.1 Formulation optimisation

PVP is a commonly used polymer in amorphous solid dispersions (ASD) formulations due to it is hydrophilic, water-soluble and bio-compatible properties (Wang et al., 2017). ODFs were thus prepared using PVP as the film forming polymer, with the aim of achieving immediate dissolution upon contact with water (Simonelli et al., 1969).

Ethanol was used as the solvent during the preparation of ODFs owing to its ability to dissolve PVP and both AB and VAL.

In a trial experiment to prepare a film using only the PVP solution, the outcome was a brittle film that lacked flexibility and was easily breakable. This is consistent with the literature (Dixit and Puthli, 2009). Therefore, to enhance the ODFs' flexibility and ease of handling, glycerol was added as a plasticiser. Glycerol is well known to be able to plasticise hydrophilic polymers like PVP through hydrogen bonding (Dixit and Puthli, 2009). The typical concentration of plasticiser is in the range between 0 to 20 % of the polymer dry weight (Rowe and Owen, 2006). A range of materials was prepared to determine the ideal ratio between glycerol and PVP. When the ratio was 10:1 v/v, a viscous solution formed on the plate and no film was generated. Upon increasing the ratio to 20:1 v/v, a sticky and wet film started to form inside the mould. However, when the mould was removed, the film shrank and collapsed. The best ODFs were obtained at a ratio of 40:1 v/v, these were firm but flexible, as is shown in Figure 3.3.

(a) **(b)**

Figure 3.3. Digital images of the blank ODFs prepared from 10% w/v PVP and glycerol at a 40:1 v/v ratio. **(a)** the film in the mould, and **(b)** the same film after removal. The film can be seen to be firm and flexible, and suitable for cutting.

3.3.2 Morphology

The surface morphology of each formulation was explored with a scanning electron microscope (SEM), and also by digital imaging (Figure 3.4). In the SEM images (Figure 3.4a), the image of AB and VAL show the APIs to have regular shaped particles with sharp edges, consistent with crystalline materials. The blank ODF (PVP/glycerol; Figure 3.4c) shows a slightly rough surface, but the film appears compact, and most of the ethanol seems to have evaporated with only a few gas bubbles trapped in the surface of the film (denoted with the blue arrows in Figure 3.4c). The latter arise due to the rapid formation of a solidified surface "skin" layer before full evaporation of the ethanol, leaving a small amount of trapped gas (Aroon et al., 2010).

Similar to the blank formulation, the single drug loaded formulations (Figure 3.4d-i) show a slightly rough surface, with only minimal presence of gas bubbles in the surface

of the films. The formulations do not resemble the original regular shape of the APIs. This suggests that amorphous solid dispersions have been formed: incomplete dissolution in the casting solution or precipitation of the drug during film formation would be expected to result in the presence of visible crystals on the films (Xu et al., 2014).

In the dual drug loaded formulations (Figure 3.4j-l), FAV1 (5% w/w of each drug) shows a similar rough surface to the blank film and single drug loaded formulations. However, when the concentration increased in FAV2 (15% w/w AB, 15% w/w VAL) and FAV3 (30% w/w AB, 30% w/w VAL), the appearance changed and some regular-shaped particles can be seen (denoted with yellow arrow in Figure 3.4k-l). This indicates some degree of precipitation of drug particles from the casting solution. When comparing the SEM images to the digital photographs of FAV1 and FAV2 (Figure 3.4m-o), the low loading formulations FAV1 and FAV2 have smooth surfaces without gas bubbles and no precipitation of APIs is visible by eye. However, when the drug concentration was raised in FAV3 (Figure 3.4, l and o), precipitation of some APIs occurred and can be seen both by SEM and as the yellowish patches in the centre of the film in the digital photographs (Figure 3.4 o). This is due to the drug concentration being higher than the loading capacity of the polymer (Wang et., 2017). As would be expected, more precipitation is noted for FAV3 than FAV2.

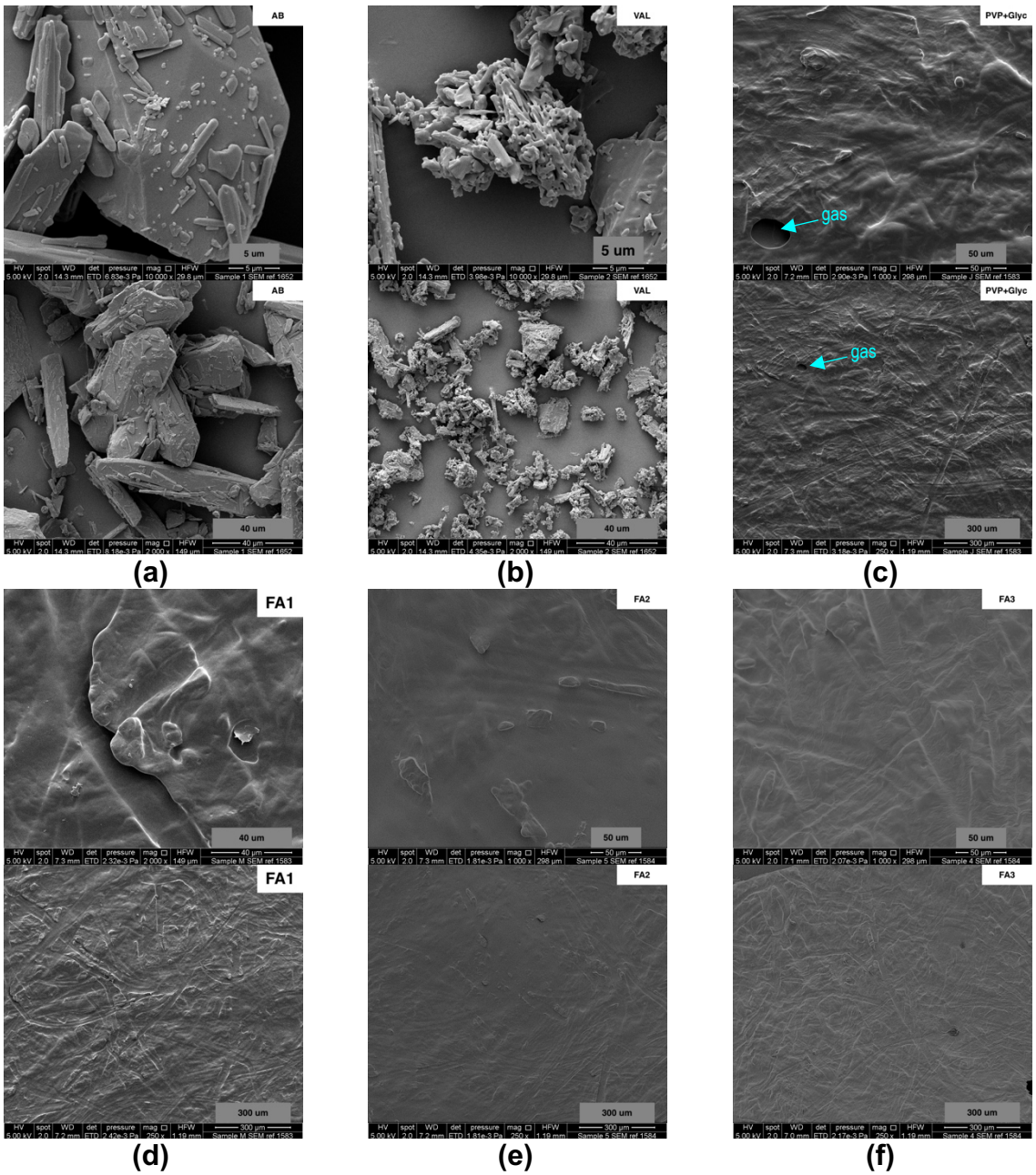
AB
5 um
AB
40 um
(a)
VAL
5 um
VAL
40 um
(b)
PVP+Glyc
gas
50 um
PVP+Glyc
gas
300 um
(c)
FA1
40 um
FA1
300 um
(d)
FA2
50 um
FA2
300 um
(e)
FA3
50 um
FA3
300 um
(f)

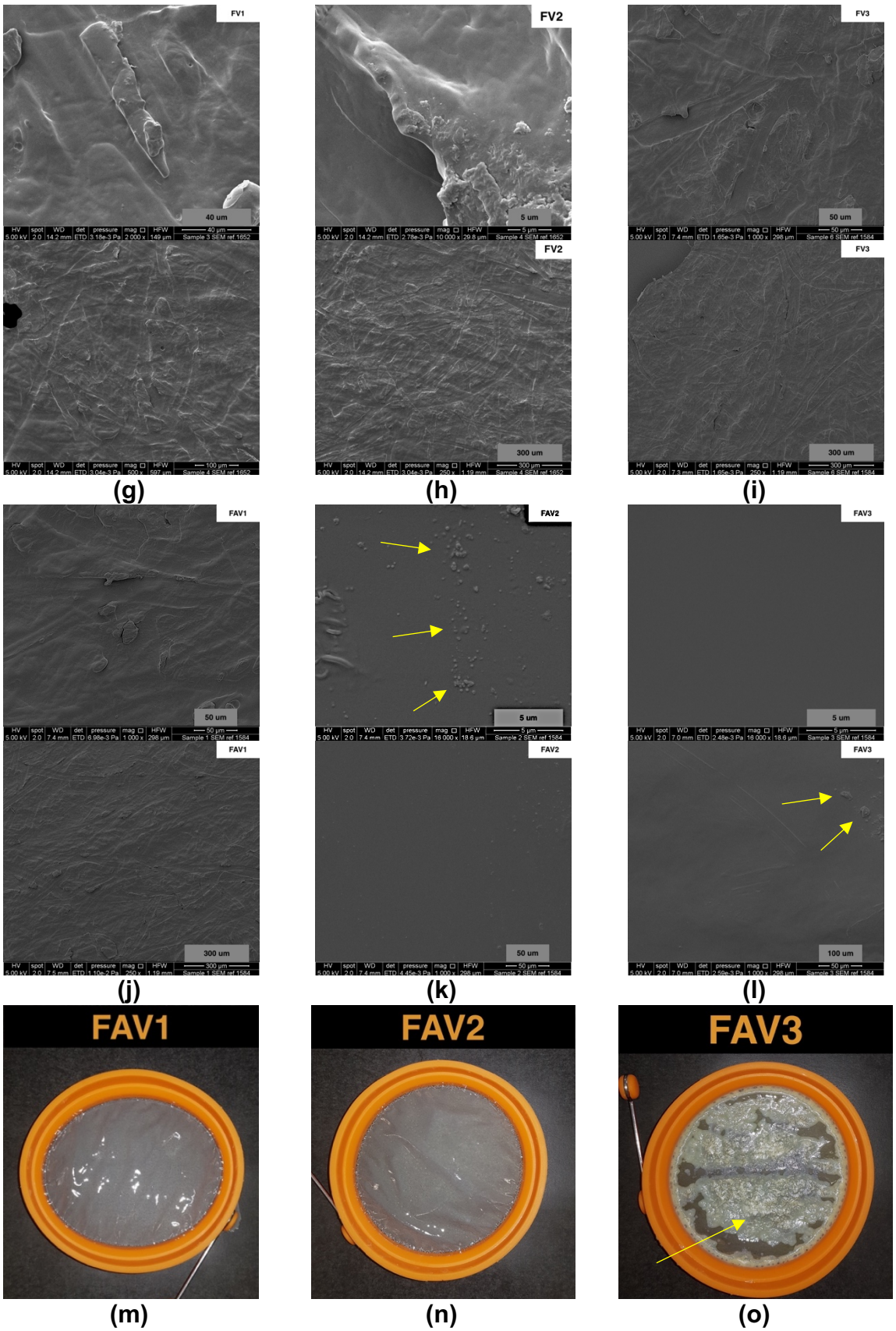

Figure 3.4. SEM images of the raw material and ODFs showing **(a)** raw AB; **(b)** raw VAL; **(c)** blank ODF (PVP+Glyc); **(d)** FA1 (5% w/w AB); **(e)** FA2 (15% w/w AB); **(f)** FA3 (30% w/w AB); **(g)** FV1 (5% w/w VAL); **(h)** FV2 (15% w/w VAL); **(i)** FV3 (30% w/w VAL); **(j)** FAV1 (5% w/w AB, 5% w/w VAL); **(k)**

FAV2 (10% w/w AB, 10% w/w VAL); and **(l)** FAV3 (30% w/w AB, 30% w/w VAL). Digital images of the ODFs **(m)** FAV1 (5% w/w AB, 5% w/w VAL); **(n)** FAV2 (10% w/w AB, 10% w/w VAL); and **(o)** FAV3 (30% w/w AB, 30% w/w VAL). Scale bars of the main SEM images= 10 µm.

3.3.3 Thickness

The thicknesses of the ODFs was determined with electronic digital Vernier calipers on a 4 cm diameter circular section of each formulation and the results are presented in Table 3.3. The thickness of the blank ODFs was around 178 ± 39 µm. An increase in the API loading led to a gradual increase in the thickness of the formulation. In the single-drug loaded formulations, the increase in thickness was not notable for the systems loaded with 5 % w/w APIs: FA1 has thickness of 167 ± 3 µm, and FV1 of 180 ± 10 µm. Further increases in the API content to 15 and 30 % w/w led to notably thicker films compared to the blank ODFs. In the dual-drug loaded materials, an increase in thickness was noticed for all the formulations FAV1, FAV2 and FAV3. This increase in thickness is directly correlated with the total amount of API in the film.

The standard deviation data show there is less variation in thickness among the formulations with lower loadings. This could be a result of the incomplete drug-in-polymer solubility in the higher loading formulations (as seen in Figure 3.4m-o). Generally, the thickness of fast dissolving films prepared by a solvent film casting found to be around 15 to 500 µm (Bala et al., 2013). Most of the ODFs here lie within this range, except for formulation FAV3 which has increased thickness due to its high total drug loading.

Table 3.3. Physical properties characterisation of the ODFs. Thickness was measured at three different points on each formulation. Folding endurance was measured on three different samples. Data are presented as mean ± S.D. (n=3).

Formulation	Thickness (μm)	Folding endurance (180°)
PVP+Glyc	178 ± 3	> 100
FA1	167 ± 3	> 100
FA2	202 ± 15	> 100
FA3	266 ± 24	> 100
FV1	180 ± 1	> 100
FV2	233 ± 17	17 ± 2
FV3	276 ± 46	0 (broke on first fold each time)
FAV1	205 ± 9	25 ± 2
FAV2	317 ± 14	19 ± 1
FAV3	937 ± 20	0 (broke on first fold each time)

3.3.4 Folding endurance

Folding endurance is mechanical property used to characterize the ability of thin films to resist cracking or breaking upon packaging and storing (Vuddanda et al., 2016). Folding endurance data are presented in Table 3.3. The folding endurance value of the blank formulation showed it to be very flexible, since it can be folded more than 100 times without breaking. In the single-drug loaded formulations, all the ODFs loaded with AB have the same level of flexibility and can be folded over 100 times without any crack formation. This high folding endurance was also reported in a previous study of AB loaded films prepared from PVP, with endurance of 75 to 135 folds observed (Maheswari et al., 2014). For the VAL-loaded formulations, an increase of drug loading led to decreased film flexibility. The same is seen in the dual-drug loaded formulations: the flexibility was acceptable for formulations FAV1 and FAV2, but FAV3 broke upon a single fold in each experiment. The decrease in folding endurance is dependent on the amount and chemical structure of the loaded drugs, which can affect the polymer chain movement resulting in mechanically weaker and

more brittle ODFs (Senthilkumar and Vijaya, 2015; Borges et al. 2015b). AB is presumably also a better plasticiser then VAL for PVP (Low et al., 2013).

3.3.5 X-ray diffraction (XRD)

XRD analysis was applied to examine the physical form of the APIs loaded in the ODFs. XRD diffraction patterns are shown in Figure 3.5.

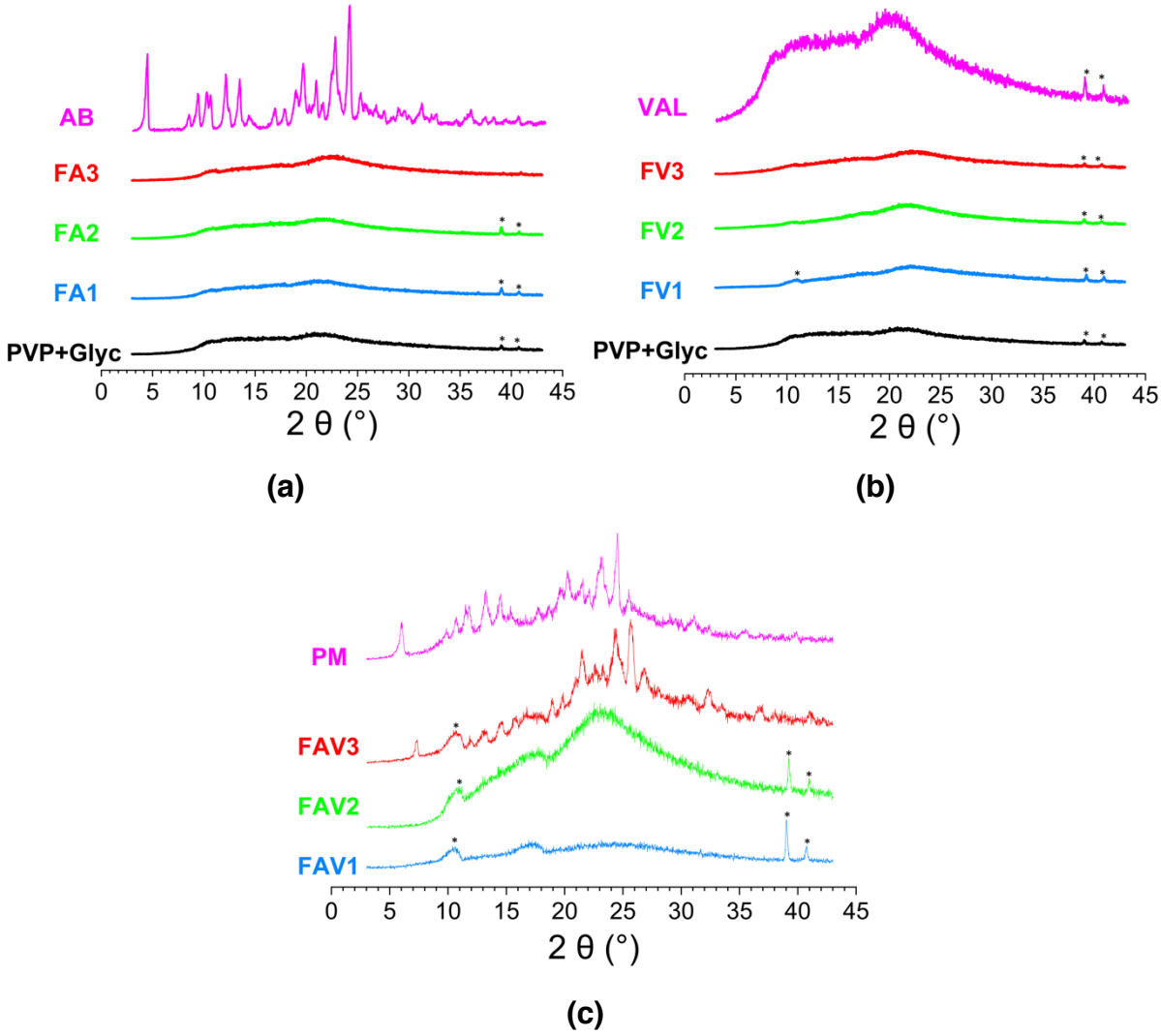

Figure 3.5. XRD diffraction patterns of the ODFs and raw materials: **(a)** AB and ODFs loaded with AB (FA1: 5%, FA2: 15%, FA3: 30% w/w); **(b)** VAL and ODFs loaded with VAL (FV1: 5%, FV2: 15%, FV3: 30% w/w); **(c)** A physical mixture combination of AB, VAL and PVP at 30:30:40 % w/w, and ODFs loaded with AB+VAL (FAV1: 5%+5%, FAV2: 15%+15%, FAV3: 30%+30% w/w). Peaks labelled with * correspond to the sample holder.

The pattern of AB shows sharp characteristics reflections at 2θ values of 5.71°, 11.13°, and 12.87°, consistent with its an anhydrous form (Koradia et al., 2010). VAL shows a diffuse X-ray pattern indicative of poor crystallinity or amorphicity. A similar X-ray diffraction pattern was obtained by Wang et al. (2013) for the commercial form of valsartan. A physical mixture of PVP, VAL and AB results in a pattern which contains the characteristic reflections of AB superimposed on an amorphous background from PVP and VAL.

The unloaded ODF only shows a broad halo in its XRD pattern, due to the amorphous nature of PVP and glycerol (Buera et al. 1992). The single-drug loaded formulations FA1 to FA3 and FV1 to FV3 have very similar patterns to the unloaded formulation, with no significant reflections visible. This indicates that all these materials comprise amorphous solid dispersions. In the pattern of the dual drug loaded formulation FAV1 and FAV2, the characteristic reflections of AB and VAL disappeared, indicating the formation of an amorphous system (Figure 3.5c). This is dependent on the ability of PVP to inhibit recrystallization from solution, most likely through steric hindrance and molecular interactions with the dissolved drug molecules, and by increasing the glass transition temperature (Broman et al., 2001). In formulation FAV3, some characteristic reflections of AB appear in the pattern, which appears similar to that of a physical mixture (PM) of AB, VAL, and PVP matching the quantities of materials in AV3. This indicates some AB was present in the crystalline form due to the high total drug loading in the ODFs.

3.3.6 Differential Scanning calorimetry (DSC)

A DSC study was performed to confirm the physical state of the APIs in the ODFs. The thermograms of all the formulations are shown in Figure 3.6.

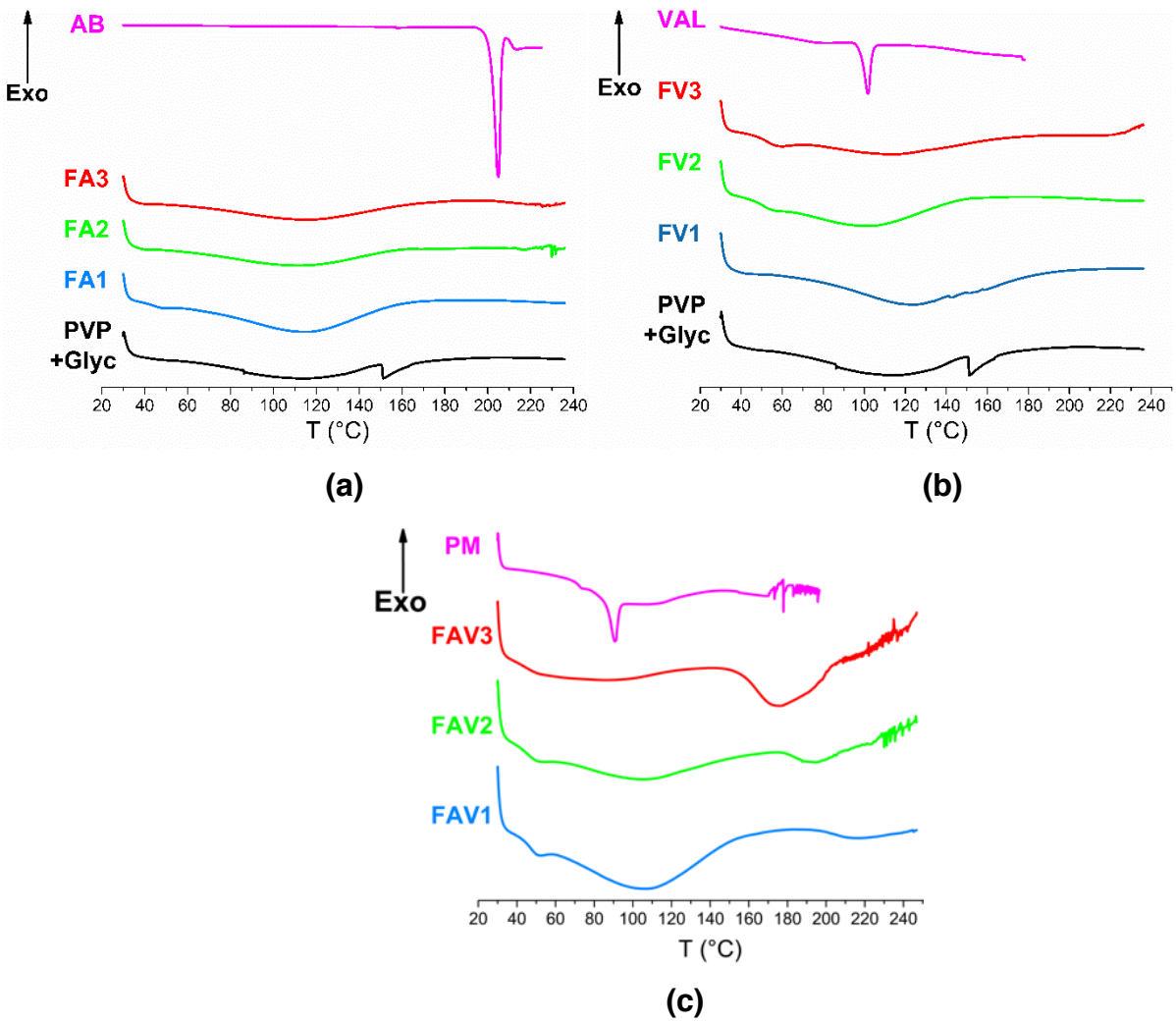

Figure 3.6. DSC data for the ODFs and raw materials: **(a)** AB and ODFs loaded with AB (FA1: 5%, FA2: 15%, FA3: 30% w/w); **(b)** VAL and ODFs loaded with VAL (FV1: 5%, FV2: 15%, FV3: 30% w/w); **(c)** A physical mixture combination of AB, VAL and PVP at 30:30:40 % w/w, and ODFs loaded with AB+VAL (FAV1: 5%+5%, FAV2: 15%+15%, FAV3: 30%+30% w/w).

The thermogram of AB shows an endothermic peak corresponding to melting at around 206 ºC. This is consistent with the melting onset between 197.5 – 200 °C

reported in the literature for the crystalline anhydrous form of AB (Rollinger and Burger, 2002). The thermogram data of VAL a show small broad peak at 60-90 ºC corresponding to water loss then glass transition with high enthalpy of relaxation at 103 ºC (Skotnicki et al., 2013). In the PVP/glycerol film, a broad endotherm between 50 and 150 ºC appears due to water evaporation from PVP (Van den Mooter et al., 1998). A sharper endothermic peak between 150 and 180 ºC arises from glycerol degradation, as reported in the literature (Kim and Ustunol, 2001; Abdorreza et al., 2011; Balqis et al., 2017).

In all the ODF thermograms, a broad endotherm appears between 50 and 150 ºC corresponding to loss of water from the formulations. However, the glycerol degradation event cannot be seen in the drug-loaded formulations. This is related to the relatively low glycerol content in the formulations and potential molecular interactions, through hydrogen bonding, with both the PVP and drug molecules (Balqis et al., 2017).

The thermograms of the single drug-loaded formulations FA1 to FA3 and FV1 to FV3 do not contain any events from AB melting or VAL relaxation, indicating that the APIs are present in the amorphous form. Considering the dual drug loaded formulations, FAV1 shows only a broad endothermic peak as a result of PVP dehydration. With the increase in drug loading from FAV1 to FAV3, the PVP content in the formulations decreases, resulting in a less distinct water loss endotherm. At the same time, an endothermic peak emerges between 170 - 200 ºC, indicating that more crystalline AB exists in the dual drug loaded formulation. The results from DSC are in agreement with the data from XRD, indicating that most of the APIs existed in a crystal form have lost

their crystal form structural alignment. However, at this level, we can not be sure that all the crystal molecules reached to complete disordered arrangement, so we assume that the raw materials comprised as either to molecular dispersion, or amorphous solid dispersions. This results can be further confirmed with stability study to assess the physical form of the APIs after storage for several months.

3.3.7 Fourier transform infrared spectroscopy (FTIR)

Infrared spectroscopy was performed to evaluate the compatibility of the components in the formulations by assessing the interactions between the APIs and the carrier PVP and glycerol. The chemical structures and spectra of the raw materials and ODFs are presented in Figure 3.7.

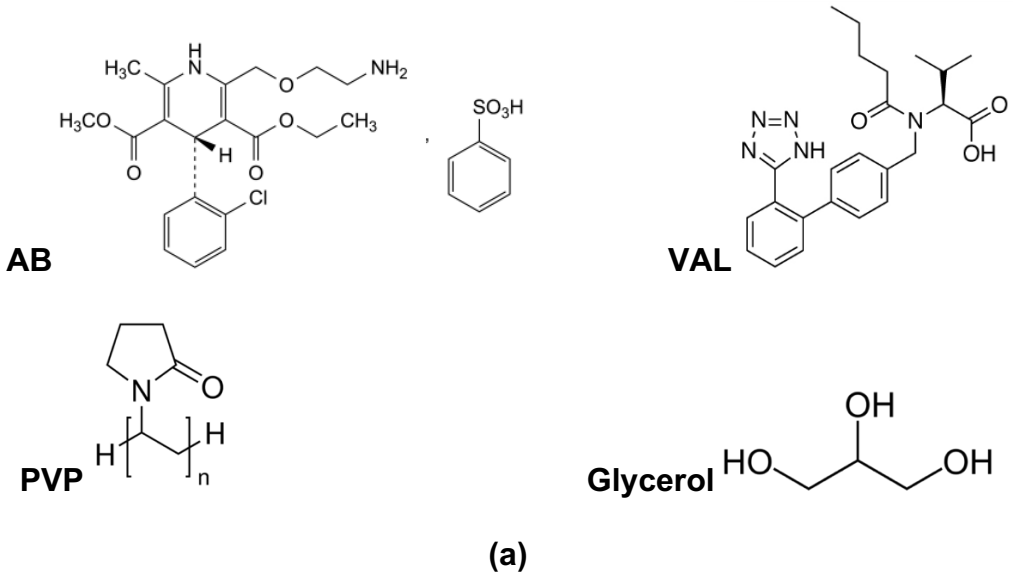

(a)

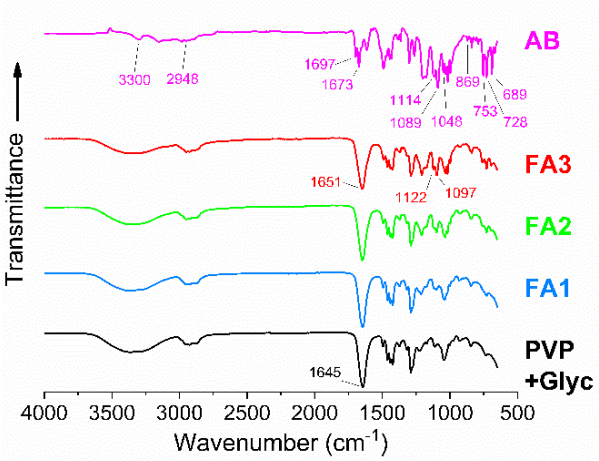

(b)

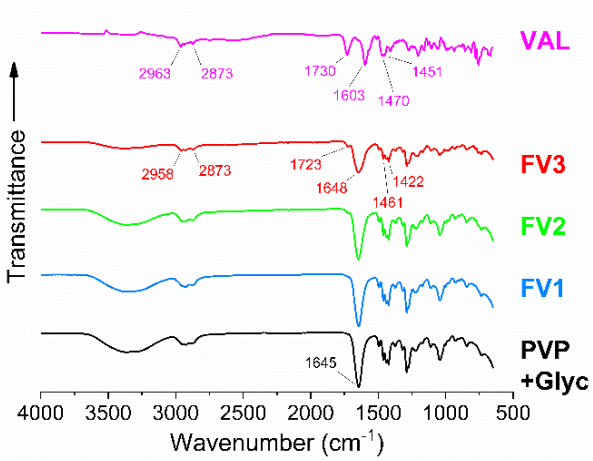

(c)

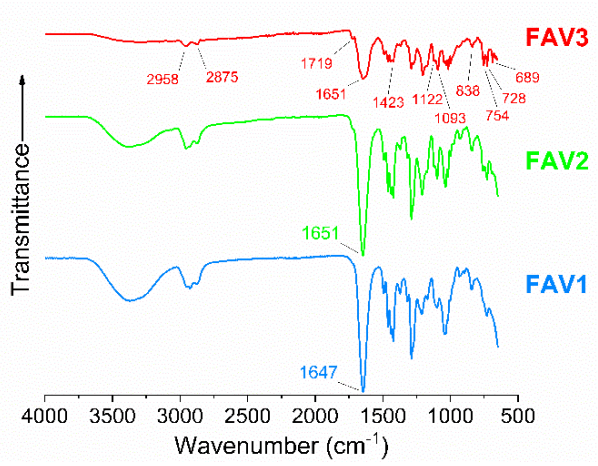

(d)

Figure 3.7. (a) The chemical structures of AB, VAL, PVP, and Glycerol; and FTIR spectra of **(b)** AB; **(c)** VAL; and, **(d)** dual-drug loaded formulations.

In the spectrum of AB (Figure 3.7, b), characteristic C=O stretches at 1697 cm^{-1} and 1673 cm^{-1} can be seen. Asymmetric stretching of C—O—C is visible as sharp peaks at 1114 cm^{-1} and 1089 cm^{-1}, and in addition bands can be seen from NH_3 wagging at 1048 cm^{-1}, —C—O bending at 869 cm^{-1}, and N—H out of plane bending at 753 cm^{-1}, 728 cm^{-1}, 689 cm^{-1}. The spectrum of VAL (Figure 3.7, c), shows distinct peaks at 3300 cm^{-1} from stretching vibrations of O—H and N—H groups, and aromatic CH_2 stretching at 2963 cm^{-1}. A C=O stretching band is present at 1730 cm^{-1}, N—C=O amide carbonyl stretching at 1603 cm^{-1}, and aromatic C=C vibrations at 1451 cm^{-1} and 1470 cm^{-1}. The spectrum of the blank film (PVP+Glycerol), (Figure 3.7, b and c), exhibits bands between 3650 – 3050 cm^{-1} from O-H stretches in glycerol and from the adsorbed water on PVP, C—H stretching between 2840 and 3010 cm^{-1}, C=O stretching at 1660 cm^{-1}, and a C—N vibration at 1290 cm^{-1} . (Koradia et al., 2010; Wang et al., 2013; Gómez-Siurana et al., 2013).

The spectra of the ODFs show changes compared to the pure raw materials. The main region that proves interactions is between 1750-650 cm^{-1}. In the FA materials (Figure 3.7, b), the two AB C=O stretching bands have merged with the PVP C=O stretching at 1651 cm^{-1}. The signal of AB (C—O—C stretching vibrations) at 1114 cm^{-1} in AB shifts to 1122 cm^{-1} in the film. The AB N-H signals present in the raw material at 753, 728, and 689 cm^{-1} have also disappeared in FA1 to FA3. Similarly, for the VAL formulations (Figure 3.7, b), the N—C=O vibrations found at 1603 cm^{-1} for the raw material have both merged with the PVP C=O stretching at 1660 cm^{-1}, and they covered the C=O vibrations at 1730 cm^{-1} which appears as a shoulder to the vibration at 1723 cm^{-1}.

In the ODF formulations (Figure 3.7, d), FAV1 and FAV2 most of the signals are also present in the spectrum of the blank PVP+glycerol film, and the distinct bands from the drugs are absent from the spectra, indicating molecular interactions such as hydrogen bonding between the drug NH or OH groups with the C=O group of PVP. However, this effect becomes weaker in the highest loading formulations: with FAV3, AB C—O—C stretching vibrations at 1114 cm^{-1} and 1089 cm^{-1}, C—O bending at 869 cm^{-1}, N-H vibrations at 753, 728, and 689 cm^{-1} can all be seen in the spectrum. This indicates that some part of the loaded drug content did not completely interact with the polymer and there is perhaps some separation of the drug(s) and polymer carrier. This hypothesis is supported by the images of FAV3 (Figure 3.4, l-o), where some regular shaped particles of the drugs can be seen at the surface of the formulation by SEM and precipitation is evident in the digital image.

3.3.8 Drug loading and encapsulation efficiency (EE)

The API loading in the ODFs was determined from three samples removed randomly from three different points throughout each formulation. The loadings were quantified by HPLC and are presented in Table 3.4. A high drug content was achieved, with EE% a little over 100% of the theoretical loading for all the formulations. Since the film casting process was in a small sized mould about 8 cm in diameter, there is little scope for loss of the drug-polymer mixture solution. The excess of loaded EE% can be attributed to some variation in film thickness across the formulations. These results are suitable for fast-dissolving ODFs and agrees with the range reported in the literature, which generally lies between 90 and 110% (Liew et al., 2014).

Table 3.4. The drug loading and entrapment efficiency of the ODFs. Data are presented as the mean ± S.D. of three independent experiments.

Formulation	AB loading (% w/w)	AB EE (%)	VAL loading (% w/w)	VAL EE (%)
FA1	5.2 ± 0.1	104.6 ± 1.6	-	-
FA2	15.7 ± 0.4	105 ± 2.3	-	-
FA3	32 ± 1	106.4 ± 3.1	-	-
FV1	-	-	5.1 ± 0.1	103 ± 2.2
FV2	-	-	16 ± 0.2	106.1 ± 1.5
FV3	-	-	32.5 ± 0.5	108.3 ± 1.8
FAV1	5.7 ± 0.4	112.4 ± 7.6	5.4 ± 0.1	106.6 ± 1.5
FAV2	16.2 ± 0.4	107.8 ± 2.4	16.2 ± 0.1	107.6 ± 0.5
FAV3	31.4 ± 1	104.7 ± 3.4	30.4 ± 0.1	101.2 ± 0.5

3.3.9 *in-vitro* drug release study

In the literature, the evaluation of drug release from the ODFs has been performed using different apparatus volumes from 5 to 900 mL (Gittings et al., 2014). Drug release was explored here in 15 mL artificial simulated saliva to better predict the dissolution behaviour into the target area of the oral cavity before swallowing. The fast dissolving ODFs should rapidly disintegrate when placed in the mouth and contact with the salivary fluid, but there is no specific maximum determined for the disintegration time (Brniak and Jachowicz, 2015). The results are given in (Figure 3.8), and the time taken for 10%, 50%, and 90 % drug release from each formulation listed in Table 3.5.

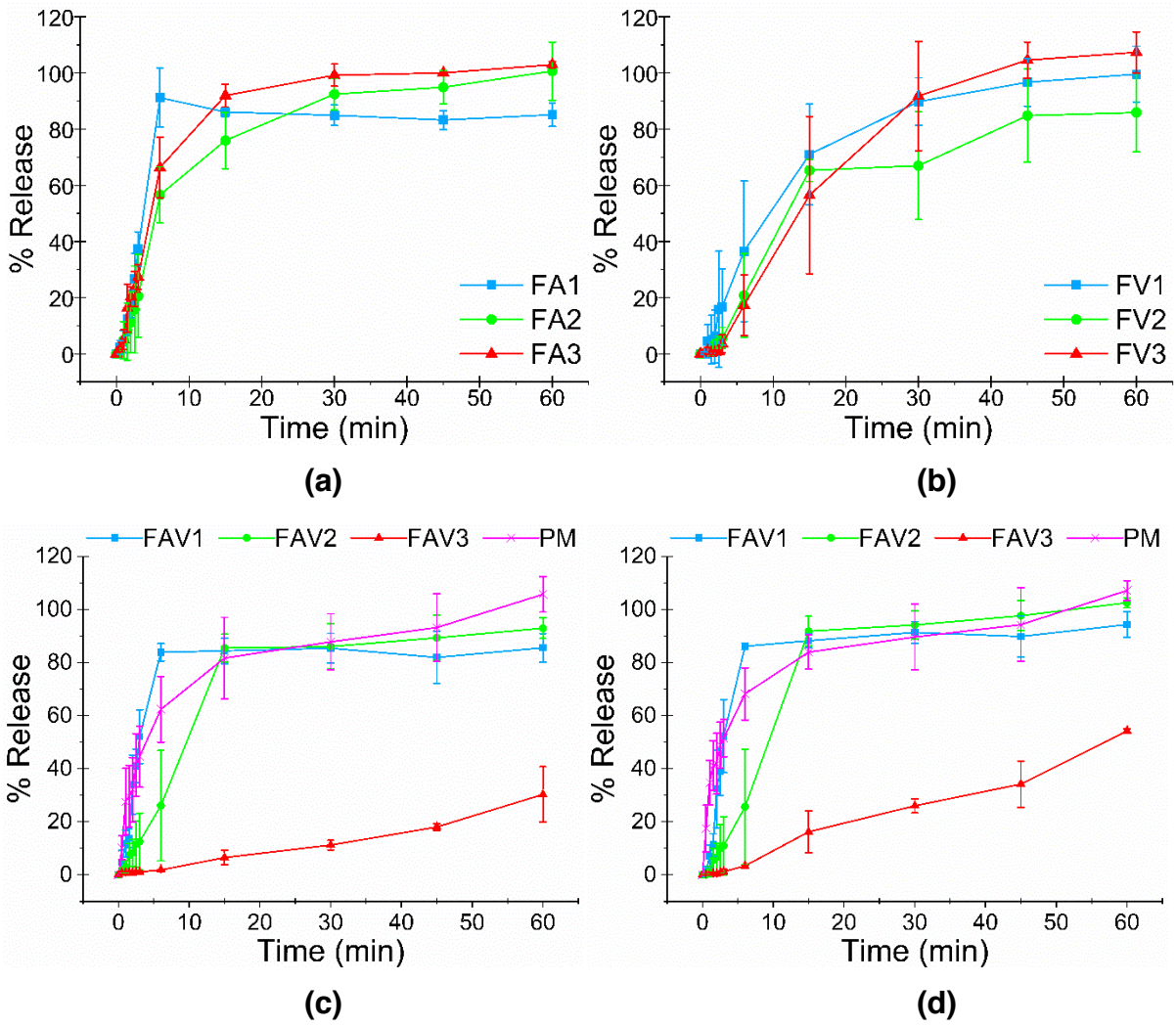

Figure 3.8. *In vitro* drug release data for **(a)** the AB-loaded formulations; **(b)** the VAL-loaded formulations; **(c)** AB release from the dual drug-loaded formulations and **(d)** VAL release from the dual drug-loaded formulations. Data are shown as mean ± S.D (n= 3).

Table 3.5. The time taken for 10, 50, and 90 % release from each formulation (calculated from the data in Figure 3.8).

Formulation	AB release (%) at time (min)			VAL release (%) at time (min)		
	10 %	50 %	90 %	10 %	50 %	90 %
FA1	1.5	> 30% in 3 min	6	-	-	-
FA2	2	6	30	-	-	-
FA3	1.5	6	15	-	-	-
FV1	-	-	-	2.5	15	30
FV2	-	-	-	6	15	60
FV3	-	-	-	6	15	30
FAV1	1	3	6	1.5	3	6
FAV2	2.5	> 26% in 6 min	45	2.5	> 25% in 6 min	15
FAV3	30	60	> 30% in 60 min	15	60	> 54% in 60 min
PM	0.5	6	35	0.5	3	30

The release of the loaded AB from the FA formulations gave 90% release of the loaded AB in the order FA1 > FA3 > FA2 (Figure 3.8a). There was first a burst release from all the FA formulations to reach over 90% from FA1, and over 50% from FA2 and FA3, within the first 6 minutes. This is owing to the high solubility of PVP, and to the amorphous state of the drug. The time of the dissolution medium penetration into the formulation is also affected by the rate of film disintegration, which is dependent on the type of the plasticiser present (Morales and McConville, 2011). It is thus postulated that the release of the remaining 50% of the AB loading from FA2 and FA3 was dependent on the time taken for the films to break and release the loaded drug. Both FA2 and FA3 showed similar drug release profiles, but FA3 was able to reach 90 % more rapidly, likely because the increased drug loading caused more plasticisation (Kasliwal et al., 2011).

The release of VAL from the FV formulations (Figure 3.8b) was much slower, reaching 50% release from all the formulations only after 15 minutes. FAV1 and FAV3 reached 90% release after 30 minutes, and FAV2 after 60 minutes. This is because the aqueous solubility of VAL is much less than that of AB.

In the dual-drug FAV formulations (Figure 3.8c-d) both APIs presented similar release profiles from each formulation. The fastest drug release was seen with FAV1, and incomplete release of both drugs arose with FAV3. The release profile of both APIs from FAV1 was similar to the fast release of AB from the single-drug formulation, due to the high content of the hydrophilic polymer PVP and hydrophilic AB assisting the fast disintegration of the ODF and releasing the amorphous drug content. In formulation FAV2, the release of AB was retarded compared to FA2, while the release of VAL was faster than from FV2. Because of the combination of AB and VAL in the same formulation, both drugs affected the release from formulation FAV2.

In formulation FAV3, incomplete disintegration of the ODFs occurred, with the samples remaining intact for more than 60 minutes and floating on the surface of dissolution medium. The reason for this was the reduced ratio of the hydrophilic polymer (40% w/w) which leads to slower permeation of the dissolution medium into the formulation. In addition, the very high loading of the APIs (30% w/w of both VAL and AB) with the presence of some crystalline material (as proved by the data from XRD and DSC; Figure 3.5 and Figure 3.6) also contribute to slow and incomplete dissolution of the APIs compared to the PM.

3.3.10 Stability study

A stability study was performed to assess the physical form of the APIs in the formulations, and detect any signs of phase separation between the loaded drug and the polymers. The storage stability of the ODF was explored for formulation FAV1 (5% w/w AB, 5% w/w VAL) since it had the best performance as a fast-dissolving ODF. XRD data and FTIR data were recorded on ODFs after storing the formulations for 6 months in different conditions denoted zone A (6.5 – 7.6 °C, 61 ± 6 % RH), zone B (16.5 – 27.5 °C, 33.5 ± 1.6 % RH), and zone C (30 - 40 °C, 21.3 ± 4 % RH), (Figure 3.9). The XRD data (Figure 3.9a) confirmed that the ODFs were largely amorphous after storing the formulations under all the different conditions, and none of the diffractograms shows any distinct Bragg reflections from AB. The FTIR data (Figure 3.9b) show samples stored under the different conditions have a similar spectrum to the fresh sample and most of the signals are also present. The spectrum from different zone look having similar peaks, only different in the intensity due to the difference in amounts of the sample tested by FTIR instrument. This indicates the good stability of the formulation for 4 months and no phase separation occurred.

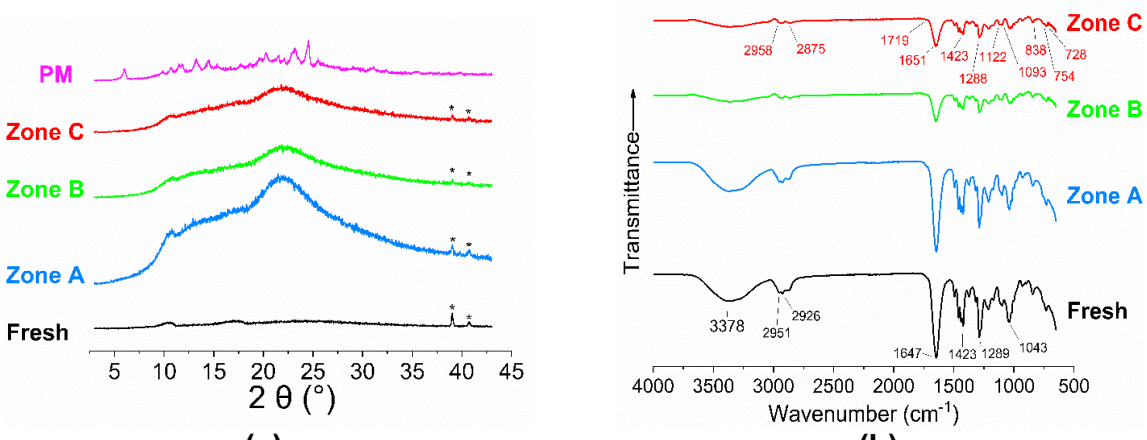

Figure 3.9. Characterisation data obtained on the aged ODF formulation FAV1 (5% w/w AB, 5% w/w VAL). **(a)** XRD data (reflections labelled with * correspond to the sample holder); **(b)** FTIR data.

3.4 Conclusion

The aim of this study was to utilize solvent film casting to prepare an FDC fast-dissolving drug delivery systems in the form of an ODF. We were able to develop ODFs with drug loadings between 5% and 30% w/w. Two types of formulation were made, loaded either with a single drug (valsartan or amlodipine besylate), or both. Characterisation of the ODF by scanning electron microscopy showed most to have smooth surfaces, but increasing the loading of both drugs to a total of 60% w/w in FAV3 resulted in phase separation of the APIs from the polymer, which can be seen from both SEM images and digital photographs. The ODFs obtained had thicknesses between 167 and 937 μm. Folding endurance was acceptable for all the AB loaded formulations FA1 - FA3, and the low drug loading formulation FV1; however, at very high drug loadings of VAL in FV3 the flexibility of the formulation was very low. Similarly, an increase of drug loading in the FDC formulations led to more brittle formulations. FTIR studies revealed intermolecular interactions between AB, VAL, and the carrier polymer PVP and glycerol were present after film casting. X-ray diffraction and differential scanning calorimetry showed the majority of the formulations to comprise amorphous solid dispersions. Entrapment efficiencies were very good at 100% in all cases. In vitro drug release from the ODF formulation FAV1, which was able to release >90% of the loaded drug within 6 minutes, that was very slower time than the expected from fast dissolving ODFs. The FAV1 FDC showed good storage at different temperature. In summary, while solvent film casting could be optimised to construct FDC formulations, the performance of most did not meet the required standards for fast dissolving ODFs. As a result, an alternative manufacturing technique will be explored in the next chapter.

3.5 References

Abed, K.K., Hussein, A.A., Ghareeb, M.M. and Abdulrasool, A.A., 2010. Formulation and optimization of orodispersible tablets of diazepam. AAPS PharmSciTech, 11(1), pp.356-361.

Ahmed, I.S. and Aboul-Einien, M.H., 2007. In vitro and in vivo evaluation of a fast-disintegrating lyophilized dry emulsion tablet containing griseofulvin. European Journal of Pharmaceutical Sciences, 32(1), pp.58-68.

Aroon, M.A., Ismail, A.F., Montazer-Rahmati, M.M. and Matsuura, T., 2010. Morphology and permeation properties of polysulfone membranes for gas separation: Effects of non-solvent additives and co-solvent. Separation and Purification Technology, 72(2), pp.194-202.

Bala, R., Pawar, P., Khanna, S. and Arora, S., 2013. Orally dissolving strips: A new approach to oral drug delivery system. International Journal of Pharmaceutical Investigation, 3(2), p.67.

Balqis, A.I., Khaizura, M.N., Russly, A.R. and Hanani, Z.N., 2017. Effects of plasticizers on the physicochemical properties of kappa-carrageenan films extracted from Eucheuma cottonii. International Journal of Biological Macromolecules, 103, pp.721-732.

Borges, A.F., Silva, C., Coelho, J.F. and Simões, S., 2015a. Oral films: current status and future perspectives: I—galenical development and quality attributes. Journal of Controlled Release, 206, pp.1-19.

Borges, A.F., Silva, C., Coelho, J.F. and Simões, S., 2015b. Oral films: Current status and future perspectives II—Intellectual property, technologies and market needs. J. Control. Release, 206, pp.108-121.

Buera, M.D.P., Levi, G. and Karel, M., 1992. Glass transition in poly (vinylpyrrolidone): effect of molecular weight and diluents. Biotechnology Progress, 8(2), pp.144-148.

Brniak, W., Maślak, E. and Jachowicz, R., 2015. Orodispersible films and tablets with prednisolone microparticles. European Journal of Pharmaceutical Sciences, 75, pp.81-90.

Broman, E., Khoo, C. and Taylor, L.S., 2001. A comparison of alternative polymer excipients and processing methods for making solid dispersions of a poorly water soluble drug. International Journal of Pharmaceutics, 222(1), pp.139-151.

Center for Drug Evaluation and Research (CEDR), (2008), Center for Drug Evaluation and Research (CEDR) Guidance for Industry Orally Disintegrating Tablets U.S. Department of Health and Human Services, U.S. Food and Drug Administration (2008).

Chella, N., Daravath, B., Kumar, D. and Tadikonda, R.R., 2015. Formulation and Pharmacokinetic Evaluation of Polymeric Dispersions Containing Valsartan. European Journal of Drug Metabolism and Pharmacokinetics, pp.1-10.

Dabbagh, M.A., Ford, J.L., Rubinstein, M.H., Hogan, J.E. and Rajabi-Siahboomi, A.R., 1999. Release of propranolol hydrochloride from matrix tablets containing sodium carboxymethylcellulose and hydroxypropylmethylcellulose. Pharmaceutical Development and Ttechnology, 4(3), pp.313-324.

Dixit, R.P. and Puthli, S.P., 2009. Oral strip technology: Overview and future potential. Journal of Controlled Release, 139(2), pp.94-107.

Garsuch, V. and Breitkreutz, J., 2010. Comparative investigations on different polymers for the preparation of fast-dissolving oral films. Journal of Pharmacy and Pharmacology, 62(4), pp.539-545.

Gittings, S., Turnbull, N., Roberts, C.J. and Gershkovich, P., 2014. Dissolution methodology for taste masked oral dosage forms. Journal of Controlled Release, 173, pp.32-42.

Gómez-Siurana, A., Marcilla, A., Beltrán, M., Berenguer, D., Martínez-Castellanos, I. and Menargues, S., 2013. TGA/FTIR study of tobacco and glycerol–tobacco mixtures. Thermochimica acta, 573, pp.146-157.

Hoffmann, E.M., Breitenbach, A. and Breitkreutz, J., 2011. Advances in orodispersible films for drug delivery. Expert Opinion on Drug Delivery, 8(3), pp.299-316.

Kasliwal, N., Negi, J.S., Jugran, V. and Jain, R., 2011. Formulation, development, and performance evaluation of metoclopramide HCl oro-dispersible sustained release tablet. Archives of Pharmacal Research, 34(10), pp.1691-1700.

Kim, S.J. and Ustunol, Z., 2001. Thermal properties, heat sealability and seal attributes of whey protein isolate/lipid emulsion edible films. Journal of Food Science, 66(7), pp.985-990.

Koradia, V., Lopez de Diego, H., Frydenvang, K., Ringkjøbing-Elema, M., Müllertz, A., Bond, A.D. and Rantanen, J., 2010. Solid forms of amlodipine besylate: physicochemical, structural, and thermodynamic characterization. Crystal Growth & Design, 10(12), pp.5279-5290.

Lai, K.L., Fang, Y., Han, H., Li, Q., Zhang, S., Li, H.Y., Chow, S.F., Lam, T.N. and Lee, W.Y.T., 2018. Orally-dissolving film for sublingual and buccal delivery of ropinirole. Colloids and Surfaces B: Biointerfaces, 163, pp.9-18.

Liew, K.B., Tan, Y.T.F. and Peh, K.K., 2014. Effect of polymer, plasticizer and filler on orally disintegrating film. Drug Development and Industrial Pharmacy, 40(1), pp.110-119.

Low, A.Q.J., Parmentier, J., Khong, Y.M., Chai, C.C.E., Tun, T.Y., Berania, J.E., Liu, X., Gokhale, R. and Chan, S.Y., 2013. Effect of type and ratio of solubilising polymer on characteristics of hot-melt extruded orodispersible films. International Journal of Pharmaceutics, 455(1-2), pp.138-147.

Maheswari, K.M., Devineni, P.K., Deekonda, S., Shaik, S., Uppala, N.P. and Nalluri, B.N., 2014. Development and evaluation of mouth dissolving films of amlodipine besylate for enhanced therapeutic efficacy. Journal of Pharmaceutics, 2014.

Morales, J.O. and McConville, J.T., 2011. Manufacture and characterization of mucoadhesive buccal films. European Journal of Pharmaceutics and Biopharmaceutics, 77(2), pp.187-199.

Plosker, G.L. and Robinson, D.M., 2008. Amlodipine/Valsartan. Drugs, 68(3), pp.373-381.

Rollinger, J. and Burger, A., 2002. Physico-chemical characterization of hydrated and anhydrous crystal forms of amlodipine besylate. Journal of Thermal Analysis and Calorimetry, 68(2), pp.361-372.

Rowe, R.C., Sheskey, P.J. and Owen, S.C. eds., 2006. Handbook of Pharmaceutical Excipients (Vol. 6). London: Pharmaceutical press.

Scarpa, M., Paudel, A., Kloprogge, F., Hsiao, W.K., Bresciani, M., Gaisford, S. and Orlu, M., 2018. Key acceptability attributes of orodispersible films. European Journal of Pharmaceutics and Biopharmaceutics, 125, pp.131-140.

Senta-Loys, Z., Bourgeois, S., Valour, J.P., Briançon, S. and Fessi, H., 2017. Orodispersible films based on amorphous solid dispersions of tetrabenazine. International Journal of Pharmaceutics, 518(1-2), pp.242-252.

Senthilkumar, K. and Vijaya, C., 2015. Formulation development of mouth dissolving film of etoricoxib for pain management. Advances in Pharmaceutics, 2015.

Shenoy, S.L., Bates, W.D., Frisch, H.L. and Wnek, G.E., 2005. Role of chain entanglements on fiber formation during electrospinning of polymer solutions: good solvent, non-specific polymer–polymer interaction limit. Polymer, 46(10), pp.3372-3384.

Simonelli, A.P., Mehta, S.C. and Higuchi, W.I., 1969. Dissolution rates of high energy polyvinylpyrrolidone (PVP)-sulfathiazole coprecipitates. Journal of Pharmaceutical Sciences, 58(5), pp.538-549.

Skotnicki, M., Gaweł, A., Cebe, P. and Pyda, M., 2013. Thermal behaviour and phase identification of Valsartan by standard and temperature-modulated differential scanning calorimetry. Drug Development and Industrial Pharmacy, 39(10), pp.1508-1514.

Van den Mooter, G., Augustijns, P., Blaton, N. and Kinget, R., 1998. Physico-chemical characterization of solid dispersions of temazepam with polyethylene glycol 6000 and PVP K30. International Journal of Pharmaceutics, 164(1), pp.67-80.

Vuddanda, P.R., Mathew, A.P. and Velaga, S., 2016. Electrospun nanofiber mats for ultrafast release of ondansetron. Reactive and Functional Polymers, 99, pp.65-72.

Wang, B., Wang, D., Zhao, S., Huang, X., Zhang, J., Lv, Y., Liu, X., Lv, G. and Ma, X., 2017. Evaluate the ability of PVP to inhibit crystallization of amorphous solid dispersions by density functional theory and experimental verify. European Journal of Pharmaceutical Sciences, 96, pp.45-52.

Wang, J.R., Wang, X., Lu, L. and Mei, X., 2013. Highly crystalline forms of valsartan with superior physicochemical stability. Crystal Growth & Design, 13(7), pp.3261-3269.

Xu, L.L., Shi, L.L., Cao, Q.R., Xu, W.J., Cao, Y., Zhu, X.Y. and Cui, J.H., 2014. Formulation and in vitro characterization of novel sildenafil citrate-loaded polyvinyl alcohol-polyethylene glycol graft copolymer-based orally dissolving films. International Journal of Pharmaceutics, 473(1-2), pp.398-406.

Chapter 4. Electrospun fixed dose formulations of amlodipine besylate and valsartan

4.1 Introduction

In chapter 3, FD-DDS in the form of ODF was prepared by solvent film casting as a conventional non-continuous manufacturing technique. In this chapter, electrospinning was utilised to formulate FD-DDS in the form of electrospun nanofibres loaded with the model drug of amlodipine besylate (AB), or valsartan (VAL), or both drugs combined in the FDC formulations. The electrospun nanofibers were prepared with the aim of improving solubility and the release profile of both drugs from the FDC formulation. The obtained electrospun nanofibres were characterised, and there in vitro performance was evaluated by HPLC as in Celebier et al. (2010).

4.2 Experimental

4.2.1 Solution preparation

10% w/v PVP solutions were prepared in ethanol, with stirring overnight to ensure complete dissolution. Drug-loaded solutions were prepared as detailed in (Table 4.1), by pre-dissolving the required amount of AB or/and VAL in 2 mL of ethanol, then combining this with 5 mL of the PVP solution. Mechanical stirring was applied at room temperature for 20 min until homogeneous solutions were formed. Drug/polymer physical mixtures (PM) were prepared for control purposes.

Table 4.1. The compositions of the spinning solutions.

Formulation		Drug loading (% w/w)	AB loading (mg)	VAL loading (mg)	Ethanol (mL)	PVP (10%w/v)
PVP fibres	PVP	-	-	-	-	5
AB formulations	A1	5	26	-	2	5
	A2	15	88	-	2	5
	A3	30	214	-	2	5
	A4	55	611	-	2	5
VAL formulations	V1	5	-	26	2	5
	V2	15	-	88	2	5
	V3	30	-	214	2	5
	V4	55	-	611	2	5
FDCs	AV1	5 + 5	28.5	28.5	2	5
	AV2	15 + 15	107	107	2	5
	AV3	30 + 30	375	375	2	5

4.2.2 Single-needle electrospinning apparatus setup and development of the fibrous formulation

Polymer solutions were loaded into 5 mL plastic syringes (Terumo, MediSupplies, UK) fitted with stainless steel dispensing needles (20G, 0.61 mm inner diameter, Nordson EFD, UK) with care taken to avoid any air bubbles. The setup of single-needle electrospinning was used for the preparation of the electrospun fibres as presented in (Figure 4.1). A voltage of +15 kV was applied to the needle (spinneret) using a HCP 35-35000 power supply (FuG Elektronik GmbH, Germany). The feed rate of the solution was optimised with a syringe pump (KDS100, Cole Parmer, UK) and was set at 1.3 mL h^{-1}. For each formulation, a batch of 5 mL of the polymeric solution was

dispensed. Electrospinning was carried out under ambient conditions (18 – 23 °C and relative humidity of 26 – 63%). The fibres were collected on a flat grounded collector (15 X 20 cm) covered with aluminium foil and situated 12 cm down under the spinneret tip. After fabrication, the electrospun fibre mats were stored in a vacuum desiccator over silica gel beads to aid evaporation of the remaining organic solvents and moisture.

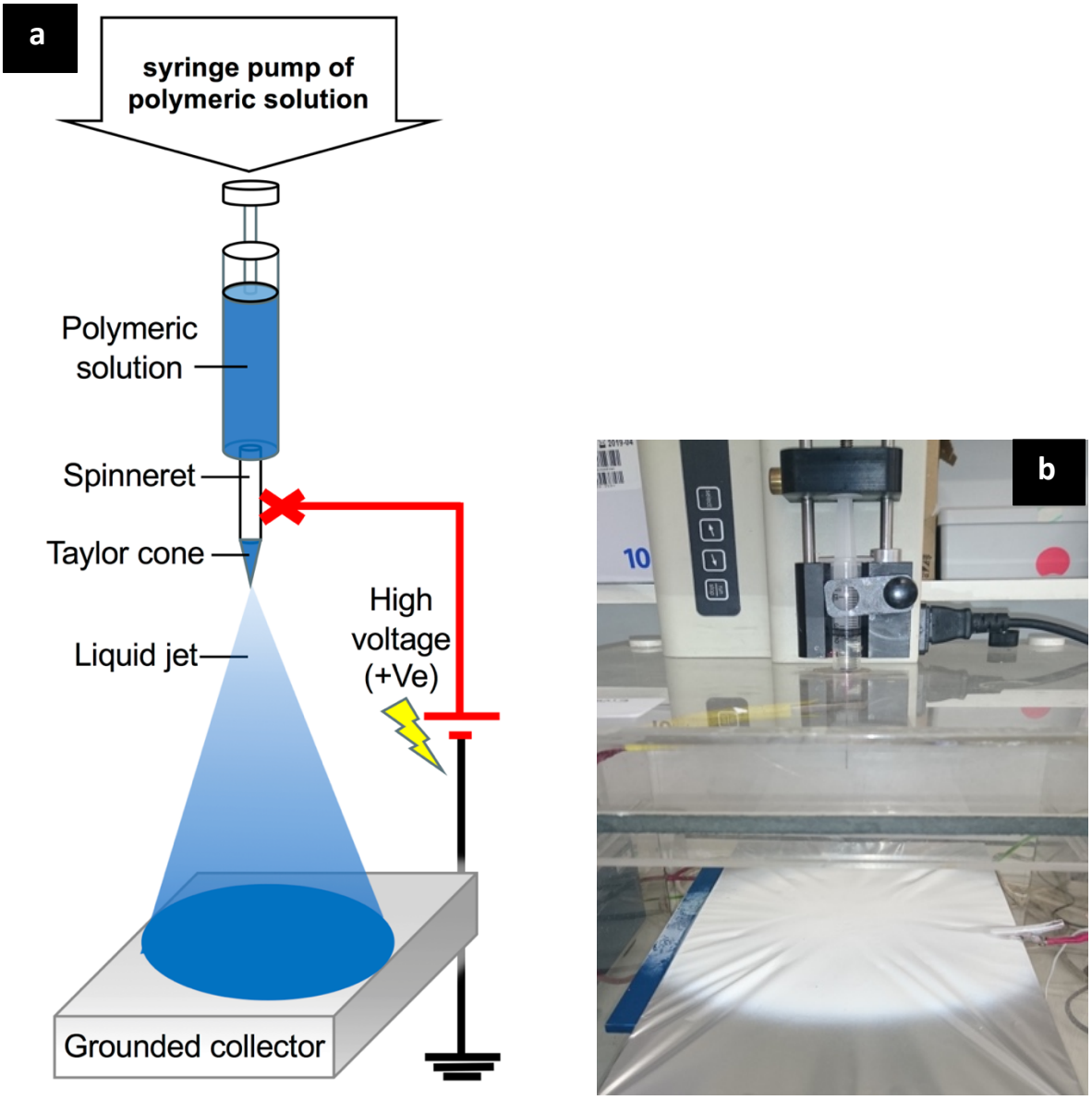

Figure 4.1. (a) A schematic diagram of the single-needle electrospinning process done for each polymeric solution to prepare the electrospun fibres. **(b)** digital image of the collected fibre mat on the flat plate collector.

4.3 Results and discussion

4.3.1 Formulation optimisation

Optimisation of the electrospinning parameters was performed first on the unloaded PVP solution to detect the possibility of electrospinning the chosen polymer and to create a blank fibre. Ethanol was a suitable solvent to dissolve PVP at the desired concentration at 10% w/v, and also 2 mL was able to dissolve the required amount of APIs to be mixed in each formulation. Also, ethanol enabled fast solvent evaporation during the electrospinning process. It was observed with experimental data for polymer/solvent systems that PVP/EtOH polymer estimated initiation of fibres+beads is around a concentration of 3% w/v, and the complete formation of fibres only is around a concentration of 7% w/v (Shenoy et al. 2005). This is due to the need for a minimum polymer concentration for fibre formation, and below this critical value, application of voltage will result in electrospraying or bead formation mainly because of a Rayleigh instability (Shenoy et al. 2005). Therefore, here we aimed to increase the concentration of the polymer solution up to 10% w/v, that was good to reach the critical minimum concentration and allows chain overlapping and entanglements to perform successful electrospinning of the blank PVP fibres.

4.3.2 Morphology

Scanning electron microscope (SEM) images of the nanofibres from all formulations are presented in (Figure 4.2).

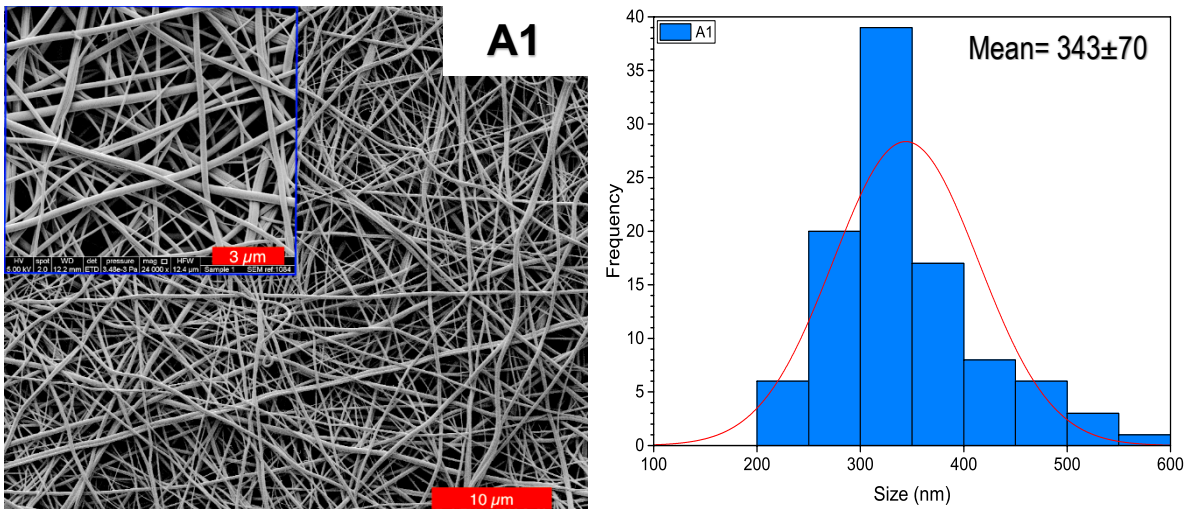
A1
3 μm
10 μm
A1
Mean= 343±70
Frequency
Size (nm)

(a)

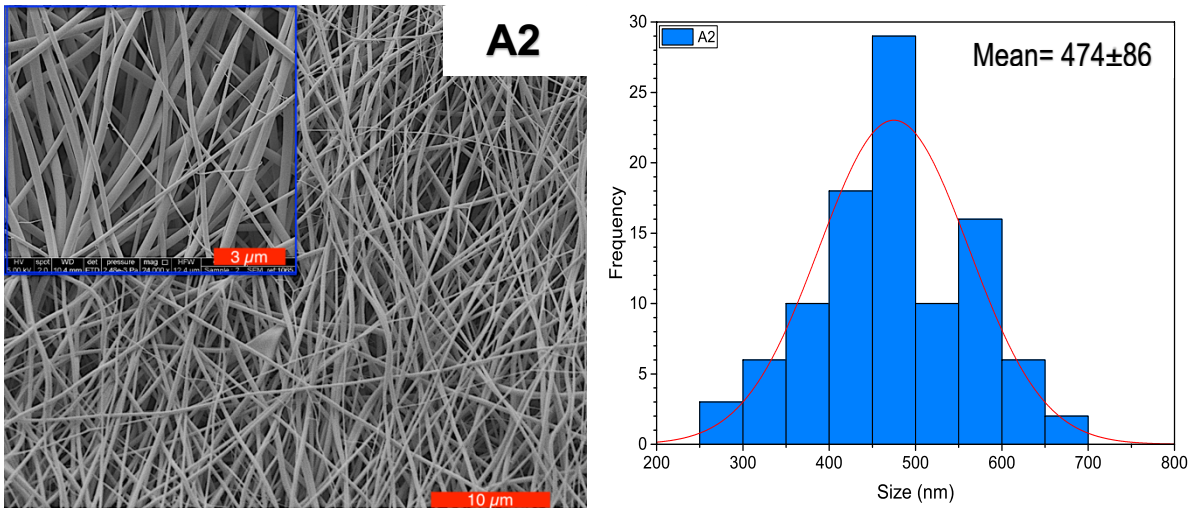
A2
3 μm
10 μm
A2
Mean= 474±86
Frequency
Size (nm)

(b)

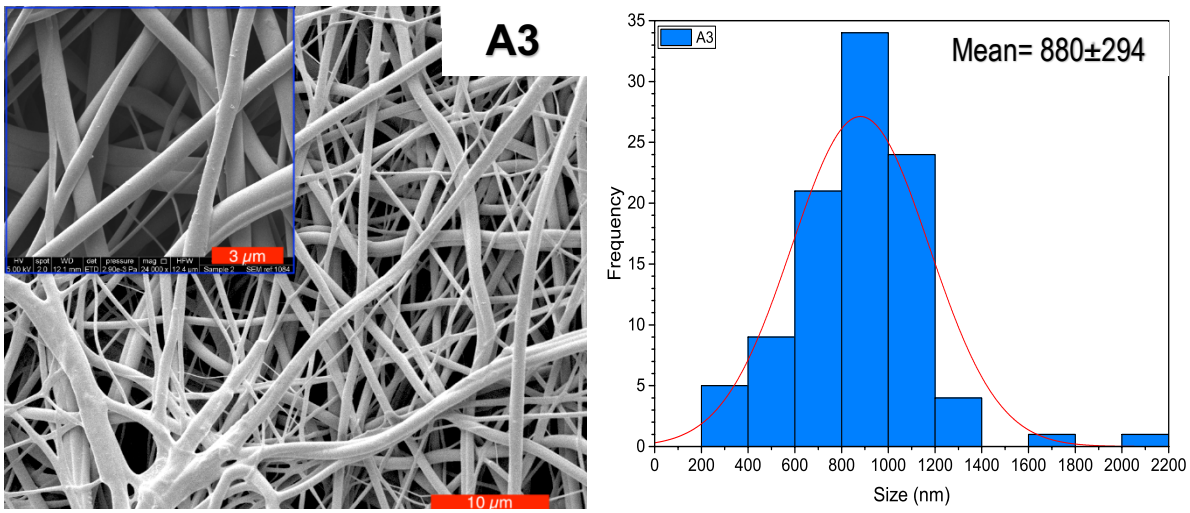
A3
3 μm
10 μm
A3
Mean= 880±294
Frequency
Size (nm)

(c)

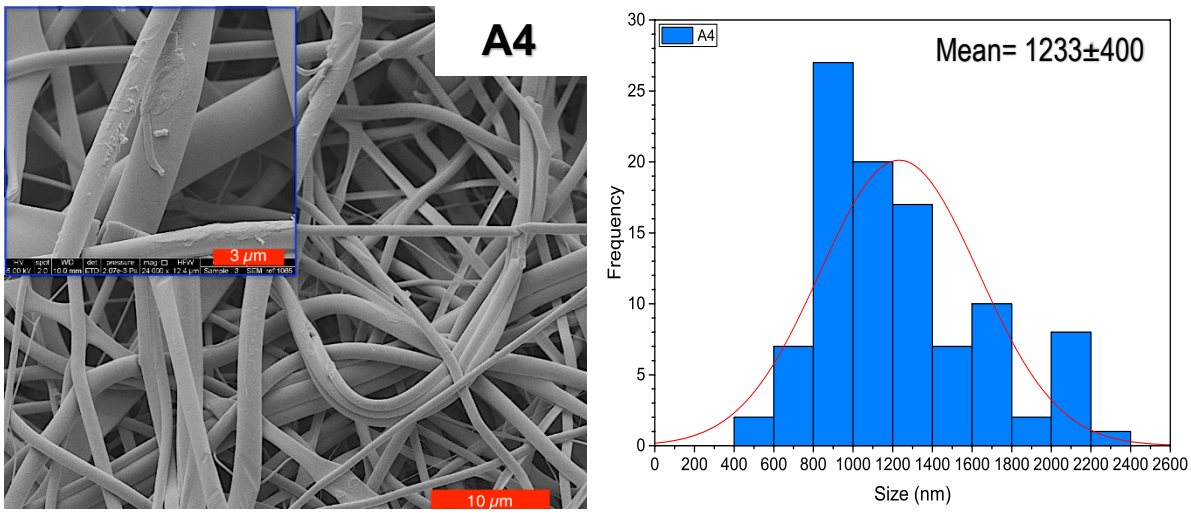
A4
3 μm
10 μm
A4
Mean= 1233±400
Frequency
Size (nm)
0
5
10
15
20
25
30
0
200
400
600
800
1000
1200
1400
1600
1800
2000
2200
2400
2600

(d)

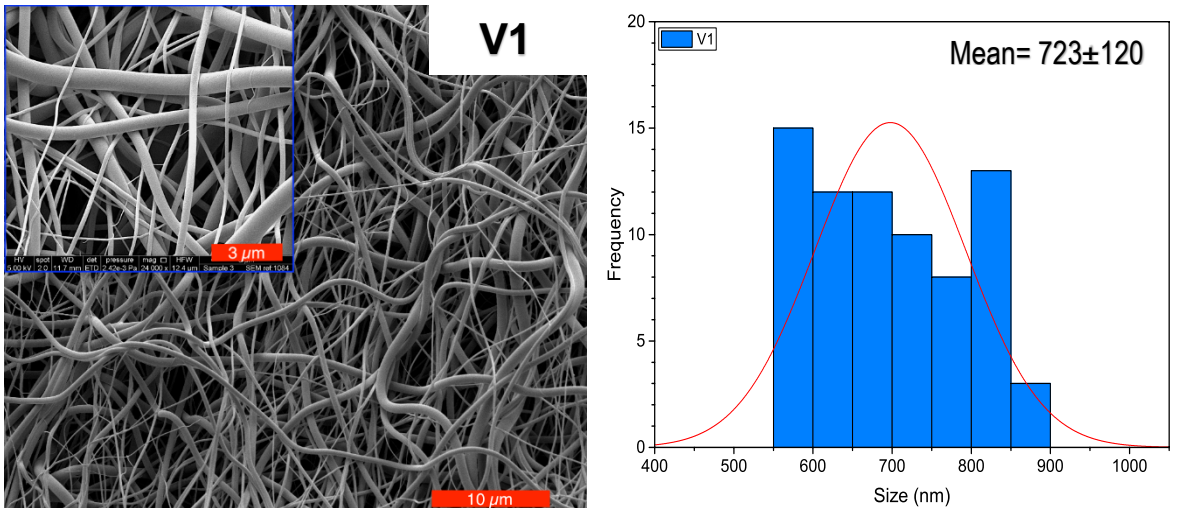
V1
3 μm
10 μm
V1
Mean= 723±120
Frequency
Size (nm)
0
5
10
15
20
400
500
600
700
800
900
1000

(e)

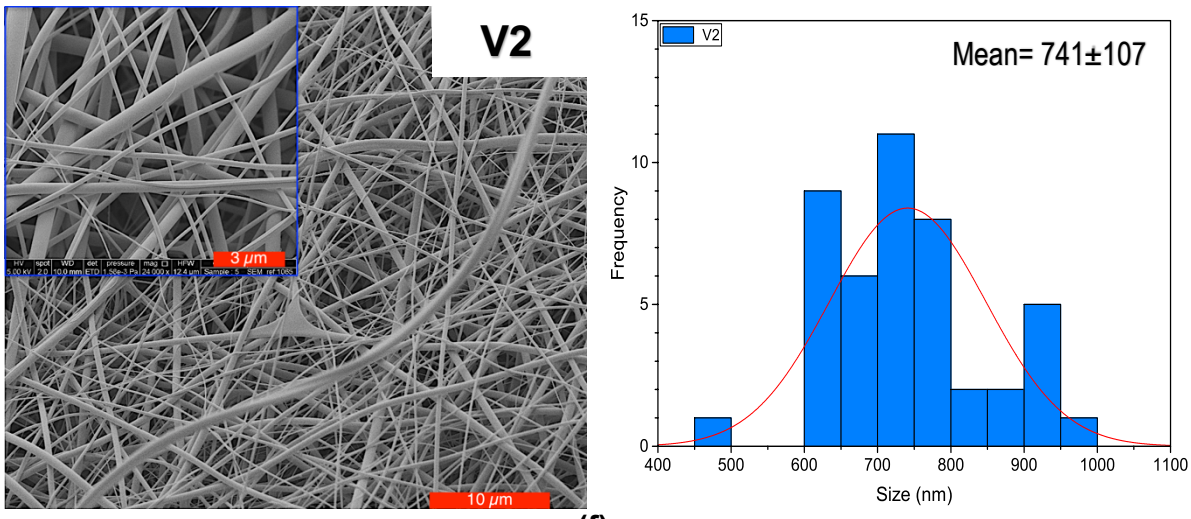
V2
3 μm
10 μm
V2
Mean= 741±107
Frequency
Size (nm)
0
5
10
15
400
500
600
700
800
900
1000
1100

(f)

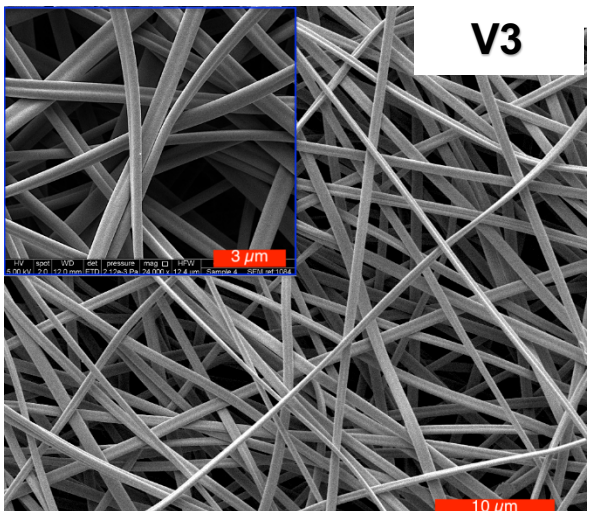
V3
3 μm
10 μm

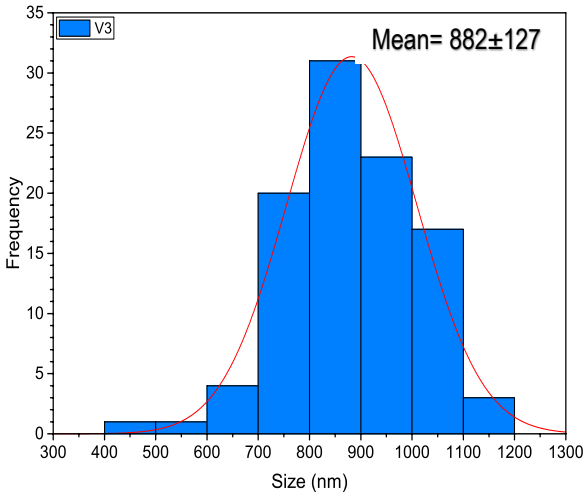
V3
Mean= 882±127
Frequency
Size (nm)

(g)

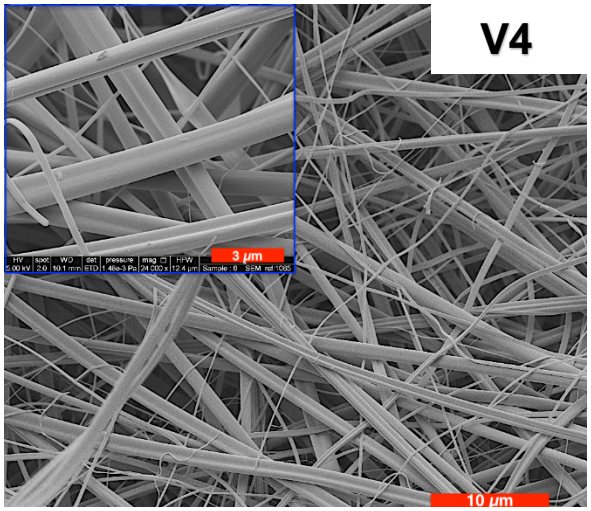
V4
3 μm
10 μm

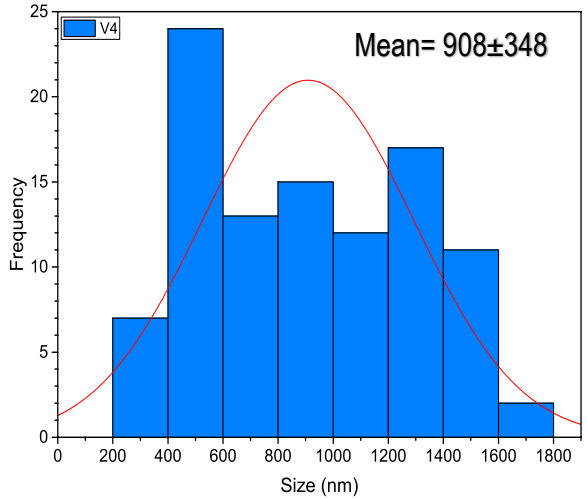
V4
Mean= 908±348
Frequency
Size (nm)

(h)

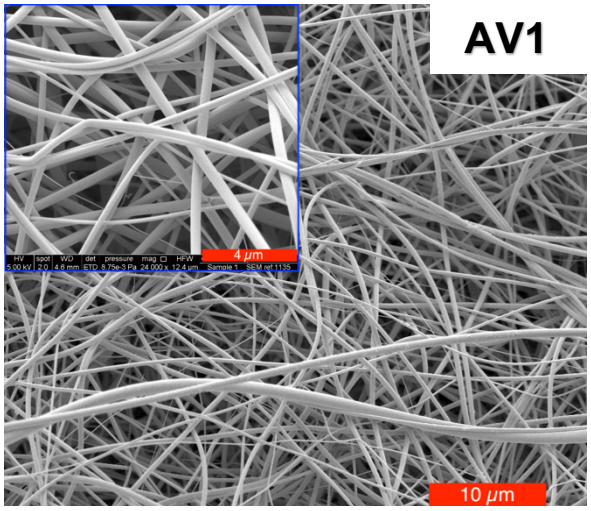
AV1
4 μm
10 μm

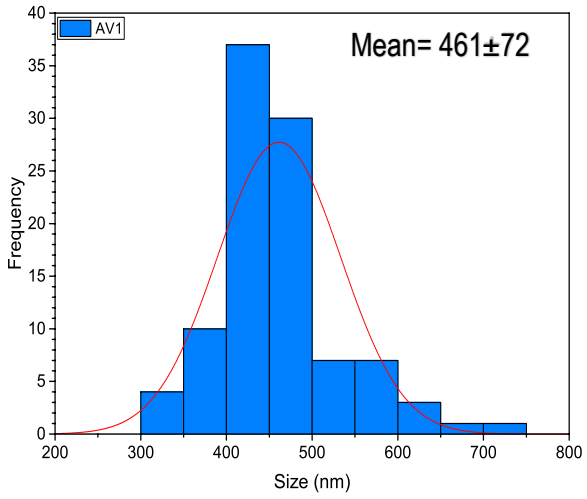
AV1
Mean= 461±72
Frequency
Size (nm)

(i)

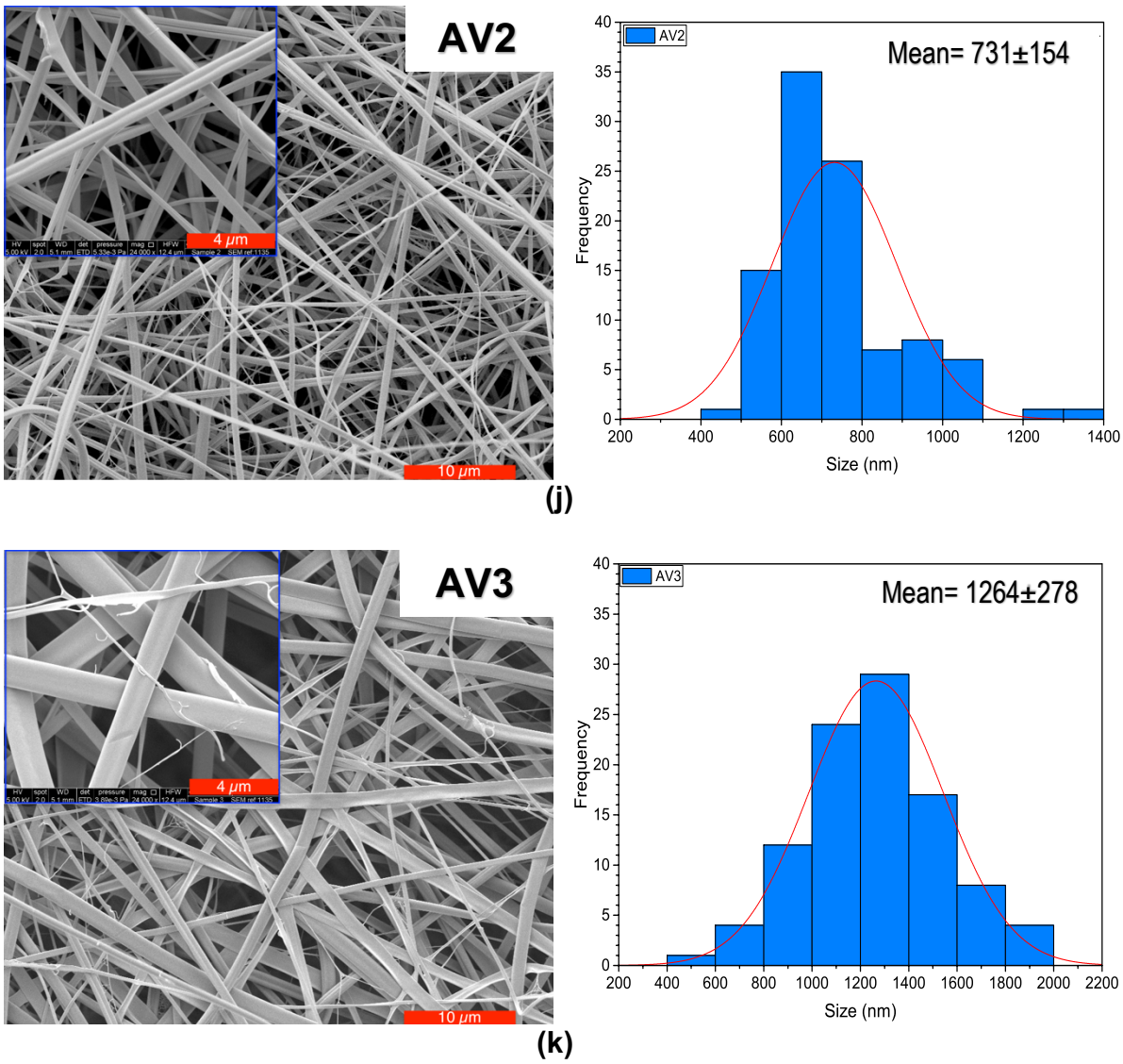

Figure 4.2. SEM images and fibres diameter distributions of the fibre formulations, showing **(a)** A1 (5% w/w AB); **(b)** A2 (15% w/w AB); **(c)** A3 (30% w/w AB); **(d)** A4 (55% w/w AB); **(e)** V1 (5% w/w VAL); **(f)** V2 (15% w/w VAL); **(g)** V3 (30% w/w VAL); **(h)** V4 (55% w/w VAL); **(i)** AV1 (5% w/w AB, 5% w/w VAL); **(j)** AV2 (10% w/w AB, 10% w/w VAL); and, **(k)** AV3 (30% w/w AB, 30% w/w VAL). Scale bars: main images 10 μm.

The images show that fibres have formed in all cases. The AB-loaded fibres A1 to A4 all have smooth cylindrical morphologies, with some small particles visible in A4. In

contrast, the VAL-containing fibres V1 to V4 and AV1 to AV3 change from cylindrical shapes to flattened ribbon-like fibres as the drug loading increases. This may be a result of the solution having high viscosity at the higher loadings, leading to incomplete evaporation and the formation of flattened fibres (Koski et al., 2004). Some precipitation of the drug was also noted during spinning with the higher concentration VAL-containing solutions like in V4 and (AV3 in Figure 4.3). Regardless of this, no drug crystals were seen on the fibre surfaces.

Figure 4.3. Polymeric solution of formulation (AV3= 30+30, % w/w) in 5 mL syringe before electrospinning was applied.

The diameters of the fibres are detailed in Table 4.2. When the drug loading percentage was increased, the fibre diameter raised. This is as expected, since an increase in drug content results in an increase in the amount of mass expelled from the spinneret per unit time and is in good agreement with literature data on the electrospinning of PVP fibres loaded (Illangakoon et al., 2014; Lopez et al., 2014; Yu et al., 2009).

4.3.3 Fibre mat thickness

The thickness of the fibre mats was measured for 4 cm circular cuts taken from different locations of each formulation (Table 4.2). The obtained data showed an increase in thickness for formulations A0 - A4 due to the increasing AB loading (0 - 55%) in their composition . In contrast, with V0 – V4 the thickness of the mat decreased with the increase in VAL loading. In the AV formulations, composed of both AB and VAL, the average mat thickness again increased with the total drug content. These changes in thickness may be attributed to the different morphology of the fibres in each formulation. The AB and AV fibres are generally all cylindrical, except for AV3. In contrast, there was formation of flat ribbon-like fibres with an increasing drug loading in the VAL systems (see formulation V4 and AV3 in Figure 4.2). Inside the fibre mat, the cylindrical fibres occupied a greater vertical bulk compared to the ribbon-like fibres. When increasing the loading of AB from A0 to A4 the fibres became thicker, causing the mat to thicken in turn. In contrast, increasing the VAL loading from V0 to V4 led to more flattened fibres accumulating and a thinner mat. A balance of these factors is operational in the AV systems, resulting overall in a small increase in thickness with the drug loading.

For oral fast dissolving formulations, the optimised film thickness range has been proposed to be between 20-500 μm (Bala et al., 2013). The results in (Table 4.2) show that the mats prepared in this work fall within this range, and suggests there is the flexibility to increase the collection time to produce thicker mats with a larger mass of drug incorporated if required.

4.3.4 Folding endurance

Folding endurance results are reported in Table 4.2. The folding endurance of the fibres decreased with an increase in drug loading, as a result of the fibres becoming more brittle and mechanically weaker (Bölgen et al., 2005). However, all the values obtained for folding endurance were generally high, and in accordance with the literature (Illangakoon et al., 2014). This indicates that all the prepared formulations showed appropriate mechanical properties to find application as oral films.

Table 4.2. Mechanical characteristics of the fibre mats. Diameters are calculated from 100 measurements in ImageJ. Thickness and folding endurance data are from three repeat experiments. All data are presented as mean ±S.D, n=3.

Formulation	Fibre diameter (nm)	Thickness (μm)	Folding endurance (number of folds)
Blank PVP fibres	**-**	320 ± 26	61 ± 2
A1	344 ± 70	338 ± 50	54 ± 15
A2	474 ± 86	340 ± 30	51 ± 10
A3	880 ± 294	352 ± 60	35 ± 4
A4	1230 ± 400	450 ± 100	30 ± 4
V1	724 ± 120	330 ± 51	80 ± 1
V2	741 ± 107	206 ± 20	72 ± 16
V3	882 ± 127	146 ± 25	46 ± 11
V4	909 ± 384	150 ± 10	17 ± 6
AV1	461 ± 72	160 ± 10	80 ± 34
AV2	737 ± 154	210 ± 10	36 ± 4
AV3	1270 ± 278	260 ± 20	17 ± 9

4.3.5 pH change

The electrospun fibres mat was designed to fast dissolve in the oral cavity prior to swallowing. The acceptable pH range of formulations for oral administration should be between pH 5-8 (Jones, 2008). Therefore, it is important to measure the alterations in the pH profile during the dissolution stage. The pH after dissolving the formulation in distilled water of pH 7.00 (at 21.8 °C) was measured and the change in pH was recorded as reported in Table 8, for each formulation. The trend of water pH change by all formulations was from neutral pH 7.00 to weak acid pH, in which the higher drug loading led to more change in pH units. This change in pH by dissolving formulations A1-4 in water was by a range between -1.54 and -1.97 pH units. While the pH change was greater, between -1.94 and -2.67, in the VAL loaded formulations V1-4, ., the change in pH was in the range between -2.14 and -2.43 in the combined-drug AV formulation. The reason for these different changes are likely due to VAL being a weak acid (pKa 4.37), resulting in solutions with pH of between 5.05 to 4.33, and for AV1 - AV3 between 4.86 to 4.33. In contrast, AB (pKa 8.6), as a weak base, did not reduce the pH of A1-A4 below 5. The resultant pH in some cases lay outside the acceptable range of pH 5-8 which may not be appropriate for the buccal mucosa (Aframian et al., 2006). For fast dissolving films, in addition to the active agents, a buffering agent can be added within 0.1-10 % dry weight concentration (Bangalore, 2008), so it can adjust the change in pH as required to bring the pH value closer to the mucosa for safe administration.

Table.4.3. pH of fibers weighing 4 ±0.5 mg dissolved in 100mL deionised water with initial pH of 7.00. The pH after dissolving the formulation in solvent was measured and the change in pH was recorded. Result are given as mean ± S.D. (n=3).

Formulation	New pH of distilled water (pH value after the fibres was fully dissolved)	Change in pH
PVP	6.7 ±0.01	-0.3 ±0.01
A1=5%	5.5 ±0.5	-1.5 ±0.4
A2=15%	5.2 ±0.4	-1.6 ±0.3
A3=30%	5.1 ±0.06	-1.9 ±0.06
A4=55%	5.0 ±0.03	-1.9 ±0.02
V1=5%	5.0 ±0.01	-1.9 ±0.01
V2=15%	4.7 ±0.2	-2.3 ±0.02
V3=30%	4.5 ±0.03	-2.5 ±0.03
V4=55%	4.3 ±0.02	-2.6 ±0.02
AV1=5%	4.8 ±0.04	-2.1 ±0.04
AV2=15%	4.7 ±0.01	-2.3 ±0.01
AV3=30%	4.6 ±0.02	-2.4 ±0.02

4.3.6 Physical form

The physical form of the drug components in the nanofibres was examined by XRD and DSC. The results of XRD are given in (Figure 4.4). The AB pattern displays a series of sharp Bragg reflections in at 2θ: of 5.71°, 11.13°, and 12.87° consistent with its anhydrous form (Koradia et al., 2010). VAL displays some reflections, but these are weak and broad. It is known that it is challenging to prepare highly crystalline VAL, and commercial materials show poor crystallinity (Wang et al., 2013). These XRD

observations are therefore all consistent with the literature. In contrast, PVP is clearly amorphous with only broad haloes in its diffraction pattern.

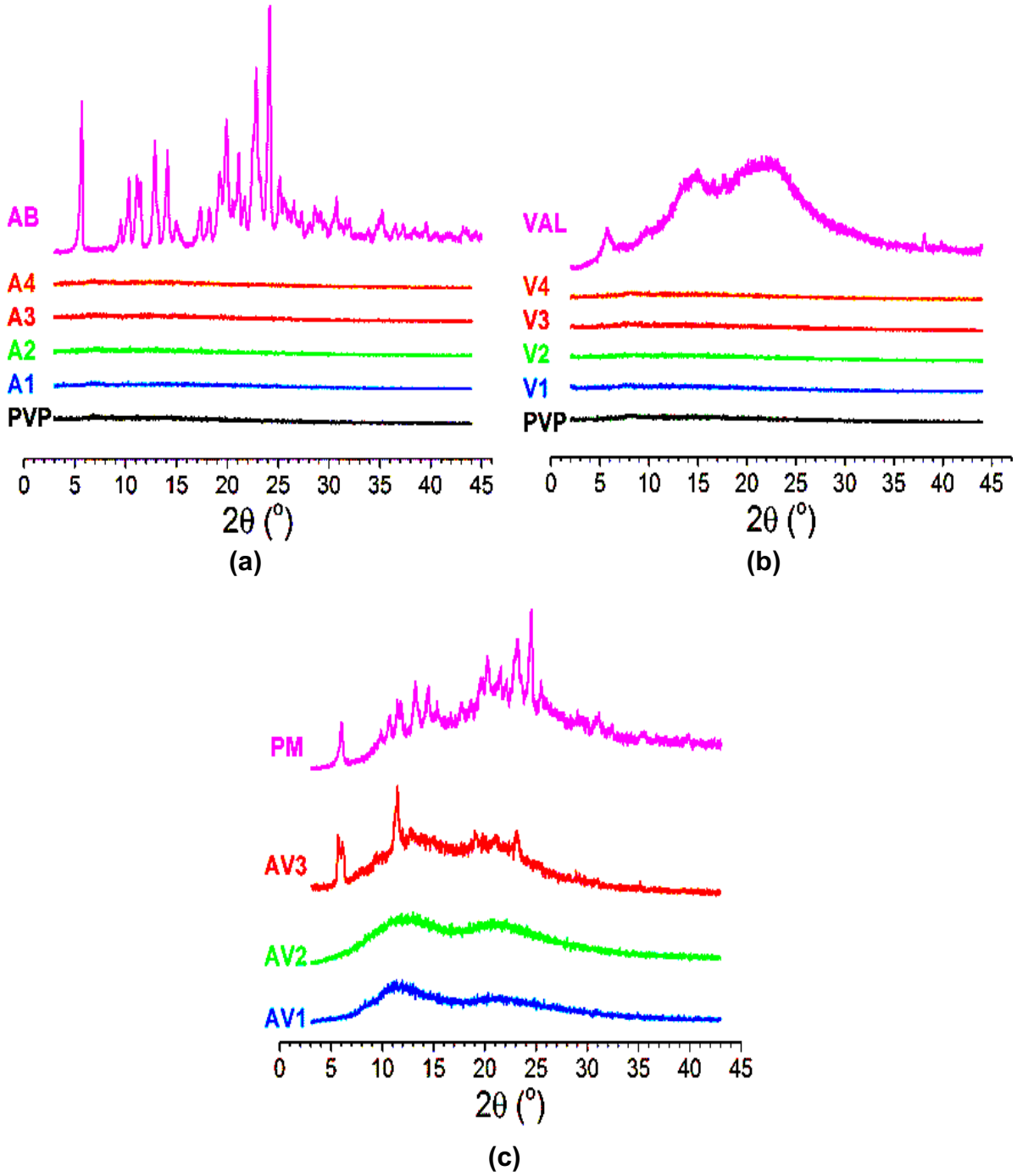

Figure 4.4. XRD diffraction patterns of the nanofibre formulations and raw materials. **(a)** AB-loaded fibres; **(b)** VAL-loaded fibres; and **(c)** AB/VAL dual drug systems. PM: physical mixture (30% AB / 30% VAL / 40% PVP by mass).

All the electrospun fibres loaded with both AB (Figure 4.4, a) and VAL (Figure 4.4, b) showed no Bragg reflections, demonstrating that the fibres comprise amorphous solid dispersions. In the patterns of AV1 and AV2, the characteristic reflections of AB and VAL again disappeared, consistent with the formation of an amorphous system (Figure 4.4, c). The formation of amorphous solid dispersions after electrospinning has been reported by a large number of studies in the literature (Jin et al., 2016; Lopez et al., 2014; Zamani et al., 2013), and arises due to the rapid evaporation of solvent induced by the process. This typically prevents the organisation of molecules into crystalline lattices, and leads to the propagation of the disordered arrangement of molecules of the initial solution into the solid products.

In formulation AV3, however, some characteristic reflections of AB can be seen in the diffraction pattern (Figure 4.4, c), and the formulation's pattern is similar to that of a physical mixture (PM) of AB, VAL and PVP in the same ratios. This indicates that some of the drug in AV3 is crystalline. This result is attributed to the high drug loading in the AV3 system.

The DSC thermograms (Figure 4.5) concurred well with the findings from XRD. The raw materials show sharp melting endothermic peaks for AB at around 206 °C. This is consistent with the literature showing melting onset around 197.5 – 200 °C reported for the crystalline anhydrous form of AB (Rollinger and Burger, 2002). The thermogram data of VAL show a small broad peak between 60-90 ºC corresponding to water loss, then glass transition with a high enthalpy of relaxation at 103 ºC (Skotnicki et al., 2013).

The latter difference agree with the XRD data and can be ascribed to the poor crystallinity of the VAL sample procured for this work. PVP presents a broad endotherm that starts at around 50 °C and finishes at ca. 135 °C, as a result of water loss. There are no melting events visible, as expected since PVP is widely known to be amorphous.

The thermograms of the electrospun fibres showed broad dehydration endotherms between around 30 and 130 °C, but in most cases there are no melting endothermic peaks visible. The loss of characteristic endotherms for A1 to A3, V1 to V4, AV1 and AV2 mean that the drug in the polymer matrix is present in the amorphous form in these fibres (Vigh et al., 2013), in agreement with the XRD data above. There are two exceptions, however. In formulation A4, a small endothermic peak appears at 201 °C, which can be ascribed to AB melting (Silva et al., 2014). Given that XRD does not show any evidence of crystalline material being present in A4, it is thought that recrystallisation must have occurred upon heating in the DSC experiment. There is also a small endotherm at approximately 195 °C in the AV3 formulation, indicating some crystalline AB is melting. This is again consistent with the XRD data, which revealed the presence of some crystalline drug at room temperature.

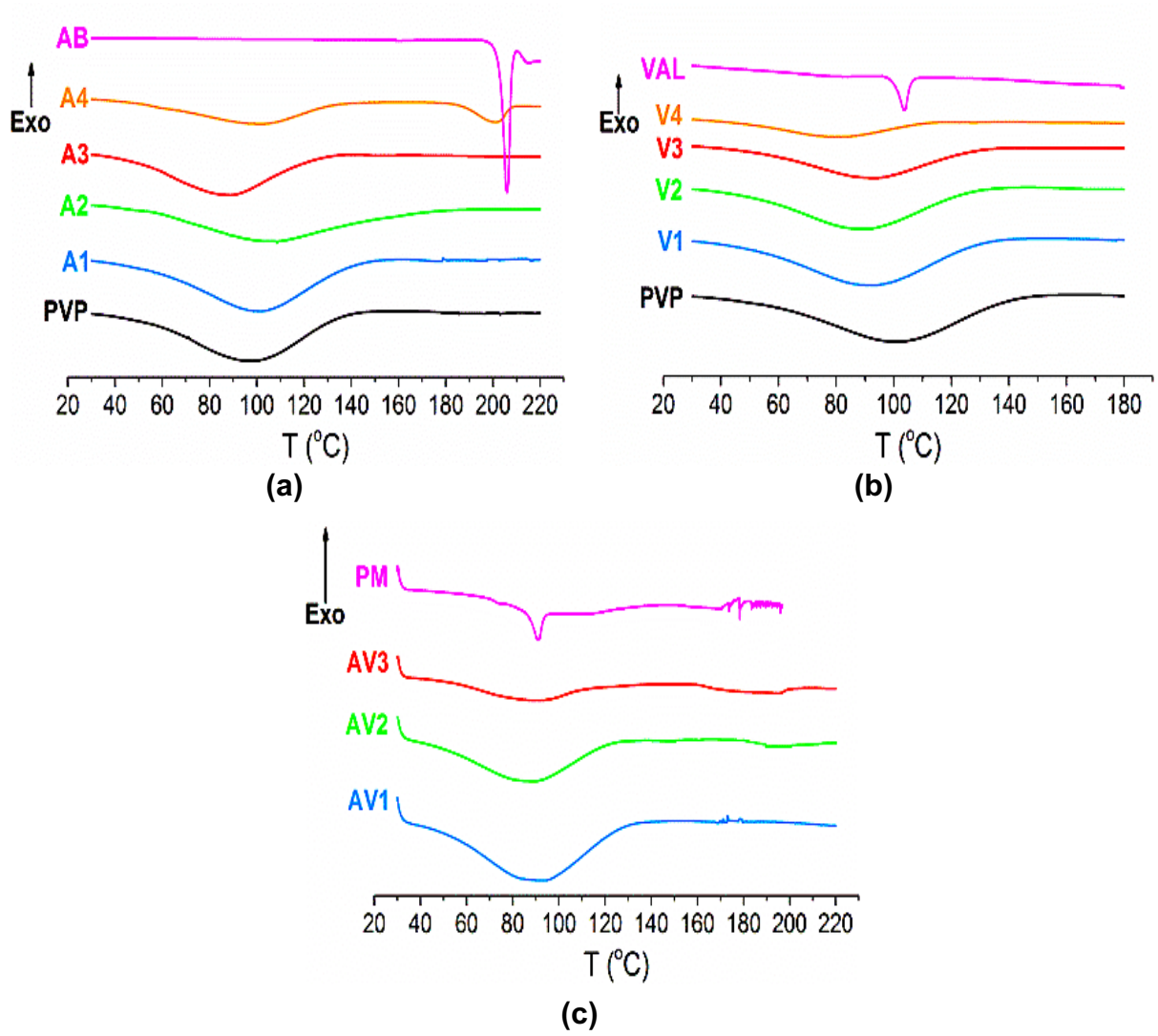

Figure 4.5. Differential scanning calorimetry data for **(a)** AB; **(b)** VAL; and **(c)** the FDC fibres. PM: a physical mixture of AB, VAL, and PVP. PM: physical mixture (30% AB / 30% VAL / 40% PVP by mass).

4.3.7 Infrared spectroscopy

The IR spectra were collected to investigate the drug-polymer interactions and help understand the compatibility of the APIs with the polymer in the fibres. Compatibility is essential for producing high quality and stable nanocomposites to prevent any solid phase separation. The molecular structures of AB and VAL are shown in (Figure 4.6,

a). IR spectra full-length and enlargements of the carboxylate region are given in (Figure 4.6, b - d).

The IR spectrum of AB shows characteristic C=O stretches at 1697cm^{-1} and 1673 cm^{-1}, and a sharp peak at 1089 cm^{-1} with a shoulder at 1114 cm^{-1} from the C-O-C asymmetric stretch. Other peaks are present at 1048 cm-1 (NH3 wagging), at 869 cm-1 (-C-O in-plane bending), and at 753 cm^{-1}, 728 cm^{-1}, and 689 cm^{-1} for (N-H vibrations). The IR spectrum of VAL has characteristic peaks at 3300 cm^{-1} (O-H, and N-H stretching vibrations), and at 2963 cm^{-1} (aromatic CH2 stretching vibration), 1730 cm^{-1} (C=O carbonyl vibration), 1603 cm^{-1} (N-C=O amide carbonyl stretching), and 1451 and 1470 cm^{-1} (aromatic C=C vibrations). Pure PVP shows bands from 3650 – 3050 cm^{-1} (O-H stretches from adsorbed water), 2840 – 3010 cm^{-1} (C-H stretches), 1660 cm^{-1} (C=O) and 1290 cm^{-1} (C-N stretch).

The spectra of the electrospun fibres show significant changes from the raw materials. These are most noticeable in the spectra of the highest drug loading formulations. The AB C=O stretches at 1697 cm^{-1} and 1673 cm^{-1} have both merged into the PVP C=O peak at 1660 cm^{-1}. Similarly, the C-O-C vibration at 1114 cm^{-1} in AB shifts to 1123 cm^{-1} in the fibres. In the spectrum of V4, the VAL peaks present at 1603 cm^{-1} (N-C=O amide carbonyl stretching) and 1470 cm^{-1} (aromatic C=C) for the pure drug are shifted to 1637 cm^{-1} and 1461 cm^{-1}. Similar findings are noted for the FDC fibres.

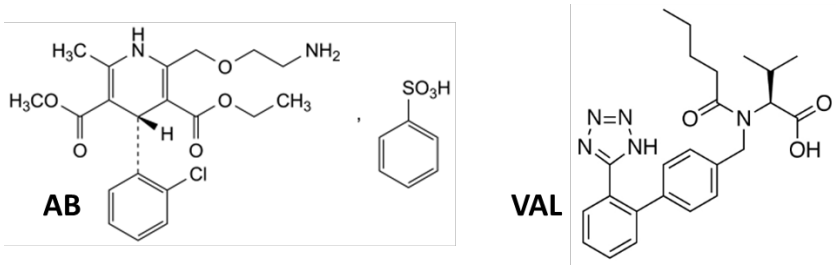
AB
VAL

(a)

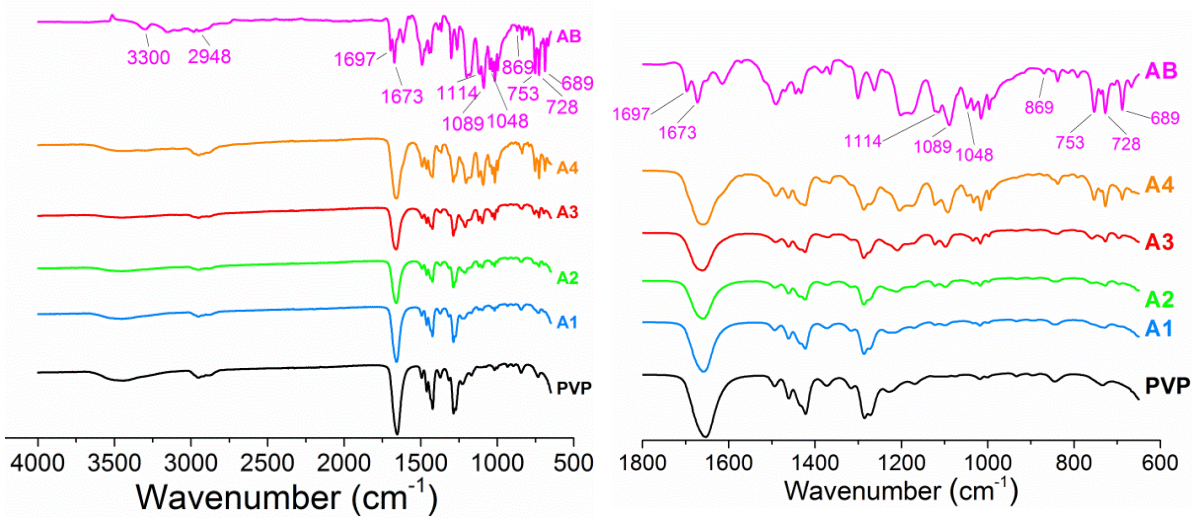
3300
2948
1697
1673
1114
1089
1048
869
753
728
689
AB
A4
A3
A2
A1
PVP
4000 3500 3000 2500 2000 1500 1000 500
Wavenumber (cm-1)
1697
1673
1114
1089
1048
869
753
728
689
1800 1600 1400 1200 1000 800 600
Wavenumber (cm-1)

(b)

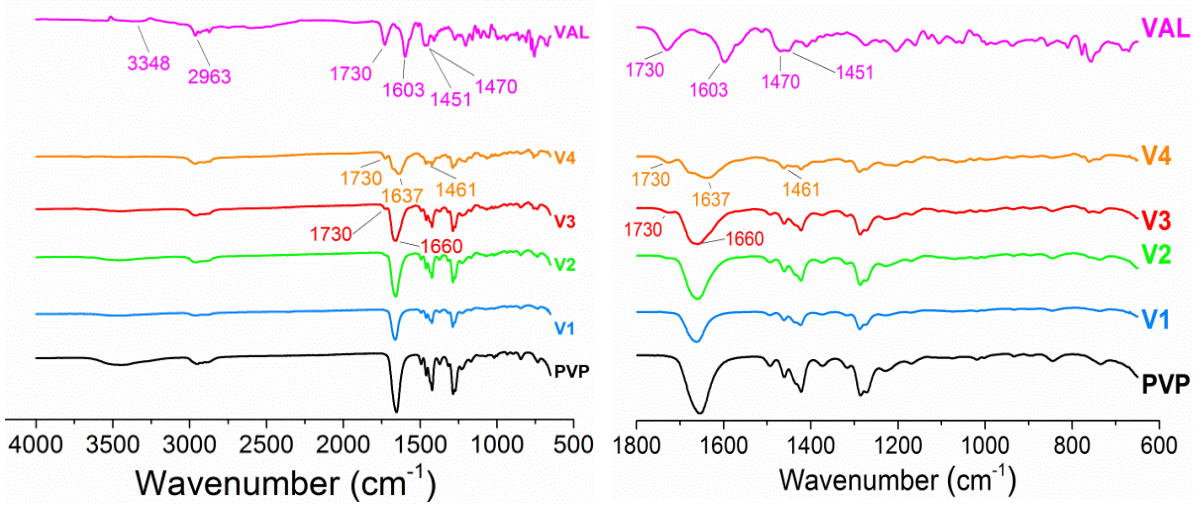
3348
2963
1730
1603
1451
1470
VAL
V4
1730
1637
1461
V3
1730
1660
V2
V1
PVP
4000 3500 3000 2500 2000 1500 1000 500
Wavenumber (cm-1)
1730
1603
1470
1451
1730
1637
1461
1730
1660
1800 1600 1400 1200 1000 800 600
Wavenumber (cm-1)

(c)

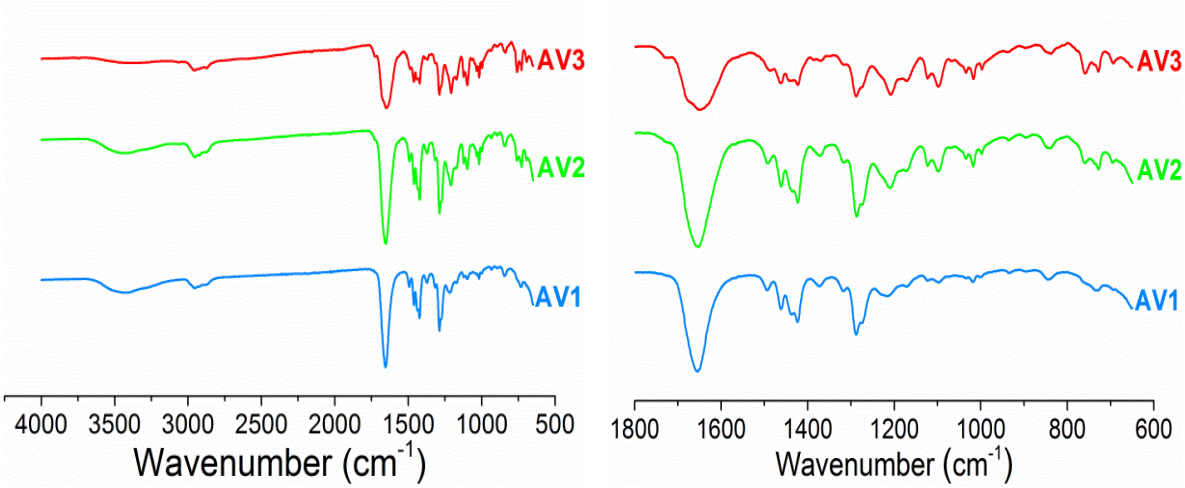

(d)

Figure 4.6. (a) The chemical structures of AB and VAL, together with IR spectra for the **(b)** AB; **(c)** VAL; and, **(d)** FDC fibres.

All these observations indicate the formation of intermolecular bonds between the drugs and PVP (Chen et al., 2008). The formation of interactions like hydrogen bonding and van der Waals interactions, and the other secondary interactions such as electrostatic interactions and hydrophobic interactions, should lead to good compatibility between the components in the fiber mat (Wu et al., 2015) and aid the long term stability of the formulations (Mukherjee et al., 2005).

4.3.8 Drug loading and encapsulation efficiency (EE)

The drug loading in the fibres mat was determined from three samples removed randomly from three different points throughout each formulation. The drug loading were quantified by HPLC (Table 4.4). The EE for all prepared formulations were found to be $\geq$ 86%, with most very close to 100%. This is as expected since there is minimal scope for loss of material in the electrospinning experiment unless there is

precipitation in the syringe. For fast dissolving ODFs this result was acceptable and agrees with the normal range of drug loading EE% between 90 to 110% (Liew et al., 2014).

Table 4.4. The drug loadings and encapsulation efficiencies (EE) of the fibers. Data are reported as mean ± S.D. from three experiments.

Formulation	AB loading (% w/w)	AB EE (%)	VAL loading (% w/w)	VAL EE (%)
A1	5.3 ± 0.3	107.3 ± 5.8	-	-
A2	14.4 ± 0.8	96.2 ± 5.4	-	-
A3	26 ± 3.4	86.8 ± 11.2	-	-
A4	56.6 ± 1.1	102.9 ± 2.1	-	-
V1	-	-	4.5 ± 0.2	90 ± 0.5
V2	-	-	14.8 ± 0.6	98.6 ± 3.9
V3	-	-	29.7 ± 0.2	99 ± 0.8
V4	-	-	54.7 ± 2.3	99.4 ± 4.2
AV1	5.4 ± 0.2	109 ± 5	5.5 ± 0.2	109.6 ± 4
AV2	14.6 ± 0.3	97.1 ± 2.7	14.9 ± 0.5	99.9 ± 3.4
AV3	27 ± 0.4	90 ± 1.4	31.3 ± 0.7	104.4 ± 2.4

4.3.9 Disintegration time

In this study, a minimal volume of artificial simulated saliva was used to simulate the amount of moisture in the mouth and the time taken for disintegration determined for formulation A1 and A3 using a high-speed camera (Figure 4.7). Complete disintegration was observed in < 1 s for A1, and < 3 s for A3. This is slightly slower than previously reported for PVP-based fibres (Illangakoon et al., 2014), but nevertheless very promising for achieving fast dissolving behaviour. Results from

other studies on oral fast dissolving formulations reported a range of disintegration times between 8 and 20 seconds (Cilurzo et al., 2011; Yu et al., 2009).

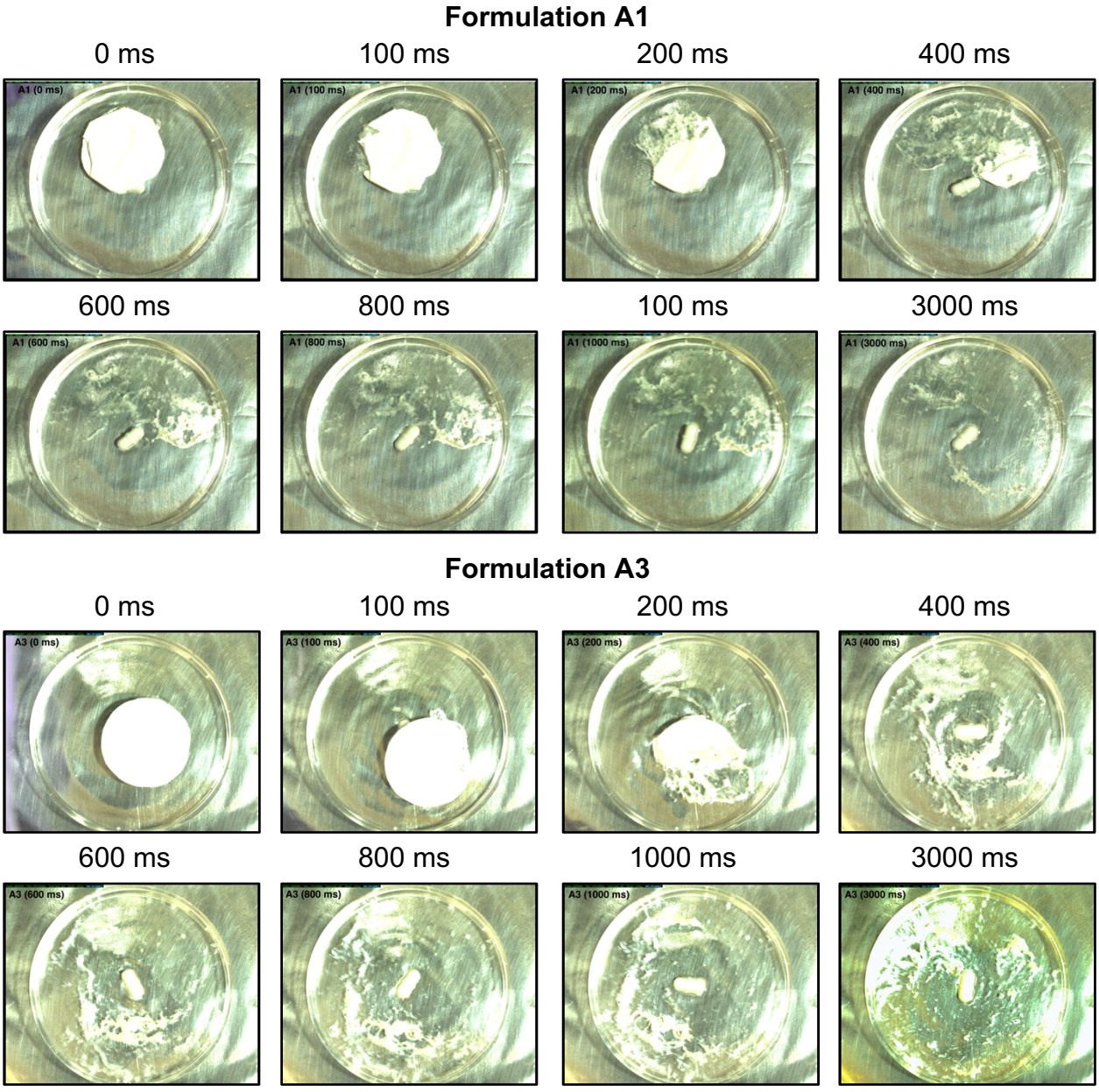

Figure 4.7. High speed camera images of the disintegration of A1 and A3 in simulated saliva.

4.3.10 In-vitro drug release

In-vitro dissolution tests were carried out in artificial simulated saliva. The results are given in Figure 4.8. The release of AB from all its single-drug fibres was very rapid: over 90% of the loading was released after 120 s for A1, A2 and A3, and after 270 s with A4 (Figure 4.8, a). Similar findings were obtained in a study by (Yu et al., 2009) on PVP electrospun fibres loaded with ibuprofen, where an increase in drug loading also extended the release time.

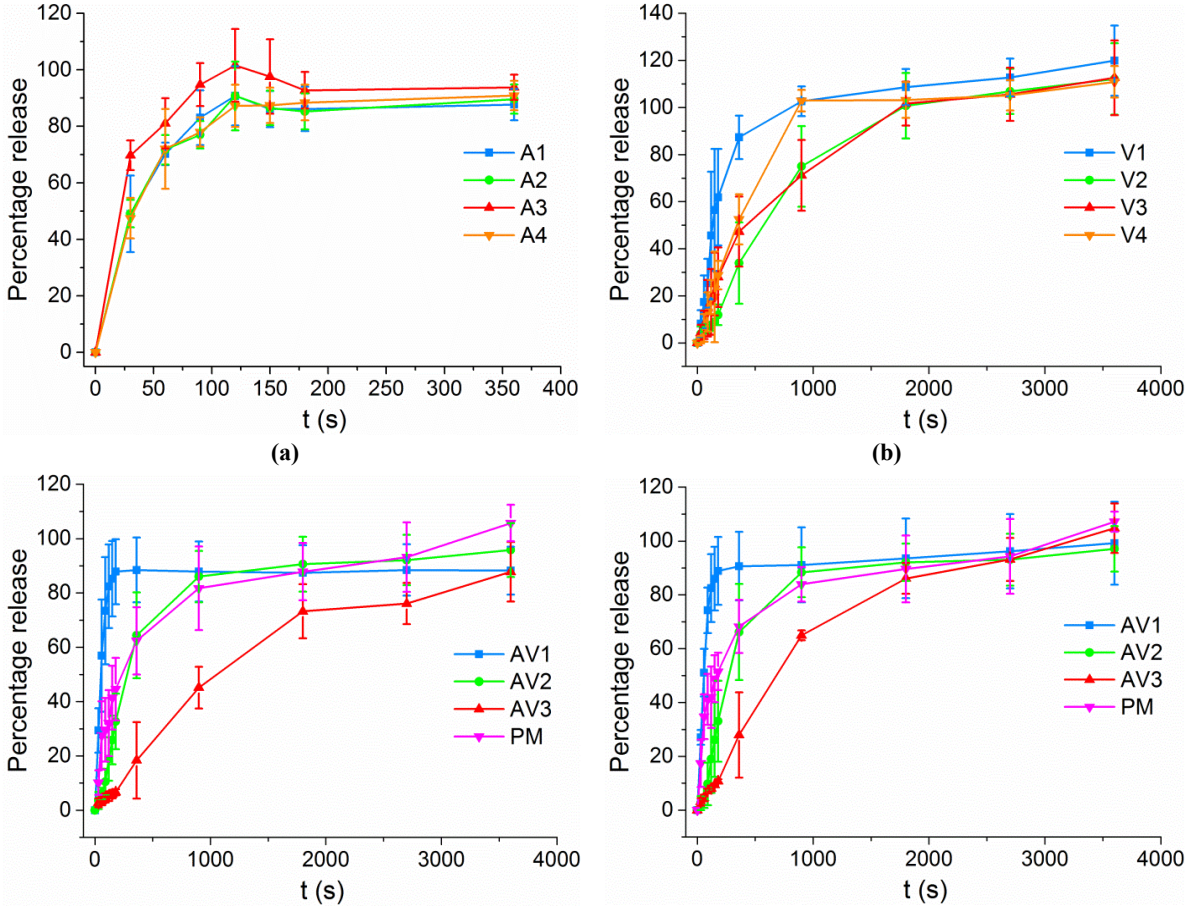

Figure 4.8. *In vitro* dissolution profiles showing **(a)** release of AB from A1 to A4; **(b)** release of VAL from V1 to V4; **(c)** release of AB from the FDC fiber mats; and, **(d)** release of VAL from FDC fibers. PM: physical mixture (30% AB / 30% VAL / 40% PVP by mass).

The release of VAL from V1 – V4 was much slower, however, drug release from V1 reached 90% only after 370 s, slightly over 6 min (Figure 4.8, b). The other VAL formulations were even slower to release, with V4 showed 90% release after 1440 s from the start of the experiment. The key factor controlling release from V1 was the presence of 95% w/w PVP in the fibres, which enhanced the disintegration of the fibres and the dissolving of VAL into solution. As the VAL loading increased, the PVP content in the fibres declined, and thus disintegration and dissolution were observed to slow down. A similar extension in release time was noted with AB from A4, but this is much less significant because AB is a salt and thus has substantially higher solubility than VAL.

In the combined-drug AV formulations, the release profiles of both APIs (Figure 4.8, c & d) were observed to be very similar in each FDC formulation. AV1 showed fast release of both drugs, 88 ± 12% for AB, and 90 ± 13% for VAL by 360 s. This presumably arises because of the high content of the hydrophilic polymer PVP and the molecular dispersion of AB and VAL in AV1. That make AV1 potentially the most appropriate formulation for fabricating fast dissolving FDC formulation with an immediate release of APIs into the oral cavity.

As for the single-drug fibres, an increase in drug loading led to decrease in the rate of drug dissolution In AV2, 90% release of AB was attained only after 1800 s (30 min), and 90% of the VAL content after 900 s. For AV3, the 90% release times > 3600 s for AB and 2190 s for VAL. Therefore, neither AV2 nor AV3 was found to show the fast dissolving behaviour as good as AV1. Indeed, AV3 dissolves more slowly than an analogous physical mixture of the drugs and PVP (Figure 4.8, c & d).

4.3.11 Stability study

Since amorphous materials tend to relax to a crystalline state over time, the storage stability of the fibres was explored. XRD data were recorded on fibres which had been stored only in (zone B) at a desiccator with silica gel, in room temperature 16.5 – 27.5 °C, with relative humidity 33.5 ± 1.6 %, for 4 months (Figure 4.9).

The diffraction data clearly show the bulk of the formulations remain amorphous over this time, and distinct Bragg reflections can only be seen for A4 and AV3. In both of these cases, there is very clear evidence for the recrystallisation of AB. VAL recrystallisation cannot be ascertained, but this is not surprising since VAL is known to be poorly crystalline, and also the presence of ions in AB encourage a more rapid reversion to an ordered form. It appears that phase separation may be starting to occur after 4 months' ageing for A4 and AV3, a phenomenon also noticed by Lopez et al., (2014) upon the ageing of PVP-based fibres.

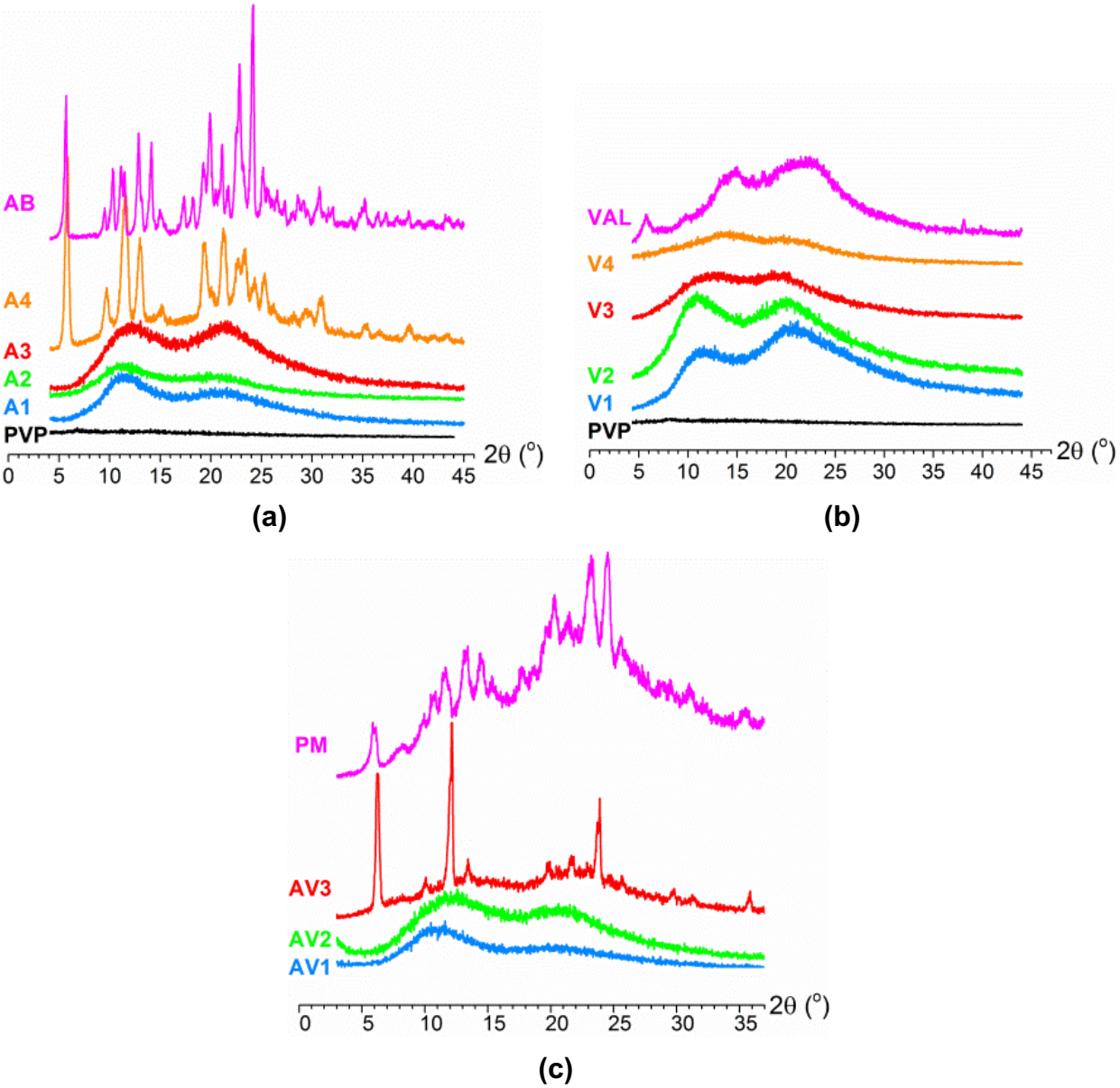

Figure 4.9. Physical characterisation data obtained on aged materials. XRD data are shown for the **(a)** AB; **(b)** VAL; and, **(c)** FDC fibres.

Overall, it is clear from this study that electrospun nanofibers can be loaded with multiple drugs to exhibit fast release in an in vitro dissolution condition mimicking the oral cavity, and that at lower doses the fibres are stable upon storage for at least four months. The drug release profile was found to be dependent on the drug loading, and these results will be helpful to guide future studies aiming to fabricate immediate

release FDC formulations for treating co-morbidities. The fast dissolving feature of the electrospun fibre systems reported here is also expected to increase acceptability for older patients with swallowing difficulties, and hence to lead to higher adherence.

4.4 Conclusions

The aim of this study was to utilize electrospinning to prepare FDC fast-dissolving drug delivery systems. We were able to develop nanofibers with drug loadings between 5% and 55% w/w. Two types of formulation were made, loaded either with a single drug (VAL or AB), or both. The SEM studies showed electrospun fibres most to be cylindrical with smooth surfaces, but with a tendency to flatten with increased valsartan loadings. The fibre mats obtained had thicknesses between 146 and 450 μm, and most showed acceptable folding endurance except at very high drug loadings. FTIR studies revealed intermolecular interactions between AB, VAL, and the polymer PVP in the composite material, and data from XRD and DSC showed the majority of the formulations (except AV3) to comprise amorphous solid dispersions. Encapsulation efficiencies were greater than 85% in all developed electrospun fibre formulations. The fibre mats formulation A1 and A3 disintegrated in under 3 s, indicating they have promise as oral fast-dissolving films. In vitro dissolution studies demonstrated that the amlodipine besylate-loaded fibres released 90% of their drug cargo within 120 s with loadings of 30% w/w and below, or 360 s from 55% w/w formulation. In contrast, the valsartan formulations released their drug cargo much more slowly, with even 5% w/w fibres only reaching 90% release at ca. 360 s, while the 55% w/w fibre required 24 min to reach this point. In the fixed-dose combination fibres, the drug release profile varied markedly with the drug loading. 90% release of both drugs was reached within 360 s

when the loading of each was 5% w/w, but the rate declined for the formulations with higher drug loading significantly. Except for those with the highest drug loadings (55% w/w), the fibres remain amorphous for at least 4 months' after storage in a desiccator.

4.5 References:

Aframian, D.J., Davidowitz, T. and Benoliel, R., 2006. The distribution of oral mucosal pH values in healthy saliva secretors. Oral Diseases, 12(4), pp.420-423.

Bala, R., Pawar, P., Khanna, S. and Arora, S., 2013. Orally dissolving strips: A new approach to oral drug delivery system. International journal of pharmaceutical investigation, 3(2), p.67.

Bangalore, S., Kamalakkannan, G., Parkar, S. and Messerli, F.H., 2007. Fixed-dose combinations improve medication compliance: a meta-analysis. The American journal of Medicine, 120(8), pp.713-719.

Bölgen, N., Menceloğlu, Y.Z., Acatay, K., Vargel, I. and Pişkin, E., 2005. In vitro and in vivo degradation of non-woven materials made of poly (ε-caprolactone) nanofibers prepared by electrospinning under different conditions. Journal of Biomaterials Science, Polymer Edition, 16(12), pp.1537-1555.

Chen, Z., Mo, X., He, C. and Wang, H., 2008. Intermolecular interactions in electrospun collagen–chitosan complex nanofibers. Carbohydrate Polymers, 72(3), pp.410-418.

Cilurzo, F., Cupone, I.E., Minghetti, P., Buratti, S., Gennari, C.G. and Montanari, L., 2011. Diclofenac fast-dissolving film: suppression of bitterness by a taste-sensing system. Drug development and Industrial Pharmacy, 37(3), pp.252-259.

Shenoy, S.L., Bates, W.D., Frisch, H.L. and Wnek, G.E., 2005. Role of chain entanglements on fiber formation during electrospinning of polymer solutions: good solvent, non-specific polymer–polymer interaction limit. Polymer, 46(10), pp.3372-3384.

Koradia, V., Lopez de Diego, H., Frydenvang, K., Ringkjøbing-Elema, M., Müllertz, A., Bond, A.D. and Rantanen, J., 2010. Solid forms of amlodipine besylate: physicochemical, structural, and thermodynamic characterization. Crystal Growth & Design, 10(12), pp.5279-5290.

Koski, A., Yim, K., Shivkumar, S., 2004. Effect of molecular weight on fibrous PVA produced by electrospinning. Mater. Lett. 58, 493–497.

Illangakoon, U.E., Gill, H., Shearman, G.C., Parhizkar, M., Mahalingam, S., Chatterton, N.P. and Williams, G.R., 2014. Fast dissolving paracetamol/caffeine nanofibers prepared by electrospinning. International Journal of Pharmaceutics, 477(1-2), pp.369-379.

Jin, M., Yu, D.G., Geraldes, C.F., Williams, G.R. and Bligh, S.A., 2016. Theranostic fibers for simultaneous imaging and drug delivery. Molecular Pharmaceutics, 13(7), pp.2457-2465.

Jones, D., 2008. Pharmaceutical solutions for oral administration, in: Pharmaceutics: Dosage Form and Design. Pharmaceutical Press, London, pp. 1–24.

Liew, K.B., Tan, Y.T.F. and Peh, K.K., 2014. Effect of polymer, plasticizer and filler on orally disintegrating film. Drug Development and Industrial pharmacy, 40(1), pp.110-119.

Lopez, F.L., Shearman, G.C., Gaisford, S. and Williams, G.R., 2014. Amorphous formulations of indomethacin and griseofulvin prepared by electrospinning. Molecular Pharmaceutics, 11(12), pp.4327-4338.

Mukherjee, B., Mahapatra, S., Gupta, R., Patra, B., Tiwari, A. and Arora, P., 2005. A comparison between povidone-ethylcellulose and povidone-eudragit transdermal dexamethasone matrix patches based on in vitro skin permeation. European Journal of Pharmaceutics and Biopharmaceutics, 59(3), pp.475-483.

Rollinger, J. and Burger, A., 2002. Physico-chemical characterization of hydrated and anhydrous crystal forms of amlodipine besylate. Journal of Thermal Analysis and Calorimetry, 68(2), pp.361-372.

Silva, A.C.M., Gálico, D.A., Guerra, R.B., Perpétuo, G.L., Legendre, A.O., Rinaldo, D. and Bannach, G., 2015. Thermal stability and thermal decomposition of the antihypertensive drug amlodipine besylate. Journal of Thermal Analysis and Calorimetry, 120(1), pp.889-892.

Skotnicki, M., Gaweł, A., Cebe, P. and Pyda, M., 2013. Thermal behaviour and phase identification of Valsartan by standard and temperature-modulated differential scanning calorimetry. Drug Development and Industrial Pharmacy, 39(10), pp.1508-1514.

Vigh, T., Horváthová, T., Balogh, A., Sóti, P.L., Drávavölgyi, G., Nagy, Z.K. and Marosi, G., 2013. Polymer-free and polyvinylpirrolidone-based electrospun solid dosage forms for drug dissolution enhancement. European Journal of Pharmaceutical Sciences, 49(4), pp.595-602.

Wang, J.R., Wang, X., Lu, L. and Mei, X., 2013. Highly crystalline forms of valsartan with superior physicochemical stability. Crystal Growth & Design, 13(7), pp.3261-3269.

Wu, Y.H., Yu, D.G., Li, X.Y., Diao, A.H., Illangakoon, U.E. and Williams, G.R., 2015. Fast-dissolving sweet sedative nanofiber membranes. Journal of Materials Science, 50(10), pp.3604-3613.

Yu, D.G., Shen, X.X., Branford-White, C., White, K., Zhu, L.M. and Bligh, S.A., 2009. Oral fast-dissolving drug delivery membranes prepared from electrospun polyvinylpyrrolidone ultrafine fibers. Nanotechnology, 20(5), p.055104.

Zamani, M., Prabhakaran, M.P. and Ramakrishna, S., 2013. Advances in drug delivery via electrospun and electrosprayed nanomaterials. International Journal of Nanomedicine, 8, p.2997.

Chapter 5. Fixed-dose combinations of ibuprofen, famotidine, and prednisone prepared by electrospinning

5.1 Introduction

In previous chapters, a comparison between the use of different manufacturing techniques to prepare FDC formulations is presented, and electrospinning shown to be able to create an ODF that combines two active pharmaceutical ingredients in the same formulation. The electrospun products further show faster drug release than ODFs prepared with conventional manufacturing techniques. The electrospinning approach used in Chapter 4 employed the most straightforward single-needle experiment. Modification of the setup in single needle electrospinning can open further strategies to fabricate advanced patient-centric drug delivery systems.

The work in this chapter aims to develop advanced FDCs using modified single-needle electrospinning processes. The method will be used to prepare 10% loaded nanofibres in two ways: by sequential electrospinning to produce multilayer fibres (L 10%) and multijet electrospinning to produce tangled fibres (T 10%). The FDC formulations will be prepared using three types of polymers: polyvinylpyrrolidone (PVP), Eudragit L100 (E-L100), and Eudragit RSPO (E-RSPO), with the aim for multiple drug release of three model drug combination in separate doses. The first dose is expected to be from PVP fibres as immediate drug release from the hydrophilic polymer that fast dissolve once contacts solvent of gastric guise. The next dose is expected to be from E-L100 fibres as delayed release triggered by pH change once the formulation reaches to gastro intestinal pH ≥ 6 (jejunum). And the final dose is expected to be from E-RSPO

fibres as extended drug release from the insoluble polymer with low permeability and pH independent swelling.

This formulation can be useful for certain conditions that demand dosing at a certain time of the day to maintain high drug concentration. Rheumatoid Arthritis (RA) is a chronic autoimmune disease, characterised by painful inflammation of joints, muscle, and fibrous tissue associated with stiffness of joints that require medication (World Health Organisation, 2019). In RA the consequences of inflammatory activities over 24-hour cycles lead to varied clinical symptoms. Joint stiffness, pain, and functional disability are common chronic clinical symptoms for rheumatic patients, which usually arises in the early morning at around 4-5 a.m. (Cutolo, 2016). These morning symptoms associate with the increase of pro-inflammatory cytokines at nighttime around 10:00 pm, and when the anti-inflammatory plasma cortisol reach lowest level at early morning (Arvidson et al., 1994; Cutolo et al., 2005). Combining various treatment with different mechanisms of action could increase the efficacy and control the possible side effects. The rationale of loading the APIs in this FDC formulation will focus on two approaches of management RA symptoms commonly disabling older patients.

The first approach aims to reduce the onset of morning joint stiffness for RA patient. The use of low dose exogenous prednisone is recommended replacement therapy of the decreased cortisol level in RA patients (Cutolo, 2016). Studies revealed that a low dose of prednisone administered at night (around 02:00 a.m.) resulted in better effect to reduce morning symptoms compared to a similar dose of conventional immediate release prednisone (around 6-8 a.m.) in the morning (Arvidson et al., 1997). However,

due to the short half-life of the low dose required at a specific time during the night, a delayed-release formulation could be more efficient for limiting the flare of inflammatory cytokines synthesis instead of treating the morning RA clinical symptoms (Maurizio, 2018).

The second approach aims for the management of pain due to inflammation in rheumatoid patients with non-steroidal anti-inflammatory drugs (NSAID). Ibuprofen has dose-dependent effectiveness to control the pain for rheumatic patients (Bello et al, 2015). The significant response for management of pain in rheumatoid arthritis requires a daily dose range of ibuprofen between 1600 to 2400 mg (Grennan et al., 1983). This is a high dose that will increase the risk of side effects like gastric ulcers and erosions and bleeding (Bhala et al., 2013). Therefore, there is a vital requirement of gastroprotection adjunctive therapy to decrease these side effects during long term use of the treatment (Bello, 2012). Famotidine is a histamine 2 (H2) antagonist that successfully combined with ibuprofen for management of the ibuprofen induced ulcer (Rostom et al., 2002). The combination available as an immediate release tablet of (ibuprofen 800 mg + famotidine 26.6 mg) prescribed for oral administration.

The final FDC formulation will be made of electrospun nanofibres loaded with three APIs: prednisone (PRED) as anti-inflammatory glucocorticoids, ibuprofen (IP) as nonsteroidal-anti-inflammatory-drug (NSAID) in high dose, and famotidine (FAM) as a protective agent from the upper gastrointestinal side effects. At separate time, doses of API expected to be released from the FDC as detailed in Table 5.1.

Table 5.1. Multiple drug release from the FDC formulation.

Polymer	Drug release profile	APIs (Dose)		
		Prednisone (5 mg/day)	**Ibuprofen (2400mg/ day)**	**Famotidine (90 mg/day)**
PVP	Immediate drug release	-	1st Dose (800mg)	1st Dose (30 mg)
E-L100	Delayed drug release at pH>6 (jejunum)	Full dose (10 mg /day)	2nd Dose (800mg)	2nd Dose (30 mg)
E-RSPO	Extended drug release	-	3rd Dose (800mg)	3rd Dose (30 mg)

5.2 Experimental

5.2.1 Solution preparation

To prepare all formulations, three base polymer solutions were used. These comprised 20% w/v (PVP; MW 360,000 Da) in ethanol, and 20% w/v Eudragit L100 (E-L100; MW 135,000 Da) or 50% w/v Eudragit RSPO (E-RSPO; MW 15,000 Da) in a solvent mixture of 8:2 (v/v) ethanol : dimethylacetamide (DMAc). The drug loading in the formulations was varied by mixing the required volume of polymer solution with a solution of APIs in methanol as detailed in (Table 5.2). Mechanical stirring was performed at room temperature for at least 6 hours, until a homogeneous solution was obtained.

Table 5.2. The compositions of the electrospinning solutions.

Formulation (ID)	Polymer solution volume (mL)		Drug loading (% w/w) Theoretical value			Drug mass (mg) in 1 mL methanol		
			IP	FAM	PRED	IP	FAM	PRED
PVP mono-layer (PVP ML)	PVP (20% w/v)	10.35	8.7	1.3	—	200.4	31.3	—
E-RSPO mono-layer (E-RSPO ML)	E-RSPO (50% w/v)	4.14	8.7	1.3	—	200.9	29.9	—
E-L100 mono-layer (E-L100 ML)	E-L100 (20% w/v	10.8	8.3	1.25	0.4	201.2	31.6	11
Multi-layer fibres L (10%)	PVP (20% w/v)	10.35	8.57	1.28	0.14	200.6	32	—
	E-RSPO (50% w/v)	4.14				200.6	30.2	—
	E-L100 (20% w/v	10.8				201.7	29.8	11.1
Tangled fibres T (10%)	PVP (20% w/v)	10.35	8.57	1.28	0.14	200.6	32	—
	E-RSPO (50% w/v)	4.14				200.6	30.2	—
	E-L100 (20% w/v	10.8				201.7	29.8	11.1

5.2.2 Development of the FDC formulation

The FDC formulations were developed in a sequence of steps. First, single-needle electrospinning was used to prepare mono-layer (ML) nanofibre mats, made from the individual drug-loaded polymer solutions (Table 5.2). The electrospinning parameters

were optimised to find the best electrospinning conditions for each polymer solution, before multi-solution processing was undertaken.

5.2.2.1 Apparatus setup

The single-needle electrospinning apparatus used was similar for each of the three polymer solutions and is shown in (Figure 5.1, a). Each polymer solution was loaded into a plastic syringe (BD plastic, MediSupplies, UK) with care taken to avoid any air bubbles. All syringes were fitted with a spinneret (stainless steel needle, 20G, 0.61mm inner diameter, Nordson EFD, UK). Fibres were collected on a grounded collector comprising a cylindrical mandrel of 7.64 cm diameter and 23.5 cm length, set to a rotation rate of 400 rpm. This gives a surface velocity of 1.6 m/s and allows enough time for fibres deposition on the collector without dispersion of the liquid-jet, which can arise due to short contact times at higher speeds (Wang et al., 2017) and leads to liquid jet breaking (Pan et al., 2006). Fibres collection was restricted to a central area of 6 cm width covered with aluminium foil, and both side areas were covered with a thick layer of parafilm as an insulator to limit fibre deposition (Figure 5.1, b).

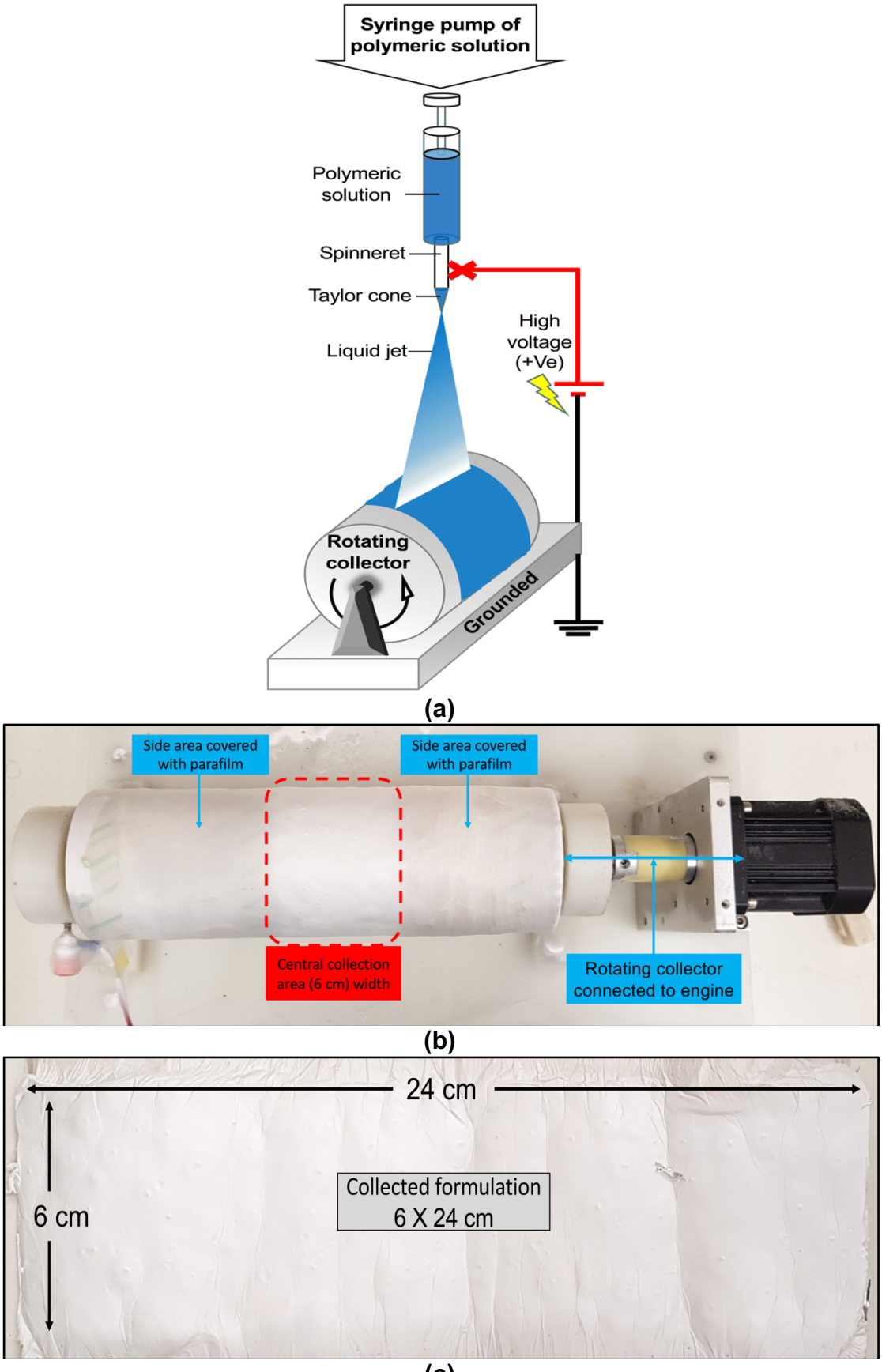

Figure 5.1. (a) A schematic diagram of the single-needle electrospinning process; **(b)** digital image of the collected fibre mat on the rotating collector; **(c)** Image of the collected fibres removed from the rotating collector.

Optimisation of the electrospinning parameters was performed under bright light (MULTI LED PT 24 High power LEDs, 84 Watt, 24 Volt, GSVitec, Germany) focused on the tip of the spinneret. This allowed us to observe the start of Taylor cone formation, and ensure that continuous liquid jets of fibres are produced. The optimisation of the electrospinning process took place in ambient conditions of 19 to 25 ºC, and 31 to 46 % RH. The electrospinning parameters were optimised to find the most appropriate flow rate, voltage, and spinneret to collector distance. The range of electrospinning parameters explored for each solution is listed in (Table 5.3).

Table 5.3. The range of parameters used for single-needle electrospinning of each polymer solution.

Polymer solution	Syringe pump flow rate (mL/hr)	Applied voltage (kV)	Spinneret to collector distance (cm)
PVP (20% w/v)	Range= 1.2 - 4 Best value= 4	Range= 15-23 Best value= 20	Range= 15-20 Best value= 15
Eudragit L100 (20% w/v)	Range= 1 - 4 Best value= 4	Range= 14-26 Best value= 18	Range= 10-16 Best value= 15
Eudragit RSPO (50% w/v)	Range= 1 - 4 Best value= 2	Range= 18-22 Best value= 22	Range= 10-16 Best value= 15

5.2.2.2 Sequential electrospinning

The first FDC formulation was prepared by sequential electrospinning of the three polymer solutions to produce multilayer electrospun nanofibers mats (Figure 5.2). The composition of the layers is described in (Table 5.2). To prepare the FDC by sequential electrospinning, collection of fibres on the rotating collector occurred in three stages to produce a multilayer nanofiber mat constructed as follows: A- PVP 20% w/v (first

layer), B- Eudragit RSPO 50% w/v (central layer), C- Eudragit L100 20% w/v (third layer). The process of sequential electrospinning for each solution was performed at the best value of flow rate, applied voltage, and distance as in (Table 5.3). The full volume of each polymer solution mixture as listed in (Table 5.2) was fully collected to prepare each layer of fibres until the syringe was empty. The multilayer fibres formulation (L %10) were all collected sequentially without drying time between layers, and then all the formulation was collected at the end of electrospinning all polymeric solutions by removing the formulation with the aluminium foil raped around the collector. The multilayer fibres were removed away from the aluminium foil and stored in a desiccator at room temperature to remove any remaining solvent.

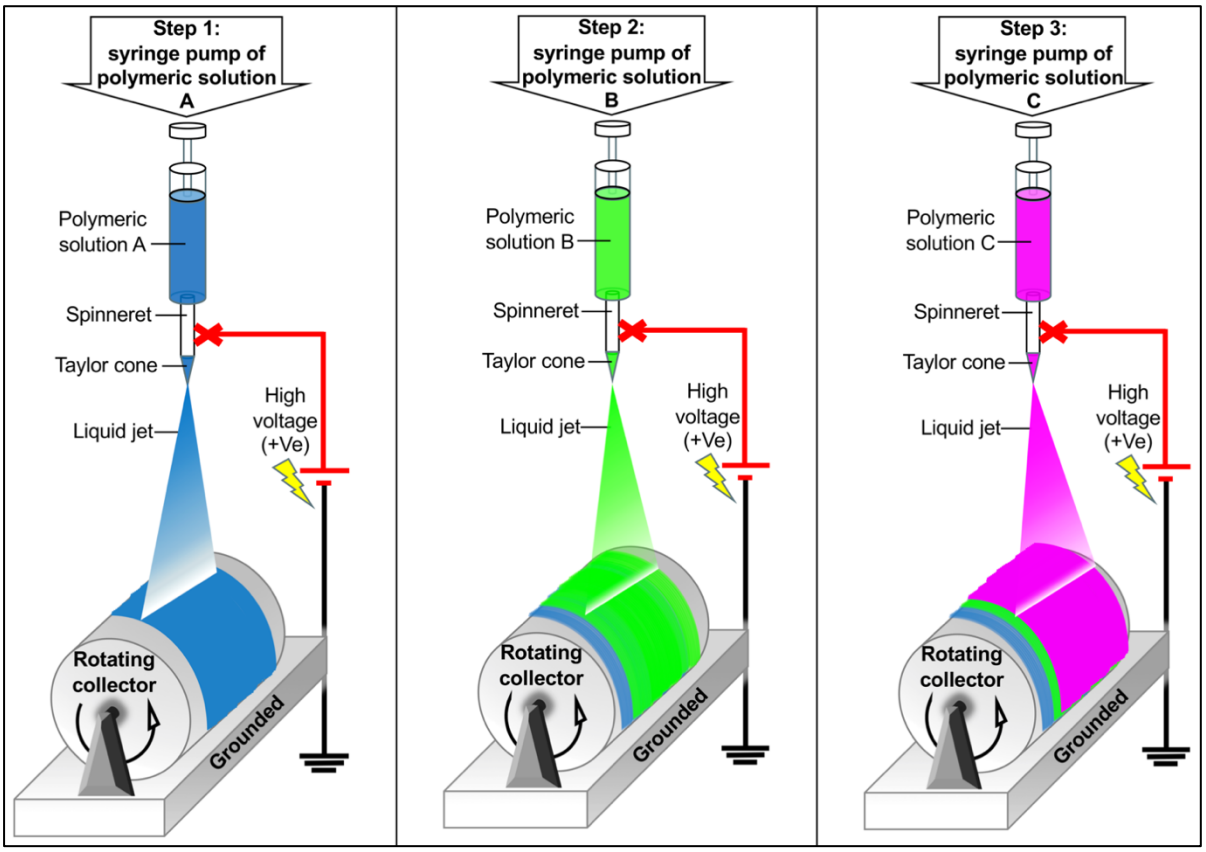

Figure 5.2. A schematic diagram of the sequential electrospinning process.

5.2.2.3 Multi-jet electrospinning

The second FDC formulation was prepared by multi-jet electrospinning to produce a mesh of tangled electrospun fibers (Figure 5.3). Three separate syringes were used at the same time, each loaded with different polymer solutions as described in (Table 5.2). Each syringe was fixed on a separate pump, and all three spinnerets were directed towards the rotating mandrel collector from three directions. All three spinneret were linked to the same high voltage power supply through a stainless steel connecting cable. Electrospinning was initiated by first rotating the collector at 400 rpm, then starting the high voltage power supply at 22 kV. For all three polymeric solution, their best value for single needle electrospinning was 20 kV for PVP, 18 kV for E-L100, and 22 kV for E-RSPO. Nevertheless, to keep constant electrospinning from all the three connected needles at once, the higher value of 22 kV was required as enough power supply for all three connected needleless to create continues multijet electrospinning process. Finally, the three pumps were turned on at the same time, and set to supply the solutions at the best flow rate values as the following: PVP at 4 mL/h, E-L100 at 4 mL/h, and E-RSPO at 2 mL/h. This flow rate also allowed equal distribution of the electrospun fibres in the tangled fibres (T %10) collected from the different total volume as in (Table 5.2). The collected fibres were removed from the collecting aluminium foil and stored in a desiccator at room temperature to dry any remaining solvent.

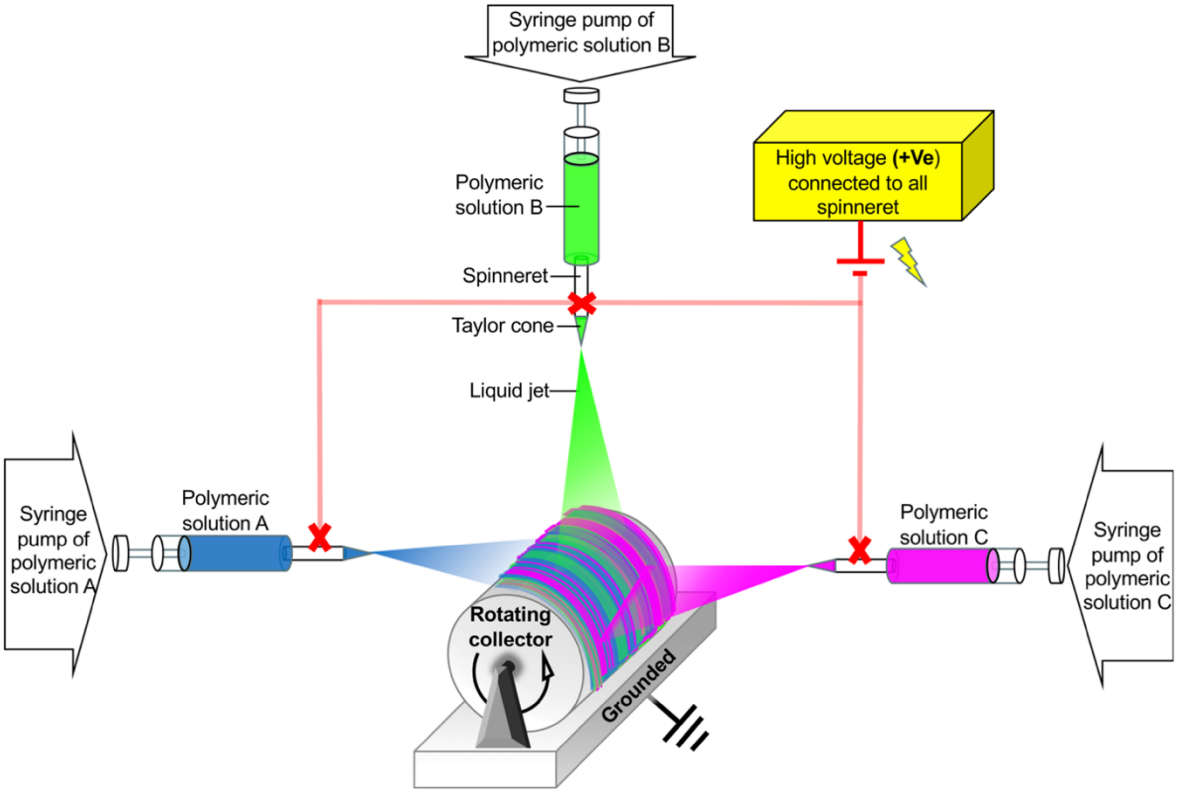

Figure 5.3. A schematic diagram of the multi-jet electrospinning process.

Characterisation of the resulting electrospun fibres mat will be done as described in Chapter 2 for morphology (2.4.1), physical form XRD (2.4.2) and DSC (2.4.3), FTIR (2.4.4), drug loading HPLC study (2.4.5.2), in-vitro drug release dissolution studies (2.6.2.2), and stability study (2.7).

5.3 Results and discussion

5.3.1 Formulation optimisation

The electrospinning process depends on key parameters that need optimisation to allow high-quality nanofiber production. Optimisation of the electrospinning parameters was performed using the single needle process to identify the most appropriate parameters for fibre production, before the generation of FDC with sequential and multi-jet electrospinning.

The selection of an appropriate solvent is essential to achieve successful electrospinning. To prepare the solutions, ethanol was found to be a suitable choice to dissolve all the three polymers used. A solution of PVP in ethanol was successfully electrospun. However, both E-RSPO and E-L100 solutions in ethanol did not allow stable electrospinning due to fast evaporation of the ethanol solvent leading to blockages forming on the tip of spinneret (Kanjanapongkul et al., 2010). Therefore, the addition of DMAc to ethanol to give a mixed solution at a 2:8 v/v ratio was explored; this enabled stable electrospinning, as a result of the reduced evaporation rate caused by adding DMAc to the solution. Similar results have been noted in the literature (Shen et al., 2011).

To enable the electrospinning process of a polymer solution, a critical minimum concentration must be reached to allow chain overlapping and entanglements (Shenoy et al., 2005). We aimed to increase higher production capacity in a shorter time by raising the concentration of each polymer solution to the maximum level that

would permit electrospinning, resulting in base solutions comprising 20% w/v PVP, 20% w/v E-L100, and 50% w/v E-RSPO. The attempt of making FDC formulation at 10%w/w drug loading was to construct formulations that show performance mainly controlled by polymer behaviour. Therefore, to make 10%w/w drug loaded formulation, it was required to prepare total-drug to polymer weight at 1:10 ratio. By using this highly concentrated polymeric solution, this ratio was prepared by less volume of the E-RSPO than using the larger volume of PVP and E-L100. Using a concentrated solution gave the advantage of faster electrospinning for the total volume instead of using a less concentrated solution with larger volume required.

The most appropriate spinneret to use was also evaluated, and this found to be a 20G flat-tipped needle (0.61mm inner diameter). Using smaller needle (0.51 mm inner diameter) resulted in solidification of the polymer solution at the needle tip and blockages forming. The reason that narrow internal diameter is unable to pass the high-viscosity polymer solutions which are created at elevated concentrations. On the other hand, a larger needle (0.84 mm inner diameter) resulted in dripping. At the tip of a large spinneret, the size of the droplet might fast increase, that makes it heavier weight. Therefore, the effect of gravity can overcome maintaining a stable Taylor cone, lead to continues polymeric solution dripping.

The starting values of the syringe pump flow rate enabled electrospinning with a stable liquid jet. However, in order to scale-up the output, the flow rate was increased more to find the maximum level that provides a stable liquid jet without solution dripping. For all the three solutions 4 mL/h was the highest value, however, in order to fix the

processing parameter for all the prepared formulations, it was preferred to use the flow rate indicated as the best values as in (Table 5.3).

The applied voltage is a highly significant parameter in electrospinning. At low voltages, drops from the polymeric solution will be suspended on the tip of the needle. For each polymeric solution, in order to find the minimum and maximum range of applied voltage allowing single needle electrospinning, the voltage was increased to the minimum critical voltage when the spherical liquid drop deformed into a Taylor cone with liquid jet elongation. Then to reach the best value that keeps continues stable electrospinning as in (Table 5.3), the power supply was increased higher while watching the presence of Taylor cone on the tip of the spinneret. To find the maximum range of the voltage with stable electrospinning, further increase of the applied voltage was possible up to the maximum point at which the stable Tylor cone was lost into many jets from the needle tip as in (Figure 5.4).

The applied voltage best values work well for each polymeric solution during single-needle and sequential electrospinning. However, for multi-jet electrospinning, all three spinnerets were connected to the same power supply. Therefore, we had to test the best value used for all polymeric solutions. At 18 kV, stable electrospinning was possible for both PVP and E-L100 but not E-RSPO that show separation of the liquid jet. Whereas, once increased to 22 kV, successfully stable electrospinning was possible from all the three connected spinnerets. This is attributed to the need for sufficient charge supply to all connected spinnerets to maintain stable electrospinning from a fast pumping flow rate with fast fibres collection.

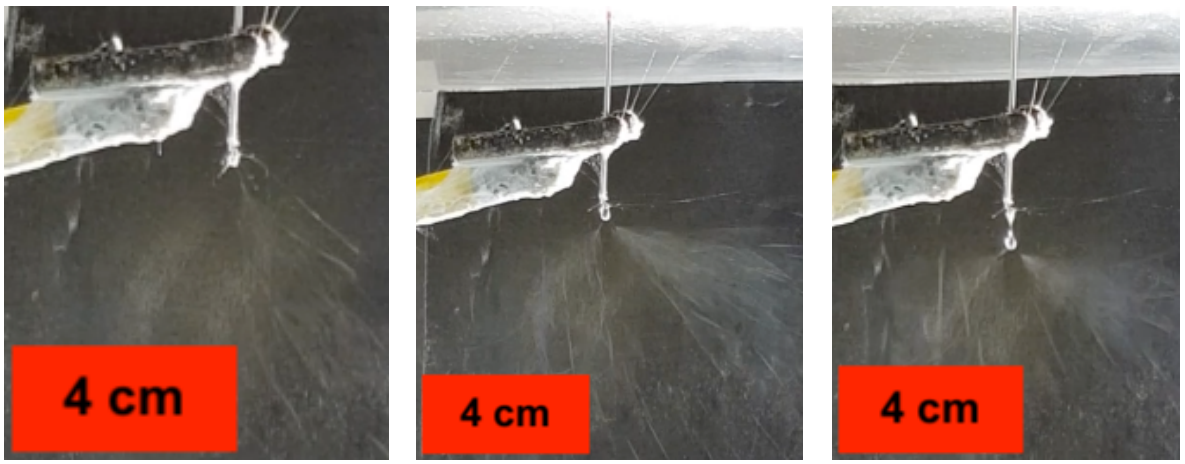

(a) Time= 1150 ms **(b)** Time= 1570 ms **(c)** Time= 2140 ms

Figure 5.4. Dispersion of Taylor cone due to the high voltage power supply in the following steps: **(a)** formation of one liquid jet from Taylor cone; **(b)** liquid jet separated into many liquid jets at different directions; **(c)** the unstable electrospinning ending by dripping of the liquid solution. Snapshots taken from a record by high-speed camera during electrospinning process of 50% w/v E-RSPO during optimisation.

The spinning process is further affected by the distance between the spinneret and the collector, which influences both the strength of the electric field and the flight time of the liquid jet. The latter needs to be long enough to permit the solvent to evaporate before reaching the collector (Ramakrishna, S., 2005). The fibres collected at short distances contained residual solvent, and the resultant wet fibres merged with fibres deposited earlier on the collector (see example in Figure 5.5). If the distance is too great, then there are significant process losses due to the low electric field strength. In all electrospinning process, fibres collection was done by setting the collector at a distance of the best values for each polymeric solution as in (Table 5.3). At this distance, the majority of fibres were successfully collected at a constant rate.

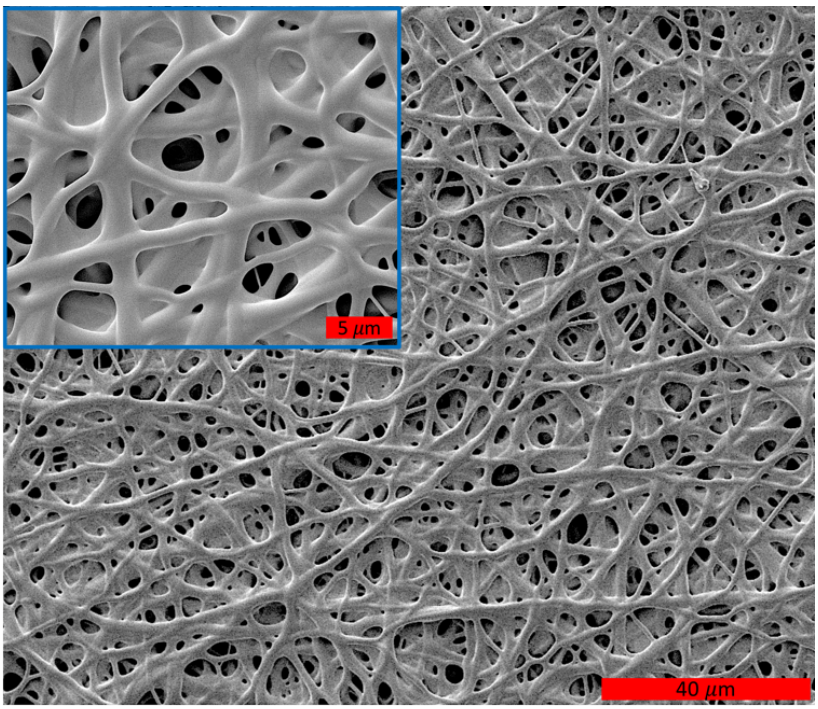

Figure 5.5. An example of merged fibres due to incomplete solvent evaporation at low collection distances. An SEM image for Eudragit RSPO prepared by single needle electrospinning at 2 mL/hr, 22kV, 15 cm, 22 ºC, and 40 % RH.

5.3.2 Morphology

The scanning electron microscope (SEM) images of the raw APIs and the electrospun fibres formulations with the fibre diameter distributions are displayed in (Figure 5.6).

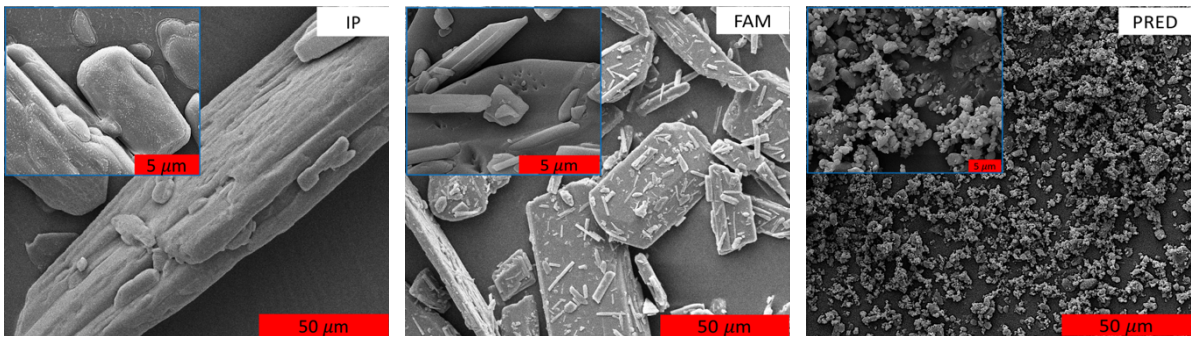

(a) (b) (c)

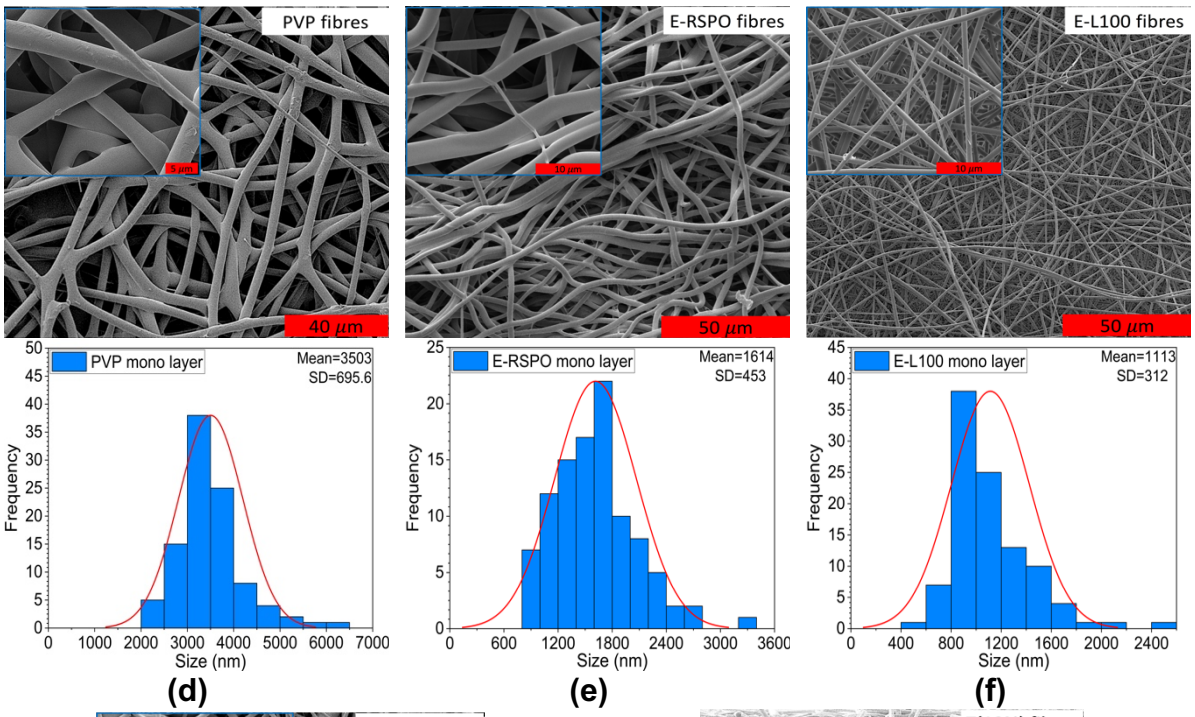
PVP fibres
40 μm
PVP mono layer
Mean=3503
SD=695.6
Frequency
Size (nm)
(d)
E-RSPO fibres
50 μm
E-RSPO mono layer
Mean=1614
SD=453
Frequency
Size (nm)
(e)
E-L100 fibres
50 μm
E-L100 mono layer
Mean=1113
SD=312
Frequency
Size (nm)
(f)

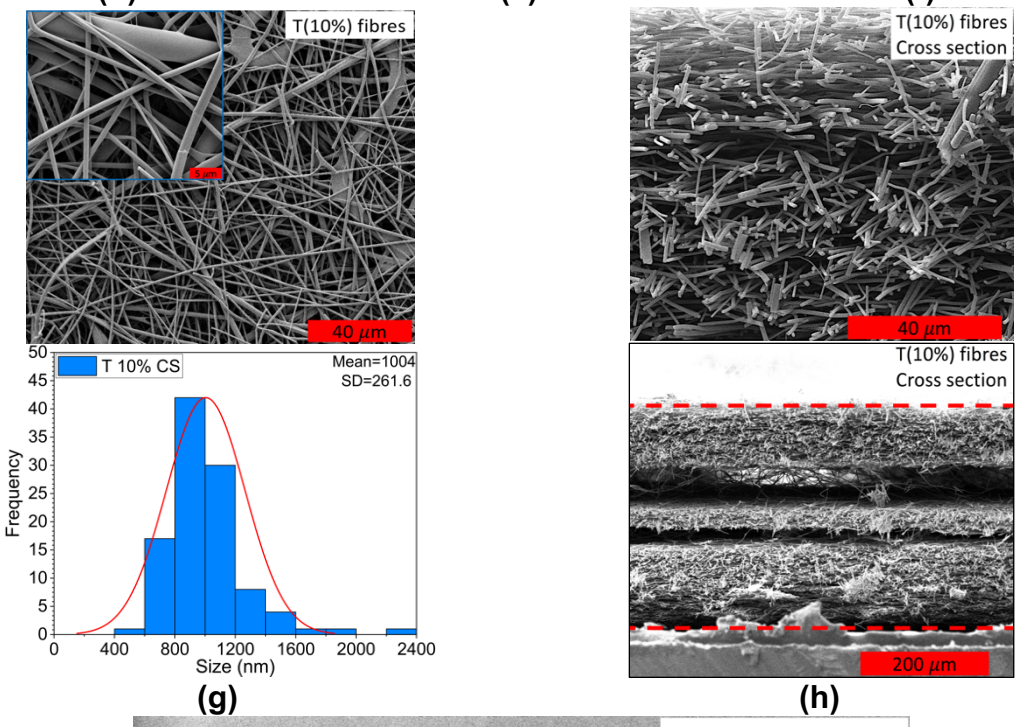
T(10%) fibres
40 μm
T 10% CS
Mean=1004
SD=261.6
Frequency
Size (nm)
(g)
T(10%) fibres
Cross section
40 μm
T(10%) fibres
Cross section
200 μm
(h)

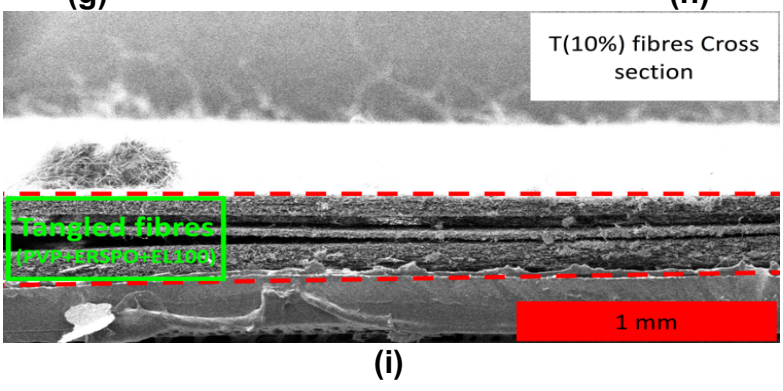
T(10%) fibres Cross section
Tangled fibres
(PVP+ERSPO+EL100)
1 mm
(i)

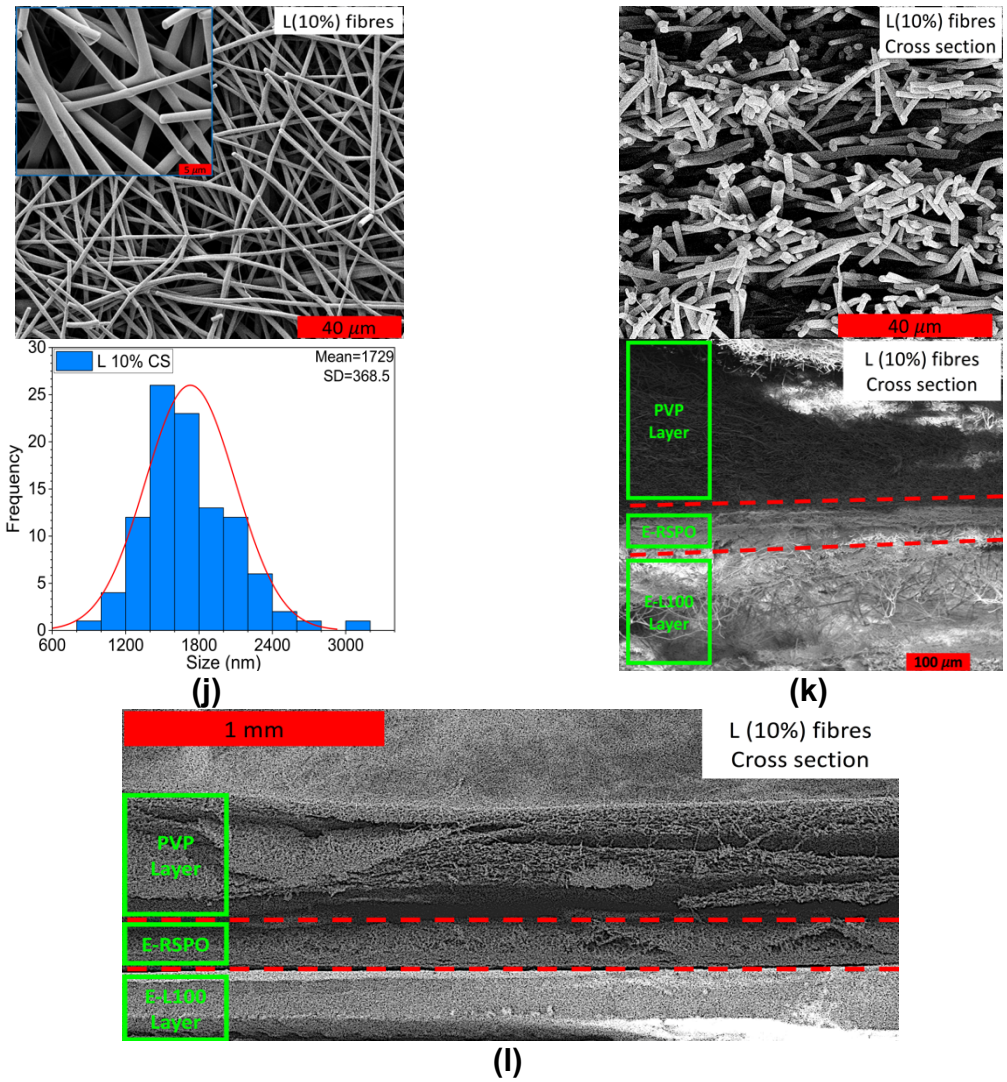

Figure 5.6. SEM images of the raw materials: **(a)** IP, **(b)** FAM, **(c)** PRED. SEM images and fibre diameter distributions of formulation: **(d)** PVP ML (8.7 % w/w IP, 1.3 % w/w FAM); **(e)** E-RSPO ML (8.7 % w/w IP, 1.3 % w/w FAM); **(f)** E-L100 ML (8.7 % w/w IP, 1.25 % w/w FAM, 0.4 % w/w PRED); **(g - i)** T (10%) (8.57 % w/w IP, 1.28 % w/w FAM, 0.14 % w/w PRED); **(j - l)** L(10%) (8.57 % w/w IP, 1.28 % w/w FAM, 0.14 % w/w PRED).

The SEM images of the raw material (Figure 5.6, a-c) shows the characteristic shape of IP as needle shape with rough surface (Rasenack and Müller, 2002); FAM elongated shape with sharp edges; and PRED small irregular particles around 5 μm each. IP and FAM have larger particles, while PRED has irregular small-sized particles. All characteristic shape of the raw materials indicates they comprise

crystalline materials. It proved possible to prepare mono-layer fibre mats from each of the individual polymer solutions in (Table 5.1), as shown in (Figure 5.6, d-f). The images of the fibres mat do not resemble the bulk structure of any of the raw APIs, suggesting that they have been successfully loaded within the fibres as an amorphous solid dispersion. As expected during the optimisation stage, all the fibres were smooth and cylindrical fibres, with a diameter size of PVP ML at 3503 ±696 nm, E-L100 ML at 1113 ±312 nm, and E-RSPO ML at 1614 ± 453 nm. Both E-RSPO and E-L100 fibres were smaller sizes compared to PVP fibre that was prepared at the same conditions. The reason for this is thought to be the different solvent mixture (8:2 v/v ethanol:DMAc) which have slower evaporation so it can extend the period of the jet in the liquid state, enabling a longer drawing time by the electric field (Yu et al., 2011). This also could result in partially fused fibres as in (Figure 5.5) as a result of the incomplete solvent evaporation. Similar effects of fibres fusion due to incomplete solvent evaporation have been reported in the literature by (Kidoaki et al., 2005; Shen et al., 2011; Yu et al., 2014).

The diameter of all fibres prepared here shows a notable increase in size, either due to the high concentration of the polymers used and/or due to the high drug loading (Huang et al., 2003; Parhizkar et al., 2016). PVP ML (Figure 5.6, d) show larger sized fibres compared to the previously reported size of made with a seemlier molecular weight polymer but with less concentration, like 5% w/v PVP produced a 700-800 nm (Quan et al., 2011), 10% w/v PVP produced 344-1270 (Bukhary et al., 2018), and over 1000 nm from 40% w/v PVP (Yu et al., 2009a). This effect could be from the higher concentration of the starting polymer solution at 20% w/v PVP that also increases with drug loading combination. Similar drug loading effect was noticed to increase the size

of E-L100 ML fibres (Figure 5.6, c), that was very high compared to blank 20% w/v E-L100 fibres around 382 ±1 nm reported in (Giram et al., 2018); or blank 25% w/v E-L100 fibres around 506 ±113 nm reported in (Li et al., 2018). The fibres prepared from E-RSPO ML (Figure 5.6, b) also show a notable increase in the size of the fibres at 1614 ± 453 nm. To the best of our knowledge, we are showing here for the first time the possibility to produce electrospun fibres from 50% w/v E-RSPO, the powder form of EUDRAGIT RS polymer. Though some reports have shown possible electrospinning of EUDRAGIT RS100 polymer, a similar based co-polymer to produce smooth fibres at 100-300 nm from 20% w/v E-RS100 as minimum concentration required, were below that concentration at 15% w/v nanobeads were mostly formed (Payab et al., 2014).

SEM images and fibres diameter distributions for the FDC formulations fabricated by multi-jet electrospinning (T10%=8.57 % w/w IP, 1.28 % w/w FAM, 0.14 % w/w PRED) are shown in (Figure 5.6, g - i). And for the FDC formulations fabricated by sequential electrospinning (L10%=8.57 % w/w IP, 1.28 % w/w FAM, 0.14 % w/w PRED) are shown in (Figure 5.6, j - l).

The surface images of both formulations T(10%) in (Figure 5.6, g) and L(10%) in (Figure 5.6, j) proved that modification of the electrospinning setup in both ways was successfully able to produce different FDC formulations from the three polymers: PVP, E-RSPO, and E-L100 in the form of tangled or multi-layer fibres mat. Both FDC formulation shows smooth surfaced fibres and with no appearance of raw API particles. Similar to the mono-layer fibre mats, this indicates a good combination of

the APIs with the polymers in both FDC formulation was successful, and that an amorphous solid dispersion was formed within the fibres mat (Bognitzki et al., 2001).
In order to find the fibres diameter size resulted from the distribution of the three polymers in the FDC formulations, the average of fibres diameter size was counted with image-J software on the cross-section image (Figure 5.6, h & k). Which was taken from the side of the fibres mat that was cut with a sharp scalpel after they both immersed in liquid nitrogen around 3 minutes (Figure 5.6, h & k). Even though both formulations were prepared from similar solutions, the average diameters in formulation T(10%) are smaller than L(10%) at 1004 ± 262 nm and 1729 ± 369 nm. This is presumably due to the differences in the electrospinning process. In the cross-section images of both formulations (Figure 5.6, i & l), show the structure of fibres mat form the side view. In the T(10%) formulation, the image of the cross-section shows an appearance of separating layers between the fibres mat T (10%) that was noticed when it occurred during the cutting of the frozen fibres mat with liquid nitrogen, but generally all the fibres are similar in size and shape (Figure 5.6, i).
In formulation L (10%) cross-section image (Figure 5.6, l) show the construction of the fibres mat, and it shows a level of difference between the fibres layers better seen in (Figure 5.6, k).

5.3.3 X-ray diffraction (XRD)

XRD analysis was used to investigate the physical form of the APIs loaded in the nanofibres. XRD diffraction patterns are shown in Figure 5.7.

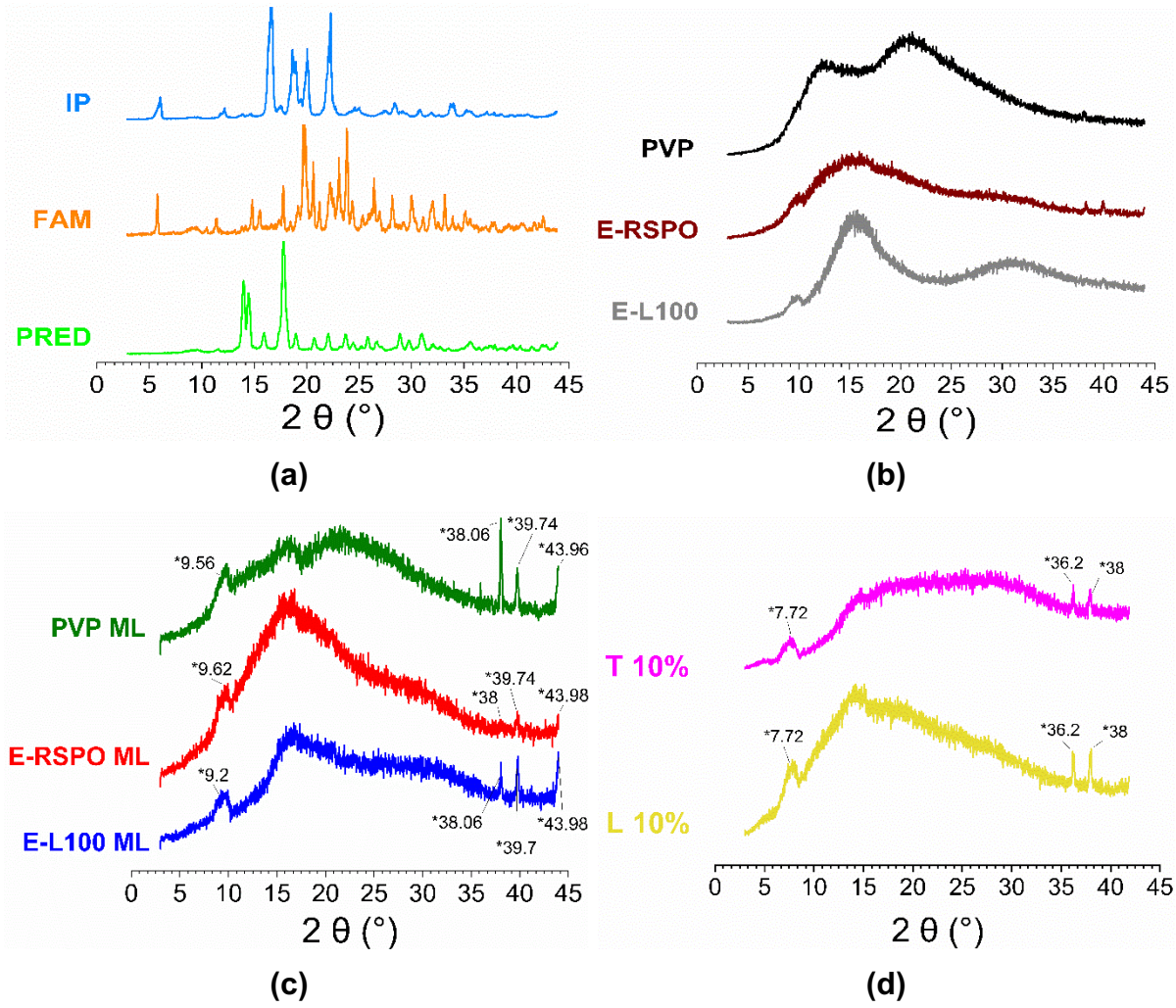

Figure 5.7. XRD diffraction patterns of the raw materials and fibre mats: **(a)** raw APIs (IP, FAM, and PRED); **(b)** the pure polymers (PVP, E-RSPO, and E-L100); **(c)** the mono-layer electrospun fibers (PVP ML, E-RSPO ML, and E-L100 ML); **(d)** the FDC fibres T(10%) and L(10%). Peaks labelled with * correspond to the sample holder.

The patterns of the API raw materials show sharp characteristics reflections for IP, FAM and PRED. The presence of these Bragg reflections demonstrates that all the APIs exist in the crystalline form before electrospinning. The data for IP (Figure 5.7, a) agree with the literature for crystalline ibuprofen (Oparin et al., 2017). FAM crystallises into three polymorphs forms A, B and C (Cheng et al., 2008; Lin et al., 2014). The XRD data are similar to those reported for the metastable form B, and it is more preferred for the commercial use (Lin, 2014). Prednisone exists in an anhydrous

crystalline form and a number of solvates, including a monohydrate and a solvate with chloroform (Vogt et al, 2007). The XRD data of prednisone here indicates it is the anhydrous crystalline form similar to the data presented by (Toehwé et al., 2017).

The patterns of the polymers PVP, E-RSPO, and E-L100 (Figure Figure 5.7, b) show only broad haloes, indicating the amorphous nature of the polymers (Giram et al., 2018). This agrees with the literature for the polymers PVP (Illangakoon et al., 2014), and E-L100 (Li et al., 2018).

The XRD pattern for each of the mono-layer electrospun nanofibres (Figure 5.7, c) shows broad haloes similar to the polymer carriers, without any characteristic Bragg reflections of the loaded APIs. This confirms that the APIs are loaded in each fibre mat as an amorphous solid dispersion. In the XRD patterns of the FDC formulations (Figure 5.7, d), similarly to the mono-layer fibres both T (10%) and L (10%) show no Bragg reflections attributable to the APIs. Both FDCs show broad haloes, confirming the APIs exist as an amorphous solid dispersion in the FDC formulations. This is consistent with the available data for electrospun fibres loaded with IP (Yu et al., 2009) and PRED (Poller et al., 2017). However, the observation of amorphous FAM here is different to previously reported nanofibres containing 50% w/w FAM, where crystalline API was observed in PVP fibres (Brettmann et al., 2013). This difference is a result of the low FAM loading here at 1.28 %w/w in the FDC formulations.

5.3.4 Differential Scanning calorimetry (DSC)

DSC thermograms of all the formulations are shown in Figure 5.8.

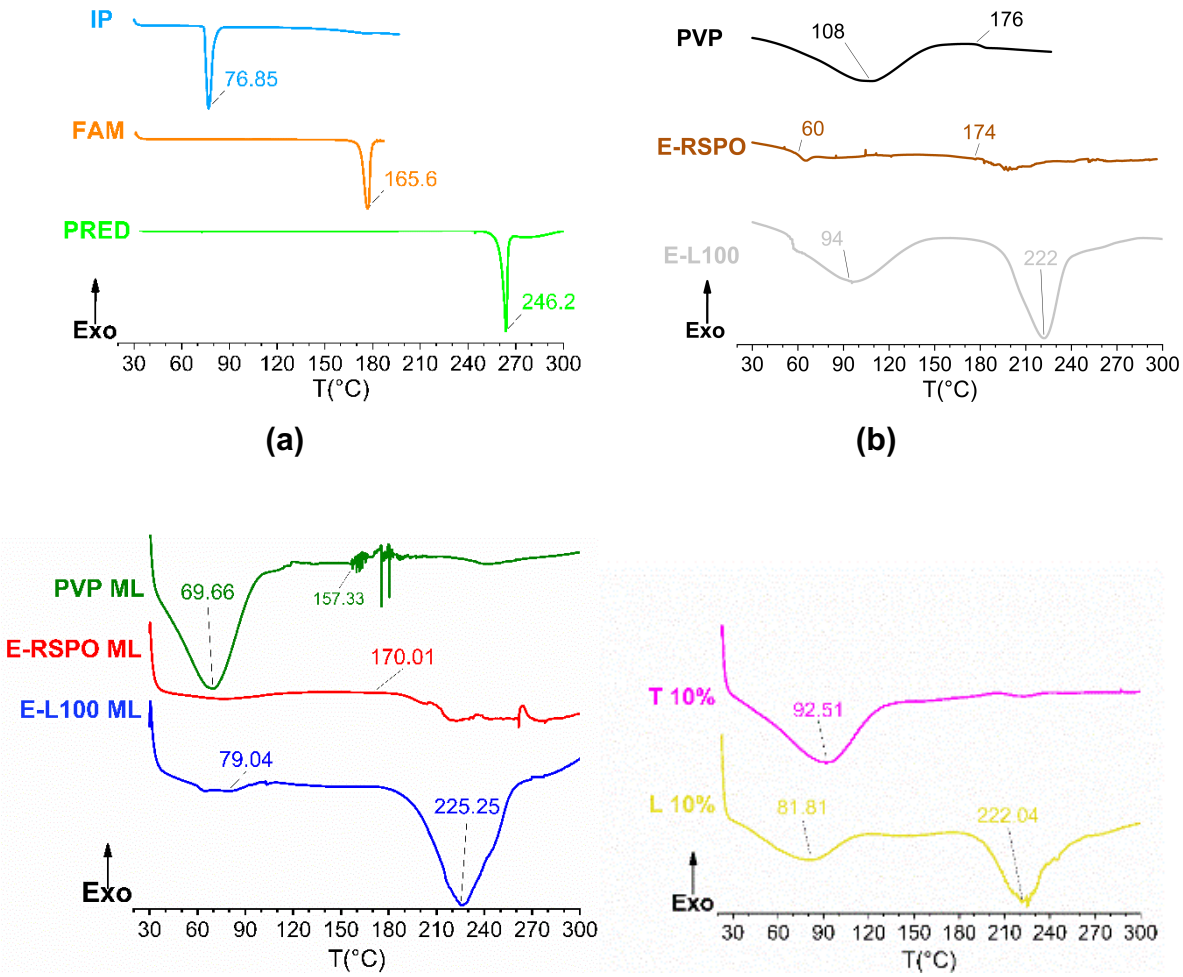

Figure 5.8. DSC data for **(a)** the pure APIs (IP, FAM, and PRED); **(b)** the polymer carriers (PVP, E-RSPO, and E-L100); **(c)** the mono-layer fibers (PVP ML, E-RSPO ML, and E-L100 ML); **(d)** the FDC fibres T(10%) and L(10%).

The data for the API raw materials (Figure 5.8a) show endothermic peaks corresponding to melting, for IP at around 76.9 ºC (similar to that given in the literature (Dudognon et al., 2008)) and for FAM at 165.6 ºC. The latter is close to the reported melting temperature of 167 ºC for FAM polymorph form B (Cheng et al., 2008). The PRED melting temperature can be seen at 246.2 ºC, within the range of 240-247 °C detailed in the literature for the anhydrous form (Toehwé et al., 2017). These results all agree with the data of XRD confirming that the APIs were originally in a crystalline form, with polymorph B of PRED having been procured.

Considering the thermograms of the pure polymers (Figure 5.8b), PVP shows a broad endotherm ascribed to dehydration at around 108 ºC, and a glass transition at 176 ºC that close to the range of the literature value at 166 ºC (Poller et al., 2017). In E-RSPO a glass transition is observed at 60 °C, intermediate between the reported temperatures of 55.6 °C (Dave et al., 2012) and 64 °C (Parikh et al., 2016). The onset at 174 °C was described by by Parikh et al. (2016) as polymer degradation in the range of 173 to176°C. E-L100 displays a broad endotherm ascribed to dehydration at around 94 ºC, and a second peak with onset around 222 ºC, as reported by Lin (Lin et al., 1995). The latter is believed to be relaxation endotherm superimposed with a glass transition at 222 ºC (Yu et al., 2013; Parikh et al., 2016). The appearance of the glass transition in the pure polymers and absence of melting endotherms are related to the amorphous nature of the polymer, which also agrees with the findings from XRD data.

The DSC data for each of the mono-layer electrospun nanofibres (Figure 5.8, c) presented thermograms similar to the polymer raw materials, with no apparent melting

endotherms from the APIs, confirming they form amorphous solid dispersions in the fibres mats as expected for drug loading in the electrospun fibres.

Similar to the mono-layer fibre mats, in the thermograms of the FDC formulations (Figure 5.8d) both display broad endothermic peaks due to dehydration centred at around 92.5 ºC in T (10%) and 81.8 ºC in L (10%). The E-L100 glass transition/relaxation event can be seen at around 222 ºC in the FDC formulations F1.

5.3.5 FTIR spectroscopy

Infrared spectroscopy was performed to assess the compatibility of the formulations by evaluating the interactions between the APIs and the carrier polymers. Good compatibility between drug and polymer should lead to improved stability of the formulation and reduce solid phase separation. This could arise from hydrophobic interactions, hydrogen bonding, or electrostatic interactions between the different components (Yang et al., 2016).

The chemical structures and IR spectra of the raw materials and electrospun fibres are presented in (Figure 5.9).

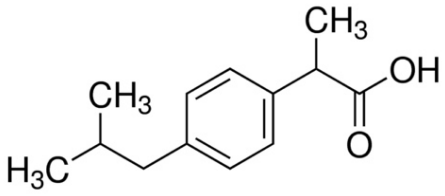

IP

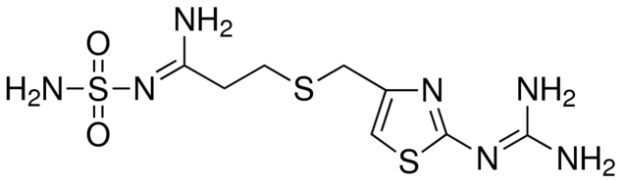

FAM

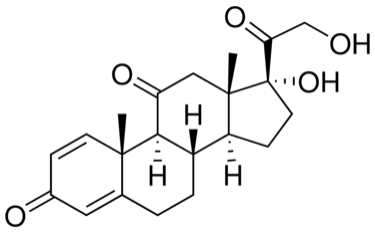

PRED

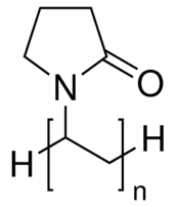

PVP

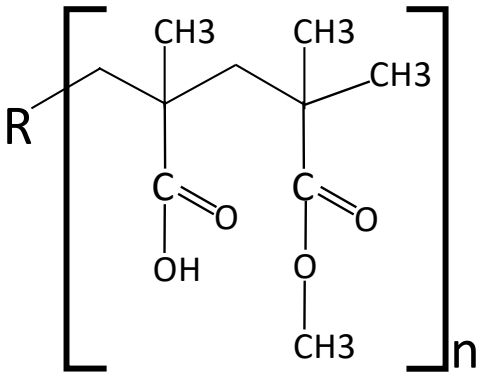

E-L100

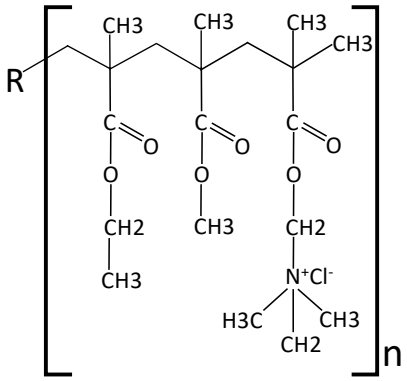

E-RSPO

(a)

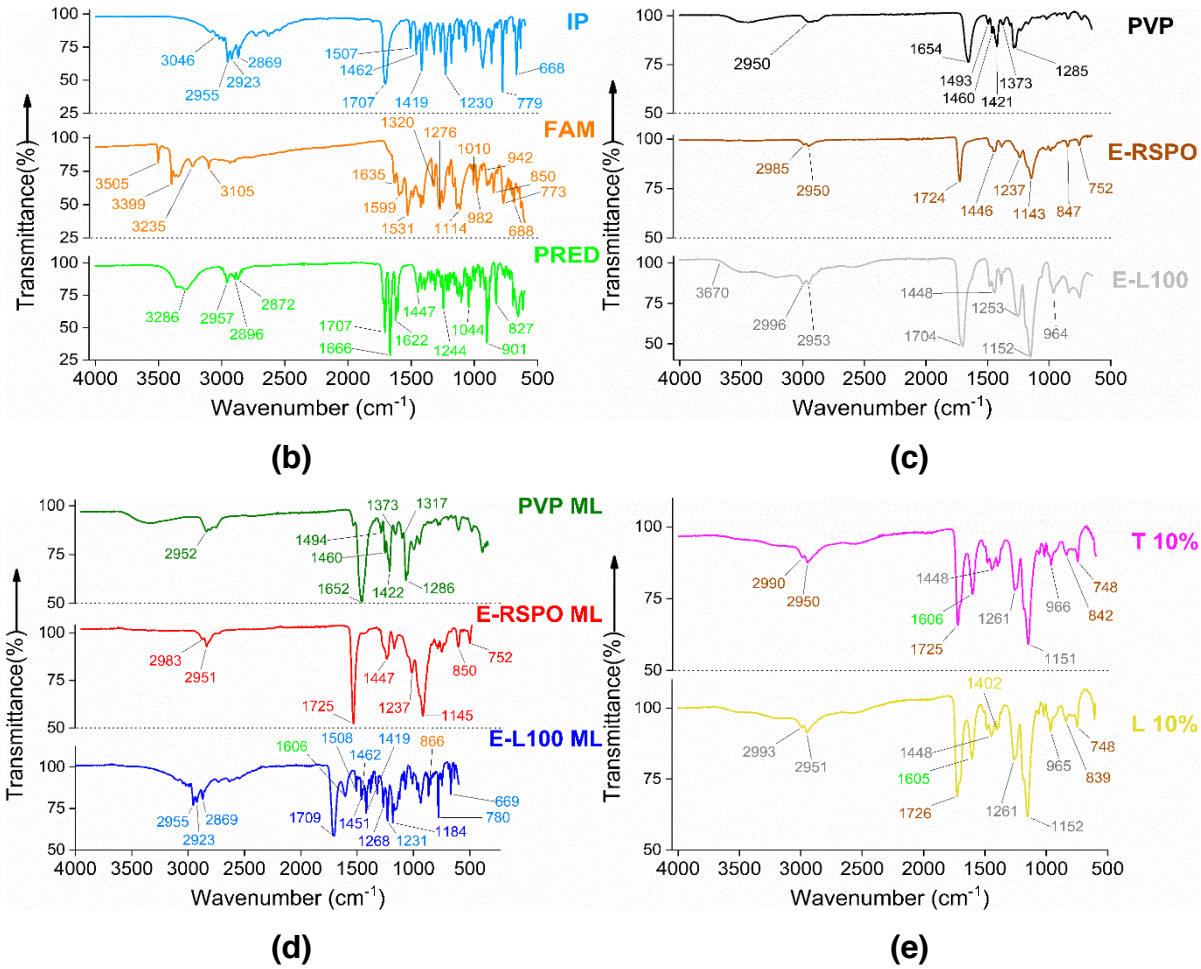

Figure. 5.9. (a) Chemical structures of the APIs and polymers, together with FTIR data for **(b)** the raw APIs; **(c)** the polymers; **(d)** the mono-layer fibres (PVP ML, E-RSPO ML, and E-L100 ML); **(e)** the FDC fibres T(10%) and L(10%).

The FTIR spectrum of the API raw materials (Figure 5.9, b) present characteristic bands for each material. In the spectrum of IP, characteristic peaks appears from O—H stretching at 2955 cm^{-1}, C=O stretching at 1707 cm^{-1}, and phenyl group C=C vibrations at 1507, 1462, 1419, 779, and 668 cm^{-1}. In the spectrum of FAM, the bands appears from C-H stretching at 3105 cm^{-1}, NH_2 stretch at 3505, 3399, 3235, 1599, and 1531 cm^{-1}, together with C=N vibrations at 1635 cm^{-1}, and O=S=O stretching at 1320 cm^{-1}. In the spectrum of PRED, absorbance bands can be seen from O—H stretches

at 3286 cm^{-1}, C—H stretches at 2957, 2986, and 2872 cm^{-1}, C=O vibrations at 1707 and 1666 cm^{-1}, and C=C stretching at 1622 cm^{-1}.

The spectra of the polymer raw materials (Figure 5.9, c) show that PVP has O—H stretches at 2950 cm^{-1} from the adsorbed water, C=O vibrations at 1654 cm^{-1}, and a C—N stretch at 1285 cm^{-1}. The spectrum of E-RSPO show C—H stretching at 2950 cm^{-1}, a C=O stretch at 1724 cm^{-1}, and C—O—C stretching at 1237 and 1143 cm^{-1}. The spectrum of E-L100 show a broad peak ranging from 3670 to about 2500 cm^{-1} from the OH groups. This is superimposed with the C—H stretch at 2953 cm^{-1}. There are also carboxylic acid C=O stretches at 1704 cm^{-1}, and C—O—C stretching at 1253 cm^{-1} and 1152 cm^{-1}. (Sagdinc and Bayarı, 2005; Gonçalves,et al., 2017).

The FTIR spectra of each mono-layer fibre mat (Figure 5.9, c) shows similar features to their raw materials, and some peaks from the loaded APIs can be seen in the spectrum. In comparison to the spectrum of pure drug, many of the peaks from the loaded APIs have shifted positions or merged with the peaks from the carrier polymers indicating that APIs can be amorphously dispersed in the fibres mat with good molecular interactions between the drug and the polymer in form of e.g. hydrogen bonding between hydrogen bond donor group (e.g. phenolic hydroxyl) and hydrogen bond acceptor group (e.g. carboxyl group) (Chen et al., 2008), which resulted in reduction of the APIs molecular phonon vibrations (Sanchez-Vazquez et al., 2017). These trends are clearest with the PVP ML and E-RSPO ML formulations. With the E-L100 ML system many peaks from IP can still be seen, such as the O—H stretch at 2955 cm^{-1}, and C=C stretches at 1507, 1462, 1419, 780, and 668 cm^{-1}. This can be

explained by the increased drug loaded in E-L100 ML compared to PVP ML and E-RSPO ML, with IP being the drug with highest loading.

In comparison to the previously presented mono-layer fibres, the FTIR spectra of the FDC formulations (Figure 5.9, d) show both formulations T(10%) and L(10%) are similarly combining the major features from all three polymers used with almost no sharp peaks from any of the APIs visible in either of the FDC formulations. Which indicate better level of molecular interaction between the amorphously distributed APIs and each carrier polymer was achieved in the FDC formulations than in the mono-layer fibres mat (Kaushal et al., 2008). This may be due to the smaller ratio of total loaded APIs to polymer in the FDC formulations, compared to the slightly increased loading of APIs in each mono-layer fibres.

5.3.6 Drug loading and encapsulation efficiency (EE)

The drug loading and EE were determined for the FDC formulations T (10%) and L (10%) by HPLC and the result as listed in (Table 5.4).

Table 5.4. The drug loadings and EE of the FDC fibres formulations. Data are reported as mean ± S.D. (n=3). Data are presented as the mean ± S.D. of three independent experiments.

Formulation	IP loading (% w/w)	IP EE (%)	FAM loading (% w/w)	FAM EE (%)	PRED loading (% w/w)	PRED EE (%)
T (10%)	9 ±0.4	105.5 ±4.6	1.3 ±0.1	100.3 ±9.1	0.15 ±0.02	92.3 ±16.3
L (10%)	8.6 ±1.2	93.8 ±14.4	1.3 ±0.2	100 ±7.3	0.16 ±0.01	109.6 ±9.7

The drug loading in the FDCs formulations T (10%) and L (10%) was determined from three samples removed randomly from three different points throughout each formulation. The loadings were quantified by HPLC and are presented in Table 5.4. Drug loading for each drug was achieved close to the percentage of drug loading designed in the formulation. EE% for each loaded drug was in high range from the theoretical drug loading within each formulation. These results showed the effectiveness of the modified electrospinning techniques with minimal loss of the loaded drug in the formulation.

5.3.7 In-vitro drug release

To evaluate the drug release from the FDCs formulations as multiple releasse in separate time as previously explained in Table 5.1. In vitro dissolution tests were carried out on both FDC formulations T (10%) and L (10%) electrospun nanofibres in two separate medium. The test carried out with separate samples in the acidic

condition of 0.1 N HCl for 4 hours, and another sample in pH 7.4 PBS for 16 hours. The in vitro drug release results are given in (Figure 5.10).

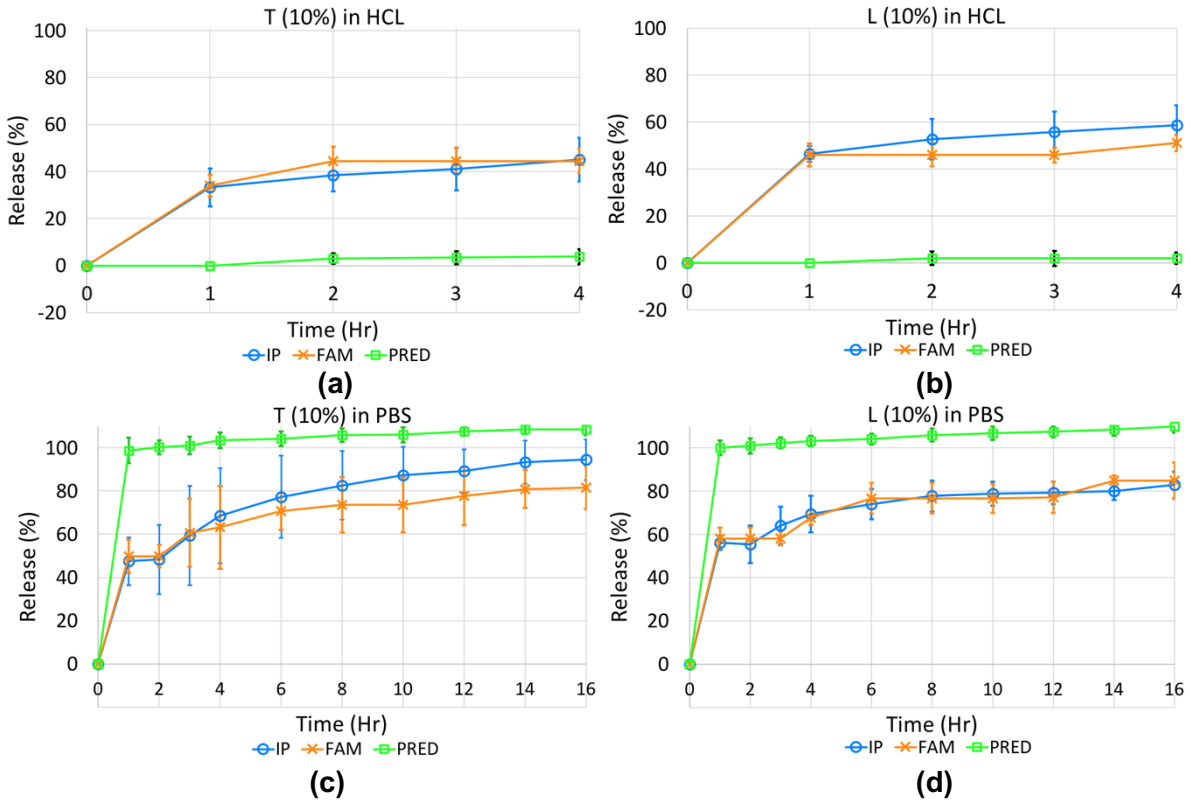

Figure 5.10. In vitro dissolution profiles showing release of IP, FAM, and PRED from the FDC formulations **(a)** T (10%) in HCL for 4 hours; (**b)** L (10%) in HCL for 4 hours; **(c)** T (10%) in PBS for 16 hours; **(d)** L (10%) in PBS for 16 hours. Result reported from Mean ± S.D. (n=3).

When both formulations were tested in the acidic medium (Figure5.10, a and b), both IP and FAM that is loaded in the PVP layer instantly released into the medium within the first hours of sampling. This is expected to happen from the PVP that have hydrophilic properties (Yu et al., 2013), so when it contacted with the dissolution medium it instantly dissolved and released the loaded drug combination. A similar full release of IP from PVP fibres within one hour as marked improved of IP dissolution

rate was observed by (Yu et al., 2009). The amount of drug released from T (10%) was around 33.27 ±8 % IP and 34 ±4.6% FAM, that equal the estimated amount of drug loaded in the PVP fibres. While from L (10%), it reached a higher percentage than the estimated amount from PVP fibres at 46.5 ±3.3 % IP and 46 ±4.9% FAM. This excess was due to the difference in fibres mat structure that was affecting the formulation porosity. Since the drug release that involves polymer dissolution require absorption, swelling, and disentanglement of the fibres mat, then end by releasing the free drug into the media (Shen et al., 2011). Formulation T (10%) made from three different polymer fibres in a twisted compact structure, that allowed the hydrophilic PVP fibres to dissolve fast within one hour once it contacted with the medium. While in formulation L (10%), PVP is a lateral layer that can fully dissolve in a faster time, then an additional release occurred could be from the microparticles located on the surface of fibres made from the other polymers (Shen et al., 2011). The amount of PRED loaded only in E-L100 fibres released low as <4%, same as expected from the insoluble fibres E-L100 in acidic medium. In (Yu et al., 2013), a similar low release in acidic conditions from E-L100 fibres was observed for the loaded drug IP.

When both formulations tested in the alkaline PBS medium (Figure5.10, c and d), all the three drug IP, FAM, and PRED released into the medium within the first hours of sampling. The amount of drug released from T (10%) was around: (IP=47.5 ±11% , FAM=49.8 ±7.6% , and PRED=98.7 ±6%), and from L (10%) was around: (IP=56 ±16%, FAM=58.2 ±5%, and PRED=100 ±3.4%). The total amount of drug released here was higher than drug released in HCL, and reaching to the estimated total drug loaded in both fibres PVP and E-L100. Also, it includes the full amount of PRED that was loaded only in E-L00. This confirms that drugs loaded in PVP fibres was fully

dissolved, and in E-L100 fibres was started to release within the first one hour and slightly increased by the second hour. This was expected since PVP is a hydrophilic polymer, and in many literatures showed that one hour is enough time to fully dissolve PVP fibres and fast release the loaded drug (Yu et al., 2009; Yu et al., 2013). And E-L100 is pH sensitive polymer that dissolves only at pH>6, at which ionisation of the polymer chain COOH groups is high enough to become soluble (Zhou et al., 2012), so when the pH value was below 6, polymer dissolution was minimal (Figure 5.10, a and b), (Li et al., 2018). But in pH 7.4 (Figure 5.10, c and d), the drug release was mainly depending on the polymer dissolution rate that started mostly to dissolve within one hour and reached by three to four hours to full drug unloading from E-L100 around 60% from each formulation. The rate of drug release from the E-RSPO fibres started to increase from three or four hours and continued at sustained drug release fashion to reach >80% after 16 hours from both formulations. This result matches with the expected release of the remaining drug loaded in E-RSPO fibres. E-RSPO is an insoluble polymer that exhibits low water permeability and pH-independent swelling (Azarmi et al., 2002) resulting in a slow drug release from the fibres composite. E-RSPO has been used as a non-erodible matrix binder in different kinds of formulations, and it showed a positive impact of extending the dissolution profile for a minimum of 3 hours and reached over 12 hours (Boza et al., 1999; Schilling et al., 2007; Dave et al., 2012; Cetin et al., 2013).

From the previous explanation, it was successfully achieved an immediate, delayed and sustained drug release by incorporating the three polymers PVP, E-L100, and E-RSPO in the same fibres mat. The drug loading was limited at 10% w/w to enable full control of the drug release as an effect of the polymer dissolving. In the clinical

conditions RA, the consequence of inflammatory activities that repeat every 24-hour cycles resulting in the clinical symptoms that mostly arise in the early morning at around 4 a.m. (Cutolo, 2016). The first dose here was achieved here as an immediate drug release from the hydrophilic polymer PVP to release most of the loaded IP and FAM within the first hour. This dose can be planned to be loading dose around 10:00 p.m., so it can reduce and maintain the symptoms appearing in the night. The gastric emptying time varies from a few minutes to longer hours, depending on the physiological state, the nature, and design of the formulations (Mudie et al., 2010). Drug administration in night time could increase its gastric residence time (Coupe et al., 1992). So this could increase the time of delaying the formulation before reaching the intestinal pH above 6. At which, drug release from the E-L100 fibres can start to release the second dose of IP, FAM, and PRED which can give its best effect in the early morning. In a similar concept to the formulations, the drug release from prednisolone tablet coated with E-L100 was observed with a lag time in the low pH, then a threshold of drug release started after one hour from changing the pH over 6 (Merchant et al., 2014). This dose is an achievement to replace the need for the early morning administration of an immediate release PRED dose around 6-8 a.m. with the delayed release of PRED that starts from around 02:00 a.m. and reach its peak concentration in four hours. Finally, the extended release from E-RSPO should keep the effective concentration of APIs in the body for an extended time and reach the peak concentration by 16 hours before the new dose administration. The two FDCs formulations prepared by the two electrospinning setup showed similar drug release profile, but with slight differences in the rate that was faster from the multi-layer formulation L (10%).

5.4 Conclusions

The aim of this study was to develop advanced FDCs using modified single-needle electrospinning processes. Three polymers PVP, E-L100, and E-RSPO were used to develop two types of formulations. The fibres mat was made either as mono-layers from each polymer separately electrospun or combined three polymers in FDCs. The FDCs was prepared in two ways: by sequential electrospinning to produce multilayer fibres (L 10%) and multijet electrospinning to produce tangled fibres (T 10%), with the aim for multiple drug release of combined three model drug IP, FAM, and PRED. Characterisation of the fibres mat by scanning electron microscopy showed a good formation of smooth and cylindrical fibres in all the mono-layers fibres mat and the FDCs formulation. The side view of the FDCs formulation showed different fibres mat structure between the tangled and the multi-layer fibres. The obtained fibres have a diameter size between 1113 and 3503 nm for the mono-layer fibres, and 1004 to 1729 for the FDC formulations. X-ray diffraction and differential scanning calorimetry showed all the formulations comprised amorphous solid dispersions unlike the data of raw APIs. FTIR studies exposed intermolecular interactions between IP, FAM, and PRED with all the carrier polymer in the mono-layer fibres and the FDC formulations. The drug loadings of the 10% w/w total loaded FDC formulation was assessed by HPLC and showed good entrapment efficiencies reaching over 90% for each loaded drug in the FDCs. In vitro drug release study on the FDCs showed a combination of multiple drug release of three model drugs in separate time as the intended design. The first release was from PVP fibres as an immediate drug release in HCL. The next release was from E-L100 fibres as a delayed release that was triggered by pH change once the formulation reached over pH 6. And the final release was from the insoluble

polymer E-RSPO fibres in extended drug release fashion. In summary, the aim of this project was achieved by developing FDC formulations combining three drugs that can effective combined for the rheumatoid arthritis patients. The performance of the FDC showed an effective outcome as intended from the formulation design.

5.5 References

Arvidson, N.G., Gudbjörnsson, B., Elfman, L., Ryden, A.C., Tötterman, T.H. and Hällgren, R., 1994. Circadian rhythm of serum interleukin-6 in rheumatoid arthritis. Annals of the Rheumatic Diseases, 53(8), p.521.

Arvidson, N.G., Gudbjörnsson, B., Larsson, A. and Hällgren, R., 1997. The timing of glucocorticoid administration in rheumatoid arthritis. *Annals of the Rheumatic Diseases*, *56*(1), pp.27-31.

Azarmi, S., Farid, J., Nokhodchi, A., Bahari-Saravi, S.M. and Valizadeh, H., 2002. Thermal treating as a tool for sustained release of indomethacin from Eudragit RS and RL matrices. International Journal of Pharmaceutics, 246(1-2), pp.171-177.

Balqis, A.I., Khaizura, M.N., Russly, A.R. and Hanani, Z.N., 2017. Effects of plasticizers on the physicochemical properties of kappa-carrageenan films extracted from Eucheuma cottonii. International Journal of Biological Macromolecules, 103, pp.721-732.

Bello, A.E., 2012. DUEXIS® (ibuprofen 800 mg, famotidine 26.6 mg): a new approach to gastroprotection for patients with chronic pain and inflammation who require treatment with a nonsteroidal anti-inflammatory drug. Therapeutic Advances in Musculoskeletal Disease, 4(5), pp.327-339.

Bello, A.E., Grahn, A.Y., Ball, J., Kent, J.D. and Holt, R.J., 2015. One-year safety of ibuprofen/famotidine fixed combination versus ibuprofen alone: pooled analyses of two 24-week randomized, double-blind trials and a follow-on extension. Current Medical Research and Opinion, 31(3), pp.407-420.

Bhala, N., Emberson, J., Merhi, A., Abramson, S., Arber, N., Baron, J.A., Bombardier, C., Cannon, C., Farkouh, M.E., FitzGerald, G.A. and Goss, P., 2013. Vascular and upper gastrointestinal effects of non-steroidal anti-inflammatory drugs: meta-analyses of individual participant data from randomised trials. The Lancet, 382(9894), pp.769-779.

Bognitzki, M., Frese, T., Steinhart, M., Greiner, A., Wendorff, J.H., Schaper, A. and Hellwig, M., 2001. Preparation of fibers with nanoscaled morphologies: electrospinning of polymer blends. Polymer Engineering & Science, 41(6), pp.982-989.

Boza, A., Caraballo, I., Alvarez-Fuentes, J. and Rabasco, A.M., 1999. Evaluation of Eudragit® RS-PO and Ethocel® 100 matrices for the controlled release of lobenzarit disodium. Drug Development and Industrial Pharmacy, 25(2), pp.229-233.

Brettmann, B.K., Cheng, K., Myerson, A.S. and Trout, B.L., 2013. Electrospun formulations containing crystalline active pharmaceutical ingredients. Pharmaceutical Research, 30(1), pp.238-246.

Bukhary, H., Williams, G.R. and Orlu, M., 2018. Electrospun fixed dose formulations of amlodipine besylate and valsartan. International Journal of Pharmaceutics, 549(1-2), pp.446-455.

Carnaby-Mann, G. and Crary, M., 2005. Pill swallowing by adults with dysphagia. Archives of Otolaryngology–Head & Neck Surgery, 131(11), pp.970-975.

Chen, Z., Mo, X., He, C. and Wang, H., 2008. Intermolecular interactions in electrospun collagen–chitosan complex nanofibers. Carbohydrate Polymers, 72(3), pp.410-418.

Cheng, W.T., Lin, S.Y. and Wang, S.L., 2008. Differential scanning calorimetry with curve-fitting program used to quantitatively analyze the polymorphic transformation of famotidine in the compressed compact. Drug Development and Industrial Pharmacy, 34(12), pp.1368-1375.

Coupe, A.J., Davis, S.S., Evans, D.F. and Wilding, I.R., 1992. Nocturnal scintigraphic imaging to investigate the gastrointestinal transit of dosage forms. Journal of Controlled Release, 20(2), pp.155-162.

Cutolo, M., 2016. Glucocorticoids and chronotherapy in rheumatoid arthritis. RMD open, 2(1), p.e000203.

Cutolo, M., Otsa, K., Aakre, O. and Sulli, A., 2005. Nocturnal hormones and clinical rhythms in rheumatoid arthritis. Annals of the New York Academy of Sciences, 1051(1), pp.372-381.

Dave, V.S., Fahmy, R.M., Bensley, D. and Hoag, S.W., 2012. Eudragit® RS PO/RL PO as rate-controlling matrix-formers via roller compaction: Influence of formulation and process variables on functional attributes of granules and tablets. Drug Development and Industrial Pharmacy, 38(10), pp.1240-1253.

Dixit, R.P. and Puthli, S.P., 2009. Oral strip technology: Overview and future potential. Journal of Controlled Release, 139(2), pp.94-107.

Dudognon, E., Danède, F., Descamps, M. and Correia, N.T., 2008. Evidence for a new crystalline phase of racemic ibuprofen. Pharmaceutical Research, 25(12), pp.2853-2858.

Fina, F., Madla, C.M., Goyanes, A., Zhang, J., Gaisford, S. and Basit, A.W., 2018. Fabricating 3D printed orally disintegrating printlets using selective laser sintering. International Journal of Pharmaceutics, 541(1-2), pp.101-107.

Giram, P.S., Shitole, A., Nande, S.S., Sharma, N. and Garnaik, B., 2018. Fast dissolving moxifloxacin hydrochloride antibiotic drug from electrospun Eudragit L-100 nonwoven nanofibrous Mats. Materials Science and Engineering: C, 92, pp.526-539.

Gonçalves, J.M., Guimarães, R.R., Brandão, B.B., Saravia, L.P., Rossini, P.O., Nunes Jr, C.V., Bernardes, J.S., Berttoti, M., Angnes, L. and Araki, K., 2017. Nanostructured alpha-NiCe mixed hydroxide for highly sensitive amperometric prednisone sensors. Electrochimica Acta, 247, pp.30-40.

Grennan, D.M., Aarons, L., Siddiqui, M., Richards, M., Thompson, R. and Higham, C., 1983. Dose-response study with ibuprofen in rheumatoid arthritis: clinical and pharmacokinetic findings. British Journal of Clinical Pharmacology, 15(3), pp.311-316.

Huang, Z.M., Zhang, Y.Z., Kotaki, M. and Ramakrishna, S., 2003. A review on polymer nanofibers by electrospinning and their applications in nanocomposites. Composites Science and Technology, 63(15), pp.2223-2253.

Illangakoon, U.E., Nazir, T., Williams, G.R. and Chatterton, N.P., 2014. Mebeverine-Loaded Electrospun Nanofibers: Physicochemical Characterization and Dissolution Studies. Journal of Pharmaceutical Sciences, 103(1), pp.283-292.

Kanjanapongkul, K., Wongsasulak, S. and Yoovidhya, T., 2010. Prediction of clogging time during electrospinning of zein solution: Scaling analysis and experimental verification. Chemical Engineering Science, 65(18), pp.5217-5225.

Kaushal, A.M., Chakraborti, A.K. and Bansal, A.K., 2008. FTIR studies on differential intermolecular association in crystalline and amorphous states of structurally related non-steroidal anti-inflammatory drugs. Molecular Pharmaceutics, *5*(6), pp.937-945.

Kidoaki, S., Kwon, I.K. and Matsuda, T., 2005. Mesoscopic spatial designs of nano- and microfiber meshes for tissue-engineering matrix and scaffold based on newly devised multilayering and mixing electrospinning techniques. Biomaterials, 26(1), pp.37-46.

Li, H., Liu, K., Williams, G.R., Wu, J., Wu, J., Wang, H., Niu, S. and Zhu, L.M., 2018. Dual temperature and pH responsive nanofiber formulations prepared by electrospinning. Colloids and Surfaces B: Biointerfaces, 171, pp.142-149.

Lin, S.Y., 2014. An overview of famotidine polymorphs: solid-state characteristics, thermodynamics, polymorphic transformation and quality control. Pharmaceutical Research, 31(7), pp.1619-1631.

Lin, S.Y., Liao, C.M. and Hsiue, G.H., 1995. Temperature-dependent anhydride formation of Eudragit L-100 films determined by reflectance FTi.r. / dsc microspectroscopy. Polymer, 36(16), pp.3239-3241.

Liu, F., Ranmal, S., Batchelor, H.K., Orlu-Gul, M., Ernest, T.B., Thomas, I.W., Flanagan, T. and Tuleu, C., 2014. Patient-centered pharmaceutical design to improve acceptability of medicines: similarities and differences in paediatric and geriatric populations. Drugs, 74(16), pp.1871-1889.

Maurizio, C., 2018. Circadian rhythms and rheumatoid arthritis. Joint Bone Spine.

Merchant, H.A., Goyanes, A., Parashar, N. and Basit, A.W., 2014. Predicting the gastrointestinal behaviour of modified-release products: utility of a novel dynamic dissolution test apparatus involving the use of bicarbonate buffers. International journal of Pharmaceutics, 475(1-2), pp.585-591.

Mesley, R.J. and Johnson, C.A., 1965. Infrared identification of pharmaceutically important steroids with particular reference to the occurrence of polymorphism. Journal of Pharmacy and Pharmacology, 17(6), pp.329-340.

Mudie, D.M., Amidon, G.L. and Amidon, G.E., 2010. Physiological parameters for oral delivery and in vitro testing. Molecular Pharmaceutics, 7(5), pp.1388-1405.

Oparin, R.D., Ivlev, D.V., Vorobei, A.M., Idrissi, A. and Kiselev, M.G., 2017. Screening of conformational polymorphism of ibuprofen in supercritical CO2. Journal of Molecular Liquids, 239, pp.49-60.

Pan, H., Li, L., Hu, L. and Cui, X., 2006. Continuous aligned polymer fibers produced by a modified electrospinning method. Polymer, 47(14), pp.4901-4904.

Parhizkar, M., Reardon, P.J., Knowles, J.C., Browning, R.J., Stride, E., Barbara, P.R., Harker, A.H. and Edirisinghe, M., 2016. Electrohydrodynamic encapsulation of cisplatin in poly (lactic-co-glycolic acid) nanoparticles for controlled drug delivery. Nanomedicine: Nanotechnology, Biology and Medicine, 12(7), pp.1919-1929.

Parikh, T., Gupta, S.S., Meena, A. and Serajuddin, A.T., 2016. Investigation of thermal and viscoelastic properties of polymers relevant to hot melt extrusion-III: Polymethacrylates and polymethacrylic acid based polymers. Journal of Excipients and Food Chemicals, 5(1), p.1003.

Payab, S., Jafari-Aghdam, N., Barzegar-Jalali, M., Mohammadi, G., Lotfipour, F., Gholikhani, T. and Adibkia, K., 2014. Preparation and physicochemical characterization of the azithromycin-Eudragit RS100 nanobeads and nanofibers using electrospinning method. Journal of Drug Delivery Science and Technology, 24(6), pp.585-590.

Poller, B., Strachan, C., Broadbent, R. and Walker, G.F., 2017. A minitablet formulation made from electrospun nanofibers. European Journal of Pharmaceutics and Biopharmaceutics, 114, pp.213-220.

Quan, J., Yu, Y., Branford-White, C., Williams, G.R., Yu, D.G., Nie, W. and Zhu, L.M., 2011. Preparation of ultrafine fast-dissolving feruloyl-oleyl-glycerol-loaded polyvinylpyrrolidone fiber mats via electrospinning. Colloids and Surfaces B: Biointerfaces, *88*(1), pp.304-309.

Ramakrishna, S., 2005. An introduction to electrospinning and nanofibers. Hackensack, NJ ; London: World Scientific.

Rasenack, N. and Müller, B.W., 2002. Ibuprofen crystals with optimized properties. International Journal of Pharmaceutics, *245*(1-2), pp.9-24.

Rostom, A., Dube, C., Wells, G.A., Tugwell, P., Welch, V., Jolicoeur, E., McGowan, J. and Lanas, A., 2002. Prevention of NSAID-induced gastroduodenal ulcers. Cochrane Database of Systematic Reviews, (4).

Rowe, R.C., Sheskey, P.J. and Owen, S.C. eds., 2006. Handbook of pharmaceutical excipients (Vol. 6). London: Pharmaceutical press.

Sagdinc, S. and Bayarı, S., 2005. Experimental and theoretical infrared spectra of famotidine and its interaction with ofloxacin. Journal of Molecular Structure, 744, pp.369-376.

Sanchez-Vazquez, B., Amaral, A.J., Yu, D.G., Pasparakis, G. and Williams, G.R., 2017. Electrosprayed Janus particles for combined photo-chemotherapy. AAPS PharmSciTech, 18(5), pp.1460-1468.

Schilling, S.U., Shah, N.H., Malick, A.W., Infeld, M.H. and McGinity, J.W., 2007. Citric acid as a solid-state plasticizer for Eudragit RS PO. Journal of Pharmacy and Pharmacology, 59(11), pp.1493-1500.

Shen, X., Yu, D., Zhu, L., Branford-White, C., White, K. and Chatterton, N.P., 2011. Electrospun diclofenac sodium loaded Eudragit® L 100-55 nanofibers for colon-targeted drug delivery. International Journal of Pharmaceutics, 408(1-2), pp.200-207.

Toehwé, L.H., Prado, L.D. and Rocha, H.V.A., 2017. Prednisone raw material characterization and formulation development. Brazilian Journal of Pharmaceutical Sciences, 53(4).

Shen, X., Yu, D., Zhu, L., Branford-White, C., White, K. and Chatterton, N.P., 2011. Electrospun diclofenac sodium loaded Eudragit® L 100-55 nanofibers for colon-targeted drug delivery. International Journal of Pharmaceutics, 408(1-2), pp.200-207.

Shenoy, S.L., Bates, W.D., Frisch, H.L. and Wnek, G.E., 2005. Role of chain entanglements on fiber formation during electrospinning of polymer solutions: good solvent, non-specific polymer–polymer interaction limit. Polymer, 46(10), pp.3372-3384.

Simonelli, A.P., Mehta, S.C. and Higuchi, W.I., 1969. Dissolution rates of high energy polyvinylpyrrolidone (PVP)-sulfathiazole coprecipitates. Journal of Pharmaceutical Sciences, 58(5), pp.538-549.

Van den Mooter, G., Augustijns, P., Blaton, N. and Kinget, R., 1998. Physico-chemical characterization of solid dispersions of temazepam with polyethylene glycol 6000 and PVP K30. International Journal of Pharmaceutics, 164(1), pp.67-80.

Vogt, M., Derendorf, H., Krämer, J., Junginger, H.E., Midha, K.K., Shah, V.P., Stavchansky, S., Dressman, J.B. and Barends, D.M., 2007. Biowaiver monographs for immediate release solid oral dosage forms: Prednisone. Journal of Pharmaceutical sciences, 96(6), pp.1480-1489.

Wang, B., Wang, D., Zhao, S., Huang, X., Zhang, J., Lv, Y., Liu, X., Lv, G. and Ma, X., 2017. Evaluate the ability of PVP to inhibit crystallization of amorphous solid dispersions by density functional theory and experimental verify. European Journal of Pharmaceutical Sciences, 96, pp.45-52.

Wang, J.C., Zheng, H., Chang, M.W., Ahmad, Z. and Li, J.S., 2017. Preparation of active 3D film patches via aligned fiber electrohydrodynamic (EHD) printing. Scientific Reports, 7, p.43924.

World health organization. 2019. Chronic rheumatic conditions. [Online]. [13 February 2019]. Available from: https://www.who.int/chp/topics/rheumatic/en/.

Yang, C., Yu, D.G., Pan, D., Liu, X.K., Wang, X., Bligh, S.A. and Williams, G.R., 2016. Electrospun pH-sensitive core–shell polymer nanocomposites fabricated using a tri-axial process. Acta Biomaterialia, 35, pp.77-86.

Yu, D.G., Branford-White, C., Bligh, S.A., White, K., Chatterton, N.P. and Zhu, L.M., 2011. Improving Polymer Nanofiber Quality Using a Modified Co-axial Electrospinning Process. Macromolecular Rapid Communications, 32(9-10), pp.744-750.

Yu, D.G., White, K., Yang, J.H., Wang, X. and Li, Y., 2012. PVP nanofibers prepared using co-axial electrospinning with salt solution as sheath fluid. Materials Letters, 67(1), pp.78-80.

Yu, D.G., Xu, Y., Li, Z., Du, L.P., Zhao, B.G. and Wang, X., 2014. Coaxial electrospinning with mixed solvents: from flat to round eudragit L100 nanofibers for better colon-targeted sustained drug release profiles. Journal of Nanomaterials, *2014*.

Yu, D.G., Zhang, X.F., Shen, X.X., Brandford-White, C. and Zhu, L.M., 2009a. Ultrafine ibuprofen-loaded polyvinylpyrrolidone fiber mats using electrospinning. Polymer International, 58(9), pp.1010-1013.

Yu, D.G., Shen, X.X., Branford-White, C., White, K., Zhu, L.M. and Bligh, S.A., 2009b. Oral fast-dissolving drug delivery membranes prepared from electrospun polyvinylpyrrolidone ultrafine fibers. Nanotechnology, 20(5), p.055104.

Yu, D.G., Williams, G.R., Wang, X., Liu, X.K., Li, H.L. and Bligh, S.A., 2013a. Dual drug release nanocomposites prepared using a combination of electrospraying and electrospinning. RSC Advances, 3(14), pp.4652-4658.

Yu, D.G., Liu, F., Cui, L., Liu, Z.P., Wang, X. and Bligh, S.A., 2013b. Coaxial electrospinning using a concentric Teflon spinneret to prepare biphasic-release nanofibers of helicid. RSC Advances, 3(39), pp.17775-17783

Xu, L.L., Shi, L.L., Cao, Q.R., Xu, W.J., Cao, Y., Zhu, X.Y. and Cui, J.H., 2014. Formulation and in vitro characterization of novel sildenafil citrate-loaded polyvinyl alcohol-polyethylene glycol graft copolymer-based orally dissolving films. International Journal of Pharmaceutics, 473(1-2), pp.398-406.

Zhou, W., An, X., Wang, J., Shen, W., Chen, Z. and Wang, X., 2012. Characteristics, phase behavior and control release for copolymer–liposome with both pH and temperature sensitivities. Colloids and Surfaces A: Physicochemical and Engineering Aspects, 395, pp.225-232.

Chapter 6. Fabrication of levodopa and carbidopa fixed-dose combinations in the form of coaxial electrospun fibres

6.1 Introduction

In Chapters 4 and 5, single needle electrospinning was employed to generate FDCs using different fibre deposition protocols. These approaches proved able to produce FDC formulations with a range of properties for the treatment of hypertension with amlodipine besylate and valsartan, and for the treatment of rheumatoid arthritis with ibuprofen, famotidine, and prednisone. In this chapter, a different approach to FDCs is explored. Rather than a monoaxial process, a concentric needle is utilised for coaxial electrospinning and the construction of a core/shell fibre (see Figure 6.1). These core/shell fibres are then explored as a DDS for two model drugs used in the treatment of Parkinson's disease: levodopa (LD) and carbidopa (CD).

The FDC formulations are prepared using two base polymer solutions containing polyvinylpyrrolidone (PVP) and Eudragit® RL PO (E-RLPO). The aim of the work is to fabricate core/shell fibre as a platform for oral FDCs giving biphasic drug release: an initial burst release of a loading dose of the drug followed by extended release. The fibres will comprise a PVP shell and E-RLPO core. An immediate burst of drug release from the PVP shell is expected, since PVP is a well known hydrophilic polymer and will dissolve rapidly upon contact with gastric fluids (Forster et al., 2001). This should be followed by extended drug release from the E-RLPO core, since the latter is an acrylic and methacrylic acid-based polymer, insoluble in water and with low permeability, but undergoing pH-independent swelling in the digestive fluid to provide time-controlled release (Yadav et al., 2012).

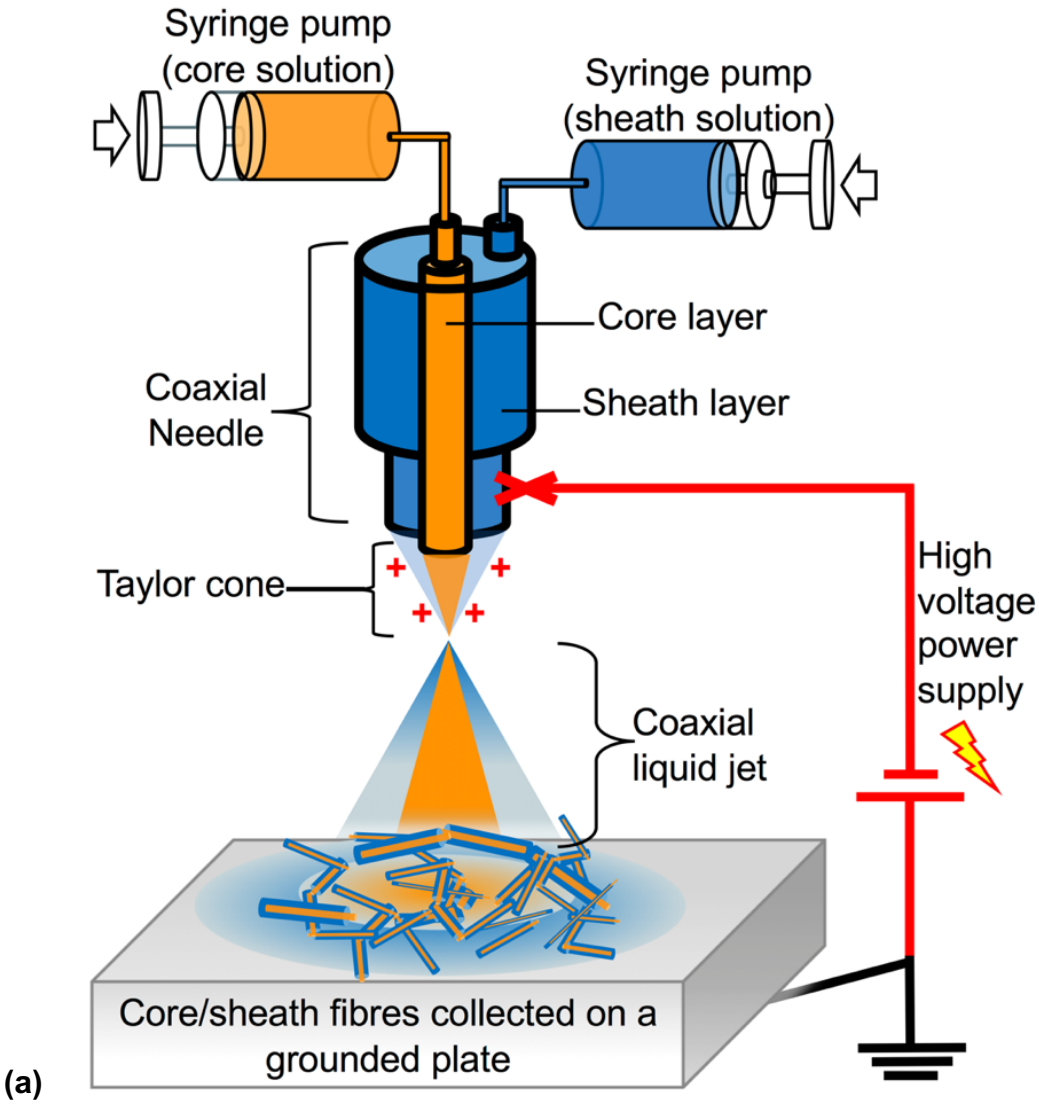

(a)

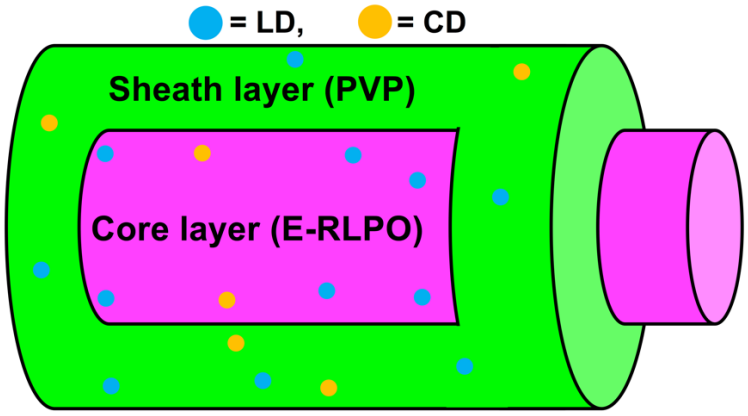

(b)

Figure 6.1. (a) A schematic diagram of the coaxial electrospinning process. The general setup for coaxial electrospinning; **(b)** a schematic diagram of the core/shell FDCs prepared in this chapter.

In coaxial electrospinning, each needle is fed with a separate liquid via two separate syringes (Greiner & Wendorff 2007). When a voltage is applied, the charge will accumulate mainly on the surface of the shell solution (Figure 6.2, a) (Greiner et al. 2006), and the shell solution will form a conical shape and ultimately emit a polymer jet (Moghe and Gupta, 2008). The deformed shell solution will extend, and by viscous dragging and contact friction will result in stretching of the core solution. (Figure 6.2, b) (Li and Xia, 2004). This leads the core solution to deform into a conical shape, and a coaxial jet is thus produced (Figure 6.2, c) (Moghe and Gupta, 2008).

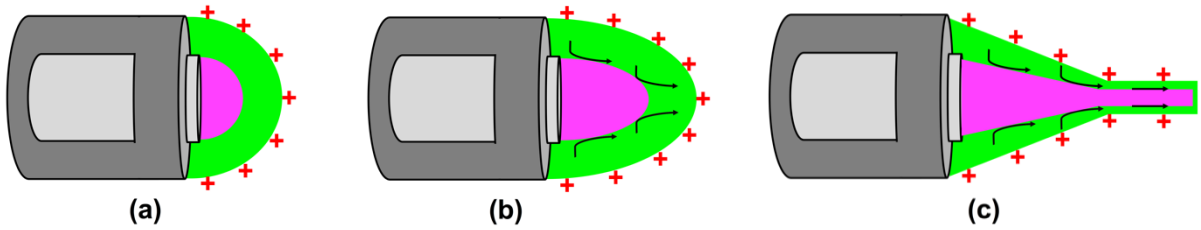

Figure 6.2. Compound Taylor cone formation in coaxial electrospinning. **(a)** Charges accumulate on the surface of the shell solution; **(b)** the deformed shell solution will exert viscous dragging on the core solution; **(c)** a core-shell compound Taylor cone continue to form as a result of continues viscous dragging. Adapted from (Moghe and Gupta, 2008).

If the coaxial electrospinning process is well optimised, the outcome should be core/shell fibres with two distinct compartments and minimal mixing of the two fluids. This result can be obtained by modifying the solution and processing parameters including the polymer concentration, the strength of the applied voltage, and the solution feed rate. All of these can potentially alter the fibre properties and structure, and the drug release kinetics (Ding and Yu, 2018).

Coaxial electrospinning of core/shell fibres has been broadly applied to create formulations with a number of benefits over monolithic systems from single-needle

electrospinning (Zhang et al., 2004; Huang et al., 2005; Yu et al. 2012). For instance, while a burst of drug release is typically observed from monolithic fibres (because of the presence of drug at the surface), this can be avoided in a core/shell system by having a drug-free shell layer (Wang et al., 2010). This is particularly true for hydrophilic small molecule drugs (Chou et al, 2015).

Other benefits of coaxial spinning lie in the development of a drug delivery system with biphasic release, as is desired here. Because coaxial electrospinning allows the combination of two polymers with very different properties (e.g. in terms of solubility/dissolution rate), it can result in release occurring at two different rates. This has been shown to be the case when PVP and zein were used to construct core/shell fibres (Jiang et al., 2012).

Another application of coaxial electrospinning involves the use of the shell layer to provide delayed release. This has been realised on a number of occasions, for instance in fabricating an oral formulation for imaging colon abnormalities. Here, fibres were successfully produced using a pH-sensitive polymer (Eudragit S100) for the shell and a bioadhesive polymer (polyethylene oxide) for the core. In vitro testing showed strong mucoadhesive forces after the dissolution of the Eudragit shell, and incorporating an imaging agent into the core was also possible (Jin et al., 2016).

Coaxial electrospinning efficiently can further help in the protection of easily denatured biological agents. This can be achieved by loading the sensitive substance(s) in a core solution, using a non-damaging solvent. For instance, peptide and protein drugs can be processed in an aqueous core, and the organic solvents usually required for

electrospinning can be confined to the shell (Huang et al., 2006). This helps to avoid the active ingredient coming into contact with an organic solvent and thus degrading. For instance, Zhang et al. (2006) studied the feasibility of encapsulating a model protein (bovine serum albumin; BSA) along with poly(ethylene glycol) (PEG) into the core of poly(ε-caprolactone) (PCL) nanofibers via coaxial electrospinning, and were able to achieve sustained release of BSA over a period of more than 5 months.

In this chapter, the creation of a coaxial FDC is explored for potential applications in the context of unintentional non-adherence by late stage Parkinson's disease (PD) patients. PD is a disabling disorder that significantly affects the quality of life (Chaudhuri et al., 2004). Treatments are available, but only 10% of PD patients fully adhere to their treatment regimens (Leopold et al., 2004). Non-adherence in PD is a serious problem linked to worsening symptoms and increased motor fluctuations (Kulkarni et al., 2008; Fernandez, 2012) (Ngwuluka et al., 2010).

Levodopa (LD) remains the most effective treatment for PD (Rajput, 2001). However, a single dosing treatment is only effective in the early phase of PD. In the severe phase, 4-5 years after diagnosis, the therapeutic window of dopamine becomes narrow, and due to its short half-life of between 0.7 to 1.4 h dosing of LD will be required every 2 h (Contin et al., 1990; Seeberger and Hauser, 2007; Grosset et al., 2009). One way to ameliorate this issue is to co-administer LD with CD. After oral administration of LD, it undergoes extensive pre-systemic metabolism to dopamine in the gut via the enzyme l-amino acid decarboxylase (AADC) (Contin et al., 1996). As a result, LD bioavailability is low with only 15-33% of LD reaching the systemic

circulation. Co-administration with peripheral AADC inhibitors such as CD in the form of an FDC can increase LD oral bioavailability to 40-70% (Contin and Martinelli, 2010).

A goal of PD pharmacotherapy has been the development of an oral formulation able to keep LD in the therapeutic plasma concentration range (Hsu et al., 2015). There exists an approved combination formulation of LD and CD, available in a dose range between 100/25 mg to 200/50 mg (Sinemet CR®; Merck). This takes the form of sustained-release (SR) tablets which release their ingredients over a 4 to 6 hour period (Stocchi, 2009; Hsu et al., 2015). This tablet is advantageous over the immediate release (IR) of LD alone, because it can reduce fluctuations of dose in the systemic circulation (Ngwuluka et al., 2010). However, LD absorption might be delayed if the SR tablet is used alone, so effective therapy often requires co-administration of an IR dose of LD/CD, particularly for the first morning dose (Hsu et al., 2015). In this chapter, we seek to combine both immediate and sustained release of LD and CD into a single formulation, with the ultimate aim of improving patient compliance in PD treatment.

6.2 Experimental

6.2.1 Solution preparation

Two base polymer solutions were used in this work. These comprised 10% w/v PVP (MW 360,000 Da; Sigma-Aldrich, UK) in ethanol, and 20% w/v Eudragit RLPO (E-RLPO; MW 150,000 Da; Evonik GmbH, Germany) in ethanol. Each solution was stirred overnight to ensure complete dissolution. The required volume of each polymer solution was mixed with a solution of the APIs dissolved in 1 M aqueous HCl (see

Table 6.1). In order to protect LD and CD from photolytic degradation, the samples were stored in dark amber glass containers. The combined drug/polymer solutions were mixed at room temperature for 6 h to obtain homogeneous solutions.

Table 6.1. The compositions of each formulation.

Formulation (ID)	Polymer solution volume (mL)		Drug loading (% w/w) Theoretical value		Drug mass (mg) in HCl (1*M*)		
			LD	CD	LD	CD	HCL (mL)
F1	E-RLPO (20% w/v) Core layer	2	19.1	4.86	100.23	25.45	1
	PVP (10% w/v) Shell layer	4			100.6	25.72	2
F2	E-RLPO (20% w/v) Core layer	5	8.8	2.2	100.23	25.45	1
	PVP (10% w/v) Shell layer	10			100.6	25.72	2

6.2.2 Development of the FDC formulation

6.2.2.1 Apparatus setup

The setup of the coaxial electrospinning apparatus is shown in Figure 6.1, a. For each formulation, the polymer solutions were loaded into separate plastic syringes (BD plastic, MediSupplies, UK) with care taken to avoid any air bubbles. Each syringe was fitted on a syringe pump (KDS100, Cole Parmer, UK) and connected with plastic tubing to infuse the polymer solution into a concentric needle (spinneret) with stainless steel needles (core: 18G, 0.83 mm inner diameter; shell: 13G, 1.83 mm inner diameter; see

Figure 6.3, a). A high voltage was applied to the spinneret using an HCP 35-35000 power supply (FuG Elektronik GmbH, Germany). To collect the fibres, a flat metal collector (5 x 5) cm covered with aluminium foil was situated 19 cm below the spinneret tip. The electrospinning process took place in ambient conditions of 19 to 26 ºC, and 31 to 49 % RH.

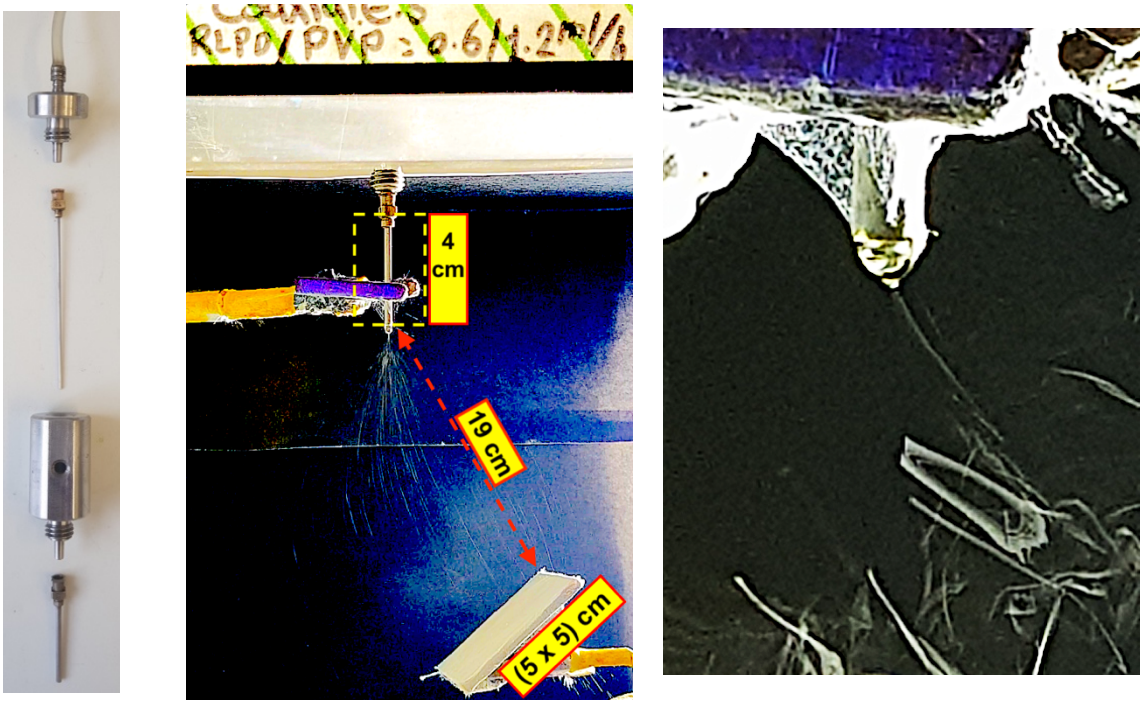

(a) **(b)** **(c)**

Figure 6.3. (a) a photo of the concentric spinneret; **(b)** an image of the coaxial electrospinning process under bright light; and **(c)** the formation of a compound Taylor cone during the optimisation process.

6.2.2.2 Coaxial electrospinning

Optimisation of the electrospinning parameters was performed to find the most appropriate flow rate, voltage, and spinneret to collector distance. Using a bright light (MULTI LED PT 24 High power LEDs, 84 W, 24 V, GSVitec, Germany) focused on the

tip of the spinneret allowed Taylor cone formation to be observed and ensure that a continuous liquid jet of fibres is produced. This was then collected on a glass slide for a few seconds to confirm fibre formation under an inverted digital microscope (EVOS XL Cell Imaging System, Thermo Fisher Scientific, UK). Electrospinning was first performed on the individual polymer solutions dispensed through the coaxial spinneret, by turning off one of the pumps. The optimisation of the electrospinning process took place in ambient conditions of 18 to 25 ºC, and 30 to 47 % RH. The electrospinning parameters were optimised to find the most appropriate flow rate, voltage, and spinneret to collector distance. The best *experimental conditions* for each solution were thus identified, and from that suitable conditions for coaxial spinning were determined (Table 6.2).

Table 6.2. The *range of experimental conditions explored in this chapter.*

Polymer solution	Syringe pump flow rate (mL/h)	Applied voltage (kV)	Spinneret to collector distance (cm)
E-RLPO (20% w/v)	Range= 0.2 – 0.6 Best value= 0.6	Range= 13-22 Best value= 22	Range= 13-19 Best value= 19
PVP (10% w/v)	Range = 0.4 – 1.3 Best value= 1.2	Range= 15 – 23 Best value= 22	Range= 10-20 Best value= 19
Coaxial ES of both polymer E-RLPO/ PVP	Range (core/shell) = 0.2/0.4 – 0.6/1.2 Best value= 0.6/1.2	Range= 18-24 Best value= 22	Range= 13-19 Best value= 19

Characterisation of the resulting coaxial electrospun fibres was performed as described in Chapter 2.

6.3 Results and discussion

6.3.1 Formulation optimisation

Ethanol was a suitable solvent for dissolving both polymers, as found in previous chapters. It proved challenging to identify a suitable solvent for LD and CD, however. This is because LD undergoes two different degradation pathways, one through decarboxylation to form dopamine, and the other via oxidation leading to the formation of melanin. It is reported that LD can be easily oxidised at alkaline pH, in the presence of water, at elevated temperatures, and by photolytic degradation. This results in the formation of a brown to black colour compound (Siddhuraju and Becker, 2001). To avoid such degradation, an acidic pH is desirable to hinder oxidation. LD has three ionisable centers with pKa1 = 2.3, pKa2 = 8.11 and pKa3 = 9.92 (Zhou et al., 2012). The drug is positively charged at pH < 2.3, and thus has highest solubility under these conditions. Hence, 1 M HCl in water was found to be an appropriate solvent to dissolve both LD and CD.

Electrospinning of PVP at 10% w/v was proven to be possible in Chapter 4, and is also well known in the literature (Yu et al., 2009; Quan et al., 2011). However, it was necessary to keep the flow rate of PVP at an optimum value to ensure formation of a composite Taylor cone with the core solution and permit a smooth and continuous electrospinning process. The electrospinning of E-RLPO was explored over a range of flow rates between 1.3 – 0.2 mL/h. Initially a concentration of 30% w/v was selected in order to maximise production rates. This concentration is similar to that reported in the literature (Pornsopone et al., 2007). However, this polymer concentration resulted

in clogging at the tip of the core needle. The concentration was hence reduced to 20% w/v, which allowed a continuous flow of solution without clogging. This is in accordance with previous findings. It was reported by Pornsopone et al. (2005) that for a fixed applied voltage of 7.5 kV, a concentration of E-RLPO at 15% w/v resulted in a combination of smooth and beaded fibres, while further increasing the solution concentration to 20% w/v created smooth fibres. When the applied voltage was raised to 22.5 kV, Pornsopone found that E-RLPO at both 15% w/v and 20% w/v gave smooth fibres, with a larger diameter at 20% w/v.

The range of values which enable a stable electrospinning process are recorded in Table 6.2. The optimal values for electrospinning each polymer solution were used to optimise coaxial electrospinning. Here, we sought to prepare coaxial fibres with equal masses of polymer in the core and sheath layers, and ensure an equal drug loading in both compartments. To do this, the flow rate of the core and shell fluids was fixed at a 1:2 ratio.

Usually in coaxial electrospinning, the flow rate of the shell layer is set to be 3- to 10-fold faster than the core layer. However, here we managed to perform electrospinning at a 1:2 flow rate ratio. This success might arise from the fact that the PVP shell is readily electrospinnable. The flow rate range that allowed fibres to be produced at the 1:2 core/shell flow rate ratio was between 0.2-0.6 mL/h (core) and 0.4-1.2 mL/h (shell). The optimum flow rate values identified were 0.6/1.2 mL/h. This gave the maximum process yield and ensured the spinneret was continuously supplied with the polymer solution without clogging or discontinuation of the Taylor cone. Reducing the flow rate both reduced the amount of product generated per unit time and led to an intermittent

cone-jet, and thus a non-continuous process. It was noted that at 0.6/1.2 mL/h, it was necessary to select a high applied voltage to maintain a continuous Taylor cone.

6.3.2 Morphology

Scanning electron microscope (SEM) images of the raw APIs and the coaxial electrospun fibres F1 and F2, together with the diameter distributions, are displayed in Figure 6.4.

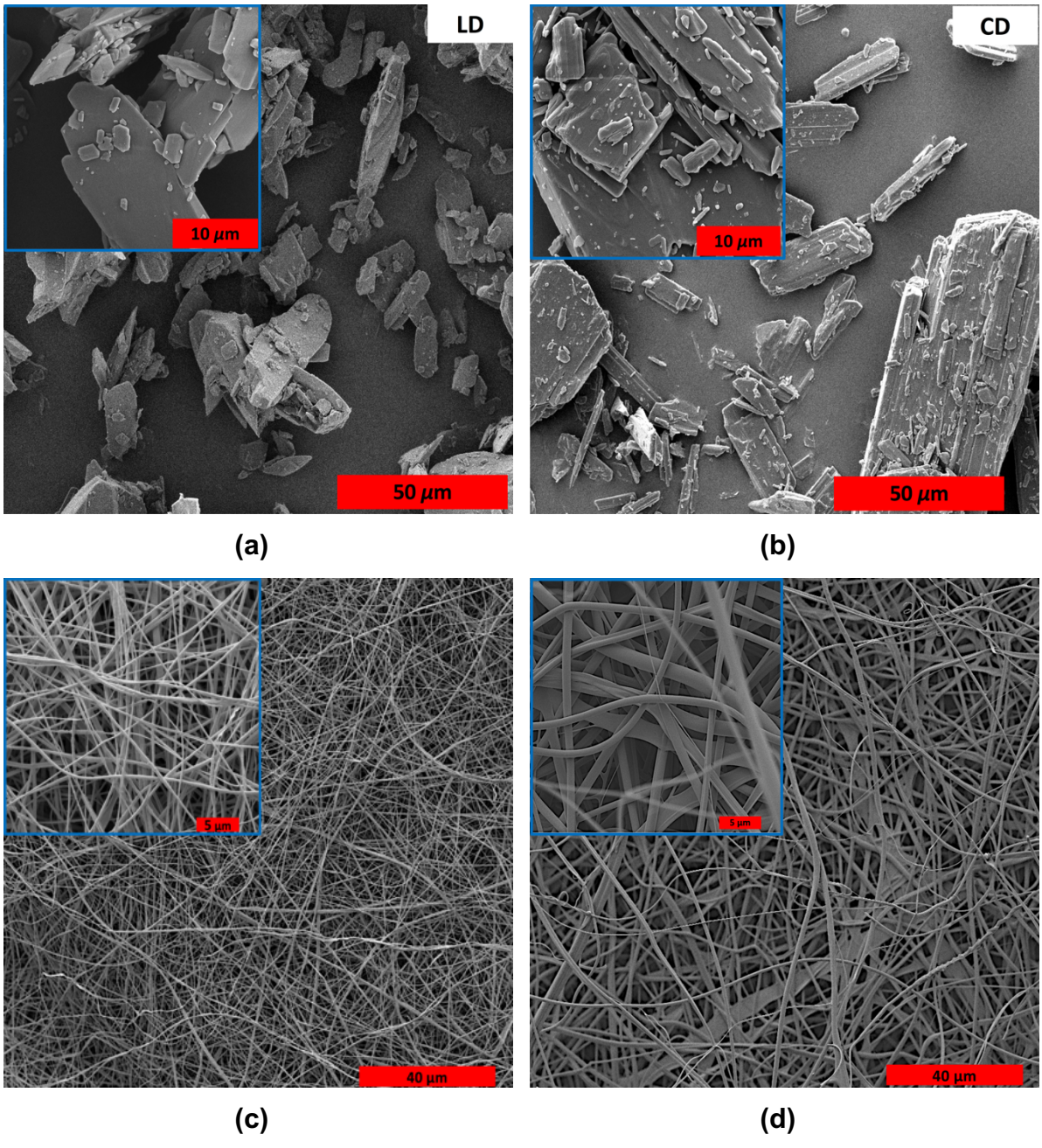

(a) **(b)**

(c) **(d)**

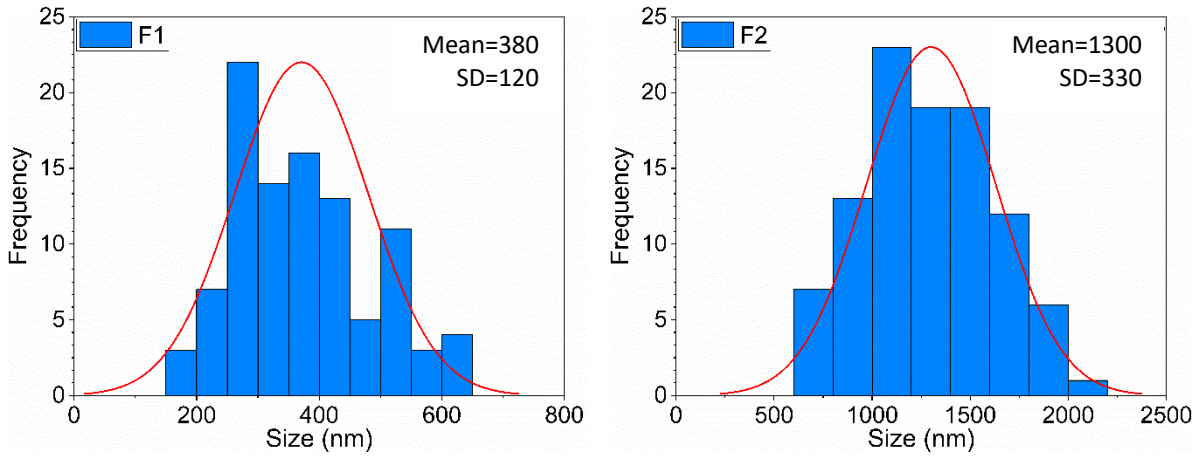

(e) (f)

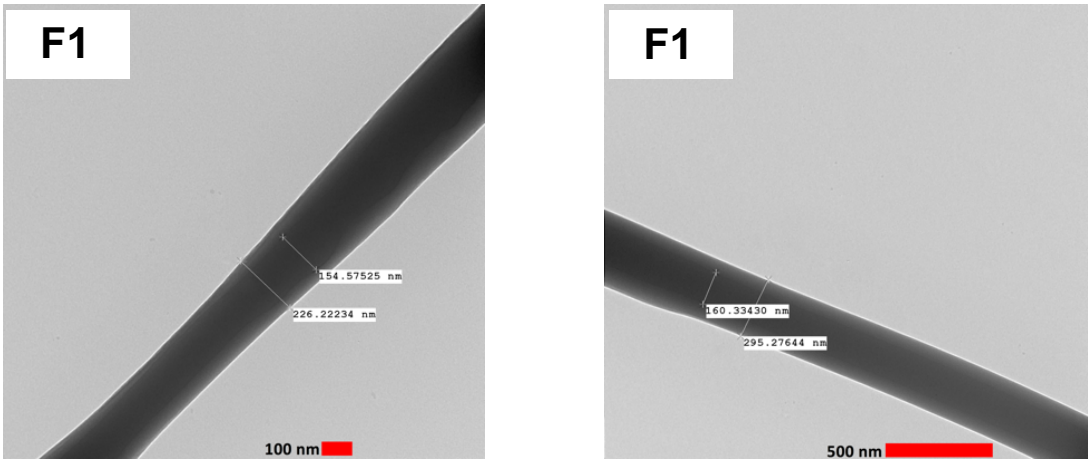

(g) (h)

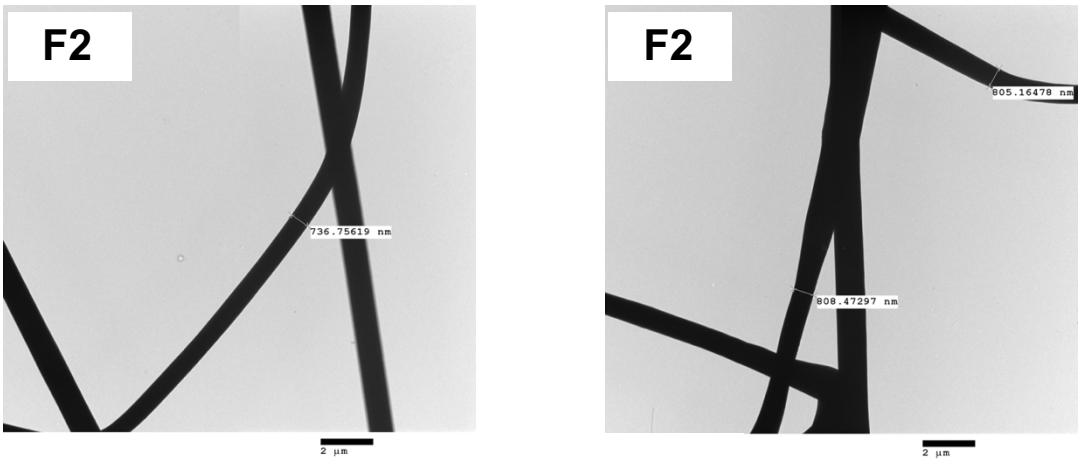

(i) (j)

Figure 6.4. SEM images of raw materials (**a)** LD; (**b)** CD; SEM images distributions of formulation (**c)** F1 (19.6/4.6 w/w LD/CD); (**d)** F2 (8.8.6/2.2 w/w LD/CD), with and fibre diameter distributions for (**e)** F1 and (**f)** F2. TEM images of formulation **(g)** F1 collected after dispensing 3 mL of liquid; **(h)** F1 collected after dispensing 6 mL; **(i)** F2 collected after dispensing 6 mL; **(j)** F2 after dispensing 12 mL.

The SEM images of the raw materials (Figure 6.4, a & b) shows LD to exist as large particles with sharp edges (Luinstra et al., 2015) and CD as elongated particles with irregular edges. The characteristic shape of both raw materials shows they are crystalline materials. The production of fibres was proved successful for both formulations as shown in Figure 6.4, c & d. The images of the fibres do not show any evidence for particles of LD or CD, indicating a solid dispersion was generated (Bognitzki et al., 2001).

The surface images of the fibres show that all have a cylindrical shape with a smooth surface. The diameter size of F1 was 376 ±120 nm and F2 1300 ± 329 nm. Even though both fibres were prepared under the same conditions, a clear difference in size can be seen. The reason for this is thought to be the variation in the amount of the polymers used. In both formulations, the amount of LD+CD was fixed at 100mg LD / 25 mg CD in each layer of the fibres in the mat (Table 6.1). However, the polymer amounts differ, with the solutions containing more polymer in the case of F2. This increase in the total amount of polymers resulted in a greater mass of solute being dispensed per unit time, and thus in larger sized fibres. Similar results have been reported in the literature by Pornsopone et al. (2005 and 2007) who produced fibres sized ~1300 nm from 20% w/v E-RLPO, and fibres sized ~2200 nm from 25% w/v E-RLPO (Pornsopone et al.2007).

The transmission electron microscope (TEM) images of the fibres are shown for F1 in Figure 6.4, g & h, and F2 in Figure 6.4, i & j. The TEM samples were collected on TEM grids after different volumes had been dispensed to confirm the continuous formation of core/shell structure fibres. The images of F1 (Figure 6.4, g & h) proved the formation

of a core/shell structure fibres in both samples collected, with a diameter of the core around 154-160 nm, and the shell at 226-295 nm. The images of F2 (Figure 6.4, i & j) do not confirm the formation of core/shell fibres, however. It is not clear why this is, but it may be that mixing of the fluids occurred during spinning.

6.3.3 X-ray diffraction (XRD)

The physical form of the drugs in the fibres was assessed with XRD and DSC. The XRD diffraction patterns are given in Figure 6.5.

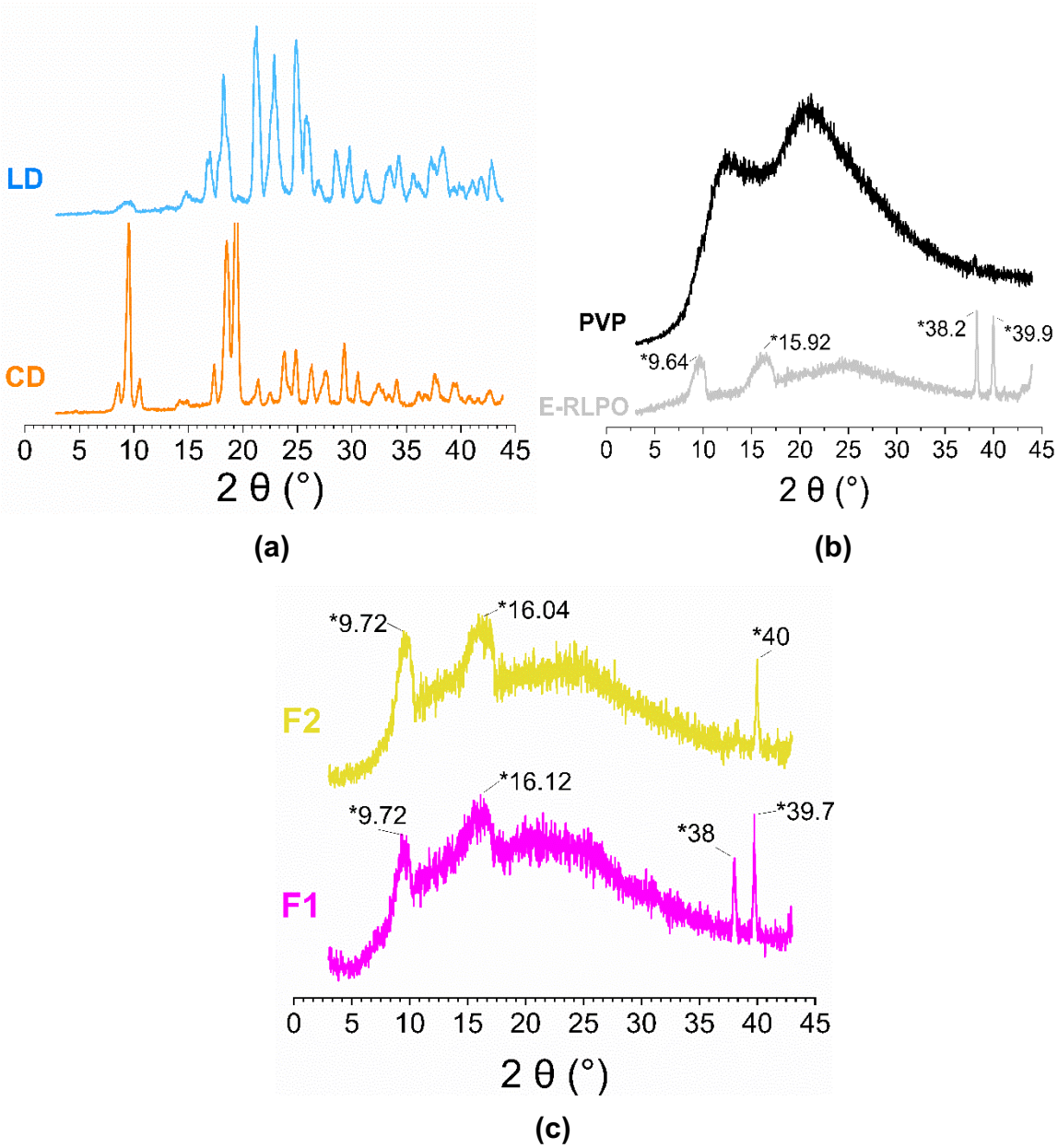

Figure 6.5. XRD diffraction patterns of the raw materials and fibres: **(a)** raw APIs (LD, and CD); **(b)** the pure polymers (PVP, and E-RLPO); **(c)** the FDC coaxial fibres F1 and F2. Peaks labelled with * correspond to the sample holder.

The patterns of the API raw materials show numerous sharp Bragg reflections for LD (e.g. at 18.36, 21.4, 22.98, and 25.08°) and CD (e.g. at 9.66, 18.66, and 19.56°) as is clear from Figure 6.5a. This illustrates that both drugs existed in a crystalline form before electrospinning. In contrast, the XRD patterns for the polymers (Figure 6.5b) shows broad haloes without any Bragg reflections, which indicates the amorphous

nature of both polymers. In the patterns of the coaxial fibre composites (Figure 6.5c), only a broad halo is seen, without the presence of any characteristic reflections from LD or CD. This confirmed that both drugs are present as amorphous solid dispersions within the coaxial fibres. This result was expected since it is known that electrospinning involves a very rapid drying process, which does not allow sufficient time for recrystallisation. Coaxial fibres prepared from PVP and other Eudragit polymers have been found to have similar amorphous structures (Illangakoon et al., 2015; Yang et al., 2018).

6.3.4 Differential scanning calorimetry (DSC)

The DSC thermograms of the raw materials and the coaxial fibres are shown in Figure 6.6.

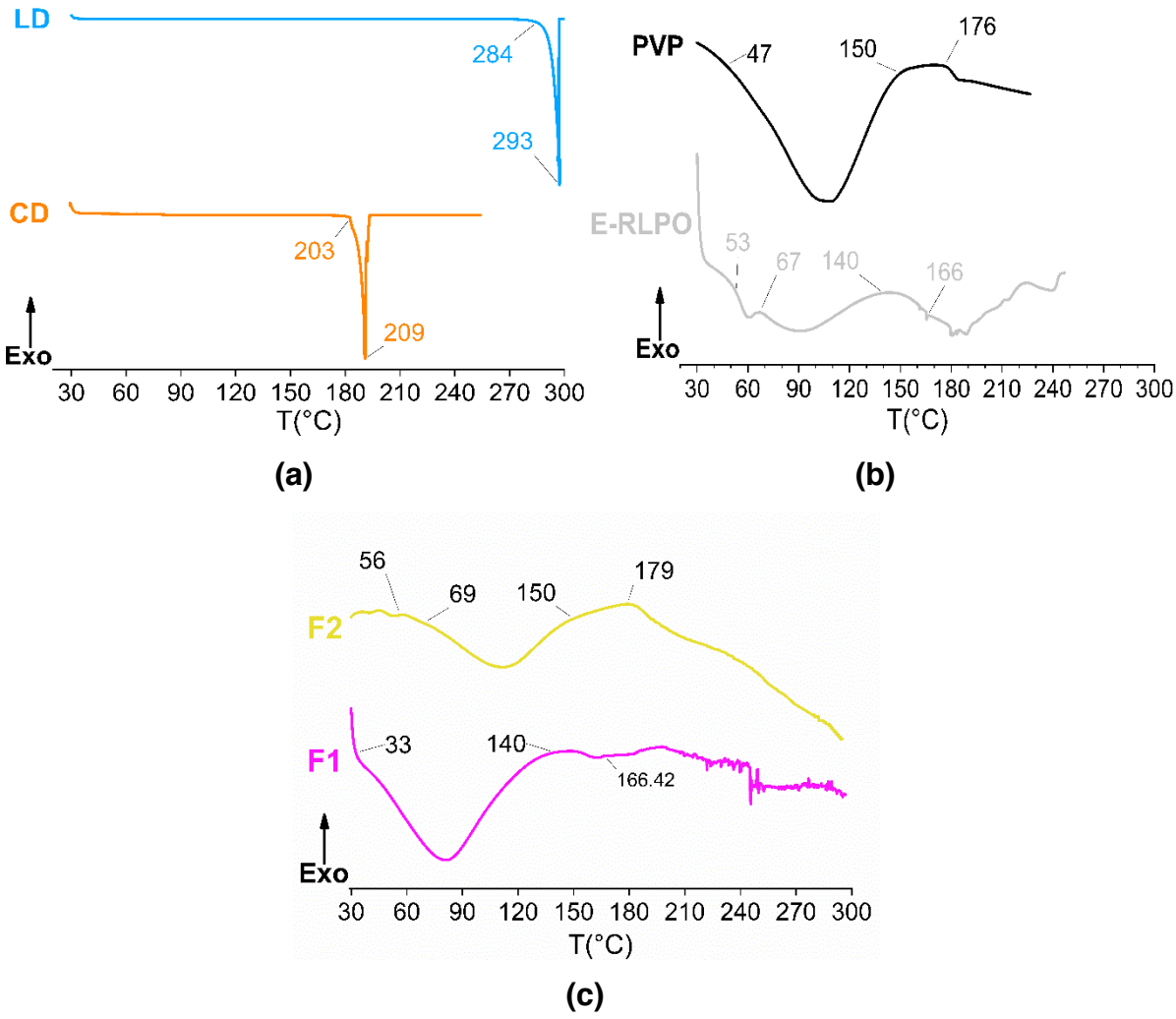

Figure 6.6. DSC data for **(a)** the pure APIs LD and CD; **(b)** the polymer carriers; **(c)** the FDC fibres F1 and F2.

The data for the APIs raw materials (Figure 6.6a) show endothermic peaks corresponding to melting, with onset for LD at 284 ºC and for CD at 196 ºC. These observed results are within the range reported in the literature for LD (284-286 ºC; O'Neil et al., 2001) and CD (203-208 ºC; British Pharmacopeia, 2013; National Center for Biotechnology Information, 2019). This observation indicates that both drugs were initially in the crystalline form before processing, which agrees with the findings from XRD.

In Figure 6.6b the data for the polymer raw materials show a broad endothermic peak for PVP at around 30 to 150 °C due to the evaporation of adsorbed water, and Tg appears at 176 ºC, close to the literature value of 166 ºC (Poller et al., 2017). E-RLPO shows a Tg at 53 ºC, followed by a broad dehydration endotherm between 67 and 140 °C. The Tg here is similar to a value previously reported for E-RLPO by (Dave et al., 2012) (53.1 °C). As with other polymers, the Tg of E-RLPO depends on the level of sorbed water in the polymer. The event observed at 166 °C for E-RLPO was described by Parikh et al. (2016) as polymer degradation. In both polymers, no melting endothermic peaks exist, confirming the amorphous nature of the polymer.

The thermograms of the coaxial fibres (Figure 6.6c) show they undergo dehydration, in the form of a broad endotherm between around 33 and 140 °C for F1, and 150 °C for F2. No melting endotherm of LD or CD was visible in the coaxial fibres, which agrees with the findings from XRD and demonstrates the fibres to comprise amorphous solid dispersions (Wu et al., 2017). The thermogram of F2 shows Tgs at 56 ºC from E-RLPO, and at 179 ºC from PVP. In F1 these glass transitions cannot be clearly observed, but the noise at ca. 166 ºC could be related to E-RLPO degradation.

6.3.5 FTIR spectroscopy

Infrared spectroscopy was performed to evaluate the drug-polymer interactions and compatibility. The chemical structures and IR spectra of the raw materials and electrospun fibres are presented in Figure 6.7.

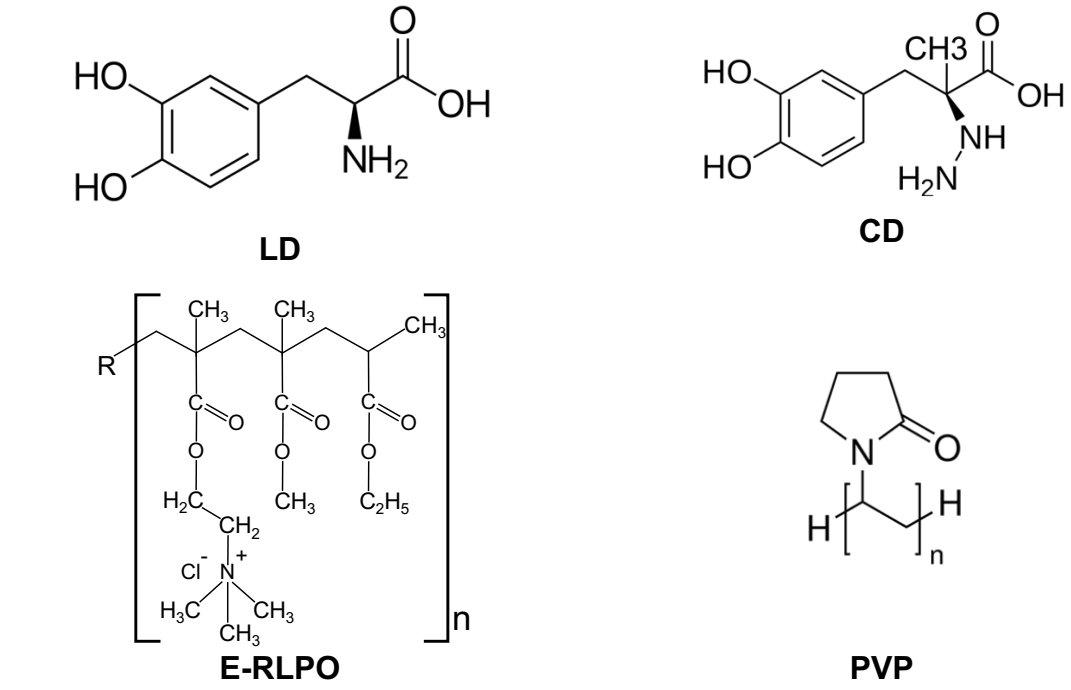

(a)

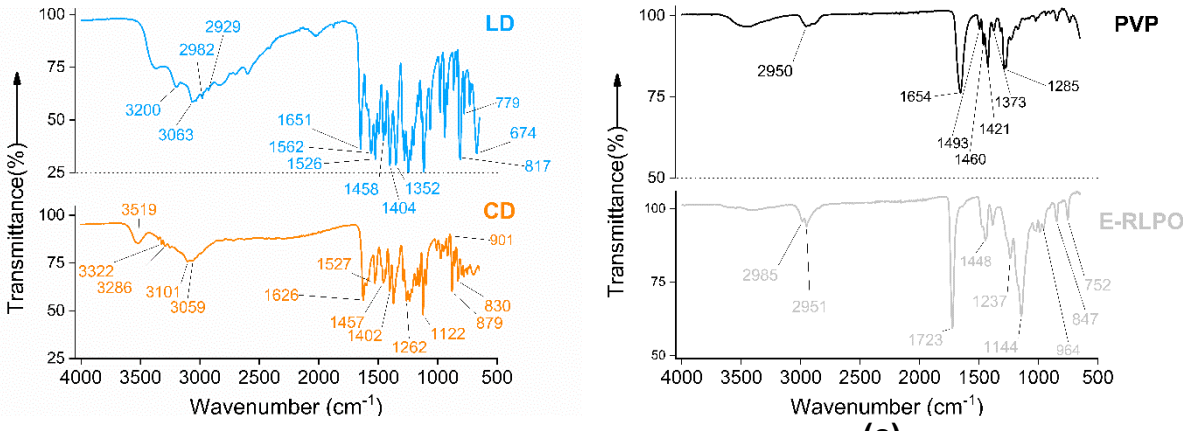

(b)

(c)

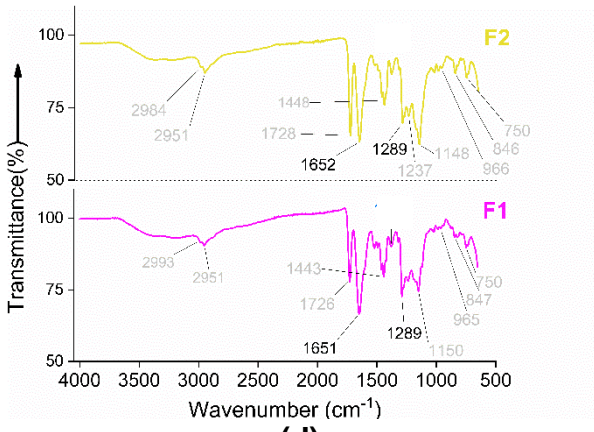

(d)

Figure 6.7. (a) Chemical structures of the APIs and polymers, together with FTIR data for **(b)** the raw APIs; **(c)** the polymers; **(d)** the FDC fibres F1 and F2.

The FTIR spectra of the API raw materials (Figure 6.7b) present characteristic bands for each material. In the spectrum of LD, characteristic peaks appear from O—H stretching at 3200, 3063, and 2982 cm^{-1}, from phenyl group C=C vibrations at 1458, 1404, 1352, 817, and 674 cm^{-1}, and from C—H stretches at 2929 and 2982 cm^{-1}. NH_2 stretches are visible at 1562 cm^{-1}, and C=O stretching at 1651 cm^{-1}. In the spectrum of CD, O—H stretching bands arise at 3519, 3322, 3286 cm^{-1}, phenyl group C=C vibrations are present at 1457, 1402, 1262, 879, and 830 cm^{-1}, with C—H stretches at 3101, 3059, and 1371 cm^{-1}. N—H and NH_2 stretches arise at 1527 cm^{-1} and 1122 cm^{-1}, and C=O stretching at 1626 cm^{-1} (Sagdinc and Bayarı, 2005). The spectra of the raw material polymer powders (Figure 6.7c) show that PVP has a broad band between 3400 to 2950 cm^{-1} corresponding to O—H stretches from the adsorbed water, C=O vibrations at 1654 cm^{-1}, and a C—N stretch at 1285 cm^{-1}. The spectrum of E-RLPO displays C—H stretching at 2951 cm^{-1} and 1448 cm^{-1}, a C=O stretch at 1723 cm^{-1}, and C—O—C vibrations at 1237 and 1143 cm^{-1} (Evonik, 2007).

In the FTIR spectra of the coaxial fibre mats (Figure 6.7d), formulation F1 shows peaks from E-RLPO at 2951 cm^{-1} from C—H stretching, at 1728 cm-1 from C=O stretching, and at 1148 cm^{-1} from C—O—C vibrations. Bands from PVP can be seen between 3400 to 2950 cm^{-1} for O—H and C-H stretches, 1652 cm^{-1} from C=O vibrations, and at 1289 cm^{-1} from C—N stretching. Similarly for formulation F2, peaks from E-RLPO can be seen at 2951 cm^{-1} from C—H stretching, at 1726 cm^{-1} from C=O stretching, and at 1150 cm^{-1} from C—O—C vibrations, and peaks from PVP at 3400 to 2984 cm^{-1}, 2950 cm^{-1}, 1651 cm^{-1}, and 1289 cm^{-1}.

In comparison to the spectrum of pure LD and CD, in the fibres many of the drug's characteristic peaks have shifted positions or merged with the peaks from the carrier polymers, indicating that APIs were successfully loaded in the fibres mat with significant molecular interactions between the drug and the polymer.

6.3.6 Drug loading and encapsulation efficiency (EE)

The drug loading and EE were determined by HPLC, and the results are listed in Table 6.3.

Table 6.3. The drug loadings and EE of the fibres. Data are reported as mean ± S.D. (n=3).

Formulation	LD loading (% w/w)	LD EE (%)	CD loading (% w/w)	CD EE (%)
F1	19.1 ± 0.6	90.1 ± 0.1	4.9 ± 0.1	66.2 ± 1
F2	8.9 ± 0.1	105.5 ± 0.1	2.2 ± 0.1	81.7 ± 0.6

For each formulation, the loading of LD was close to the theoretical percentage, and hence the EE is > 90%. However, for CD the drug loading and EE are notably lower. This decrease in CD could be a result of degradation during either the electrospinning or HPLC sample preparation processes.

6.3.7 *In vitro* drug release

In the British Pharmacopoeia (BP), it is recommended to perform dissolution testing of the LD/CD combination SR tablet in 0.1M HCl (British Pharmacopeia Commission,

2016). The dose of the selected tablet contains LD/CD at 200/50 mg. This is relatively high, and thus the high drug-loaded formulation F1 seemed more appropriate for study here. Further, the TEM images of F2 did not confirm the formation of core/shell fibres.

The F1 fibres were manually loaded into a hard gelatin capsule (size 0) since the intention is to deliver the formulation orally (see Figure 6.8). The in-vitro drug release results are given in Figure 6.9.

Figure 6.8. A photograph of the coaxial electrospun fibres loaded in a hard gelatin capsule (size 0).

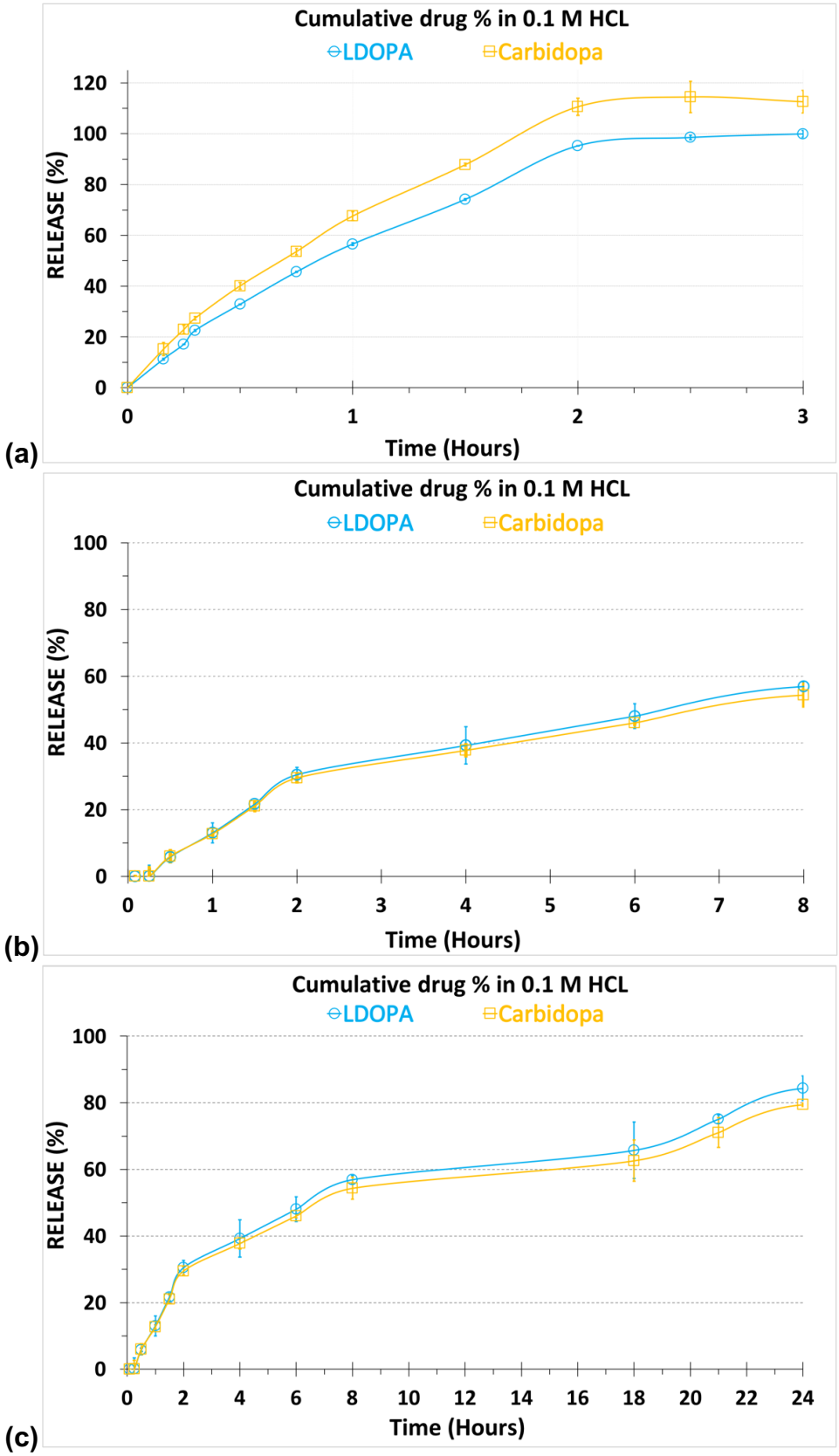

Figure 6.9. In vitro dissolution profiles showing **(a)** release of LD and CD from Sinemet CR® 200/50 mg tablets; **(b)** release of LD and CD from F1 over the first 8 hours; **(c)** release of LD and CD from F1 over 24 hours. Data are reported as mean ± S.D. (n=3).

In Figure 6.9a, the release of both drugs from the Sinemet CR tablet show similar trends, with ca. 50% of the loaded drug released in the first hour, and the remaining 50% in the second hour. This release was faster than the expected release from Sinemet CR, which should give sustained release over 4 to 6 hours (Goole and Amighi, 2009).

To allow a direct comparison with the SR tablet, drug release from the formulations was explored in HCl. This will allow the drugs to be released and dissolve into the acidic medium of the stomach, avoiding degradation. They can then transit into the small intestine where they will lose their charge and permeate. Since the fibres are expected to have mucoadhesive properties, they could be developed into gastro-retentive systems to this end. The in vitro drug release data are presented for the first 8 hours of the experiment in Figure 6.9b, and over 24 h in Figure 6.9c. The release of both drugs was similar, showing a biphasic release profile. In the first 2 h, over 25% of the loaded drug was rapidly released, followed by another 25% drug release over the next 6 h. Half the loading of each drugs is present with hydrophilic PVP in the shell layer, and it is expected that it is this half of the dose which was freed in the first phase of release. A similar fast release pattern was also noticed from coaxial fibres made of a PVP shell and ethyl cellulose core (Yu et al., 2013). These results concur with the aim of the formulation, delivering half the drug content as an immediate drug release.

In Figure 6.9c the second phase of release from the E-RLPO core can be seen from 8 to 24 h. As described earlier, E-RLPO is known to be a water-insoluble polymer with low permeability, but it undergoes pH-independent swelling allowing it to slowly release a drug cargo (Dave et al., 2012). The slow release of LD and CD observed

from E-RLPO arises due to diffusion of the loaded drug through and out of the polymer matrix (Yadav et al., 2012). This ER from the core layer is a comparable to results reported by Pornsopone et al. (2007) who showed the release from E-RLPO fibres loaded with 10% w/w indomethacin to reach only 18% cumulative release within 24 h. Overall, it is clear that the formulation prepared provides the desired biphasic release profile.

6.4 Conclusions

This study aimed to employ coaxial electrospinning to fabricate a core/shell fibre with biphasic drug release. Two polymers, PVP and E-RLPO, were used to build the core/shell fibres. In each layer, two model drugs (LD and CD) were loaded, resulting in an FDC which could be used for the treatment of PD. We were able to develop fibres with theoretical drug loadings of LD+CD at 19.1+4.86 % (F1) and 8.9+2.24 % w/w (F2). SEM images showed the production of cylindrical fibres with smooth surfaces. TEM images confirmed the formation of coaxial structure in the F1 fibres, but not for F2. Physical form characterisation studies with XRD and DSC revealed that both formulations comprised amorphous solid dispersions. Drug-polymer interactions between both drugs and the polymers were confirmed with FTIR studies. Encapsulation efficiencies for LD were over 90% in both FDC formulations, while CD lay between 66% to 81%. An *in vitro* dissolution study revealed the ability of the core/shell fibres to provide biphasic release profiles, providing an immediate burst release (giving a loading dose) followed by extended release for longer than was observed with commercial controlled release tablets. These results show the ability of coaxial electrospinning to fabricate LD/CD co-loaded coaxial electrospun fibres as a

novel drug delivery system. Such a formulation should be able to help maintain constant LD plasma concentration, extend the dosing frequency, and reduce undesirable side effects from overuse of the conventional treatments in PD.

6.5 References

British Pharmacopoeia commission, 2016, Co-careldopa Tablets, Appendix XII B. ANNEX: Recommendations on dissolution testing, British Pharmacopeia, London, England: stationary office.

British pharmacopeia, 2013, Carbidopa Assay Standard, EC Regulation No 1907/2006/EC, Article 31 Version number 1 of the European Parliament and of the Council of 16 December 2008 on classification, labeling and packaging of substances and mixtures, amending and repealing Directives 67/548/EEC and 1999/45/EC, and amending Regulation (EC) No 1907/2006.

Chaudhuri, K.R., Taurah, L.S., MacMahon, D.G., Turner, K., Kelly, L., Burn, D., Forbes, A., Bowron, A. and Foster, O.J., 2004. PD LIFE--a prospective multi-centre longitudinal audit of Quality of Life in Parkinson's disease across the UK. Journal of Neurology, Neurosurgery and Psychiatry, 75(3), pp.516-518.

Chen, Z., Mo, X., He, C. and Wang, H., 2008. Intermolecular interactions in electrospun collagen–chitosan complex nanofibers. Carbohydrate Polymers, 72(3), pp.410-418.

Chou, S.F., Carson, D. and Woodrow, K.A., 2015. Current strategies for sustaining drug release from electrospun nanofibers. Journal of Controlled Release, 220, pp.584-591.

Contin, M. and Martinelli, P., 2010. Pharmacokinetics of levodopa. Journal of Neurology, 257(2), pp.253-261.

Contin, M., Riva, R., Albani, F. and Baruzzi, A., 1996. Pharmacokinetic optimisation in the treatment of Parkinson’s disease. Clinical Pharmacokinetics, 30(6), pp.463-481.

Contin, M., Riva, R., Martinelli, P., Procaccianti, G., Cortelli, P., Avoni, P. and Baruzzi, A., 1990. Response to a standard oral levodopa test in parkinsonian patients with and without motor fluctuations. Clinical Neuropharmacology, 13(1), pp.19-28.

Dave, V.S., Fahmy, R.M., Bensley, D. and Hoag, S.W., 2012. Eudragit® RS PO/RL PO as rate-controlling matrix-formers via roller compaction: Influence of formulation and process variables on functional attributes of granules and tablets. Drug Development and Industrial Pharmacy, 38(10), pp.1240-1253.

de Sousa, I.P. and Bernkop-Schnürch, A., 2014. Pre-systemic metabolism of orally administered drugs and strategies to overcome it. Journal of Controlled Release, 192, pp.301-30

Evonik Roehm, 2007, Product Specification, Info 7.7/E, Specifications and test methods for Eudragit RL 100 and Eudragit RL PO, Eudragit RS 100 and Eudragit RS PO, Evonik Roehm GmbH, Pharma Polymers.

Fernandez, H.H., 2012. Updates in the medical management of Parkinson disease. Cleve Clin J Med, 79(1), pp.28-35.

Forster, A., Hempenstall, J. and Rades, T., 2001. Characterization of glass solutions of poorly water-soluble drugs produced by melt extrusion with hydrophilic amorphous polymers. Journal of Pharmacy and Pharmacology, 53(3), pp.303-315.

Goole, J. and Amighi, K., 2009. Levodopa delivery systems for the treatment of Parkinson's disease: an overview. International Journal of Pharmaceutics, 380(1-2), pp.1-15.

Greiner, A. and Wendorff, J.H., 2007. Electrospinning: a fascinating method for the preparation of ultrathin fibers. Angewandte Chemie International Edition, 46(30), pp.5670-5703.

Greiner, A., Wendorff, J.H., Yarin, A.L. and Zussman, E., 2006. Biohybrid nanosystems with polymer nanofibers and nanotubes. Applied Microbiology and Biotechnology, 71(4), pp.387-393.

Grosset, D., Antonini, A., Canesi, M., Pezzoli, G., Lees, A., Shaw, K., Cubo, E., Martinez-Martin, P., Rascol, O., Negre-Pages, L. and Senard, A., 2009. Adherence to antiparkinson medication in a multicenter European study. Movement disorders: official journal of the Movement Disorder Society, 24(6), pp.826-832.

Hsu, A., Yao, H.M., Gupta, S. and Modi, N.B., 2015. Comparison of the pharmacokinetics of an oral extended-release capsule formulation of carbidopa-levodopa (IPX066) with immediate-release carbidopa-levodopa (Sinemet®), sustained-release carbidopa-levodopa (Sinemet® CR), and carbidopa-levodopa-entacapone (Stalevo®). The Journal of Clinical Pharmacology, 55(9), pp.995-1003.

Huang, Z.M., Zhang, Y. and Ramakrishna, S., 2005. Double-layered composite nanofibers and their mechanical performance. Journal of Polymer Science Part B: Polymer Physics, 43(20), pp.2852-2861.

Huang, Z.M., He, C.L., Yang, A., Zhang, Y., Han, X.J., Yin, J. and Wu, Q., 2006. Encapsulating drugs in biodegradable ultrafine fibers through coaxial electrospinning. Journal of Biomedical Materials Research Part A: An Official Journal of The Society for Biomaterials, The Japanese Society for Biomaterials, and The Australian Society for Biomaterials and the Korean Society for Biomaterials, 77(1), pp.169-179.

Illangakoon, U.E., Yu, D.G., Ahmad, B.S., Chatterton, N.P. and Williams, G.R., 2015. 5-Fluorouracil loaded Eudragit fibers prepared by electrospinning. International Journal of Pharmaceutics, 495(2), pp.895-902.

Jiang, Y.N., Mo, H.Y. and Yu, D.G., 2012. Electrospun drug-loaded core–sheath PVP/zein nanofibers for biphasic drug release. International journal of pharmaceutics, 438(1-2), pp.232-239.

Jin, M., Yu, D.G., Wang, X., Geraldes, C.F., Williams, G.R. and Bligh, S.A., 2016. Electrospun Contrast-Agent-Loaded Fibers for Colon-Targeted MRI. Advanced healthcare materials, 5(8), pp.977-985.

Kanjanapongkul, K., Wongsasulak, S. and Yoovidhya, T., 2010. Prediction of clogging time during electrospinning of zein solution: Scaling analysis and experimental verification. Chemical Engineering Science, 65(18), pp.5217-5225.

Kulkarni, A.S., Balkrishnan, R., Anderson, R.T., Edin, H.M., Kirsch, J. and Stacy, M.A., 2008. Medication adherence and associated outcomes in medicare health maintenance organization-enrolled older adults with Parkinson's disease. Movement disorders: official journal of the Movement Disorder Society, 23(3), pp.359-365.

Leopold, N.A., Polansky, M. and Hurka, M.R., 2004. Drug adherence in Parkinson's disease. Movement disorders: official journal of the Movement Disorder Society, 19(5), pp.513-517.

Lewandowski, Z., 2001. Rheological aspects of fiber spinning from cellulose solutions in N-methylmorpholine-N-oxide. Journal of Applied Polymer Science, 79(10), pp.1860-1868.

LeWitt, P.A., Giladi, N. and Navon, N., 2019. Pharmacokinetics and efficacy of a novel formulation of carbidopa-levodopa (Accordion Pill®) in Parkinson's disease. Parkinsonism & Related Disorders.

Li, D. and Xia, Y., 2004. Direct fabrication of composite and ceramic hollow nanofibers by electrospinning. Nano Letters, 4(5), pp.933-938.

Luinstra, M., Grasmeijer, F., Hagedoorn, P., Moes, J.R., Frijlink, H.W. and de Boer, A.H., 2015. A levodopa dry powder inhaler for the treatment of Parkinson’s disease patients in off periods. European Journal of Pharmaceutics and Biopharmaceutics, 97, pp.22-29.

Moghe, A.K. and Gupta, B.S., 2008. Co-axial electrospinning for nanofiber structures: preparation and applications. Polymer Reviews, 48(2), pp.353-377.

National Centre for Biotechnology Information, 2019. PubChem Database. Carbidopa, CID=34359, https://pubchem.ncbi.nlm.nih.gov/compound/34359 (accessed on Apr. 24, 2019)

Ngwuluka, N., Pillay, V., Du Toit, L.C., Ndesendo, V., Choonara, Y., Modi, G. and Naidoo, D., 2010. Levodopa delivery systems: advancements in delivery of the gold standard. Expert Opinion on Drug Delivery, 7(2), pp.203-224.

Nyholm, D., Remahl, A.N., Dizdar, N., Constantinescu, R., Holmberg, B., Jansson, R., Aquilonius, S.M. and Askmark, H., 2005. Duodenal levodopa infusion monotherapy vs oral polypharmacy in advanced Parkinson disease. Neurology, 64(2), pp.216-223.

Nyholm, D., Lennernäs, H., Gomes–Trolin, C. and Aquilonius, S.M., 2002. Levodopa pharmacokinetics and motor performance during activities of daily living in patients with Parkinson's disease on individual drug combinations. Clinical Neuropharmacology, 25(2), pp.89-96.

O'Neil, M.J., Smith, A., Heckelman, P.E. and Budavari, S., 2001. The Merck Index-An Encyclopedia of Chemicals, Drugs, and Biologicals. Whitehouse Station, NJ: Merck and Co. Inc, 767, p.4342.

Parikh, T., Gupta, S.S., Meena, A. and Serajuddin, A.T., 2016. Investigation of thermal and viscoelastic properties of polymers relevant to hot melt extrusion-III: Polymethacrylates and polymethacrylic acid based polymers. Journal of Excipients and Food Chemicals, 5(1), p.1003.

Poewe, W.H., Lees, A.J. and Stern, G.M., 1986. Low-dose L-dopa therapy in Parkinson's disease: a 6-year follow-up study. Neurology, 36(11), pp.1528-1528.

Pornsopone, V., Supaphol, P., Rangkupan, R. and Tantayanon, S., 2005. Electrospinning of methacrylate-based copolymers: Effects of solution concentration and applied electrical potential on morphological appearance of as-spun fibers. Polymer Engineering & Science, 45(8), pp.1073-1080.

Pornsopone, V., Supaphol, P., Rangkupan, R. and Tantayanon, S., 2007. Electrospun methacrylate-based copolymer/indomethacin fibers and their release characteristics of indomethacin. Journal of Polymer Research, 14(1), pp.53-59.

Quan, J., Yu, Y., Branford-White, C., Williams, G.R., Yu, D.G., Nie, W. and Zhu, L.M., 2011. Preparation of ultrafine fast-dissolving feruloyl-oleyl-glycerol-loaded polyvinylpyrrolidone fiber mats via electrospinning. Colloids and Surfaces B: Biointerfaces, 88(1), pp.304-309.

Rajput, A.H., 2001. Levodopa prolongs life expectancy and is non-toxic to substantia nigra. Parkinsonism & Related Disorders, 8(2), pp.95-100.

Sagdinc, S. and Bayarı, S., 2005. Experimental and theoretical infrared spectra of famotidine and its interaction with ofloxacin. Journal of Molecular Structure, 744, pp.369-376.

Seeberger, L.C. and Hauser, R.A., 2007. Optimizing bioavailability in the treatment of Parkinson's disease. Neuropharmacology, 53(7), pp.791-800.

Siddhuraju, P. and Becker, K., 2001. Rapid reversed-phase high performance liquid chromatographic method for the quantification of L-Dopa (L-3, 4-dihydroxyphenylalanine), non-methylated and methylated tetrahydroisoquinoline compounds from Mucuna beans. Food Chemistry, 72(3), pp.389-394.

Stocchi, F., 2009. The hypothesis of the genesis of motor complications and continuous dopaminergic stimulation in the treatment of Parkinson's disease. Parkinsonism & Related disorders, 15, pp.S9-S15.

Wang, C., Yan, K.W., Lin, Y.D. and Hsieh, P.C., 2010. Biodegradable core/shell fibers by coaxial electrospinning: processing, fiber characterization, and its application in sustained drug release. Macromolecules, 43(15), pp.6389-6397.

Yadav, S.K., Mishra, S. and Mishra, B., 2012. Eudragit-based nanosuspension of poorly water-soluble drug: formulation and in vitro–in vivo evaluation. AAPS PharmSciTech, 13(4), pp.1031-1044.

Yang, Y.Y., Zhang, M., Wang, K. and Yu, D.G., 2018. pH-sensitive polymer nanocoating on hydrophilic composites fabricated using modified coaxial electrospraying. Materials Letters, 227, pp.93-96.

Yu, D.G., Zhang, X.F., Shen, X.X., Brandford-White, C. and Zhu, L.M., 2009. Ultrafine ibuprofen-loaded polyvinylpyrrolidone fiber mats using electrospinning. Polymer International, 58(9), pp.1010-1013.

Yu, D.G., Li, X.Y., Wang, X., Yang, J.H., Bligh, S.A. and Williams, G.R., 2015. Nanofibers fabricated using triaxial electrospinning as zero order drug delivery systems. ACS applied materials & interfaces, 7(33), pp.18891-18897.

Yu, D.G., Wang, X., Li, X.Y., Chian, W., Li, Y. and Liao, Y.Z., 2013. Electrospun biphasic drug release polyvinylpyrrolidone/ethyl cellulose core/sheath nanofibers. Acta Biomaterialia, 9(3), pp.5665-5672.

Yu, D.G., Shen, X.X., Branford-White, C., White, K., Zhu, L.M. and Bligh, S.A., 2009. Oral fast-dissolving drug delivery membranes prepared from electrospun polyvinylpyrrolidone ultrafine fibers. Nanotechnology, 20(5), p.055104.

Zhang, Y., Huang, Z.M., Xu, X., Lim, C.T. and Ramakrishna, S., 2004. Preparation of core− shell structured PCL-r-gelatin bi-component nanofibers by coaxial electrospinning. Chemistry of Materials, 16(18), pp.3406-3409.

Zhou, Y.Z., Alany, R.G., Chuang, V. and Wen, J., 2012. Studies of the Rate Constant of l-DOPA Oxidation and Decarboxylation by HPLC. Chromatographia, 75(11-12), pp.597-606.

Chapter 7. Research summary and future work

7.1 Research summary

This research project investigated the ability to develop FDC formulation to deliver multiple APIs in a single formulation to overcome the polypharmacy challenge and ultimately improve the adherence in patients with multimorbidities. Two different pharmaceutical manufacturing techniques were selected to prepare the FDC as multiple drug-polymer composite systems. The first method was solvent film casting as a conventional manufacturing technique, and the second method was single needle electrospinning as novel fabrication technique. For both studies, the FDC was made as a solid dispersion of the model drugs amlodipine besylate and valsartan with the appropriate polymeric solution polyvinylpyrrolidone (PVP). Assessment of the prepared formulations and performance of both manufacturing techniques were discussed in chapter 3: amlodipine besylate and valsartan FDCs prepared by film-casting; and chapter 4: electrospun FDCs of amlodipine besylate and valsartan.

Fast-dissolving ODFs and electrospun nanofibres were prepared by solvent film casting and single-needle electrospinning, respectively. For each technique, two types of formulation were made, loaded either with a single drug (valsartan or amlodipine besylate), or both as FDC. Drug loading was between 5% and 30% w/w for all ODF formulations while between 5% and 55% w/w for electrospun fibres incorporating single drug, and 5% and 30% w/w for the FDC.

Surface morphology study with scanning electron microscopy showed that solvent casting enabled a homogeneous layer with a smooth surface in most films, but partial drug dissolved at the highest loaded formulation 30%+30% AB+VAL. Similarly, electrospinning fibres formation was confirmed with smooth surfaces for all the fibres mat and cylindrical shape that tends to flatten with increased valsartan loadings. Thicknesses obtained for ODFs were between 167 and 937 μm, whereas for fibre mats between 146 and 450 μm. Folding endurance for all FDCs was more flexible at each time in the fibres mat formulation compared to the ODFs at similar loading. FTIR studies revealed good intermolecular interactions between both drugs AB and VAL with the carrier composite of the polymer PVP and glycerol in the ODFs, and a similar result was obtained for the PVP fibres mat. The physical characterisation studies with XRD and DSC showed that amorphous solid dispersions incorporated successfully in all the ODFs and the electrospun fibres mat FDC formulations loaded with AB+VAL up to 15%+15% w/w. Encapsulation efficiencies were very good at 100% for all the ODFs, while electrospun fibres were mostly above 90% except for one formulation at 86%. The fastest disintegration time of fast dissolving film was achieved under 3 s only from the electrospun fibres, indicating a promising oral fast-dissolving film.

The performance of all formulations was assessed as fast dissolving drug delivery system in simulated saliva. The in vitro dissolution studies demonstrated that all the AB loaded formulation at 30% w/w and below, released 90% of their drug cargo within 2 minutes from the fibres mat, and within 15 minutes from the ODFs. All the VAL loaded formulation at 30% w/w and below, released 90% of their drug cargo within 25 minutes from the fibres mat, and within 60 minutes from the ODFs. In the FDCs, the fastest release of both drugs to reach over 90% was achieved within 6 minutes from

the 5%+5% w/w loaded fibres. Whereas, the fastest release of both drugs to reach over 90% was achieved within 60 minutes for AB and 15 min for VAL from the 15%+15% w/w loaded ODFs. From the presented findings, both methods proved the ability to produce a drug-polymer composite that combines two active pharmaceutical ingredients in the same formulation. The performance of both formulations was compared, and we concluded that faster drug release was obtained from the electrospun fibres, making it more promising FD-DDS of the FDCs. However, this was best proved at the lower drug loading of AB+VAL limited to 5%+5% w/w to release 90% release of both drugs within 360 s. Though, at higher drug loading the rate declined significantly making the successful preparation of ODFs limited by drug loading and constricted to drugs that highly potent at a lower dose.

The electrospinning approach used in Chapter 4 employed the most straightforward single-needle experiment. Modification of the setup in single needle electrospinning opened further strategies to fabricate advanced patient-centric drug delivery systems. In Chapter 5 and Chapter 6, electrospinning was employed to generate FDCs with tailored drug release profiles for multiple drugs. In Chapter 5: FDC of ibuprofen, famotidine, and prednisone prepared by electrospinning; the aim was to employ a modification to the fibre deposition protocols from the single needle electrospinning. In this way, it was possible to develop the first formulation as multilayer fibres L (10%) using sequential electrospinning and to develop the second formulation as tangled fibres T (10%) using multi-jet electrospinning. Both formulations were successfully made from three selected polymers polyvinylpyrrolidone (PVP), Eudragit L100 (E-L100), and Eudragit RSPO (E-RSPO). Each formulation was loaded with a combination of three model drug ibuprofen, famotidine, and prednisone in separate

doses. The SEM surface images of both formulations proved that modification of the electrospinning setup in both ways was successfully able to produce different FDC formulations of electrospun fibres with average diameters of formulation T (10%) at 1004 ± 262 nm, and L(10%) at 1729 ± 369 nm. The physical characterisation studies XRD and DSC data displayed that all loaded drug was an amorphous solid dispersion. Drug-polymer interaction was confirmed with FTIR. Drug loading and EE was achieved the three drug combinations in both FDC. In vitro drug release studies showed the desired multi-phasic drug release could be obtained from the FDCs formulation T (10%) and L (10%). The multiple drug release from this fibres mat directly affected by the formulation final shape without damaging the fibres mat and need to be kept in shape until the end-user uses it. Therefore, studies to select the proper packaging of the fibres mat formulation will be required.

In Chapter 6: fabrication of levodopa and carbidopa FDCs in the form of coaxial electrospun fibres; the aim was to fabricate core/shell fibre as a platform for FDC with combined immediate then extended drug release. A concentric needle was utilised for coaxial electrospinning. The selected polymers PVP and E-RLPO were appropriate to build the fibres in core/shell structure. Coaxial fibres were developed with highest theoretical drug loadings of LD+CD at 19.1+4.86 % w/w, and EE of LD at 90.1 ± 0.07 %, and CD at 66.2 ± 0.9%. Morphology study with SEM showed that cylindrical fibres with smooth surfaces were formed in all formulations, and TEM images confirmed the formation of core/shell fibres structure in the 19.1+4.86 % w/w LD+CD loaded fibres with a diameter of the core around 154-160 nm, and the shell at 226-295 nm. Physical characterisation studies with XRD and DSC confirmed that both drugs were comprised as amorphous solid dispersions in all formulations. Molecular interactions between

loaded drugs with the carrier polymers was confirmed by FTIR studies. The in vitro dissolution study revealed the ability of the core/shell fibres to provide similar release of both drugs, showing a multiple drug release profile, as immediate from PVP burst release followed by the extended release from E-RLPO. So we concluded that coaxial electrospinning was a feasible technique to fabricate a novel drug delivery system the desired biphasic release profile. The most challenging part for producing this coaxial fibre was the production of small amount at milligram level over extended time over long hours because of the low flow rate used. The setup of the coaxial spinneret used here was limited to use one concentric needle. However, it would be feasible to optimise the scaleup production of coaxial fibres through a multiple-spinneret set up so that the production rate can be accelerated at a higher amount. The limitation in this study was the selection of LD+CD as an insoluble drugs in ethanol as the commonly used solvent for electrospinning. So they did require a step of pre dissolving the APIs in the required solvent of 1 M HCL as a different uncommon solvent to be added with the electrospinning polymer solution.

In conclusion, the main aims of the thesis were achieved by developing FDCs as multiple drug-polymer composite systems utilising advanced pharmaceutical manufacturing techniques for the ultimate goal of treating geriatric conditions requiring combined therapies. The rationale for selecting and optimising the processing method for each formulation enabled the production of a different platform as a drug delivery system. Each platform was efficiently designed to improve the performance of the FDCs prescribed for certain conditions commonly known among the geriatric populations. In all cases, the loaded drug in different formulations mostly changed from crystal form into amorphous solid dispersion, which potentially improves the

dissolution performance of a drug mainly the one with low aqueous solubility. Overall this thesis explored the application of solvent film casting and electrospinning as pharmaceutical manufacturing technique to develop FDCs as a strategy to manage polypharmacy.

7.2 Future work

7.2.1 Electrospun FDCs of amlodipine besylate and valsartan

The fast dissolving electrospun fibres showed a promising performance as fast dissolving drug delivery system in the artificial saliva. However, the acceptability of a dosage form is a fundamental aspect needs to be considered during formulation development. Limited knowledge is known for patient mouthfeel, palatability and acceptability of the electrospun fibres as fast dissolving film. Further studies can be focused on patient acceptability of this type of formulation.

7.2.2 FDCs of ibuprofen, famotidine, and prednisone electrospun fibres

The work in Chapter 5 employed electrospinning of three different polymers at the highest tested rate to possibly reach 4 mL/hr. The ability to collect the fibres mat on the rotating drum enabled fast fibres collection. Scale-up and further attempt to increase the production of the fibres can be applied to determine the optimum parameters to manufacture advanced formulations at a larger scale.

7.2.3 Levodopa and carbidopa FDCs in the form of coaxial electrospun fibres

The produced core/shell fibrous formulation showed the opportunity of combining two drugs to show immediate then extended drug release profiles. The design of this formulation ultimately aims to reduce the side effects related to the administration of multiple doses over the day. In order to assess the achievement of this aim, in vivo animal pharmacokinetics study can be applied to further optimise the pharmacokinetic profile of LD/CD from the formulation. Which can be an initial data towards the clinical studies in the context of reducing levodopa dosing and the undesirable side effects related to the repeated multiple dose.

Appendix 1. Calibration curve of the HPLC detection study

1- Amlodipine besylate and valsartan

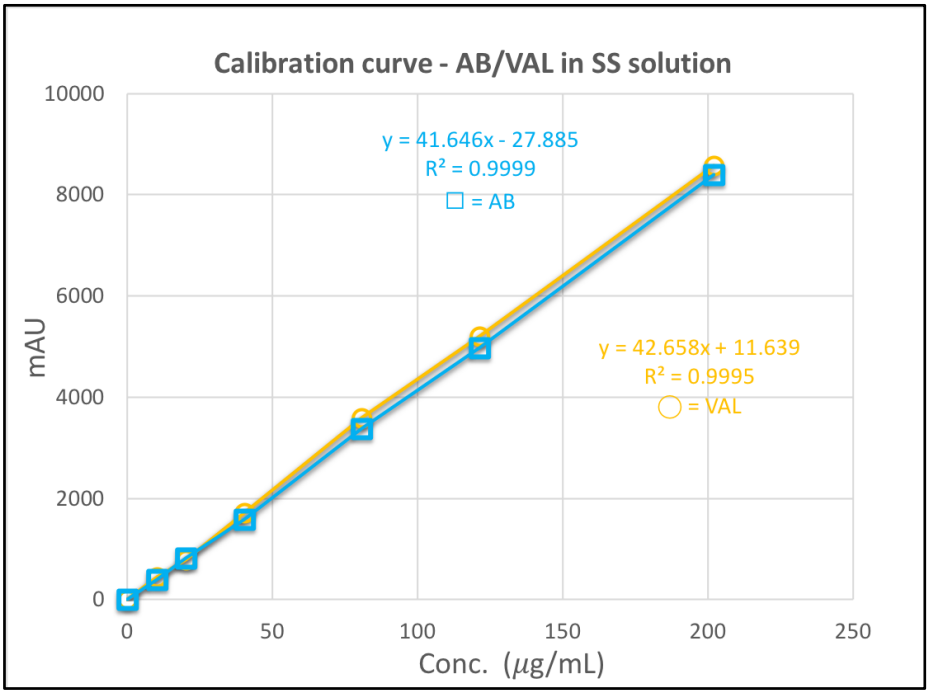

2- Ibuprofen, famotidine, and prednisone determination

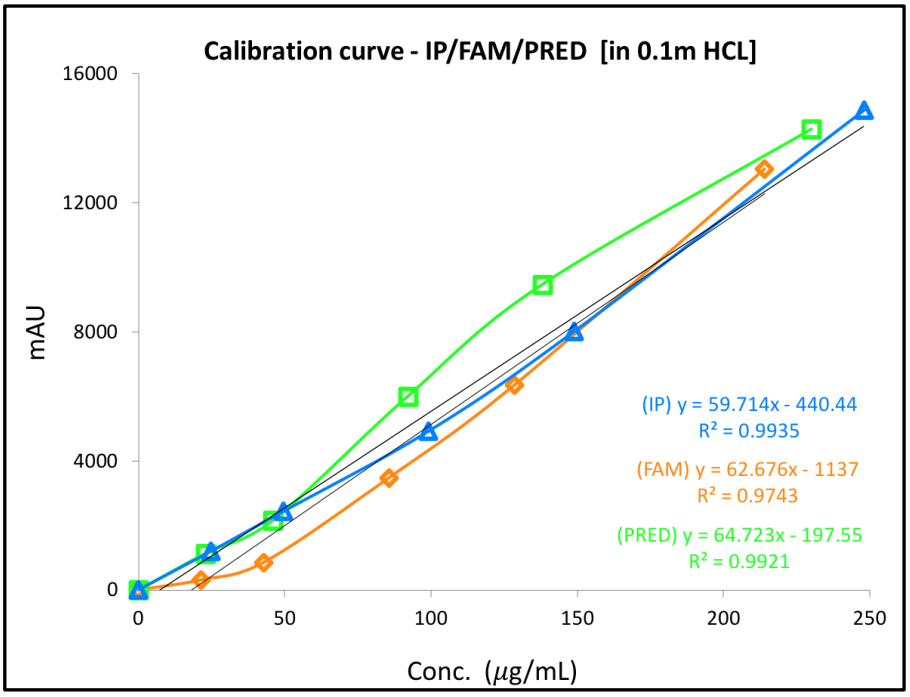

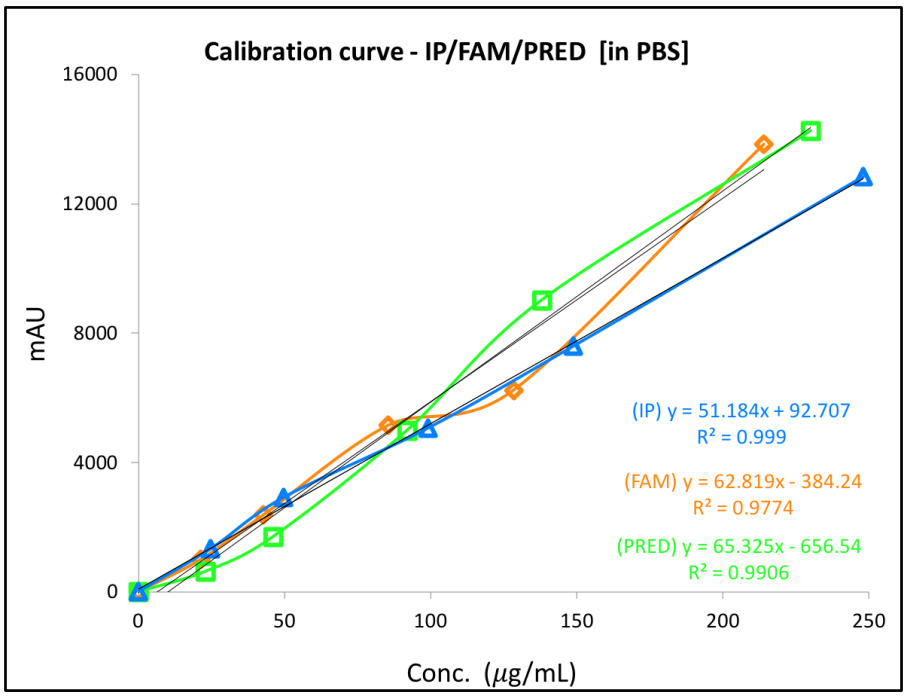

3- Levodopa and carbidopa determination